THE PROBABILISTIC ASSESSMENT OF SMALL HOMOGENEOUS UK EARTHFILL DAMS AFFECTED BY CLIMATE CHANGE; PRECIPITATION

by

Marie-Christine Preziosi

MEng (Honours)

Dissertation submitted in fulfilment of the requirement for the award of PhD

in

Civil Engineering

School of Engineering and Mathematical Sciences

City University

London

September 2011 (Resubmission January 2013)

VOLUME 1: TABLE OF CONTENTS

LIST OF FIGURES

LIST OF TABLES

ACKNOWLEDGEMENTS

I would like to express my sincerest gratitude to my supervisor, Dr. Tatyana Micic, for her continual advice, help and encouragement throughout my research project.

I would also like to thank Professor Neil Taylor for his valuable advice on the geotechnical aspect of this project.

I am also indebted to the Building Research Establishment, Environmental Agency and UK Climate Projections (UKCP09) for providing the tools and datasets I have used during the research process.

Lastly, I wish to thank my family and husband for their financial and moral support throughout my studies.

DECLARATION

I grant powers of discretion to the University Librarian to allow this dissertation to be copied in whole or in part without further reference to me. This permission covers only single copies made for study purposes, subject to normal conditions of acknowledgements.

ABSTRACT

The focus of this research is on small, well-established, homogeneous earthfill embankment dams that are currently in use and whose performance was previously outside the Reservoirs Act 1975, but are now governed by the new Flood and Water Management Act 2010. Many uncertainties are associated with such structures, a situation that can lead to the threat of dam failure when extreme climate conditions develop. Therefore, merely carrying out a deterministic assessment for such structures is insufficient and more sophisticated models, which reflect uncertain conditions of the dam site are required. This research presents the new advanced probabilistic slope stability model with precipitation effects (APSMP) developed by integrating the First Order Second Moment method (FOSM) with the deterministic slope stability model with precipitation (ASMP) using sliding block formulation. For the purpose of this study, the selected precipitation scenarios (rainfall intensity and duration) are obtained from past Met Office rainfall records and by applying the latest probabilistic model for predicting future precipitation projections for the UK (UKCP09).

It is demonstrated that by implementing APSMP the notional reliability and probability of upstream and downstream slope failure for small homogeneous earthfill embankment dams can be quantified. To reflect the critical conditions conducive to slope failure a benchmark has been developed, as a reference for comparison of the effect of precipitation on the notional reliability and performance classification of the embankment's slopes. By considering the probabilities of failure collated from APSMP and their associated performance, the impact critical precipitation effects could have on the notional level of engineering risk associated with slope failure is also identified. Hence, the dam's risk, as categorized by the Flood and Water Management Act 2010, can be reassessed in terms of engineering risk.

From the results obtained using APSMP a more informed assessment of small homogeneous earthfill embankment dams using limited information, including the level of uncertainty associated with the available site data, can therefore be carried out. Such an approach is therefore well placed to support and enhance the decision making process when evaluating the likelihood of dam failure, its impact on infrastructure performance and public safety, especially in relation to future climate effects.

NOTATION

Symbol	Description
A_{fu}, A_{fc}, A_{fd}	Total area of foundation (upstream/core/downstream)
A_{ju}, A_{jd}	Allocated areas in the upstream slope, core and downstream slope
A_{Tu}, A_{Td}	Total area of the slope (upstream/downstream)
b	Total base width of the embankment
b_u, b_d	Base width of the slope (upstream/downstream)
c	Cohesion
c'	Effective cohesion
CW	Crest width
e	Void ratio
FoS_U, FoS_D	Factor of safety (upstream/downstream)
$g(x_i)$	Linear limit state function
G_s	Specific gravity
H	Maximum height of the embankment
H'	Embankment's freeboard
H_{avu}, H_{avd}	Average height of the idealized phreatic line
H_f	Height of the embankment's foundation
H_U, H_D	Total horizontal driving force (upstream/downstream)
H_w	Headwater height of the reservoir
H_{xU}, H_{xD}	Embankment fill's average height above phreatic line
i_{flt},i_{slp}	Infiltration rate for flat and sloped surfaces
K(Θ)	Unsaturated hydraulic conductivity as a function of Θ
K(ψ)	Unsaturated hydraulic conductivity as a function of ψ
K_a	Active earth pressure coefficient
K_p	Passive earth pressure coefficient
K_r	Relative hydraulic conductivity
K_s	Saturated hydraulic conductivity
L_{up}, L_c, L_{dwn}	Vertical depth of infiltrated water through embankment fill for the upstream slope, core and downstream slope
L_{xflt}, L_{xslp}	Depth of infiltrated water normal to the flat and sloped surfaces
n_s	Porosity
P_{aU}, P_{aD}	Total active earth pressure force (upstream/downstream)
P_f	Probability of failure
P_{pU}, P_{pD}	Total passive earth pressure force (upstream/downstream)
P_s	Structure's reliability
P_w	Pore water pressure force
P_{XC}, P_{XU}, P_{XD}	Total active earth pressure force from the core, upstream and downstream slopes
P_{XUj}, P_{XCj}, P_{XDj}	Component active earth forces exerted by the upstream slope, core and downstream slope
R_U, R_D	Resultant shearing force (upstream/downstream)
S_r	Degree of saturation (saturation level)

'j' denotes 1 (above the phreatic line), 2 (below the phreatic line) and 3 (within the slope and its foundation)

Symbol	Description
t	Rainfall duration
t_{pflt}, t_{pslp}	Time to surface ponding for flat and sloped surfaces
u_{ju}, u_{jc}, u_{jd}	Component pore pressures present in upstream slope, core and downstream slope
u_{vu}	Pore pressure acting in the vertical direction
x_i	Random variable
α_1, α_2	Slope gradient (upstream/downstream)
α_i	Sensitivity index
α_{slp}	Slope angle
β	Reliability index
β_{HL}	Hasofer-Lind reliability index
β_U, β_D	Reliability index for upstream and downstream structural slope failure
γ_{fu}, γ_{fc}, γ_{fd}	Foundation's unit weight of soil (upstream/core/downstream)
γ_m	Partially saturated unit weight of soil
γ_{sat}	Saturated unit weight of soil
γ_{sub}	Effective (Submerged) unit weight of soil
γ_w	Unit weight of water
θ	Moisture content
Θ	Effective saturation of the soil
θ_r	Residual moisture content
θ_s	Saturated moisture content
μ_{xj}	Mean
σ_x	Standard deviation
σ_{Fu}, σ_{Fd}	Total vertical stress ≡ Effective weight of slope (upstream/downstream)
σ_{hju}, σ_{hjc}, σ_{hjd}	Component horizontal stresses present in the upstream slope, core and downstream slope
σ_{hju}', σ_{hjc}', σ_{hjd}'	Component horizontal effective stresses present in the upstream slope, core and downstream slope
σ_{vju}, σ_{vjc}, σ_{vjd}	Component vertical stresses present in the upstream slope, core and downstream slope
σ_{vju}', σ_{vjc}', σ_{vjd}'	Component vertical effective stresses present in the upstream slope, core and downstream slope
τ_u', τ_d'	Total effective shear stress (upstream/downstream)
φ	Internal friction
φ'	Effective internal friction
ψ	Wetting front suction head
ω_{eu}, ω_{ed}	Total effective weight of the slope (upstream/downstream)
ω_{euj}, ω_{edj}	Component effective weights within the slope (upstream/downstream)

'j' denotes 1 (above the phreatic line), 2 (below the phreatic line) and 3 (within the slope and its foundation)

ABBREVIATIONS

AFOSM	Advanced First Order Moment Methods
BRE	Building Research Establishment
CCIRG	Climate Change Impacts Review Group
CDF	Cumulative Density Function
CMF	Cumulative Mass Function
COV	Coefficient of Variance
DEFRA	Department for Environment, Food and Rural Affairs
DETR	Department of Environment Transport and the Regions
EA	Environment Agency
FM	Failure Mode
FORM	First Order Reliability Method
FOSM	First Order Second Moment Method
FP	Future Precipitation
G-A	Green-Ampt method
LC	London Clay
M1 to M6	Soil Model
MC	Monte Carlo simulation
MS	Medium Silt
PCP	Probabilistic Climate Projections
SBM	Sliding Block Method
SG	Slope gradient configuration
SORM	Second Order Reliability Method
SWCC	Soil-Water Characteristic Curve
UKCIP	UK Climate Impacts Programme
UKCP09	UK Climate Projections 2009
USACE	U.S. Army Corps of Engineers
VG	van Genuchten method
JCSS	Joint Committee on Structural Safety

ACRONYMS FOR DEVELOPED PROGRAMS

APSMP	Advanced Probabilistic Slope Stability Model with Precipitation Effects
ASMP	Advanced Slope Stability Model with Precipitation Effects
PSSM	Probabilistic Slope Stability Model

CHAPTER 1 : INTRODUCTION

1.1 Current Status of Small Embankment Dams in the UK

Many UK dams have been in existence for over a hundred years and as recorded by Baxter and Hope (2009: p.8) '*the average age of large dams is 110 years*'. Landowners, farmers and/or industrial companies originally constructed many of the oldest recorded small dams and their associated reservoirs. They were primarily used for storage of water for irrigation, farming and industrial purposes. More recently, small reservoirs have been either built or reclaimed by different individuals such as large companies who operate them for either industrial purposes or power generation. Many of the older reservoirs are still in operation and appear to be used for more commercial and leisure purposes. This includes fishing clubs, fish farms, charities, conservationists and private individuals. However, as these small dams continue to age they inevitably suffer from deterioration and assessing their overall safety is becoming more difficult, especially for those dams whose embankments were originally constructed of earthfill, of an unknown consistency.

In 1988, the UK's national dam database was formed as part of the Government's DETR Reservoir Safety Research Programme. This database was held by the Building Research Establishment (BRE) and contained detailed information '*on some 2650 dams which impound the 2500 reservoirs that come within the ambit of the Reservoirs Act 1975*' (Tedd, Skinner & Charles 2000: p.181). Over the years, this database has been continuously expanded and updated, increasing the usefulness of the available data. Since 2004 the Environment Agency, who is the current Enforcement Authority for England and Wales, holds the latest register of all existing dams and associated

reservoirs, which previously fell within the ambit of the Reservoirs Act 1975 and are now subject to the new Flood and Water Management Act 2010 (UK Statute Law Database, 2010). This register includes any revised information on individual dams, minor or major incidents that may have occurred, as well as any remedial works carried out at the dam site.

In order to identify the most common types of dams constructed in the UK, the national dam database from 2003 was considered and the following information obtained:

- 70 %, or 2066 of the 2965, registered dams are classified as Earthfill (TE) of which 61 % had not been allocated a flood risk category (identifies the potential effect should a dam breach occur) in 2003.
- Approximately 28 %, or 574, of the registered earthfill dams have an embankment height $\leq$ 5.0 m.

For consistency, BRE applied the same dam type codes as defined by the International Commission on Large Dams – ICOLD (BRE, 2003). As observed by Hinks and Williams (2004), approximately 38 % of the registered dams in the national dam database have a capacity of less than 100,000 m^3. Hinks and Williams (2004) also noted that of these, many are in private ownership and rarely generate sufficient income to pay for periodical inspections and supervisions under sections 10 and 12 of the Reservoirs Act 1975 (UK Statute Law Database, 2008) or for improvements and remedial works to be carried out. Dams are vital infrastructure components and any form of failure would result in severe consequences, so extensive regulation is in place to ensure their safe operation.

1.1.1 Summary of current legislations for UK dam safety

The first safety legislation for dams and their associated reservoirs was introduced in 1930, which was later replaced by the Reservoirs Act 1975 (Brown & Gosden, 2004). This provided the legal framework required to ensure the safety of all large raised reservoirs, whose minimum reservoir capacity was 25,000 m^3 above the lowest point of naturally occurring ground level or the level at which the reservoir could drain out if it were to fail (Brown & Gosden, 2000; UK Statute Law Database, 2008). More recently, the Flood and Water Management Act 2010 has replaced the Reservoirs Act 1975. With the recent introduction of the Flood and Water Management Act 2010, many reservoirs

that previously did not fall under the Reservoirs Act 1975, but whose capacities are greater than 10,000 m^3, will now have to comply with the new Act as they are re-categorized as large raised reservoirs (UK Statute Law Database, 2010). This new legislation also includes new arrangements for reservoir safety based on risk rather than just on the reservoir's capacity. Thus, new specific methodologies are needed to perform detailed assessments for those small dams that must now comply with the new legislation, due to high uncertainties associated with these structures.

1.2 Rationale for the Research

As all large raised reservoirs had to comply with the Reservoirs Act 1975, there are many well-established procedures, reports relating to their potential modes of failure and the overall safety of the specific reservoir. However, for small dams that will now have to comply with the new Flood and Water Management Act 2010 it is unlikely detailed consistent data is available, as:

- Few regulations were in place when these dams were originally designed and built.
- Undertakers (owner or user) of these dams may have a limited budget to carry out detailed dam site tests, which can be both expensive and time consuming.
- Certain physical properties will be either largely unknown or visibly differ between available data samples.
- Inconsistent monitoring and/or only a small number of data samples could have been extracted since the dam's formation.

It would therefore be difficult to accurately assess the integrity of such dams and establish their rate of deterioration (Preziosi, 2008), resulting in decision-makers being faced with the problem of obtaining quantitative performance measures for such structures.

As the new Act will now base reservoir safety on risk rather than just on the reservoir's capacity, carrying out a deterministic assessment may no longer be sufficient. Furthermore, as acknowledged by Hughes, Bowles and Morris (2009: p.9) '*the effect of such legislation is that many smaller reservoirs are likely to fall within the proposed*

new Act, significantly increasing the number of individual dam owners for whom an effective, proportionate risk analysis method would be beneficial. Estimates suggest that the number of reservoirs falling within such legislation would rise to around 7500 from the current 2100 in England and Wales. (There are already another 760+ reservoirs in Scotland and there could be many more.)'

Reports published also indicate that failures have occurred and in the future such dams may continue to fail (Tedd, Skinner & Charles, 2000; Hamilton-King, 2010). Hamilton-King (2010) recorded several incidents between 2004 and 2009 concerning non-statutory reservoirs and small raised reservoirs whose capacities are between 25,000 m^3 and 10,000 m^3. The majority of these structures failed due to instability of the embankment and overtopping of the dam, resulting in external erosion of the crest and downstream face. As reported by Charles, Tedd and Warren (2011) '*a variety of causes of slope instability have been recorded in both upstream and downstream shoulders; particularly the presence of water causing a decrease in effective stress, from rain, leakage through the dam, broken supply pipe within the dam, spray over the dam or flows from valley sides. Other causes include removal of trees, rapid reservoir drawdown and construction*' (p.48).

In addition, due to recent extreme rainfall events, public bodies and insurers are starting to take a greater interest in the impact extreme rainfall events could have on dam failure at key dam sites. Specifically, in order to identify the change, if any, in the dam's risk classification outlined in the new legislation. More comprehensive information is therefore required to assess the future behaviour (performance) of the dam, including site-specific lifecycle issues (such as maintenance, repair and dam use). In order to determine if the safety of such dams has or will be compromised during its lifetime, models that reflect uncertain conditions of the dam's embankment are required as even the smaller dams can still cause damage to their surrounding environments.

1.2.1 Classification of small embankment dams in the UK

For clarity when describing a dam and its reservoir as 'small', either of the following parameters can be considered (Kennard, Hopkins & Fletcher, 1996; Brown & Gosden, 2000):

- The overall height of the dam.
- The maximum capacity of water stored by the reservoir.

In the UK, dams are primarily defined by their reservoir capacity rather than the height of the dam (Brown & Gosden, 2000). Therefore, for a dam to be classified as small and remain outside of the new Flood and Water Management Act 2010 c.29, its reservoir must not exceed '*10,000 cubic metres of water above the natural level of any part of the surrounding land*' (UK Statute Law Database, 2010: p.62). This is a change in practice and there are a number of dams associated with reservoirs smaller than 25,000 m^3 that have become subject to the new legislation. According to Stephens (2010), an earthfill embankment can be categorized as small when:

- The embankment's height does not exceed 5.0 m from the streambed to the crest level. However, Smout and Shaw (1999) classify an embankment as small when its overall height is less than 3.0 m.
- The embankment's freeboard is not less than 0.5 m, but the preferred height is between 0.75 m and 1.0 m (Stephens, 2010: p.53).

As there are several methods that could be applied when classifying a dam and its reservoir as 'small', a more suitable approach is to consider both parameters, the overall height of the embankment and reservoir's maximum capacity.

It is unlikely that the impact the changing climate could have on the dam's embankment was originally addressed when small earthfill dams were designed and built. Furthermore, as changes in UK climate are dependent on global climate change, the exact nature and scale of these changes will continue to retain a degree of uncertainty. What is certain, however, is that climate change will take place in the UK, and will result in changes to the frequency of seasonal events, such as precipitation, and other forms of climate change, along with their related hazards. It is therefore important to identify how the different modes of failure, associated with these structures, can be affected by the UK's changing climate.

Due to the high level of uncertainties associated with small earthfill dams, it is necessary to develop a probabilistic approach to assess the performance of the embankment's upstream and downstream slopes, as a function of their notional reliability (probability of failure), and quantify the effects of uncertainty in basic parameters. In order to identify the change, if any, in the classification of the slope's behaviour and performance level, due to precipitation, a benchmark will be developed. It will therefore be possible to document the structure's risk classification, according to engineering risk, to check compliance with the current guidelines, such as the Flood and Water Management Act 2010.

1.3 Assessment of Climate Effects on Slope Stability

There are many uncertainties surrounding the composition of most small earthfill embankments, a situation that may be exacerbated by the likely increase in extreme adverse conditions predicted by climate change estimates. To date numerous applications have been developed to assess the effect rainfall can have on the behaviour of earthfill slopes. Such analyses have been carried out using both experimental and empirical methods, deterministic and probabilistic approaches.

The Bionics project (Glendinning et al., 2006) applied an experimental approach by building a full-scale embankment, representing transport infrastructure in the UK, and under controlled conditions monitored the effect of climate change on the embankment. Davis et al. (2008) developed a deterministic model for hydraulic boundary conditions that includes the geotechnical finite difference code, FLAC. This method also applies a hydrological model to measure the exact depth of water infiltration through the embankment, but does not consider vegetation cover. From their model, Davis et al. (2008) observed that climate change, in the form of precipitation, may not have a significant effect on slope stability, but indicated that due to the increase in precipitation different outcomes may be present in other parts of the UK. Using experimental data from Bionics, Rouainia et al. (2009) developed a model for pore water pressure changes and diagnostic embankment evaluating the effects on deformation and stability.

Rouainia et al. (2009) and Kilsby et al. (2009) both identified that future climate scenarios in the UK will have an effect on the behaviour and maintenance of transport infrastructure slopes, such as those constructed of over-consolidated clays.

To evaluate rainfall-induced slope instability Lee, Gofar and Raharjo (2009) presented an effectively deterministic model, PERSIS, which incorporates the statistical analysis of rainfall and the key properties of the unsaturated soil. When Lee, Gofar and Raharjo (2009) compared the suction envelope and factor of safety calculated using the PERSIS model with those obtained using the readily available deterministic uncoupled seepage analysis program SEEP/W and slope stability analysis program SLOPE/W similar results were observed. Mahmood and Kim (2011) used SEEP/W to assess the effect short rainfall durations have on the stability of an unsaturated embankment and observed the difference between the soils and rainfall patterns. As the analytical methods presented still rely on data that has been either extracted, collated or derived from soil samples taken from the embankment or other sources, they are all effectively a deterministic approaches and rather expensive to implement throughout.

Using experimental methods, Liang, Nusier and Malkawi (1999) presented a methodology that considered the risk level of slope failure, where the slope's reliability index was obtained theoretically by applying the First Order Second Moment Method (FOSM), which was combined with the Fellenius method of slices. Yet they did not consider the effect of climate change. In a similar manner to Davis et al. (2008) and Rouainia et al. (2009), Zhang, Zhang and Tang (2005) developed a coupled hydromechanical finite element modelling program and a finite element based slope stability analysis program to investigate the performance and stability of unsaturated soil slopes during a rainstorm. They observed that prior to rainfall only the soil properties affect the slope's factor of safety, but after rainfall, the slope's factor of safety is influenced by the soil's hydraulic properties as they change the pore water pressures in the embankment. In contrast, Zhan, Zhang and Chen (2006) used the seepage analysis program SEEP/W to assess the effect of seasonal climate change on the slope's factor of safety by simulating the change in pore water pressures in the slope, due to changes in the reservoir level.

Taking into account climate effects, Hudacsek et al. (2009) investigated experimentally the long-term performance of compacted clay embankments subject to controlled climatic conditions using centrifuge model testing. They observed that soil movement occurred mostly during the simulated winter months compared to those recorded during the simulated summer months. More recently, Lee et al. (2010) developed a wireless sensor network based slope monitoring system to measure the slope's unsaturated hydraulic soil properties, such as the variability of the soil's matric suction, for reliable slope stability estimation. They also presented a reliability based slope stability assessment method, which automatically considers the measured matric suction and applies the Advanced First Order Reliability Method (AFORM) to quantify the risk of slope failure during a rainfall event. From their research, they identified that the slope's reliability index decreases during rainfall, most notably at the slope's surface. However, in practice it would have been very difficult to have sufficient site measurements for such analysis.

Santoso, Phoon and Quek (2010) applied subset simulation to estimate the probability of failure for unsaturated infinite soil slopes by modelling the change in the soil's matric suction due to rainfall infiltration using a finite element transient seepage analysis. They ascertained that for unsaturated soil slopes, the failure surface and factor of safety changed with time. Furthermore, Santoso, Phoon and Quek (2010) and Lee et al. (2010) demonstrated that their proposed methodologies were more efficient than standard Monte Carlo simulation when determining the slope's probability of failure. As an alternative, Ching, Phoon and Hu (2010) proposed a method based on the importance sampling technique, which applies the ordinary method of slices to establish the suitable locations of the importance sampling probability density function, to calculate the slope's probability of failure. However, they did not consider climate effects. As the slope's factor of safety is dependent on its dimensions, soil type, hydraulic properties and the rate at which the reservoir level changes, more sophisticated models that reflect uncertain conditions are required. By extending this approach, it will be possible to assess and obtain a clearer and more detailed understanding of the risks associated with selected environmental threats in the future. Unfortunately, simulation techniques are associated with very high computational costs.

Currently, there has been no comprehensive probabilistic model that could include precipitation. As summarised by Cheung and Tang (2005) and in the Probabilistic Model Code according to the Joint Committee on Structural Safety (JCSS) (Baker, Calle & Rackwitz, 2006), when performing a slope reliability analysis for earthfill embankments, the probabilistic model should be capable of incorporating uncertainties relating to:

- Embankment geometry.
- Geological profile of the embankment fill.
- Soil strength parameters.
- Spatial variability of soil properties within the embankment fill.
- Climate effects, specifically diverse precipitation scenarios.

Considering recent legislation changes and evidence about changing climate, it is evident that there is a need to consider comprehensively the effect of climate change on the embankment's slopes, especially when looking at old well-established earthfill embankments dams, were not taken into account at the time of their design and construction. Due to uncertainties associated with such structures it is important to analyse probabilistically the specific impact that new circumstances may have on their overall stability.

1.4 Aims of Research

The aim of this research is to first develop a new and sophisticated probabilistic slope stability model to quantitatively measure the notional reliability and probability of upstream and downstream slope failure when exposed to variable seasonal precipitation scenarios. Secondly, to develop a benchmark classification that reflects the critical conditions conducive to slope failure. Lastly, to establish a methodology that can be used to identify the impact future extreme rainfall events could have on the structure's risk classification, as categorized by the Flood and Water Management Act 2010.

It must be noted that the aims of this research are selected to complement the existing risk assessments and to improve the quality of data used by the decision-makers

(Undertakers, Panel Engineers, Environment Agency, etc.) when determining the slope's behaviour and performance level, in relation to variable precipitation scenarios.

1.5 Objectives of Research

To carry out this research, the following objectives must be completed.

1. Establish the physical model for a generic small homogeneous earthfill embankment whose reservoir capacity is between 25,000 m^3 and 10,000 m^3.
2. Define the relevant failure modes associated with upstream and downstream slope failure and define the critical limit state functions to include the uncertain random variables associated with uncertain parameters:
    i The embankment's geometry.
    ii The embankment fill's mechanical and hydraulic soil properties.
    iii The water level of the reservoir.
    iv Climate effects.
3. Develop the deterministic slope stability model for the upstream and downstream slopes, which encompasses:
    i The physical model of the embankment.
    ii The steady seepage flow model.
    iii The infiltration model.
    iv The unit weights of the embankment fill and the embankment's foundation.
4. Identify the appropriate methodology required to perform the reliability analysis that includes uncertainties and generic formulation of the failure modes.
5. Identify the common climate variables and climate change scenarios associated with UK climate change, in order to:
    i Identify the impact that these scenarios could have on the dam's long-term performance.
    ii Establish different precipitation scenarios and future extreme rainfall scenarios, using historic Met Office rainfall records and future UKCP09 precipitation projections.
    iii Examine the impact precipitation could have on the engineering risk associated with slope instability.

6. Integrate the considered reliability analysis with the deterministic slope stability model, in order to identify the impact variable precipitation events could have on the performance of the embankment's slopes. Demonstrate the methodology by performing parametric studies for:
   i Various soil models.
   ii Distinct slope gradient configurations.
   iii Different fill saturation levels and associated hydraulic soil properties.
7. Demonstrate how the engineering risk associated with slope failure, of small homogeneous earthfill embankment dams, could be related to the risk classification, as categorized by the Flood and Water Management Act 2010.

1.6 Structure of Report

This thesis has been divided into seven chapters and 10 appendices. The individual chapters are summarised as follows:

Chapter 1: Introduction to thesis, presenting the rationale, aim and objectives of the research that will be carried out.

Chapter 2: The significant failure modes and their local factors associated with the performance of small homogeneous earthfill embankment dams are identified. A summary of the methodologies used to develop the physical model, which incorporates the steady seepage model is presented. The equations used to characterise the embankment fill's soil properties are also presented. The deterministic slope stability models are outlined in detail and several worked examples presented. The engineering risk associated with such failure events and its relation to the risk classification, as categorized by the Flood and Water Management Act 2010, is discussed.

Chapter 3: Provides an outline of the methodology required to perform a reliability analysis. Different forms of uncertainty fundamental to engineering models are defined, focusing on the Level 2 structural reliability analysis. The probabilistic slope stability model (PSSM), developed by integrating the First Order Second Moment method (FOSM) with the modified deterministic sliding block slope stability model is presented. The relevant

failure modes and their limit state functions are defined. A simple slope stability example is presented, demonstrating the application of PSSM. The methodology used to establish site-specific engineering risk associated with the limit states as well.

Chapter 4: Performance level benchmark is developed. In chapter 4, results obtained using PSSM for selected soil types, with respect to their mechanical properties, assuming the generic dam site conditions are presented. From the parametric probabilistic slope stability analysis the performance of the embankment's upstream and downstream slopes, as a function of their notional reliability, using the benchmark classifications is established. The sensitivity factors that reflect the importance of all random variables for each limit state are also identified.

Chapter 5: The common climate variables and climate change scenarios associated with UK climate change and their current and future trends are identified. The impact that external and internal threats have on the long-term performance of small earthfill embankment dams are categorized and their influence on the selected failure modes examined. The advanced deterministic slope stability model with precipitation (ASMP), which incorporates rainfall infiltration within the sliding block formulation for the upstream and downstream slopes, is outlined in detail and several worked examples, using ASMP, presented.

Chapter 6: Seasonal precipitation scenarios are selected from past Met Office rainfall records and UKCP09 future precipitation projections and used to generate future extreme rainfall scenarios. The effect that precipitation can have on the performance of the embankment's individual slopes, as a function of their notional reliability (probability of failure), is evaluated for selected clay soil models. The sensitivity factors of the uncertain variables, for each limit state, are also assessed for the selected clay soil models. The engineering risk associated with such structures is established and related to the risk classification identified by the Flood and Water Management Act 2010, in respect to the effect of precipitation.

Chapter 7: Draws conclusions from thesis and discusses the scope of future research and practical applications.

CHAPTER 2 : ANALYSIS AND PERFORMANCE CHARACTERISATION FOR SMALL EARTHFILL EMBANKMENT DAMS

2.1 Introduction

In this chapter, the design terminology and performance characterisation of small homogeneous earthfill embankment dams will be studied in detail. The significant failure modes, relating to structural, hydraulic and seepage failures, and their local factors associated with the embankment's performance will also be identified. Selected specific failure modes will be discussed in depth. The methodology used to develop the physical model, for the cross section of the embankment and its reservoir level, is explained and illustrated. A general overview of the soil characteristics and properties of the embankment fill is given. The fundamental definitions of the implemented soil mechanics and the detailed equations, with which the fill's soil properties are characterised, are presented. The steady seepage methodology applied to estimate the position of the idealised phreatic line through the cross-section of the embankment will be summarized, and its importance in dam construction and maintenance explained. For the slope stability analysis, several well-established methodologies are considered. The equations implemented to perform the slope stability analyses for the upstream and downstream slopes are presented in detail. Several worked examples are given, demonstrating the methodology. Finally, the general procedure required for probabilistic slope stability analysis will be summarised.

2.2 Types of Embankments Used to Construct Small Dams.

For small dams, as defined by Kennard, Hopkins and Fletcher (1996); Stone (2003); and Stephens (2010), the four most common types of embankment designs are:

- Lined embankments
- Zoned embankments
- Diaphragm embankments
- Homogeneous embankments

These are standard forms and for a brief description see *Appendix I: Subsection I.2*. As these types of embankments do not exert a great deal of pressure directly onto their foundation, it is possible to construct them on different soil type foundations. Depending on the dam site, and the dam's use, different embankment types are preferred, but the type of material used for the embankment fill and the type of material available for the dam's foundation are still key factors when designing and constructing the embankment. The principal materials used for the embankment fill are:

- Rockfill
- Earthfill
- Or a combination of both materials

Rockfill embankments contain an array of compacted or dumped rockfill, whereas the majority of earthfill embankments are constructed using good quality compacted soil (Kennard, Hopkins & Fletcher, 1996). When constructing rockfill or earthfill embankments a large amount of material is required, as each layer of the embankment fill needs to be compacted to reduce the threat of seepage or overturning occurring. Consequently, the dam's foundation has to be capable of supporting the entire weight of the embankment and reservoir when at full capacity, without substantial settlement occurring during or just after the dam's construction. Considering that this research is focused on embankments that were not governed by the Reservoirs Act 1975, only small earthfill embankment dams will be examined.

2.3 Review of Small UK Homogeneous Earthfill Embankment Dams

The majority of small UK dams generally have a homogeneous earthfill embankment and are typically constructed in areas where there is an abundance of natural material, so the embankment's fill would have had the minimal amount of handling during the dam's construction. This makes them more suitable in areas where earthquakes, landslides, and unexpected floods are more common. However, as earthfill embankments are not impervious they will undergo some form of seepage, due to water seeping through the structure, over the dam's lifecycle. In some cases, seepage appears on the downstream slope where, for instance, there is no toe or drainage incorporated into the embankment's downstream slope. Subsequently slope instability can arise due to shear failure within the embankment or its foundation. As documented by Hamilton-King (2010) and Hope (2009) in the annual reports for post-incident reporting for UK dams, one of the main triggers of dam failure is due to embankment stability caused by internal erosion through the embankment. Earthfill embankments are also prone to damage due to external erosion, deformation, overtopping, seepage, etc.

This research project will only focus on small homogeneous earthfill embankment dams, Figure 2.1, as:

- Homogeneous earthfill embankments are relatively simple in design and the majority of small UK dams are constructed using this type of embankment (Kennard, Hopkins & Fletcher, 1996).
- They can have a wide range of foundations, as the foundation requirements are less stringent when constructing such dams (Stephens, 2010).
- It is likely that the embankment and its foundation are constructed using local material excavated at or near the dam site, or quarried from within the reservoir basin itself (Kennard, Hopkins & Fletcher, 1996).
- Earthfill embankments can resist movement and settlement better than other dam type (Stephens, 2010).

As a result of the earthfill embankment's simplistic design, the embankment can only resist sliding and slope instability due to the sheer weight of the embankment fill (Stephens, 1991). Furthermore, earthfill embankments are *'easily damaged or destroyed*

due to water flowing on, over or against it' (Stephens, 2010; p.13). Stephens (2010) also explains that *'a failed dam, however small, is not only a matter of a lost structure but can result in loss of life and considerable expense for those downstream'* (p.8).

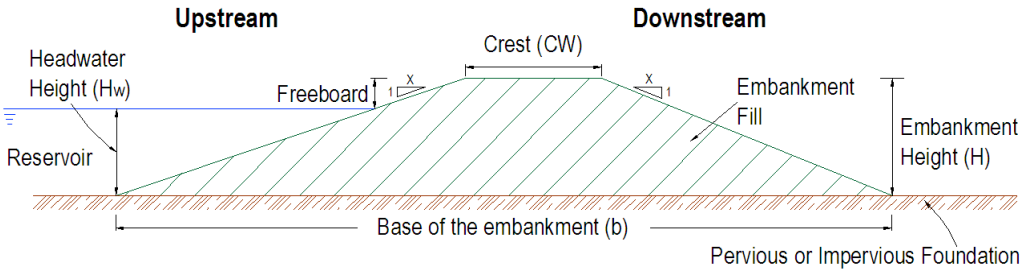

Figure 2.1 Cross sectional diagram of a homogeneous embankment

Due to the uncertainties associated with small homogeneous earthfill embankment dams, it is important to analyse and discuss the impact new circumstances, such as extreme adverse conditions, may have on the structure's reliability. This is crucial when assessing those dams that until now were not covered by the Reservoirs Act 1975, but now fall under the Flood and Water Management Act 2010, as it is unlikely that detailed consistent data is available, as the requirements at the design stage and during construction was generally less stringent. As only those dams considered old and well established are dealt with here, the effect of construction, compaction and settlement of the embankment fill will not be considered in this investigation. This is a fair approach, as the effects of those processes would have diminished with the passage of time.

2.3.1 Lifetime effects on homogeneous earthfill embankments

During the dam's lifecycle, its physical and mechanical properties will have changed in some form. This can be due to environmental impacts (climate change) or some form of failure (such as deterioration, seepage etc.) occurring during its use (Baxter & Hope, 2009). Changes in the surrounding environment such as an increase in precipitation intensity and number of dry days can cause the properties of the embankment fill to change by either increasing its moisture content or reducing its permeability or void ratios. Therefore, as the embankment fill becomes more saturated, water can seep through the fill causing seepage to occur. The physical contour of the embankment and its reservoir could also have changed due to some form of compaction, erosion, or deterioration of the embankment fill as well as any remedial actions carried out on the

embankment. For these reasons, all uncertainties have to be considered when researching old well-established dams.

2.4 Failure Modes for Small Homogeneous Earthfill Embankment Dams

In practice, the behaviour of the earthfill embankment is monitored using both visual surveillance techniques and monitoring instrumentations set by the supervising engineer. Modes of failure can be grouped into three main classifications (Johnston et al., 1999):

Structural failure Involves the separation of the embankment fill's material and/or foundation material.

Hydraulic failure Occurs from the uncontrolled flow of water over and adjacent to the embankment, due to the water's erosive action on the embankment's slopes over a period of time.

Seepage failure Can only be controlled by the volume of water in the reservoir and its flow rate through the embankment and/or its foundation.

From incident reports published by the Environment Agency (EA), the most common forms of failure for old, well-established, earthfill embankments dams was linked to:

Structural Failure	⇨	Settlement Internal erosion Slope instability
Hydraulic Failure	⇨	Overtopping External erosion
Seepage Failure	⇨	Seepage through the embankment fill and foundation

These failure modes are also influenced by a combination of site-specific local factors, which can play a vital role in the embankment's performance as well as the extent and location of the failure in the embankment. These local factors can be grouped into four categories, as shown in Table 2.2.

Table 2.1 Local factors affecting the performance of small earthfill embankments[1]

LOCAL FACTORS			
Internal	External	Environmental	Human
Moisture content	Reduction in crest	Gullying	Age of embankment
Friction angle	Settlement of crest	Leakage	Distance from human habitats
Unit weight of soil	Localised dipping of crest	Animal burrows	Agriculture
Plastic index	Cracking/ Sloughs/ Bulges/ Other irregularities in the dam	Water volume in reservoir	Enforced legislation
Cohesion	Sink holes	Flow content	
Foundation properties	Vegetation cover	Climate conditions	
Compaction	Cracking along the crest	Tree growth through or near embankment	
Inner temperature	Bulging at the downstream toe		

To take into account the internal (local) factors complete understandings of the embankment fill's soil type, geology and composition with respect to its hydraulic and mechanical properties is essential. In an ideal situation, detailed data of the embankment and reservoir, including geological and geotechnical reports, review reports as well as monitoring and surveillance data should be available (Fell et al, 2000). However, this information is often incomplete or unknown, then soil samples are required from the dam site to identify the soil type and its structural composition, but those are expensive to obtain and therefore limited in number.

The external (local) factors are relatively easy to identify through visual inspections, as they only affect the embankment's surface. One of the main sources of uncertainty is the surrounding environment of the dam as there is no direct control over it. Therefore, the environmental factors also have to be investigated as they can influence the dam's performance and failure rate and relate to the physical factors surrounding the dam.

Humans can also have a direct impact on the type and rate of failure of an embankment. One of the main causes is due to the lack of maintenance and knowledge of the embankment and its fill properties. Thus, the behaviour of the dam is dependent on:

- The embankment's location.

[1] Extracted from Crookes (2004a: pp.14-17)

- The reservoir's maximum allowable capacity.
- The hydraulic and mechanical properties of the soil present in the embankment fill and foundation.

2.4.1 Structural failure of the embankment

When different failure modes are analysed together with related local factors, it is important to consider each component of the dam separately to establish how they may fail, due to either operating conditions or surrounding environment. One or more of the failure modes may affect an individual component, depending on the dam's design characteristics, material and its location within its surroundings. Most likely forms of failure, in order of importance, are now identified, as they will affect the dam's long-term behaviour in some form.

2.4.1.1 Settlement

Settlement is a form of structural failure and is proportional to the height of the embankment (Almog, Kelham & King, 2011). Internal erosion is one of the causes of settlement. This results in sinkholes, which appear either in or around the embankment's crest (Charles et al., 1996). If no sinkholes are present, another method of checking for settlement at present is to inspect the toe of the downstream slope for the presence of seepage (Tedd, Charles & Holton, 1997).

2.4.1.2 Internal erosion

Johnston et al. (1999: p.14) state that *'for old embankment dams internal erosion is the most common cause of in-service incidents and failures*'. As documented by Charles (2002) and Cameron (2010) the majority of earthfill embankments, especially older ones, have experienced some form of internal erosion over their lifetime. Embankments constructed of silt or fine-grained soils are more prone to internal erosion, compared to those constructed of clay. One of the causes of internal erosion is due to the flow of water through the dam's embankment or foundation (Charles, 2002). As the water seeps through the embankment or foundation, the eroded soil is washed out either at the downstream face or into the dam's foundation (Almog, Kelham & King, 2011).

An indicator of internal erosion is the presence of piping or sinkholes, as this form of failure is hidden and usually localised phenomenon (Johnston et al., 1999). Piping occurs through the embankment while sinkholes form on the surface of the embankment. Piping can appear in the downstream section of the embankment as a hole or seam discharging water and contains soil particles from the embankment fill (Creager et al., 1945b). The rate at which internal erosion occurs is dependent on the type of soil, its soil properties and characteristics.

2.4.1.3 Slope instability

There are several triggers of slope instability, such as shear failure in the embankment or the embankment and its foundation, leakage due to piping, hydraulic fracture, etc. (Johnston et al., 1999). In the case of homogeneous earthfill embankments, slope instability due to shear failure can occur in the form of shearing along a slip surface, which can be circular in shape (Craig, 1992). However, if there are any weak zones and layers within the embankment's foundation and embankment fill, the slip surface can be non-circular and shear failure could occur in the form of sliding along the base of the embankment (Stephens, 2010).

With respect to stability of embankment slopes Vaughan, Kovacevic and Ridley (2002) observed that extreme changes in the surrounding environment could also result in slope failure, in the form of sliding or slope instability. One of the more common forms of slope instability is due to increased pore-water pressures (Almog, Kelham & King, 2011), which can develop in the downstream slope's embankment fill (Stephens, 2010). Homogeneous earthfill embankments, which are old and well established, will be more vulnerable to slope instability due to changes in their embankment fill's soil properties and the rate at which water, from the reservoir and rainfall, can infiltrate the soil.

2.4.2 Hydraulic failure of the embankment

2.4.2.1 Overtopping

Overtopping is a form of hydraulic failure and accounts for approximately 30 % of all reported earthfill embankment failures throughout the UK (Hughes & Hoskins, 1994). The main cause of overtopping is due to inadequate spillways at the dam site (Cameron, 2010). This causes the water to flood over the embankment washing any loose soil

downstream. A number of small earth dams do not have a spillway thus increasing the likelihood of failure due to overtopping or flooding of the reservoir (Hughes & Hoskins, 1994).

2.4.2.2 External erosion

External erosion is a result of the erosive action and uncontrolled nature of the water present on or close to the embankment. Johnston et al. (1999: p.20) identified that the main causes of external erosion can be due to:

- Overtopping of floodwater.
- Wave action on the upstream slope.
- Toe erosion on the downstream slope.
- The accumulation of water on the surface of the embankment after heavy rainfall or thawing of snow or ice.

One of the primary causes of surface erosion on the embankment's crest and downstream slope is due to local runoff or water remaining on the embankment's surface during or just after rainfall has occurred (Leong, Low & Rahardjo, 1999; Almog, Kelham & King, 2011). Erosion of the upstream slope is more likely to develop because of overtopping when the reservoir exceeds its maximum capacity, due to flooding or wave action (ter Horst, Jonkman & Vrijling, 2006). However, the surface erosion due to changes in surrounding environment can lead to changes in the hydraulic and mechanical properties of the embankment fill's surface layers, which can have a noticeable impact on the rate water is absorbed through the fill.

2.4.3 Seepage failure through the embankment

As *'all earth dams will have some seepage and it is unrealistic not to expect this'* (Stephens, 2010: p.54), failure due to seepage or leakage flow must always be considered, as it accounts for approximately 40 % of all embankment failures (Johnston et al., 1999). Seepage and leakage flows have the same impact on the embankment, but manifest slightly differently from one another (Johnston et al., 1999).

Seepage flow Occurs when a slow uniform body of water flows through the porous material of the dam's embankment.

Leakage flow Occurs when there is an uncontrolled flow through either the defects or cracks that have formed in or at the surface of the dam's embankment.

If slope instability or slope failure occurs, either upstream or downstream of the embankment, then seepage flow is considered the primary cause of the dam's decrease in overall safety. However, should there be a significant decrease in the reservoir's water level, or piping is present, then leakage flow will be the likely cause of the embankment's failure.

Seepage occurs in older earthfill embankments as over a long period of time the water stored within the reservoir, is constantly trying to find ways of seeping through the upstream slope into the embankment. As the water seeps slowly through the embankment, it saturates the fill causing the dam's embankment to become weak. This can be due to the effects of:

- Increased pore pressures in the embankment and the dam's foundation.
- Smaller soil particles being washed away, leading to internal erosion or slumping.

The impact of seepage through the embankment and the dam's foundation can result in slope instability occurring, due to shear failure within the embankment or its foundation. Therefore, seepage is a safety issue that can cause either internal erosion or result in the development of slope instability (Gosden & Brown, 2000).

2.4.4 Deformation of the embankment

Deformation of the embankment is one of the indicators of the dam's long-term behaviour. The mechanisms that can cause movements within the embankment are largely associated with the magnitude and direction of the stresses acting on the embankment influenced by the fill's soil properties, such as the soil's moisture content, permeability and matric suction, as well as any fluctuations in the reservoir level during normal operations (Hunter & Fell, 2003). Environmental factors specifically relating to climate conditions, such as prolonged drought, or increased precipitation, variations in the saturation level, or moisture content, would be reflected in the embankment's surface layers, as well as the reservoir's water level. Due to seasonal fluctuations, shrink-swell related deformations can also develop as a direct effect of the embankment fill's moisture content (Tedd, Charles & Holton, 1997).

2.4.5 Summary of failure modes

The failure modes summarised on page 17 are all dependent, to a degree, on the type of soil used for the embankment fill, including the soil's mechanical and hydraulic properties. Therefore, before carrying out a dam safety assessment, the embankment fill's soil type and its mechanical behaviour have to be clearly defined using soil mechanics. Obtaining detailed and current data about the embankment fill is important, as over the dam's lifecycle, the mineralogy of the embankment fill may have changed. This is largely due to continuous exposure to seasonal and extreme changes in its surrounding environment as well as the presence of seepage through the embankment and its foundation. This can eventually cause internal erosion to develop, due to an increase in the soil's saturation level and pore-water pressures.

For this analysis failure due to slope instability (structural failure), which combines the effect of seepage failure is considered. The local factors listed in Table 2.2, which influence these failure modes, are considered. These are associated with the soil properties of the embankment's foundation and its embankment fill, the water level of the reservoir and the climate conditions at the dam site. Here the only environmental factor will be precipitation, in the form of rainfall.

2.4.6 Implications of failure modes on risk classification

As the new legislation, Flood and Water Management Act 2010, bases reservoir safety on risk rather than just on the maximum allowable capacity of the reservoir, engineering risk has to be taken into account. Engineering risk is the product of the probability of the event (P_f) and the consequence of the event (such as dam failure), as defined by Hartford and Baecher (2004). Once the engineering risk associated with such failure events is established, it will then be related to the risk classification, as categorized by the Flood and Water Management Act 2010. *'The consequence of a dam failing depends on many factors. These include the volume of water in the reservoir, the height of the dam and the slope and nature of the ground downstream of the dam'* (Cameron, 2010: p.8).

Current guidelines, such as the Flood and Water Management Act 2010, classify the dam's risk classification as high risk (The UK Statute Law Database, 2010), where dam failure is defined as low probability, high-consequence events (Hartford & Baecher, 2004). However, the probability of failure scenario occurring would have a significant effect on engineering risk, effectively the embankment's risk classification. For instance, as the dam's embankment is exposed to the different seasons, its level of engineering risk could vary due to changes in the embankment's soil composition, its geometry, slope configuration, etc. As stated by Almog, Kelham and King (2011) the defined risk classification using engineering risk *'has significant limitations when applied to the management of reservoir safety risks for events of low probability and high-consequence'* (p.4). Therefore, due to high level of uncertainties associated with old, well established, small homogeneous earthfill embankment dams it is necessary to implement a probabilistic approach in order to determine its engineering risk and check its compliance with the Flood and Water Management Act 2010.

For completeness, a model of the cross section of a generic small homogeneous earthfill embankment can be assessed, for specific failure events, and a realistic engineering risk exposure quantified for selected climate change scenarios.

2.5 The Physical Model of the Embankment

The physical model considered here is based on a generic, long-established, small homogeneous earthfill embankment where no drainage was adopted at the downstream toe and the soil type used is uniform throughout the entire embankment and foundation. It has a known foundation height (H_f), embankment height (H), and its reservoir level has a height H_w. Figure 2.2 shows the generic cross section of the embankment model with the key parameters required for its design and construction, including its associated reservoir level. Therefore, the geometry of the cross section of the embankment is a function of the following parameters:

- The height of the embankment (H)
- Crest width (CW)
- Slope gradients of the upstream and downstream slopes (α_1 and α_2)

- Total base width of the embankment (b)
- The height of the embankment's foundation (H_f)
- The maximum reservoir level (H_w) and freeboard (H')

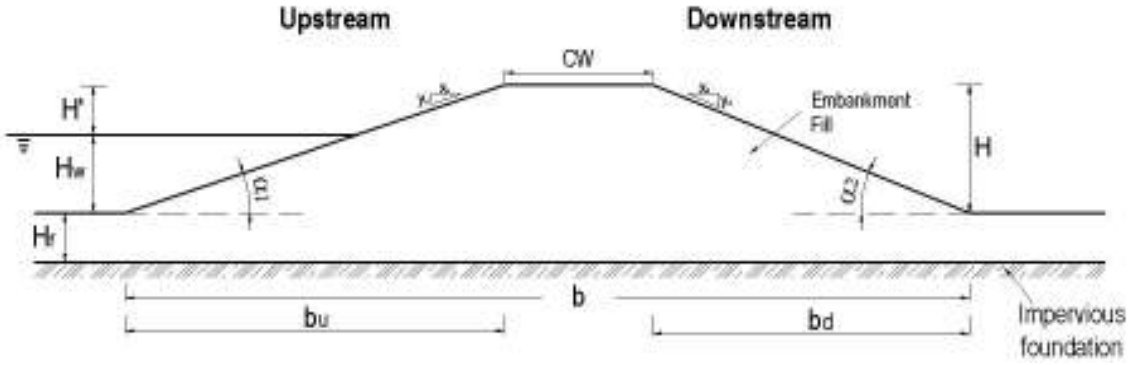

Figure 2.2 Cross section of the physical embankment model

The maximum height of the embankment (H) is determined from the lowest point of the downstream toe where it meets the natural foundation level, to the top of the embankment where the crest originates as outlined by (Tancev, 2005). The embankment's crest width is dependent on *'the size of the dam, the catchment characteristic and topography, and whether road or other access will be required across the embankment'* (Stephens, 2010: p.54). As the crest width (CW) is dependent on the height of the embankment (H), the embankment's minimum allowable crest width can be calculated using either Eqn. (2.1), when the embankment's height is greater than 5.0 m, or directly from Table 2.3 so long as the embankment's height does not exceed 3.0 m.

Table 2.2 Minimum crest widths of the embankment when its height does not exceed 3.0 m[2]

Embankment height (H)	Minimum Crest width (CW)
Any height up to 2.0 m	2.5 m
2.1 – 3.0 m	2.8 m

$$CW = 1.65 \cdot H^{1/2} \tag{2.1}$$

As stated by Stephens (2010), in all cases, CW should be no less than 2m to ensure safe passage of equipment and plants required when constructing small earth dams.

[2] Extracted from Stone (2003).

Throughout this report, the embankment will have a maximum height of 3m and from Table 2.3 its crest width will be equal to 2.8m.

As defined by Creager et al. (1945a) the embankment's foundation (H_f) is usually excavated to a depth of approximately 0.5m. This is to ensure removal of all the topsoil at the base of the dam's embankment and its reservoir. However, the stability of the embankment is also influenced by the angle of the foundation's incline (Kennard, Hopkins & Fletcher, 1996). For the foundation's incline not to affect the embankment's stability, it has to have a slope gradient less than 1V: 10H, or 5°. Most soil types have sufficient strength to bear the weight of any arbitrary small earthfill dam. However, they should have relatively low permeability to ensure no, or very little, water seeps into the dam's foundation from the reservoir. For simplification, it will be assumed that the embankment's foundation has a uniform depth across the total width of the embankment, was constructed without an incline and using the same material as the embankment fill.

To calculate the total span of the base of the embankment (b), the slope gradients ($X_{u/d}$ and $Y_{u/d}$) and the width of the upstream and downstream slope sections (b_u and b_d) have to be established, see Figure 2.2. The embankment's upstream and downstream slope angles are a measure of its steepness, and are dependent on the type and use of the embankment as well as the nature of the material/s used in its construction. As defined by Stephens (2010), the side slopes of a small earth embankment must not be steeper than 1: 2.0 on the upstream and 1: 1.75 on the downstream slope. The gradients of the individual slopes are site specific and the width of the base of the upstream (b_u) and downstream (b_d) slopes can be evaluated using the following equations:

Upstream:
$$b_u = H \cdot \left(\frac{X_u}{Y_u} \right) \tag{2.2}$$

Downstream:
$$b_d = H \cdot \left(\frac{X_d}{Y_d} \right) \tag{2.3}$$

where: $\left(\frac{X_u}{Y_u}\right)$ and $\left(\frac{X_d}{Y_d}\right)$ are the ratios of the upstream and downstream slope gradients, as replicated in Figure 2.2.

Thus, the total span of the base of the embankment (b) can be simply found:

$$b = b_u + CW + b_d \tag{2.4}$$

As the embankment's upstream and downstream slopes behave independently from one another, they are subjected to different forces, stresses and strains. The upstream and downstream slope angles (α_1 and α_2) can be calculated using Eqns. (2.5 and 2.6), as functions of the embankment's height and the width of the base of their corresponding slopes.

Upstream slope gradient:

$$\alpha_1 = \tan^{-1}\left(\frac{H}{b_u}\right) \tag{2.5}$$

Downstream slope gradient:

$$\alpha_2 = \tan^{-1}\left(\frac{H}{b_d}\right) \tag{2.6}$$

However, over the dam's lifetime the upstream and downstream faces and crest width may have undergone some form of surface erosion due to heavy rainfall events, further settlement of the embankment fill, the formation of sinkholes, bulging at the toe, etc. This will result in the embankment's geometry having a degree of uncertainty over the dam's lifetime and in the following model inclusion of these uncertainties is enabled.

The embankment's freeboard (H') is measured between the reservoir's headwater height (H_w) and the crest of the embankment and must never be less than 0.5m, but should ideally be between 0.75m and 1.0m (Stephens, 2010). The freeboard effectively safeguards the dam's embankment should the reservoir exceed its maximum allowable capacity, due to unforeseen circumstances such as overtopping of the embankment due to floodwater from a secondary reservoir or a result of heavy (high intensity) rainfall.

Since the reservoir's headwater height (H_w) is usually measured at the time of the dam's inspection, it can be positioned anywhere along the face of the upstream slope of the physical model, see Figure 2.2. H_w is measured from the base of the reservoir to its maximum design capacity. During the dam's lifetime, the reservoir is never truly at a constant level due to sedimentation of silt in the reservoir, fluctuations in the volume of water stored in the reservoir, inconsistent measurements of the reservoir level, etc. Therefore, the adopted physical model includes variations in the reservoir's headwater height.

Most dams with an earthfill embankment are not impervious, causing water to seep steadily through the embankment from the reservoir or its foundation over its lifetime. Therefore, as the average recorded age of UK embankments is 110 years (Hughes, Bowles & Morris, 2009: p.8), failure associated with seepage flow has to be considered and incorporated within the embankment physical model.

2.6 The Steady Seepage Flow Model

The stability of the individual slopes, subject to specific conditions, can only be determined once the embankment's geometry, soil conditions of its embankment fill and foundation, and the distribution of pore-water pressure through the embankment and its foundation are established. To determine the soil conditions and pore-water pressures in the embankment and its foundation, a seepage flow model has to be established, which will then be incorporated into the applied slope stability model. The distribution of the pore pressures, are largely dependent on the trajectory of the phreatic line or seepage flow line, through the embankment. The flow of water through the embankment can occur in the form of either:

Steady seepage flow: Dependent on the properties and permeability of the soil including the hydraulic boundary conditions that control the rate of seepage into and through the embankment fill (Bromhead, 1992).

Unsteady seepage flow: '*the equilibration of non-equilibrium porewater pressures to the steady sate'* (Bromhead, 1992: p.185).

When considering unsteady seepage flow, it is difficult to model its effect, as its flow rate will vary both in direction and speed with time. As the water level in the reservoir associated with homogeneous earthfill dams does not vary significantly over a short space of time, it allows a state of steady seepage flow. Thus, when carrying out a slope stability analysis, steady seepage flow is considered, as its applied methodology defines the seepage flow line outlining the saturated and partially saturated embankment fill.

The next step is to formulate the trajectory of the phreatic line through the embankment when the reservoir has a given headwater height using standard seepage theory (Cedergren, 1989).

2.6.1 Methodology used to formulate the idealised trajectory of the phreatic line

The path that the water takes through the cross section of the embankment can be represented by a series of flow lines or by the phreatic line. The phreatic line represents the upper flow boundary of the seepage flow through the embankment (Bowles, 1984). It can be easily modelled using standard seepage theory based on Darcy's Law of flow (Chowdhury, Flentje & Bhattacharya, 2010). The trajectory of the phreatic line is largely dependent on the headwater height of the reservoir (Cedergren, 1989), as illustrated in Figure 2.3. As the reservoir's headwater height is increased, the trajectory of the phreatic line will change allowing more water to seep through the embankment fill. However, this is only true if the water in the reservoir remains at its new height for a significant length of time. For old, well-established, homogeneous dams the effect of steady seepage flow through its embankment, defined by the phreatic line, is considered especially if its reservoir's water level has remained relatively constant (Bromhead, 1992).

Here, the idealised position of the phreatic line is formulated using standard flow net theory proposed by Casagrande (1937), as demonstrated by Creager et al. (1945); Bowles (1984); and Bromhead (1992). Figure 2.3 illustrates the empirical model and the parameters required to determine the idealised trajectory of the phreatic line through the physical embankment model in this analysis. The point where the phreatic line exits the downstream face is only dependent on the embankment's geometry and is not influenced by the soil's permeability, as the embankment fill is homogeneous (Creager et al., 1945) and isotropic with respect to permeability (Craig, 1992). As there is no drainage adopted at the downstream toe the embankment's foundation is impervious, see Figure 2.2, and the reservoir's headwater height has remained relatively constant, the seeped water will exit on the downstream slope just above the toe.

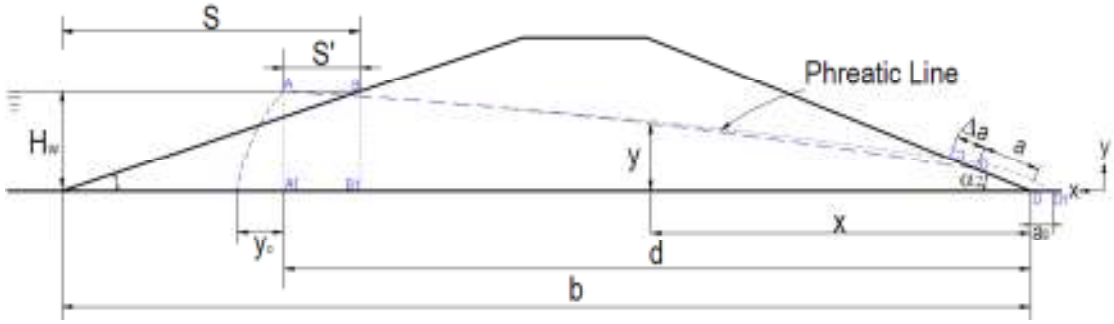

Figure 2.3 Empirical model of the phreatic line through the physical embankment model

Using the empirical model, Figure 2.3, and the following equations, Eqns. (2.7 to 2.14), the position of the phreatic line through the embankment is established. The first step is to calculate the horizontal projection of the wetted upstream slope (S), which is the initial point of the basic parabola, and the horizontal distance (S') between points AB, as derived by Craig (1992) and Bowles (1984). Subsequently, the trajectory of the phreatic line through the cross section of the embankment model is established.

$$S = \frac{H_w}{\tan \alpha_1} \tag{2.7}$$

$$S' = 0.3S \tag{2.8}$$

where: S is dependent on H_w and the angle of the upstream slope (α_1); S' is the distance between the apparent origin of the phreatic line, point A, and where the phreatic line intersects the upstream face, point B.

Using Eqns. (2.4, 2.7 and 2.8), the total horizontal projection (d) of the phreatic line, Eqn. (2.9), can be obtained. This is the horizontal distance from point D to point A_1, as indicated in Figure 2.3. Thus, y_o can be calculated, Eqn. (2.10), which is the horizontal distance between point A_1 and where it intersects the foundation upstream of the embankment, see Figure 2.3.

$$d = b - \left(S - S'\right) \tag{2.9}$$

$$y_0 = \sqrt{H_w{}^2 + d^2} - d \tag{2.10}$$

Subsequently the distance a_0 between point D (toe of the downstream slope) and point D_1 along the baseline can be established, where point D_1 is the point where the phreatic line would intersect the foundation if it continued to follow the path of its parabola.

$$a_0 = \frac{y_0}{2} \tag{2.11}$$

The next step is to determine the trajectory of the phreatic line through the physical embankment model using Eqn. (2.12) (Craig, 1992; Bowles, 1984).

$$y = \sqrt{2y_0x + {y_o}^2} \qquad 0 < x \leq d \tag{2.12}$$

where: y is the vertical height of the phreatic line at a distance x through the embankment and x is the horizontal distance of the phreatic line from point D towards the upstream toe along the base of the embankment.

As the phreatic line is assumed parabolic in shape, it will exit the downstream slope at point C, as shown in Figure 2.3. This produces a wetting zone between points C and D, distance 'a' on the surface of the downstream slope, Figure 2.3, and is dependent on the angle of the downstream slope (α_2). When the angle of the downstream slope (α_2) is less than or equal to 30º, then Eqn. (2.13) is applied (Bowles, 1984). If α_2 is greater than 30º, the standard practice is to use the long established empirical formulations and graph developed by Casagrande (1937), summarised by Creager et al. (1945: p.667) and Das (2008: p.264), to determine the base parabola in the downstream slope. For the present embankment physical model, it is unlikely that the downstream slope's angle (α_2) will be greater than 30º, as its slope gradient cannot exceed 1: 1.75 ($\alpha_2 \sim 29.7°$) (Stephens, 2010). Therefore, only the following quadratic equation, Eqn. (2.13), is required for this analysis.

$$a = \sqrt{{H_w}^2 + d^2} - \sqrt{d^2 - {H_w}^2 \cot\alpha_2} \qquad \alpha_2 \leq 30° \tag{2.13}$$

Thus, the slant distance between points D and C_1 on the downstream slope, a + Δa, on the downstream face is found using Eqn. (2.14).

$$a + \Delta a = \frac{y_0}{1 - \cos\alpha_2} \tag{2.14}$$

where: Δa is the distance between points C and C_1 on the downstream slope, Figure 2.3.

The phreatic line position is also assumed theoretically independent of the soil type used for the embankment fill. This means that above the phreatic line there is no hydrostatic pressure, as there is no pore water pressure present within the embankment fill. Therefore, changes in the surrounding environment, such as rainfall events and

temperature changes, will primarily affect the embankment fill above the phreatic line. The applied formulation for the position of the phreatic line therefore reflects the site-specific uncertainties associated with variations in the embankment fill's unit weight of soil, as illustrated in Figure 2.4.

2.6.2 Zoning of the different unit weights of the embankment fill

As the height of the phreatic line could fluctuate, variations in the unit weights of the embankment fill (partially saturated, saturated and effective) above and below the phreatic line, as illustrated in Figure 2.4, including the pore pressures present within the embankment fill and foundation can be identified. However, the embankment's upstream and downstream slopes effectively behave independently from one another, as they are subject to different stress conditions.

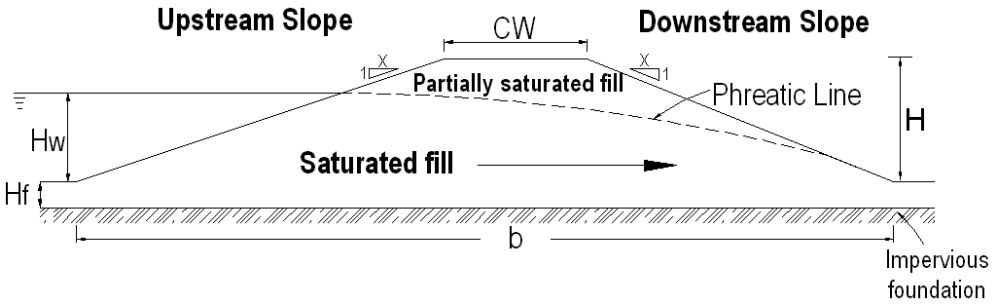

Figure 2.4 Zoning of the unit weights of soil in the embankment's fill and foundation

It will therefore be possible to evaluate the stability of the embankment's slopes using a simple slope stability method, where the steady seepage flow model is incorporated into the formulation.

Using the applied methodology, the upstream and downstream slope's factor of safety can be determined. To determine if slope failure is likely to occur, its calculated factor of safety is compared to target factors of safety to differentiate between the different slope failures (Bowles, 1984). As this analysis is only focusing on old, well-established, homogeneous earthfill embankment dams, the effect of construction, compaction and settlement of the embankment fill and foundation will not be included in the modelling process.

2.7 Soil Modelling

Since the soils used to construct a small homogeneous earthfill embankment dams vary between sites, due to external changes, such as source location, environment conditions during and after formation, loading etc. (White, 1993), it is important to identify the geology and mechanical behaviour of the soil. In practice, soil samples are required to identify the soil type and associated properties of the embankment's fill and foundation. To ensure variations within the embankment fill are taken into account, soil samples must also be taken at different depths across the embankment. Modelling of the soil is also dependent on the sampling and testing conditions employed (Reeves, Sims & Cripps, 2006).

Even with samples taken, the mechanical and hydraulic properties of the soil are still largely unknown as only a specific number of samples can be taken without disturbing the overall stability of the embankment under consideration (Pohl, 1999). Hence, when carrying out a standard deterministic analysis, the soil properties are taken as constant values and are usually based on experience and judgement (Liang, Nusier & Malkawi, 1999). However, uncertainties arise when trying to determine the exact soil composition of the embankment's fill and foundation. As in almost all site investigations, the soil profile examined and modelled usually represents only a small fraction of the total volume of soil (White, 1993). This is generally due to limited data and the number of soil samples taken at the dam site. In order to allow for inclusion of these uncertainties, a comprehensive soil model needs to be included.

2.7.1 Unit weights of the Soil

Once the embankment fill's soil type is established, the unit weights of the embankment fill (partially saturated, saturated and effective) can be easily derived using the standard formulae (Barnes, 2000), Eqns. (2.15 to 2.17). Here, the unit weight of soil below the phreatic line in the downstream slope is defined as the effective (submerged) unit weight (γ_{sub}) (Creager et al., 1945). The effective unit weight of soil is particularly important in slope stability analysis (Bowles, 1984), as water seeps freely through the

soil. Its unit weight is equal to the saturated unit weight of soil reduced by the unit weight of water, Eqn. (2.17).

Saturated unit weight of soil (γ_{sat}):

$$\gamma_{sat} = \left(\frac{G_s + e}{1 + e} \right) \gamma_w \qquad (2.15)$$

Partially saturated unit weight of soil (γ_m):

$$\gamma_m = \left(\frac{G_s + S_r e}{1 + e} \right) \gamma_w \qquad (2.16)$$

Effective unit weight of soil (γ_{sub}):

$$\gamma_{sub} = \gamma_{sat} - \gamma_w \qquad (2.17)$$

where: G_s = Specific gravity; e = Void ratio; γ_w = Unit weight of water ($\gamma_w = g \cdot \rho_w$); The value for S_r (degree of saturation) is used in the decimal form ($0.0 \leq S_r \leq 1.0$) and not as a percentage in Eqn. (2.16).

By using standard soil mechanics, the relationships between the physical properties of the soil, as well as other key parameters can be determined (Barnes, 2000), as demonstrated in *Appendix I: Subsection I.4*. It is only once the soil's mechanical behaviour is understood, can the conditions with which the structure could fail be predicted (Whitlow, 1995).

2.7.2 Internal friction and cohesion of soils (c - φ)

Soils are materials that have some form of cohesion (c) and internal friction (φ) (Atkinson, 1993). These are crucial parameters when performing a slope stability analysis, as most soils contain some measure of internal friction and cohesion, either one or both stress parameters can have a value equal to, or greater than, zero (Bowles, 1984). Internal friction is defined as the angle of shear stress and normal effective stresses at which shear failure of the slope occurs (Bell, 1992), Whereas cohesion is the force that holds the soil particles together within the soil and is usually found from laboratory tests (Atkinson, 1993).

When constructing a small homogeneous dam, different soil types can be used, but as outlined by Kennard, Hopkins and Fletcher (1996: p.150) '*a homogeneous embankment should contain generally not less than 20% nor more than 30% clay, the remainder being well-graded sand and gravel. Such a soil is likely to be stable even when subject*

to significant changes in moisture content.' Thus in the current project, sample clay like soils that can be found in the UK will be considered.

2.7.3 Shear strength of soils

Liu and Evett (2006: p.41) state that '*the ability of the soil to support an imposed load is determined by its shear strength*'. The shear strength depicts the soils maximum strength at a point where plastic deformation occurs due to an applied shear stress (Hough, 1969). It varies considerably between soil types due to their associated physical proprieties. As defined by Bowles (1984), the soil's shear strength is affected by:

- The type and composition of the soil.
- The soil's loading conditions.
- The soil's initial state (defined by the effective normal stress and shear stress of the soil).
- The structure of the soil.

The shear strength for drained and un-drained soil can be expressed by the standard Coulomb equation (Bell, 1992), Eqn. (2.18). Therefore, if the soil's shear stress normal to the shear plane (σ_n) becomes equal to its shear strength (τ) then failure will occur (Craig, 1992).

$$\tau = \sigma_n \tan \varphi + c \qquad (2.18)$$

where: σ_n = Normal stress (dependent on the slope's gradient and the unit weight of the soil); φ = Angle of internal friction; c = Cohesion of the soil.

As explained by Atkinson (1993), the soil's behaviour (such as shear strength, compression and distortion) is governed by a combination of its total normal stress (σ_n) and pore pressure (u). The difference between the parameters, σ_n and u, is called the effective stress (σ'), which is fundamental in obtaining an accurate value for the soil's shear strength (σ).

2.7.4 Pore pressures

In order to estimate the shear strength of a slope in terms of its effective stress (σ'), the pore pressure (u) must be established. However, the significant source of inaccuracy in

slope stability is due to the estimation of the pore pressures in the embankment fill (Abramson et al., 2002). When establishing the pore pressure within the embankment, the three main conditions usually considered are:

- At the point just after construction of the embankment.
- When rapid drawdown of the reservoir occurs.
- When steady seepage flow develops from the reservoir.

In natural slopes, distribution of the pore pressures can be highly complicated due to possible changes in the soil properties, at varying depths within the embankment. These pore pressures are generally measured from site investigations, by taking soil samples from various points along the embankment. If steady seepage flow is present, then the pore pressures within the embankment's fill can be calculated deterministically, by applying either a flow net or using the steady seepage flow model, to establish the soil conditions within the embankment fill (Cedergren, 1989). As there is no hydrostatic pressure above the phreatic line, pore pressure (u) will only be present below the surface of the phreatic line. This is simply calculated using the following equation.

$$u = \gamma_w \cdot z \tag{2.19}$$

where: γ_w = Unit weight of water; z = Depth of water below the idealised phreatic line.

Variations in the reservoir's headwater height will cause the pore water pressures within the embankment and the vertical effective stresses acting on the embankment to change. This in turn causes the soil's shear strength to vary. Therefore, any increase in water present within the soil, will cause the pore pressures to increase resulting in the soil's shear strength to decrease (Chowdhury, Flentje & Bhattacharya, 2010). For instance, if embankment fill is completely saturated, then the shear strength is so low that the embankment's slopes are susceptible to instability (Bromhead, Harris & Watson, 1999).

2.7.5 Effective shear stress of soils

The effective stress (σ') is calculated from the total stress normal to the shear plane (σ_n) minus the pore pressure (u) acting on the same plane (Abramson et al., 2002), Eqn. (2.20). This represents the average stress carried by the soil skeleton.

$$\sigma' = \sigma_n - u \tag{2.20}$$

The soil's shear strength therefore depends on its effective stresses (σ') and effective stress parameters (c' and φ') and not on its total stresses and stress parameters. Consequently, the soil's shear strength (τ) will be expressed as a function of its effective normal stress (σ') and the soil's effective stress parameters (Bell, 1992; Atkinson, 1993), as expressed in Eqn. (2.21). Thus, a more accurate evaluation of the soil's total shearing resistance can be established.

$$\tau' = \sigma' \tan \varphi' + c' \tag{2.21}$$

where: τ' = Total effective shear stress.

Currently, the data used to model the soil's behaviour is limited, as the available soil models cannot replicate 'real' soil behaviour (Potts & Zdravkovic, 2001). As stated by Bowles (1984), the following soil parameters will therefore be considered uncertain:

- unit weight of the soil
- cohesion
- internal friction

Furthermore, for this specific analysis the effective stresses (σ') and effective stress parameters, c' and φ', will be implemented in the slope stability analysis.

2.8 Slope Stability Analysis for Small Homogeneous Earthfill Dams

The main factors of slope instability, as defined by Möllmann and Vermeer (2007); and Hammouri, Malkawi and Yamin (2008) arise from the slope's geometry, the material properties of the soil, along with the forces acting on the slope. Fell, MacGregor and Stapledon (1992) describe the same problem in terms of the embankments pore pressures, shear strength (relating to the soil's cohesion and internal friction) and the implemented stability methodology. Craig (1992) and Whitlow (1995) both describe slope instability in relation to the seepage and gravitational forces on the embankment slope. Whitlow (1995) also goes on to explain that the combination of the soil's shear strength and the geometry of the slope are key factors in reducing slope failure. Therefore, a slope stability analysis has to be implemented so that site-specific information about a specific embankment's geometry and soil conditions of its embankment fill, mechanical and hydraulic properties, are taken into account. This can

be achieved by obtaining explicit formulation for the governing equation for slope stability.

The stability of a given slope is most commonly evaluated using limit equilibrium methods (Baker, 2006). Such methods have been in use for over 70 years and are governed by the linear Mohr-Coulomb principle (Hammouri, Malkawi & Yamin, 2008). These deterministic approaches quantify the slope stability in terms of its factor of safety (FoS), which is the ratio between the slope's available resisting forces (shear strength) and the gravitational forces (weight of the embankment fill) required to maintain stability acting on the slope. Once the critical failure surface is established, standard limit equilibrium procedures, well-established failure theories, can be implemented. The most common limit equilibrium methods that are applied are:

- Circular Arc Method
- Method of Slices
- Finite Element Method
- Sliding Block Method

All these methodologies are well documented in most slope stability, soil mechanics and geotechnical textbooks. As the embankment's geometry and the seepage line position are dependent on uncertain variables, and therefore uncertain themselves, for application of common limit equilibrium methods (i.e. Method of Slices, Circular Arc Method, etc.) computational meshing would have to reflect the variability in slope domain, which needs to be discretized, and variability of the soil properties within the domain. Bowles (1984) has pointed out that for Method of Slices errors are associated with the soil properties and the location of the slope's failure, rather than the shape of the assumed failure surface. As the limit equilibrium methods only differ by their assumed hypothesis, the results obtained are still acceptable when analysing a slope with the same conditions (Das, 2005). In addition, none of the limit equilibrium methods (Circular Arc Method, Method of Slices and Finite Element Method), summarised in *Appendix I: Subsection I.5* can be considered precise methodologies with which to determine a slope's FoS (Michalowski, 1995).

To respond to modelling requirements in the presence of uncertainties and with the view of precipitation scenarios that are due to be implemented, the Sliding Block Method will

be considered for the slope stability analysis. Michalowski (1995) also explains that the factor of safety (FoS) calculated using the rigid-block translation mechanism, sliding block method, is equivalent to that obtained using the limit equilibrium method, assuming the same discrete failure pattern. Furthermore, the FoS obtained using the Sliding Block Method, is comparable to that obtained using the Method of Slices (Jansen et al., 1988).

The Circular Arc Method, Finite Element Method and Method of Slices are summarised in *Appendix I: Subsection I.5*, as these are commonly applied limit equilibrium methods, and so are well documented. However, these limit equilibrium methods, while suitable when simulation methods are applied, are not appropriate for envisaged probabilistic analysis. In particular, the generic formulation for the position of phreatic line and inclusion of the soil's variable hydraulic conductivity, of the embankment fill, would disproportionately increase computing time if these alternative methods are implemented.

2.8.1 Sliding block method (SBM)

The Sliding Block Method (SBM) originated in the USA in the 1940s (Tancev, 2005). Its methodology is generally applied to slopes that have a foundation, which comprises of one or more thin, weak, horizontal stratums of soil (Chowdhury, Flentje & Bhattacharya, 2010; USACE, 2003). Therefore, the slope's plane of weakness will occur close to the base of the slope's foundation, as indicated by the failure surface in Figure 2.5. As with all limit equilibrium methods, this method also assumes that all points along the failure surface are on the verge of failure (Eberhardt, 2003).

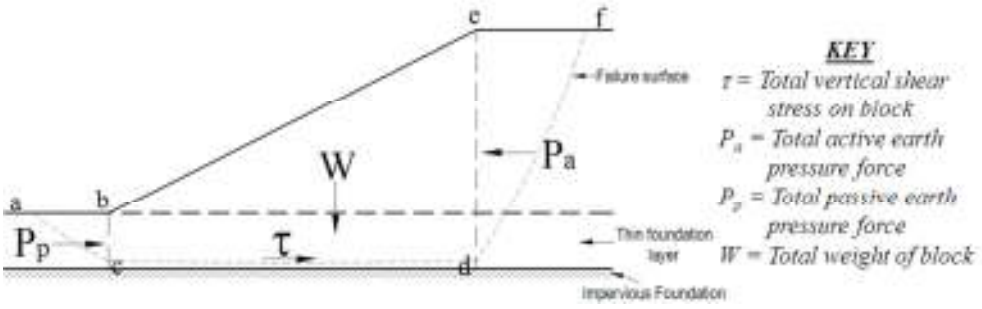

Figure 2.5 Sliding Block Method for analysis of slopes with a weak foundation layer

Unlike the other limit equilibrium methods, the sliding bock method (SBM) assumes that the slope's initial movement is translatory and not rotational (Craig, 1992). This occurs as all forces acting on the slope pass through the centroid of the block, Block 2 in Figure 2.6 (Eberhardt, 2003). Therefore, slope failure occurs in the form of sliding and will be parallel to the slope.

2.8.2 Application of the SBM for slope stability analysis

As shown in Figure 2.6, the slip surface comprises of three sections. Block 1 is the passive wedge at the slope's toe, Block 2 is the central block and Block 3 is the active wedge at the head of the slide (Tancev, 2005). The arrows labelled A in the same figure indicate where the plane of sliding is likely to occur. As passive resistance is usually not available at the slope's toe, the stresses present along the plane of sliding are assumed to be constant (Hammah, 2003).

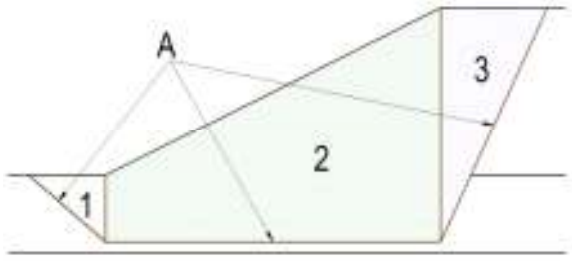

Key
Block 1 (Passive wedge)
Block 2 (Central block)
Block 3 (Active wedge)
Arrows A (Plane of sliding)

Figure 2.6 Active, passive and central blocks used for SBM

When carrying out the SBM the following assumptions are made:

- The physical embankment model has a unit thickness of 1.0 m.
- The embankment slope is a rigid body.
- All points along the failure surface, as shown in Figure 2.5, are close to failure.
- Slope failure is due to sliding only.
- The foundation is a thin layer of soil.
- All forces acting on the slope pass through its central block (Block 2), Figure 2.6.
- The soil, defined by c' and φ', of the embankment fill follow the Mohr-Coulomb failure criterion.
- There are no tension cracks within the embankment's slopes.

In order to determine the slope's factor of safety using the Sliding Block Method, the resultant active (P_a) and passive (P_p) earth forces, including the shear force or unit

shearing resistance (T) have to be calculated. Unlike P_a and P_p, the shear force (T) is simply the effective shear stress (τ') multiplied by the length of the central block, Eqn. (2.22), (Chowdhury, Flentje & Bhattacharya, 2010).

$$T = \tau' \cdot b_x \tag{2.22}$$

where: b_x is the width of the embankment slope or as shown Figure 2.5 is the length (cd) of the central block.

As outlined by Bowles (1984), the sliding block formulation for the slope includes the shear strength and resultant active (P_a) and passive (P_p) earth pressure forces, which are themselves sensitive to the soil's effective strength parameters and pore pressures present within the embankment fill. Thus, the known position of the phreatic line and the saturation of the fill below and above the phreatic line will determine the corresponding pore pressures used in the sliding block formulation. By using the Sliding Block Method, a realistic model for the overall stability of the upstream and downstream slopes of the embankment is established.

2.8.2.1 Active (P_a) and passive (P_p) earth forces

As shown in Figure 2.5, the active earth force (P_a) occurs at the top of the slide (Block 3) and is the horizontal driving force exerted by the soil, whereas the passive earth force (P_p) is the horizontal resisting force acting at the slope's toe (Tancev, 2005). By applying Bells' method, which determines lateral earth pressure for cohesive soils using either the Rankine or Coulomb methods, the active (P_a) and passive (P_p) earth forces, per metre length, can be established in terms of their active (σ_a) and passive (σ_p) earth pressures (Bowles, 1984; Atkinson, 1993). Atkinson (1993) goes on to explain that the active (σ_a) and passive (σ_p) earth pressures, represent the effective active (σ_a') and passive (σ_p') earth pressures, as σ_a' and σ_p' increase linearly with depth. Thus, σ_a' and σ_p' are evaluated using Eqns. (2.23 and 2.24).

$$\sigma_a' = \sigma_v'(K_a) - 2c'\sqrt{K_a} \tag{2.23}$$

$$\sigma_p' = \sigma_v'(K_p) + 2c'\sqrt{K_p} \tag{2.24}$$

$$K_a = \left(\frac{1-\sin\varphi'}{1+\sin\varphi'}\right) = \tan^2\left(45^\circ - \frac{\varphi'}{2}\right) \tag{2.25}$$

$$K_p = \left(\frac{1+\sin\varphi'}{1-\sin\varphi'}\right) = \tan^2\left(45^\circ + \frac{\varphi'}{2}\right) \quad (2.26)$$

where: σ_v = Vertical stress in the embankment fill; c' and φ' are the effective soil parameters cohesion and internal friction; K_a = Active earth pressure coefficient defined as *'a condition of loosing strains where the friction resistance is mobilized to reduce the force necessary to hold the soil in position.'* Bowles (1984: p.504); K_p = Passive earth pressure coefficient, which is *'a condition of densifying the soil by a lateral movement into the soil mass.'* Bowles (1984: p.504).

Once the effective active (σ_a') and passive (σ_p') earth pressures are established, then the active (P_a) and passive (P_p) earth pressure forces are found by integrating σ_a' and σ_p', Eqns. (2.27 and 2.28).

$$P_a = \int_0^{H_x} \sigma_a' \, dH_x = \frac{1}{2}\sigma_a' H_x \quad (2.27)$$

$$P_p = \int_0^{H_f} \sigma_p' \, dH_f = \frac{1}{2}\sigma_p' H_f \quad (2.28)$$

where: H_x = Height of phreatic line; H_f = Foundation height.

2.8.2.2 Factor of safety, FoS

For the traditional deterministic analysis, the stability of the slope is defined by its factor of safety (FoS) with respect to its shear strength (Baker, 2006). Therefore, the slope's FoS as derived by Eqn. (2.29), can be evaluated in terms of the resultant driving forces (P_a) and the available shearing resistance (sum of the passive earth force (P_p) and unit shear strength) (Bowles, 1984).

$$FoS = \frac{\tau' \cdot b_x + P_p}{P_a} = \frac{\left(\sigma' \tan\varphi' + c'\right) b_x + P_p}{P_a} \quad (2.29)$$

where: b_x = Width of the block; τ' = Total effective shear force; P_a = Active earth pressure force; P_p = Passive earth pressure force.

If the calculated FoS is low, slope instability will occur due to shear failure within the embankment's foundation or within the embankment itself (Atkinson, 1993). Under ideal conditions, as defined by Duncan and Wright (2005), the slope would be deemed stable when FoS is greater than 1, but only if the forces were measured with absolute accuracy. However, as the values used to determine the FoS have a degree of

uncertainty, to ensure that the slope remains stable and failure kept to a minimum, its FoS has to be greater than 1.25 (Bowles, 1984; BS 6031:2009).

From extensive studies, Bowles (1984: p.559) differentiated between the different factors of safety and the slope's corresponding failure event, where:

FoS < ~ 1.07	Failures are common due to slope instability.
1.07 < FoS ≤ 1.25	Failures will occur, as the slope has low stability.
FoS > 1.25	Failures are a rare occurrence, as the slope is completely stable under its current conditions.

Due to the uncertainties involved in determining the forces acting on the slope as well as the deterministic mechanical and hydraulic properties of the soil, the FoS is based largely on engineering judgement and local experiences. By implementing a probabilistic approach within the sliding block method, these uncertainties can be taken into account. However, as stated by Duncan (2000) deterministic slope stability analyses should not be abandoned in favour of reliability analyses rather that the two methodologies complement each other and should be applied in tandem.

2.9 Sliding Block Model for Small Homogeneous Earthfill Embankment Dams

As the physical embankment model shown in Figure 2.2 has a thin foundation layer and is assumed to contain the same soil type as the embankment's fill, the Sliding Block Method (SBM) will be implemented for the slope stability analysis, see Figure 2.5 (downstream) and Figure 2.7 (upstream), as it can easily incorporate:

- The embankment's geometry.
- The updated position of the phreatic line using the seepage flow model.
- Pore pressures acting on the slope and the varying soil conditions.

This limit equilibrium method will also be relatively straightforward to incorporate into the considered reliability methodology, when developing the probabilistic slope stability model.

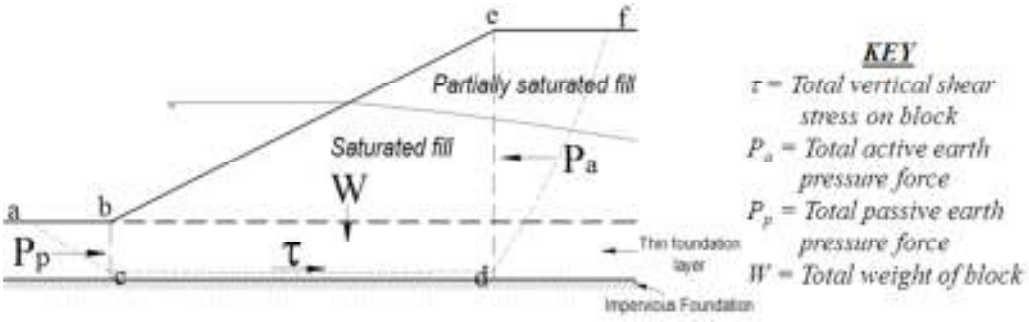

Figure 2.7 Application of Sliding Block Method for slope stability analysis

As with most slope stability models, each embankment slope is analysed independently from the rest of the structure. This means that the forces acting on the slope from the core and its opposing slope appear to be ignored. However, as the embankment comprises of a core and two slopes, how these slopes behave in relation to the whole structure will be analysed within the proposed upstream and downstream slope stability models. The modified slope stability models will incorporate the forces acting on the slope from the core and opposing slope, as demonstrated in Figure 2.8.

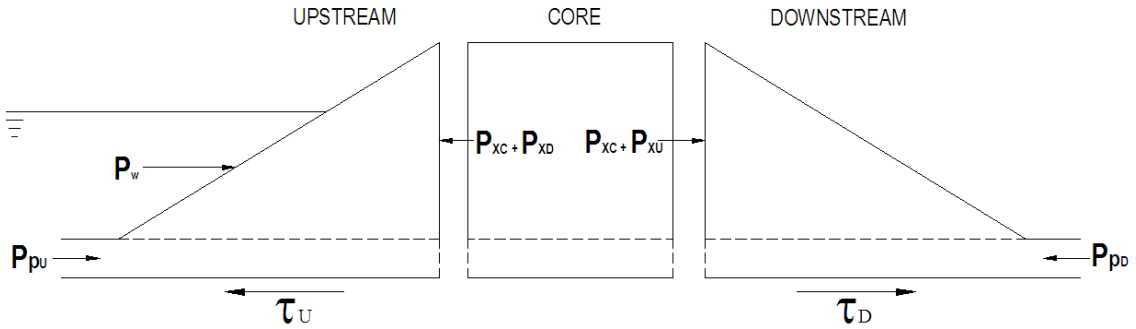

Figure 2.8 Sketch of active, passive and shear effective forces acting on the upstream and downstream slopes

From Figure 2.8 and Eqns. (2.30 and 2.31), FoS_U and FoS_D for the upstream and downstream slope stability models are established.

$$FoS_U = \frac{\tau_U \cdot b_u}{\left(P_{x_C} + P_{x_D}\right) - \left(P_w + P_{p_U}\right)} \tag{2.30}$$

$$FoS_D = \frac{\tau_D \cdot b_d}{\left(p_{x_C} + p_{x_U}\right) - p_{p_D}} \tag{2.31}$$

where: 'U' and 'D' denote the upstream and downstream slopes respectively; $FoS_{U/D}$ = Factor of safety; $\tau_{U/D}$ = Effective shear stress; P_W = Pore water pressure force; P_{XC} = Total active effective

earth force exerted by the core; $P_{XU/D}$ = Total active effective earth force exerted by the slopes; $P_{PU/D}$ = Total passive effective earth force.

2.9.1 Slope stability model for the upstream slope using sliding block formulation (SBM)

The upstream slope stability model, using SBM is now established by evaluating the total effective stresses and pore pressures above and below the surface of the idealised phreatic line, through the foundation and cross section of the embankment.

2.9.1.1 Zoning of the embankment fill above and below the phreatic line

The first step in modelling the distribution of the varying unit weights of soil and pore pressures within the slope, is to establish the idealised position of the phreatic line through the upstream slope, using the seepage flow methodology derived in *Subsection 2.6.1*. Thus the points where the phreatic line enters (point a) and leaves (point b) the upstream slope indicated in Figure 2.9 can be identified.

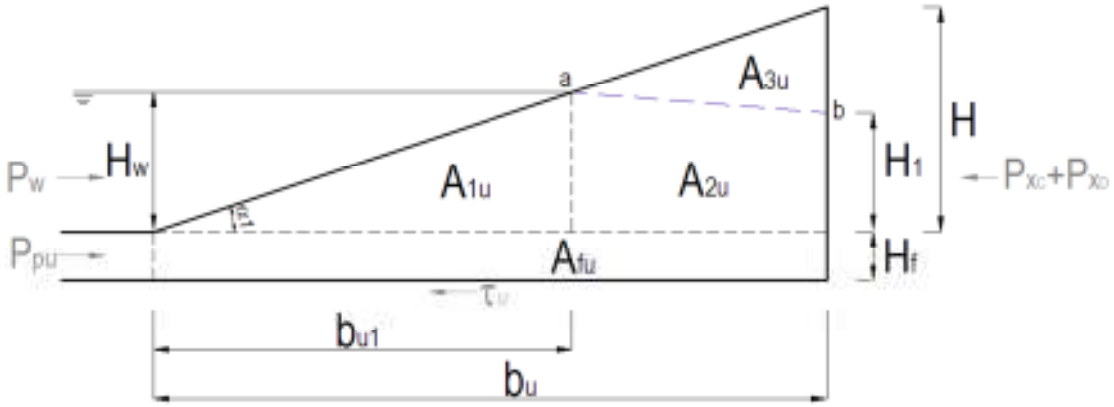

Figure 2.9 Position of the idealised phreatic line in the upstream slope

As b_{u1} is dependent on H_w, it is found as the horizontal projection of the wetted upstream slope (S), Eqn. (2.7).The height (H_1) that the phreatic line exits the upstream section of the embankment, Figure 2.9, is calculated using Eqn. (2.32), where H_w and b_u are taken as constant values.

At point a: $$b_{u1} \equiv S$$

At point b: $$H_1 = \sqrt{2x_0(b - b_u) + x_o^{\,2}} \qquad (2.32)$$

Thus, the average height (H_{av_U}) of the idealised phreatic line, mean point between points a and b, Eqn. (2.33), and the embankment fill's average height (H_{x_U}) above the idealised phreatic line, Eqn. (2.34), are established.

$$H_{av_U} = \frac{H_w + H_1}{2} \tag{2.33}$$

$$H_{x_U} = H - H_{av_U} \tag{2.34}$$

The next step is to calculate the areas (A_{1u} to A_{3u}) in the upstream slope, the area of the foundation (A_{fu}) see Eqn. (2.35), identified in Figure 2.9, and the total area of the slope (A_{Tu}), Eqn. (2.36).

$$A_{fu} = b_u H_f \tag{2.35}$$

$$A_{Tu} = \frac{1}{2} b_u H \tag{2.36}$$

Then A_{1u} and A_{2u} below the phreatic line are given by Eqns. (2.37 and 2.38), where A_{2u} is the integration of Eqn. (2.12) bounded by the total base width of the slope (b_u) and the horizontal projection of the wetted upstream slope (b_{u1}). Thus, the area of the embankment fill above the phreatic line (A_{3u}), Eqn. (2.39), is simply found by subtracting the total area of the slope (A_{Tu}) from the areas (A_{1u} and A_{2u}) below the phreatic line.

$$A_{1u} = \frac{1}{2} b_{u1} H_w \tag{2.37}$$

$$A_{2u} = \int_{b_{u1}}^{b_u} y \, dx = \frac{1}{3y_0}\left[\left(2y_0 b_u + y_0^{\,2}\right)^{\frac{3}{2}} - \left(2y_0 b_{u1} + y_0^{\,2}\right)^{\frac{3}{2}}\right] \tag{2.38}$$

$$A_{3u} = A_{Tu} - (A_{1u} + A_{2u}) \tag{2.39}$$

where: y_o is the horizontal distance between points A_1 and B_1 defined in Figure 2.3: *Subsection 2.6.1*.

2.9.1.2 Pore pressures present in the upstream slope

As the embankment fill contains solid soil particles and water, the pore pressures u_{1u} (above the phreatic line), u_{2u} (below the phreatic line) and u_{3u} (within the upstream slope and its foundation) are established by applying Eqns. (2.40 to 2.42). As the effect of rainfall is not considered at this stage of the analysis, the effect of pore pressure is only included for the fill below the phreatic line and in the slope's foundation.

Therefore, there is no hydrostatic pressure above the phreatic line, so u_{1u} is equal to zero, Eqn. (2.40).

Here, the pore pressure (u_{2u}) below the idealised phreatic line takes into account the changing height of the phreatic line, as it traverses through the slope. Therefore, to calculate u_{2u}, the average height (H_{av_U}) of the idealised phreatic line is applied, Eqn. (2.41). Since the slope's foundation is composed of the same material as the embankment model, the explicit formulation for pore pressure (u_{3u}) acting through the upstream slope and its foundation has to be established, Eqn. (2.42).

$$u_{1u} = 0 \tag{2.40}$$

$$u_{2u} = \gamma_w H_{av_U} \tag{2.41}$$

$$u_{3u} = \gamma_w \cdot \left(H_{av_U} + H_f\right) \tag{2.42}$$

where: H_{av_U} = Average height of the idealised phreatic line; H_f = Foundation height; γ_w = Unit weight of water.

For the slope stability model the normal stresses and effective stresses, in the vertical and horizontal direction at any given point within the soil mass have to be calculated. This ensures that the total stresses and pore pressures present within the embankment are accurately modelled. Here, the effective stresses, in the vertical and horizontal direction, are differentiated as the vertical effective stress (σ_v'), Eqn. (2.43), and horizontal effective stress (σ_h') Eqn. (2.44).

$$\sigma_v' = \sigma_v - u \tag{2.43}$$

$$\sigma_h' = \sigma_h - u \tag{2.44}$$

where: σ_v = Normal stress in the vertical direction; σ_h = Normal stress in the horizontal direction; u = Pore pressure.

2.9.1.3 Vertical effective stresses present in the upstream slope

To determine the vertical effective stresses (σ_{v1_u}', σ_{v2_u}' and σ_{v3_u}') acting on the upstream slope, the vertical stresses (σ_{v1_u}, σ_{v2_u} and σ_{v3_u}) must be first identified. As the embankment fill is homogeneous, the unit weights of the soil above and below the phreatic line and in the foundation are taken as constant values.

Above the phreatic line, the embankment fill is partially saturated and its saturation level is dependent on the environmental conditions surrounding the dam. Thus the vertical stress (σ_{v1_u}) is calculated using Eqn. (2.45). Below the phreatic line, the embankment fill is assumed to be completely saturated and so the vertical stress (σ_{v2_u}) is found by applying Eqn. (2.46). Eqn. (2.47) defines the vertical stress (σ_{v3_u}), which is the total vertical stress acting on the entire upstream slope and its foundation.

$$\sigma_{v1_u} = \gamma_m(H - H_{av_U}) = \gamma_m(H_{x_U}) \quad (2.45)$$

$$\sigma_{v2_u} = \sigma_{v1_u} + \gamma_{sat}(H_{av_U}) \quad (2.46)$$

$$\sigma_{v3_u} = \sigma_{v2_u} + \gamma_{f_{up}}(H_f) \quad (2.47)$$

where: γ_{fup} = Average unit weight of foundation (upstream).

Once the vertical stresses (σ_{v1_u}, σ_{v2_u} and σ_{v3_u}) and pore pressures (u_{1u}, u_{2u} and u_{3u}) are evaluated, the vertical effective stresses (σ_{v1_u}', σ'_{v2_u} and σ_{v3_u}'), above and below the phreatic line and in the upstream slope and its foundation, as defined in Eqns. (2.48 to 2.50), can be calculated by applying Eqn. (2.43).

$$\sigma_{v1_u}' = \sigma_{v1_u} - u_{1u} \quad (2.48)$$

$$\sigma_{v2_u}' = \sigma_{v2_u} - u_{2u} \quad (2.49)$$

$$\sigma_{v3_u}' = \sigma_{v3_u} - u_{3u} \quad (2.50)$$

2.9.1.4 Total passive earth pressure force (P_{pU})

The total passive earth pressure force (P_{pU}) acts in the same direction as the water pushing against the upstream slope. To calculate P_{pU}, the first step is to determine the passive effective earth pressure (σ_{pU}'), which is found using Eqns. (2.24 and 2.26) to form Eqn. (2.51). The horizontal passive earth pressure (σ_{pU}) is then evaluated, by adding the pore pressure u_{3u} derived by Eqn. (2.42) to σ_{pU}', Eqn. (2.52). Once σ_{pU} is established, then the total passive earth pressure force (P_{pU}) can be found using Eqn. (2.53).

$$\sigma_{p_U}' = \sigma_{v3_u}'(K_p) + 2c'\sqrt{K_p} \quad (2.51)$$

$$\sigma_{p_U} = \sigma_{p_U}' + u_{3u} \quad (2.52)$$

$$P_{p_U} = \frac{1}{2}\sigma_{p_U} H_f \tag{2.53}$$

where: K_p = Coefficient of passive earth pressure, (Eqn. 2.26); H_f = Foundation height; c' = Cohesion.

2.9.1.5 Pore water pressure force (P_w)

The pore water pressure force (P_w) is the force of the water acting on the slope's surface, from the reservoir, and is calculated using the standard equation:

$$P_w = \frac{1}{2}\gamma_w H_w^{\,2} \tag{2.54}$$

2.9.1.6 Total active earth pressure force (P_{aU}) acting on the upstream slope

In order to determine the total horizontal driving force (H_U) of the upstream slope, the total active earth pressure force (P_{aU}) has to be calculated. This is the sum of the forces acting on the upstream slope from the core (P_{XC}) and downstream slope (P_{XD}) of the embankment, as shown in Figure 2.8.

2.9.1.6.1 Active earth pressure force (P_{XC}) from the embankment's core

To establish the total active earth pressure force of the core (P_{XC}), the following pore pressures, stresses and effective stresses in the vertical and horizontal direction have to be established:

The vertical stresses (σ_{v1_c}, $\sigma_{v2_c}$and σ_{v3_c})

The pore pressures (u_{1c}, u_{2c} and u_{3c})

The vertical effective stress (σ_{v1_c}', σ_{v2_c}' and σ_{v3_c}')

The horizontal effective stresses (σ_{h1_c}', σ_{h2_c}' and σ_{h3_c}')

The horizontal stresses (σ_{h1_c}, σ_{h2_c} and σ_{h3_c}')

Methodology described above is implemented again.

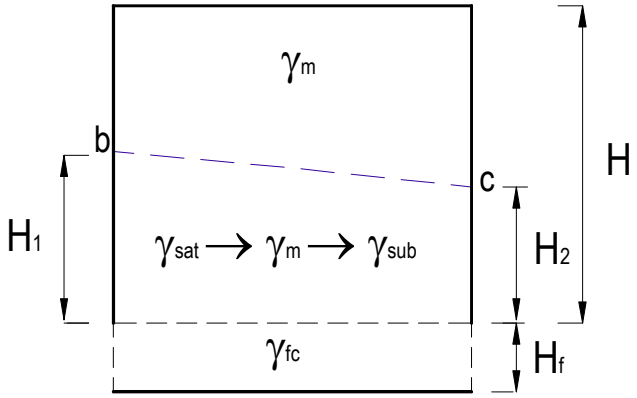

Figure 2.10 Idealised allocation of the different unit weights of soil defined in the core

where: H_1 and H_2 = Height of the idealised phreatic line at the point where it enters and leaves the core; H_f = Foundation height; H = Height of embankment; γ_{fc} = Unit weight of foundation (core); γ_{sat} = Saturated unit weight of soil; γ_m = Partially saturated unit weight of soil; γ_{sub} = Effective (submerged) unit weight of soil.

As the core is not in direct contact with the reservoir, the unit weight of soil within the core's embankment fill will be different above and below the phreatic line, and in the foundation to a degree, Figure 2.10. Above the phreatic line, the residual embankment fill will remain partially saturated. However, below the phreatic line, the embankment fill will have a combination of saturated, moist and effective unit weight of soil, as the core is not in direct contact with the reservoir. Thus, for the vertical stresses (σ_{v1_c}, σ_{v2_c} and σ_{v3_c}) and pore pressures (u_{1c}, u_{2c} and u_{3c}), the following equations are required.

Above the phreatic line:

$$\sigma_{v1_c} = \gamma_m\left(H - H_{av_c}\right) \tag{2.55}$$

$$u_{1c} = 0$$

Below the phreatic line:

$$\sigma_{v2_c} = \sigma_{v1_c} + \left(\frac{\gamma_{sat} + \gamma_m + \gamma_{sub}}{3}\right) H_{av_c} \tag{2.56}$$

$$u_{2c} = \gamma_w\left(H_{av_c}\right)$$

Core and foundation:

$$\sigma_{v3_c} = \sigma_{v2_c} + \gamma_{fc}(H_f) \tag{2.57}$$

$$u_{3c} = \gamma_w\left(H_{av_c} + H_f\right)$$

where: $H_{av_c} = \frac{H_1 + H_2}{2}$ = Average height of the idealised phreatic line through the core (mean point between points b and c in Figure 2.10); γ_w = Unit weight of water; γ_{fc} = Unit weight of foundation (core).

By applying Eqns. (2.58 to 2.60), the core's vertical effective stresses (σ_{v1_c}', σ_{v2_c}' and σ_{v3_c}') are established.

$$\sigma_{v1_c}' = \sigma_{v1_c} - u_{1c} \tag{2.58}$$

$$\sigma_{v2_c}' = \sigma_{v2_c} - u_{2c} \tag{2.59}$$

$$\sigma_{v3_c}' = \sigma_{v3_c} - u_{3c} \tag{2.60}$$

Once the core's vertical effective stresses are established, the horizontal effective stresses ($\sigma_{h1_c}', \sigma_{h2_c}'$ and σ_{h3_c}') and horizontal stresses ($\sigma_{h1_c}, \sigma_{h2_c}$ and σ_{h3_c}) can be evaluated. The horizontal effective stresses ($\sigma_{h1_c}', \sigma_{h2_c}'$ and σ_{h3_c}') are simply derived using Eqn. (2.23) and are equated using the following equations:

$$\sigma_{h1_c}' = \sigma_{v1_c}'(K_a) - 2c'\sqrt{K_a} \tag{2.61}$$

$$\sigma_{h2_c}' = \sigma_{v2_c}'(K_a) - 2c'\sqrt{K_a} \tag{2.62}$$

$$\sigma_{h3_c}' = \sigma_{v3_c}'(K_a) - 2c'\sqrt{K_a} \tag{2.63}$$

Subsequently the horizontal stresses (σ_{h1_c}, σ_{h2_c} and σ_{h3_c}) can be calculated by implementing Eqn. (2.64), which determines the standard horizontal stress (σ_h) by adding the horizontal effective stress (σ_h') and the relative horizontal pore pressure together. Thus, σ_{h1_c}, σ_{h2_c} and σ_{h3_c} can be established, Eqns. (2.65 to 2.67).

$$\sigma_h = \sigma_h' + u \tag{2.64}$$

$$\sigma_{h1_c} = \sigma_{h1_c}' + u_{1c} \tag{2.65}$$

$$\sigma_{h2_c} = \sigma_{h2_c}' + u_{2c} \tag{2.66}$$

$$\sigma_{h3_c} = \sigma_{h3_c}' + u_{3c} \tag{2.67}$$

The last step is to determine the total active earth pressure force (P_{XC}) by applying Eqn. (2.28) to calculate the active earth pressure forces (P_{XC1}, P_{XC2} and P_{XC3}) above, below and through the core's foundation. Thus, total active earth pressure force (P_{XC}) acting on the upstream slope from the embankment's core is established, Eqn. (2.71).

$$P_{XC1} = \frac{1}{2}\sigma_{h1_c}\left(H - H_{av_c}\right) \tag{2.68}$$

$$P_{XC2} = \left(\frac{\sigma_{h1_c} + \sigma_{h2_c}}{2} \right) H_{av_c} \tag{2.69}$$

$$P_{XC3} = \left(\frac{\sigma_{h2_c} + \sigma_{h3_c}}{2} \right) H_f \tag{2.70}$$

$$P_{XC} = P_{XC1} + P_{XC2} + P_{XC3} \tag{2.71}$$

2.9.1.6.2 Active earth pressure force (P_{XD}) from the downstream slope

By applying the same principles used to determine P_{XC}, the total active earth pressure force (P_{XD}) acting on the upstream slope from the downstream slope can be obtained, see Figure 2.11. Here, the following have to be established.

The vertical stresses (σ_{v1_d}, $\sigma_{v2_d}$and σ_{v3_d})

The pore pressures (u_{1d}, u_{2d} and u_{3d})

The vertical effective stress (σ_{v1_d}', σ'_{v2_d} and σ_{v3_d}')

The horizontal effective stresses (σ_{h1_d}', σ_{h2_d}' and σ_{h3_d}')

The horizontal stresses (σ_{h1_d}, σ_{h2_d} and σ_{h3_d})

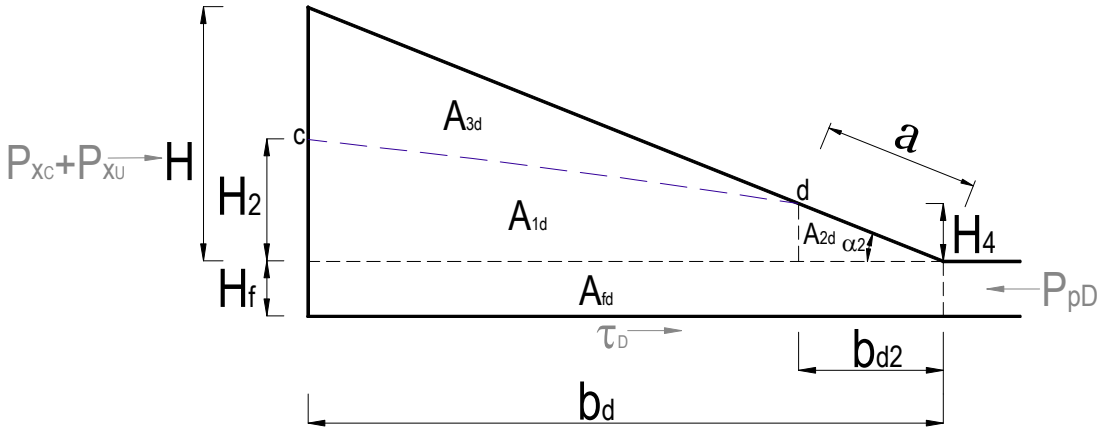

Figure 2.11 Position of the idealised phreatic line in the downstream slope

The first step is to determine the vertical stresses (σ_{v1_d}, σ_{v2_d} and σ_{v3_d}) and pore pressures (u_{1d}, u_{2d} and u_{3d}), above and below the phreatic line and within the upstream slope and its foundation using the following equations. Here, the embankment fill's unit weight of soil is classified as partially saturated above the phreatic line and at the slope's toe, and effective below the phreatic line.

Above the phreatic line:

$$\sigma_{v1_d} = \gamma_m\left(H - H_{av_d}\right) \quad (2.72)$$

$$u_{1d} = 0$$

Below the phreatic line:

$$\sigma_{v2_d} = \sigma_{v1_d} + \left(\gamma_{sub} H_{av_d}\right) + \left(\gamma_m \frac{H_4}{2}\right) \quad (2.73)$$

$$u_{2d} = \gamma_w \left(H_{av_d} + \frac{H_4}{2}\right)$$

Downstream slope and foundation:

$$\sigma_{v3_d} = \sigma_{v2_d} + \gamma_{fd}(H_f) \quad (2.74)$$

$$u_{3d} = \gamma_w \left(H_{av_d} + \frac{H_4}{2} + H_f\right)$$

where: H_2 and H_4 = Height of the phreatic line at the point where it enters and leaves the downstream slope; $H_{av_d} = \frac{H_2+H_4}{2}$ = Average height of the idealised phreatic line through the downstream slope (mean point between points c and d in Figure 2.11); H = Height of embankment; H_f = Foundation height; γ_{fd} = Unit weight of foundation (Downstream); γ_w = unit weight of water; γ_m = Partially saturated unit weight of soil; γ_{sub} = Effective (submerged) unit weight of soil.

Subsequently, the vertical effective stresses (σ_{v1_d}', σ_{v2_d}' and σ_{v3_d}') can be established using the following set of equations.

$$\sigma_{v1_d}' = \sigma_{v1_d} - u_{1d} \quad (2.75)$$

$$\sigma_{v2_d}' = \sigma_{v2_d} - u_{2d} \quad (2.76)$$

$$\sigma_{v3_d}' = \sigma_{v3_d} - u_{3d} \quad (2.77)$$

Once the vertical effective stresses are calculated, the horizontal effective stresses (σ_{h1_d}', σ_{h2_d}' and σ_{h3_d}') can be equated, Eqns. (2.78 to 2.80).

$$\sigma_{h1_d}' = \sigma_{v1_d}'(K_a) - 2c'\sqrt{K_a} \quad (2.78)$$

$$\sigma_{h2_d}' = \sigma_{v2_d}'(K_a) - 2c'\sqrt{K_a} \quad (2.79)$$

$$\sigma_{h3_d}' = \sigma_{v3_d}'(K_a) - 2c'\sqrt{K_a} \quad (2.80)$$

where: K_a= Coefficient of active earth pressure.

Lastly, the horizontal stresses (σ_{h1_d}, σ_{h2_d} and σ_{h3_d}), Eqns. (2.81 to 2.83) can be derived.

$$\sigma_{h1_d} = \sigma_{h1_d}' + u_{1d} \quad (2.81)$$

$$\sigma_{h2_d} = \sigma_{h2_d}' + u_{2d} \quad (2.82)$$

$$\sigma_{h3_d} = \sigma_{h3_d}' + u_{3d} \quad (2.83)$$

Thus, the individual active earth pressure forces (P_{XD1}, P_{XD2} and P_{XD3}) of the downstream slope can be determined, Eqns. (2.84 to 2.86), and subsequently the total active pressure force (P_{XD}), Eqn. (2.87).

$$P_{XD1} = \frac{1}{2}\sigma_{h1_d}\left(H - H_{av_d}\right) \tag{2.84}$$

$$P_{XD2} = \left(\frac{\sigma_{h1_d} + \sigma_{h2_d}}{2}\right)H_{av_u} \tag{2.85}$$

$$P_{XD3} = \left(\frac{\sigma_{h2_d} + \sigma_{h3_d}}{2}\right)H_f \tag{2.86}$$

$$P_{XD} = P_{XD1} + P_{XD2} + P_{XD3} \tag{2.87}$$

2.9.1.7 Total horizontal driving force (H_U) acting on the upstream slope

The total horizontal driving force is determined by subtracting the total active earth pressure forces from the core and downstream slope, P_{XC} and P_{XD}, with the total passive earth pressure force (P_{pU}) and the pore water pressure force (P_w), as demonstrated in Figure 2.8.

$$H_U = \left(P_{x_C} + P_{x_D}\right) - \left(P_w + P_{p_U}\right) \tag{2.88}$$

2.9.1.8 Total vertical effective stress (σ_{vu}') acting on the upstream slope

The total vertical effective stress (σ_{vu}') acting vertically through the upstream slope is independent of the stresses acting horizontally through the slope. This is calculated by establishing the total effective weight of the slope that is the function of the total area of the slope's embankment fill and corresponding unit weights of the soil, which is equal to the vertical stress (σ_{Fu}), as well as the pore pressure acting in the vertical direction (u_{vu}).

The first step is to establish the effective weights above and below the phreatic line in the slope, as well as the effective weight of the slope's foundation. To determine the effective weight above (ω_{eu1}) and below (ω_{eu2}) the phreatic line, of the slope, and the effective weight of the foundation (ω_{eu3}) Eqns. (2.89 to 2.91) are used. Subsequently, the total effective weight (ω_{eu}) of the upstream slope can be evaluated, Eqn. (2.92).

Above the phreatic line: $$\omega_{eu1} = \gamma_m(A_{3u}) \quad (2.89)$$

Below the phreatic line: $$\omega_{eu2} = \gamma_{sat}(A_{1u} + A_{2u}) \quad (2.90)$$

In the foundation: $$\omega_{eu3} = \gamma_{fup}(A_{fu}) \quad (2.91)$$

$$\omega_{eu} = \omega_{eu1} + \omega_{eu2} + \omega_{eu3} \quad (2.92)$$

In order to calculate the total vertical effective stress (σ_{vu}'), the pore pressure acting in the vertical direction (u_{vu}), through the embankment fill, must be found by evaluating Eqn. (2.93). Unlike the pore pressures acting in the horizontal direction, the width of the upstream slope's base (b_{u1}) is also incorporated into the equation.

$$u_{vu} = \frac{\left(\gamma_w H_w b_{u1}\right) + \left(\gamma_w H_{av_U}\left(b - b_{u1}\right)\right)}{b_u} \quad (2.93)$$

where: H_{avu} = Average height of the idealised phreatic line (upstream) (mean point between points a and b in Figure 2.9); γ_w = Unit weight of water; b = Total base width of the embankment; b_{u1} = Horizontal projection of the wetted upstream slope; b_u = Total base width of the slope (upstream).

Hence, σ_{vu}' is calculated by subtracting the total vertical stress (σ_{Fu}), with the pore pressure (u_{vu}) acting in the vertical direction of the upstream slope, as expressed in Eqn. (2.94). Thus, the total vertical effective shear stress (τ_U') and resultant shearing force (R_U) for the upstream slope can be evaluated.

$$\sigma_{vu}' = \sigma_{Fu} - u_{vu} \quad (2.94)$$

2.9.1.9 Resultant shearing force (R_U)

R_U is calculated in terms of the total effective shear stress (τ_U') and the total width of the base of the upstream slope (b_u).

$$R_U = \tau_U' \cdot b_u \quad (2.95)$$

where: $\tau_U' = \sigma_{vu}' \tan\varphi' + c'$

2.9.1.10 Factor of safety (FoS_U) of the upstream slope

The upstream slope's factor of safety is therefore simply evaluated by dividing the total resultant shearing force (R_U) by the slope's horizontal driving force (H_U), as defined in Eqn. (2.30).

2.9.2 Slope stability model for downstream slope using sliding block formulation (SBM)

To determine the downstream slope's factor of safety (FoS_D), the relevant equations relating to its slope stability model, using SBM, are established. The downstream slope stability model is determined using the same sliding block formulation implemented in the slope stability model for the embankment's upstream slope, however taking into account that the downstream slope is not in direct contact with the reservoir.

2.9.2.1 Zoning of the embankment fill above and below the phreatic line

Figure 2.11 in *Subsection 2.9.1.6.2* shows the idealised position of the phreatic line through the downstream slope, calculated using the seepage flow methodology derived in *Subsection 2.6.1*. Thus, by applying Eqns. (2.96 to 2.98), the position where the phreatic line enters (point c) and leaves (point d) the downstream slope, identified in Figure 2.11, are obtained. Hence, the average height (H_{avd}) of the idealised phreatic line, in the downstream slope, is found using Eqn. (2.99).

At point c:

$$H_2 = \sqrt{2y_0(b_d) + {y_o}^2} \tag{2.96}$$

At point d:

$$H_4 = a \sin \alpha_2 \tag{2.97}$$

$$b_{d2} = a \cos \alpha_2 \tag{2.98}$$

$$H_{av_d} = \frac{H_2 + H_4}{2} \tag{2.99}$$

where: α_2 = Angle of the downstream slope; y_o is the horizontal distance between point A_1 and where it would intersect the foundation on the upstream side of the embankment, point B_1, illustrated in Figure 2.3.

As shown in Figure 2.11, *Subsection 2.9.1.6.2*, the downstream slope and its foundation have has been divided into areas (A_{1d} to A_{3d}, and A_{fd}), which correspond to a specific unit weight of soil. Thus, it will be possible to quantify the total effective weight and forces acting on the slope. The area below (A_{1d}) and above (A_{3d}) the phreatic line, at the

downstream toe (A_{2d}) and the area of the slope's foundation (A_{fd}), are derived using the same formulae implemented for the upstream slope. Using Eqns. (II.2 to II.5) in *Appendix II: Subsection II.1.1*, A_{1d} to A_{3d}, and A_{fd} are established.

2.9.2.2 Pore pressures, vertical stresses and vertical effective stresses present in the downstream slope

As defined in *Subsection 2.9.1.6.2*, the vertical stresses (σ_{v1_d}, σ_{v2_d} and σ_{v3_d}), pore pressures (u_{1d}, u_{2d} and u_{3d}) and vertical effective stresses (σ_{v1_d}', σ_{v2_d}' and σ_{v3_d}') present in the downstream slope are evaluated using the same set of equations. The vertical stress (σ_{v1_u}) and pore pressure (u_{1d}) present above the phreatic line, and the vertical stress (σ_{v2_u}) and pore pressure (u_{2d}) present below the phreatic line are calculated by applying Eqns. (2.72 and 2.73). The total vertical stress (σ_{v3_u}) and pore pressure (u_{3d}) acting on the entire downstream slope and its foundation are found by implementing Eqn. (2.74). Therefore, to establish the vertical effective stresses (σ_{v1_d}', σ_{v2_d}' and σ_{v3_d}'), in the downstream slope, the pore pressures (u_{1d}, u_{2d} and u_{3d}) are subtracted from the vertical stresses (σ_{v1_d}, σ_{v2_d} and σ_{v3_d}) by applying Eqns. (2.75 to 2.77).

2.9.2.3 Total passive (P_{pD}) and active (P_{aD}) earth pressure forces acting on the downstream slope

The total passive earth pressure force (P_{pD}) defines the force acting on the downstream slope from its foundation and is established using Eqns. (II.6 to II.7), formulated in *Appendix II: Subsection II.1.2*. The total active earth pressure force (P_{aD}) is the sum of the forces acting on the downstream slope from the embankment's core (P_{XC}) and upstream slope (P_{XU}), shown in Figure 2.9. From the stability model illustrated in Figure 2.10, the total active earth pressure force (P_{XC}) acting on the downstream slope from the core is identical to that acting on the upstream slope. Therefore, the same methodology defined earlier is applied, and from Eqn. (2.71) the total active earth pressure force (P_{XC}) acting on the downstream slope from the embankment's core is established.

Applying the same methodology used to determine P_{XC}, the total active earth pressure force (P_{XU}) acting on the downstream slope from the upstream slope can be ascertained.

To determine P_{XU}, the pore pressures, stresses and effective stresses in the vertical and horizontal direction are calculated, see *Appendix II: Subsection II.1.3* for all equations. Thus, the active earth pressure forces (P_{XU1}, P_{XU2} and P_{XU3}) and the total active earth pressure force (P_{XU}) acting on the downstream slope from the upstream slope are established. For further details on the applied methodology and equations used to determine P_{XU}, see *Appendix II: Subsection II.1.3*.

2.9.2.4 Total horizontal driving force (H_D) acting on the downstream slope

To calculate the total horizontal driving force (H_D), the following equation is applied, Eqn. (2.100), where the downstream slope's passive earth pressure force (P_{pD}) is subtracted from the total active earth pressure force (P_{aU}).

$$H_D = P_{a_D} - P_{p_D} = \left(P_{x_C} + P_{x_U}\right) - P_{p_D} \tag{2.100}$$

where: P_{pD} is the total passive earth pressure force , acting on the downstream slope from its foundation, formulated using Eqn. (II.7) in *Appendix II: Subsection II.1.2* and the total active earth pressure forces P_{XC} and P_{XU}, acting on the downstream slope from the core and upstream slope, are calculated using Eqn. (2.71), *Subsection 2.9.1.6.1*, and Eqn. (II.21), *Appendix II: Subsection II.1.3*, respectively.

2.9.2.5 Total vertical effective stress (σ_{vd}') acting on the downstream slope

By applying the same methodology defined in *Subsection 2.9.1.8*, the vertical effective stress (σ_{vd}'), acting through the downstream slope, is established by calculating the total effective weight of the downstream slope (ω_{ed}) and pore pressure acting in the vertical direction (u_{vu}). To determine ω_{ed} the first step is to calculate the effective weights above (ω_{ed1}) and below (ω_{ed2}) the phreatic line and the effective weight of the slope's foundation (ω_{ed3}), by applying Eqns. (II.22 to II.25) defined in *Appendix II: Subsection II.1.4*. Therefore, the total vertical stress (σ_{Fd}), which is equal to the total effective weight (ω_{ed}) of the downstream slope can be determined by using Eqn. (2.92).

The next step is to calculate the pore pressure (u_{vd}) acting in the vertical direction, through the downstream slope's embankment fill, by applying Eqn. (2.101). Hence, the total vertical effective stress (σ_{vd}') can be defined by Eqn. (2.102). Here, σ_{vd}' is found by subtracting the total vertical stress (σ_{Fd}) with the pore pressure (u_{vd}), and then dividing

the difference by the total base width of the downstream slope (b_d). Thus, the total effective shear stress (τ_D') and resultant shearing force (R_D) for the downstream slope can be evaluated.

$$u_{vd} = \left(\gamma_w H_f b_d\right) + \left(\gamma_w H_{av_d}\left(\frac{b_d - b_{d2}}{2}\right)\right) \tag{2.101}$$

$$\sigma_{vd}' = \frac{\sigma_{Fd} - u_{vd}}{b_d} \tag{2.102}$$

where: H_{av_d} = Average height of the idealised phreatic line (downstream); H_f = Foundation height; γ_w = Unit weight of water.

2.9.2.6 Resultant shearing force (R_D)

As expressed in Eqn. (2.103), the resultant shearing force (R_D) is found by multiplying the total effective shear stress (τ_D'), defined by Eqn. (2.22), with the total width of the base of the downstream slope (b_d).

$$R_D = \tau_D' \cdot b_d \tag{2.103}$$

where: $\tau_D' = \sigma_{vd}' \tan\varphi' + c'$

2.9.2.7 Factor of safety (FoS_D) of the downstream slope

By inputting the calculated total resultant shearing force (R_D) and horizontal driving force (H_D) into Eqn. (2.31), the downstream slope's factor of safety is established.

2.10 Deterministic Example of the Upstream and Downstream Slope Stability Model

Now that the traditional limit state formulation has been established to a great level of detail, the application of the deterministic upstream and downstream slope stability model, for a specific small homogeneous earthfill embankment, is demonstrated here, for two different soils. For comparison, London Clay (LC) and Medium Silt (MS) are selected for the embankment fill and are subjected to the same dam site conditions. Their soil properties and derived unit weights of soil (partially saturated, saturated and effective) are summarised in Table 2.4. Due to a lack of actual data, the soil properties and unit weights of soil for LC and MS were modelled using the standard formulae defined in *Subsection 2.7.1*.

Table 2.3 London Clay (LC) and Medium Silt (MS): Soil properties and unit weights of soil

Soil properties		Units	Soil Type	
			LC[3]	MS[4]
Void ratio (e)			0.69	0.43
Moisture content (θ)		%	56	56
Cohesion (c)		kN/m^2	5	0
Internal friction (φ)		°	20	26
Unit weight of embankment fill	γ_m	kN/m^3	17.0	18.7
	γ_{sat}		20.1	21.1
	γ_{sub}		10.3	11.3
Unit weight of foundation	γ_{fup}		20.1	21.1
	γ_{fc}		23.7	25.6
	γ_{fd}		13.6	15

2.10.1 Physical embankment model

Figure 2.12 shows the dimensions of the cross-section of the generic homogeneous earthfill embankment and the reservoir level considered for the deterministic analysis. For this specific embankment model, its upstream and downstream slopes have a slope gradient of 1: 3.0 and 1: 4.0 respectively.

[3] Extracted from Kovacevic et al. (2001)
[4] Extracted from Bell (1992)

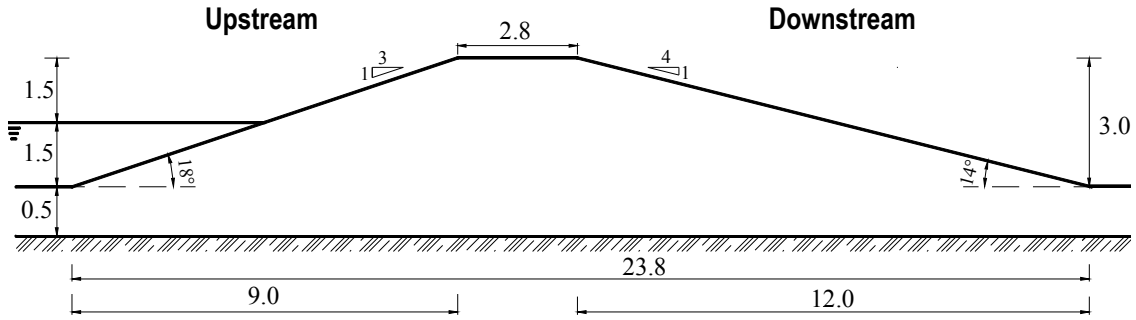

Figure 2.12 Dimensions (m) of the embankment model (Upstream 1: 3.0 Downstream 1: 4.0)

2.10.2 Idealised trajectory of phreatic line through the physical embankment model

For the embankment, the steady seepage flow model is applied and the trajectory of the idealised phreatic line established. Figure 2.13 shows the calculated dimensions used to determine the trajectory of the idealised he phreatic line through the cross section of the considered physical embankment model.

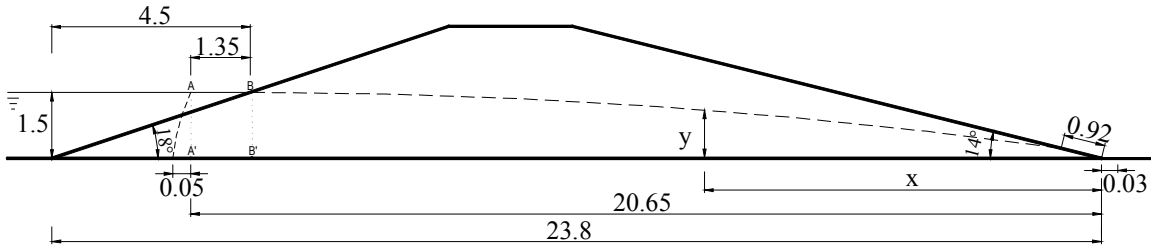

Figure 2.13 Dimensions (m) of the idealised phreatic line through the cross section of the embankment model

Figure 2.14 highlights the position of the idealised phreatic line, and the point where it enters and leaves the upstream, core and downstream sections of the embankment, assuming steady seepage flow through the embankment. This ensures that the unit weights of the embankment fill (partially saturated, saturated and effective) above and below the phreatic line, including the embankment's foundation, as illustrated in Figure 2.4, are explicitly considered.

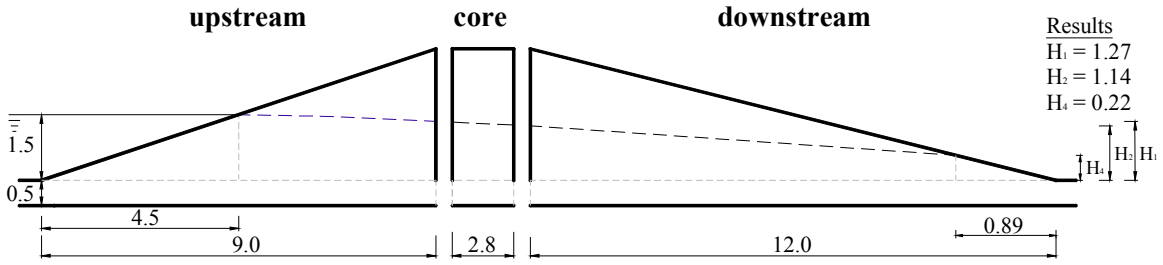

Figure 2.14 Position and points where the idealised phreatic line enters and leaves the upstream slope, core and downstream slope (m)

2.10.3 Areas allocated in the upstream and downstream slopes and their foundation

Details of sliding block application for the slope stability analysis are shown in Figure 2.15. The embankment fill of the upstream and downstream slopes was divided into sections using the formulae defined earlier. Figure 2.15 shows the calculated areas allocated below and above the phreatic line, and in the foundation.

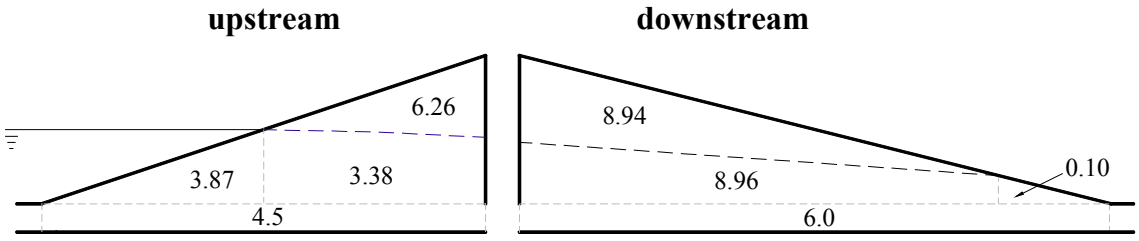

Figure 2.15 Areas (m^2) allocated within the upstream and downstream slopes and foundation

2.10.4 Pore water pressure force (P_w)

As the pore water pressure force (P_w), acting on the upstream slope from the water in the reservoir, is solely dependent on the reservoir's headwater height and the unit weight of water ($\gamma_w = 9.81$ kN/m^3), it will be the same for both soil models. By applying Eqn. (2.54), the pore water pressure force (P_w) was established:

$$P_w = \frac{1}{2}\gamma_w {H_w}^2 = \frac{1}{2} \cdot 9.81 \cdot 1.5^2 = 11.036 \text{ kN per metre length of dam}$$

By applying the upstream and downstream slope stability models, as defined in *Subsections 2.9.1* and *2.9.2*, the factor of safety for the upstream and downstream slopes were calculated.

2.10.5 Slope stability model: London Clay Embankment

Firstly, the embankment model is assumed to be constructed solely of London Clay. The results obtained for the vertical and horizontal stresses, pore pressures and associated effective stresses acting on the individual slopes are tabulated in *Appendix III*. From these results, the total resultant shearing force and horizontal driving force acting on the upstream and downstream slopes were calculated.

2.10.5.1 Factor of safety for the upstream slope

Once the total active earth pressure forces from the core and downstream slope (P_{XC} and P_{XD}), the total passive earth pressure force (P_{pU}) and the pore water pressure force (P_w) were calculated, see *Appendix III* for results, the total horizontal driving force (H_U) acting on the upstream slope was established.

$$H_U = \left(P_{x_C} + P_{x_D}\right) - \left(P_w + P_{p_U}\right) = (44.88 + 38.55) - (11.04 + 32.07) = 40.33 \text{ kN per m length of dam}$$

From the tabulated results in *Appendix III*, the total vertical effective shear stress (τ_U') and resultant shearing force (R_U) for the upstream slope were evaluated.

$$\tau_U' = \sigma_{vu}' \tan\varphi' + c' = 23.87\tan 20 + 5 = 13.69 \text{ kN/m}^2$$

$$R_U = \tau_U' \cdot b_u = 13.87 \cdot 9.0 = 123.2 \text{ kN per m length of dam}$$

Hence, the factor of safety of the upstream slope (FoS_U) was obtained.

$$FoS_U = \frac{R_U}{H_U} = \frac{123.2}{40.33} = 3.05$$

2.10.5.2 Factor of safety for the downstream slope

By applying the methodology, defined in *Subsection 2.9.2*, for the downstream slope stability model, the downstream slope's factor of safety (FoS_D) was also calculated. Here, the total horizontal driving force (H_D) acting on the downstream slope was calculated by subtracting the total active earth pressure force (P_{aU}) from the downstream slopes passive earth pressure force (P_{pD}), see calculation below.

$$H_D = \left(P_{x_C} + P_{x_U}\right) - P_{p_D} = (43.77 + 44.88) - 29.05 = 59.59 \text{ kN per metre length of dam}$$

Thus, the resultant shearing force (R_D) was calculated, as shown below, by multiplying the total effective shear stress (τ_D') with the total width of the base of the downstream slope (b_d).

$$\tau_D{}' = \sigma_{vd}{}' \tan\varphi' + c' = 19.29\tan 20 + 5 = 12.02\ \text{kN/m}^2$$

$$R_D = \tau_D' \cdot b_d = 12.02 \cdot 12.0 = 144.57\ \text{kN per metre length of dam}$$

By dividing the resultant shearing force with the horizontal driving force, the downstream slope's factor of safety was established.

$$\text{FoS}_D = \frac{R_D}{H_D} = \frac{144.25}{59.59} = 2.42$$

2.10.6 Slope stability model: Medium Silt Embankment

Subsequently the embankment fill is considered to be homogeneous but with Medium silt, which is a cohesionless soil (c' = 0). The calculated vertical and horizontal stresses, pore pressures and associated effective stresses, using the applied slope stability models, are tabulated in *Appendix III*. Thus, the total resultant shearing force and horizontal driving force acting on the individual slopes was calculated.

2.10.6.1 Factor of safety for the upstream slope

After evaluation of the total active earth pressure forces (P_{XC} and P_{XD}), the total passive earth pressure force (P_{pU}) and pore water pressure force (P_w) into Eqn. (2.76), the total horizontal driving force (H_U) was calculated.

$$H_U = \left(P_{x_C} + P_{x_D}\right) - \left(P_w + P_{p_U}\right) = (57.30+49.51) - (11.04+37.60) = 58.17\ \text{kN per m length of dam}$$

The resultant shearing force (R_U) for the upstream slope was established by multiplying the total effective shear stress (τ_U') with the total base width of the slope (b_u). However, as MS is cohesionless, the effective shear strength (τ_U') of the slope is solely dependent on the soil's angle of internal friction.

$$\tau_U{}' = \sigma_{vu}{}' \tan\varphi' = 26.40\tan 26 = 12.88\ \text{kN/m}^2$$

$$R_U = \tau_U' \cdot b_u = 12.88 \cdot 9.0 = 115.89\ \text{kN per metre length of dam}$$

Dividing R_U and H_U, the factor of safety of the upstream slope was obtained.

$$FoS_U = \frac{R_U}{H_U} = \frac{115.89}{58.17} = 1.99$$

2.10.6.2 Factor of safety for the upstream slope

For the downstream slope, the total horizontal driving force (H_D) was calculated.

$$H_D = \left(P_{x_C} + P_{x_U}\right) - P_{p_D} = (56.99 + 57.30) - 34.74 = 79.55 \text{ kN per metre length of dam}$$

From the results tabulated in *Appendix III*, the total vertical effective shear stress (τ_D') and resultant shearing force (R_D) for the downstream slope were calculated.

$$\tau_D{}' = \sigma_{vd}{}' \tan\varphi' = 22.01\tan 26 = 10.74 \text{ kN/m}^2$$

$$R_D = \tau_D' \cdot b_d = 10.74 \cdot 12.0 = 128.84 \text{ kN per metre length of dam}$$

Therefore, the downstream slope's factor of safety was established.

$$FoS_D = \frac{R_D}{H_D} = \frac{128.84}{79.55} = 1.62$$

From the set of traditional deterministic analyses, the factors of safety for the upstream and downstream slopes are visibly different between the two soils. For the embankment model constructed of London Clay, its slopes have a high factor of safety (FoS > 2.0). This indicates that under the embankment's current conditions, slope failure is unlikely to occur, as the slopes are stable. Comparing the factors of safety, the upstream slope has a much higher factor of safety compared to the downstream slope. This occurs as the embankment fill in the upstream slope has a higher overall unit weight compared to the fill in the downstream slope.

In comparison, the factors of safety for the embankment's upstream and downstream slopes constructed of Medium Silt are much lower. However, under the embankment's current conditions they are still classified as stable (FoS > 1.25). If results such as those for Medium Silt were obtained, in practice, more comprehensive investigations would have to be performed to ensure that the embankment's slopes did not fail under varying

dam site conditions. Thus, a realistic formulation for the limit states is identified and will provide the base for inclusion of probabilistic modelling.

2.11 Concluding Remarks

Due to the uncertainties associated with small homogeneous earthfill embankment dams, merely carrying out a deterministic assessment for the dam's safety will not be adequate and more sophisticated models that reflect uncertain conditions are required. In order to take into account the entire embankment when determining upstream and downstream slope stability, the sliding block method was identified as the most appropriate methodology.

To develop the slope stability model for the slopes, a physical embankment model has been developed that incorporates:

- The embankment's geometry.
- The soil properties of the embankment fill.
- The calculated position of the idealised phreatic line through the cross-section of the embankment.

The equations implemented for carrying out the deterministic slope stability models are also clearly outlined in this chapter. An example has been presented to demonstrate the application of the sliding block model for a generic embankment with different homogeneous fills.

In the next chapter, the methodology used to develop the probabilistic upstream and downstream slope stability model, for a generic small homogeneous earthfill embankment dam, will be presented. By applying a probabilistic approach, it will be possible to obtain notional performance measures of the slopes and obtain a clearer understanding of the risks associated with the dam's embankment in the future. This form of analysis is particularly important when looking at old well-established dams, where such effects were not initially considered at the time of their design and construction.

CHAPTER 3 : UNCERTAINTY ANALYSIS FOR HOMOGENEOUS EARTHFILL EMBANKMENT DAMS

3.1 Introduction

There are many sources of uncertainty relating to small earthfill dams, in particular, when considering older dams that have been in use for a significant length of time and have not been subject to the Reservoirs Act 1975. Furthermore, El-Ramley, Morgenstein and Cruden (2002) explain that deterministic limit equilibrium methods for slope stability analysis do not consider uncertainties such as the inherent variability of the soil properties, scarcity of representative data, simplifications and approximations adopted in geotechnical modelling, etc. However, they all need to be taken into consideration when carrying out a slope stability analysis (Abramson et al., 2002) for small earthfill dams. Here, a probabilistic approach is developed that will enable us to take into account the uncertainties associated with:

- The embankment's geometry.
- The mechanical and hydraulic properties of the embankment fill.
- The water level of the reservoir, which is site specific.
- Climate change effects, specifically relating to diverse precipitation scenarios.

This chapter will provide an outline of the methodology required to perform a reliability analysis on a homogeneous earthfill embankment dam. As uncertainties are fundamental to engineering models, the different forms of uncertainty will be defined. Finally, developed probabilistic slope stability model (PSSM) will be implemented in

order to determine the likelihood of structural failure due to the loss of overall stability of the upstream and downstream slopes under specific conditions.

3.2 Uncertainty in Engineering Modelling

The term uncertainty describes a variability of the outcome that does not have any explicit pattern. In engineering, uncertainty could be taken as a parameter, which describes the variability in natural properties and events (Hartford & Baecher, 2004), including the possible errors associated with a structure's behaviour, geometry and variability of its material properties (Murphy et al., 2011). In engineering, as defined by Thoft-Christensen and Baker (1982); Ditlevsen and Madsen (2007), it is important to differentiate between the following forms of uncertainty:

- Physical uncertainty
- Statistical uncertainty
- Model uncertainty

3.2.1 Physical uncertainty

This describes the physical characteristics of the key variables under consideration (Thoft-Christensen & Baker, 1982), such as the dimensions of the dam's embankment and its reservoir's headwater height. These variables have physical uncertainty as they can and will vary independently from each other during the dam's lifecycle. Changes to these variables can be either very subtle or very apparent and are not entirely dependent on a given timescale. Similarly, due to practical and economic considerations there will always be some degree of physical uncertainty due to several factors, such as:

- Human and/or technological errors during construction, resulting in differences between the final dimensions and those outlined in the dam's original design.
- Some form of consolidation and deterioration due to ageing of the dam, which could affect the gradient of the slopes including the height of the embankment.
- Changes to the composition of the embankment fill over time, due to variations in the dam's surrounding environment.

As the earthfill embankment fill is composed of naturally formed materials, their physical properties are variable due to inconsistencies in the soil itself and its soil

profile (Mettananda & Kulathilaka, 2002). Physical uncertainty can only be reduced and not entirely eliminated, as it exists regardless of the amount of data available (Vrijling, van Gelder & Voortman, 2004).

3.2.2 Statistical uncertainty

In addition to the physical uncertainty, the precision and accuracy of measurements has to be taken into account using statistical uncertainty. This relies on experimental data, provided by a sample of finite size, to estimate the uncertainty (Thoft-Christensen & Baker, 1982; Ditlevsen & Madsen, 2007). In practice, a large number of sample data is required to provide a good estimate of the numerical values of the parameters. For infrastructures, such as the embankment of an old well-established small dam, the lack of information is exceptionally high.

3.2.3 Model uncertainty

Model uncertainty is a result of the limitations of the applied model used to replicate the 'real' or actual structure mathematically. Therefore, '*model uncertainty is due to the necessary idealizations on which the physical model formulation and the distributional model formulation are based'* (Ditlevsen & Madsen, 2007: p.341). For engineering applications, the mathematical model does not take into consideration all aspects of the structure's behaviour (Thoft-Christensen & Baker, 1982). This can be related to either the limit state equation itself, or the distribution function of the input parameters (Melchers, 1999), such as the embankment's dimensions or the embankment fill's soil properties (Vrijling, van Gelder & Voortman, 2004). These uncertainties reflect the natural variability of the structure, as well as the limited knowledge relating to the precision of the developed model (Baecher & Christian, 2003).

In recent times, these forms of uncertainty (physical, statistical and model) are frequently classified as either epistemic or aleatory uncertainty. Aleatory uncertainty refers to the inherent randomness or natural variations in the physical world (Faber & Stewart, 2003; Hartford & Baecher, 2004). This includes geological processes such as the embankment fill's soil properties (Huber, Vermeer & Moormann, 2011). Epistemic uncertainty relates to the lack of representative data, simplifications and approximations adopted in the geotechnical modelling, etc. (Hartford & Baecher, 2004). This stems

from our lack of perfect knowledge due to limited data about the structure, effectiveness of the selected analytical method, scale of site tests, etc. (Baecher & Christian, 2003; Faber & Vrouwenvelder, 2008). Typically, epistemic uncertainty can be reduced by obtaining more data and improving the model of the structure, whereas aleatory uncertainty cannot be reduced by improving the model or the procedure (Murphy et al., 2011).

As the selected analytical model (Sliding Block) is implemented for all analyses, the applied probabilistic modelling is limited to aleatory uncertainties. Here, the aleatory uncertainties are associated with (Preziosi & Micic, 2009, 2011a; Abramson et al., 2002):

- The geometry of the embankment and its foundation.
- The soil properties of the embankment fill.
- Environmental effects, specifically diverse precipitation scenarios.

By introducing specific random variables, uncertainties are incorporated into the applied reliability analysis.

3.3 Analysis with Uncertainty

The probability of dam failure is being investigated using mathematical methods, as *'in a narrow sense, it is the probability that a structure will not attain each specified limit state (ultimate or serviceability) during a specified reference period'* (Thoft-Christensen and Baker, 1982: p.8). We have introduced numerous variables and extensive mathematical modelling. The probabilistic methodology therefore forms the basis with which to incorporate uncertainty into the computational model in a coherent manner.

Structural reliability has both a mathematical and general meaning. Here, each failure mode is associated with the limit state of the model, and it is evaluated separately and any correlation between variables is taken into account. We consider a limit state to be a function $g(x_i)$, Eqn. (3.1), that is a complex function of several variables (x_i) and has some probability distribution function, $F_{g(x_i)}$.

$$g(x_i) = g(x_1, x_2, \dots\dots, x_n) \quad (3.1)$$

where: x_i are variables that could be deterministic and/or probabilistic.

3.3.1 Probabilistic modelling

The established convention states that there are four levels of probabilistic modelling, identified as Level 1 to Level 4. Each Level is dependent on the amount, and complexity, of the available information for the structural problem (Thoft-Christensen & Baker, 1982).

Level 1 represents the analysis when only one characteristic value for each variable in Eqn. (3.1) is available and is the simplest form of probabilistic modelling (Melchers, 1999). This methodology is based on probabilistic principles, but does not require any probabilistic calculations to be carried out (Ang & Tang, 1984). Thus, it is effectively a deterministic analysis usually associated with load and resistance variables including any predefined characteristic values for the applied variables.

Level 2 refers to cases where relevant variables in Eqn. (3.1) are characterised by their mean (μ_{x_i}) and standard deviation (σ_{x_i}), taking into account correlation between parameters (Sørensen, 2004). The reliability index methodology applied in Level 2 provides an approximation of the model's probability of failure as well as its system, (Thoft-Christensen & Baker, 1982). For this level of probabilistic modelling, by applying First Order Second Moment Reliability Method (FOSM) and simulation methods, estimates of the structure's probability of failure can be established (Melchers, 1999). By carrying out a Level 2 analysis, it is possible to obtain an idea of the notional safety of the model due to its design or the uncertainties influencing the structure's design.

Level 3 probabilistic modelling applies when there is sufficient knowledge of all the combined distributions of the uncertain parameters relating to the model. As for Level 2 probabilistic modelling, FOSM and simulation techniques can be applied. The disadvantage of a Level 3 reliability analysis is that it can only be implemented when the probability of failure is assumed to be a measure. It is also very time consuming

when considering complex failure modes with many random variables, as it requires a clear understanding of the combined distribution of all the uncertain parameters of the structure and a large number of tests to be carried out (Haldar & Mahadevan, 2000).

A Level 4 analysis is only carried out when it is possible to attain a reliability index that encompasses other technological systems in society (Melchers, 1999). This level of probabilistic modelling compares both a reference and a structural analysis, which must take into account all the principles of the engineering economic analysis under uncertainty (Thoft-Christensen & Baker, 1982). This may include the cost of failure, benefits of construction, maintenance, repair and possible failure modes of the structure (Madsen, Krenk & Lind, 1986). When considering large important economic structures, a Level 4 analysis is crucial as the structure's risk criterion and cost of failure are used as a measure of its reliability (Sørensen, 2004), where risk is defined as the product of probability and consequence (Hartford & Baecher, 2004).

For older dams, soil property records are incomplete, outdated or lost over the years, so Level 3 and Level 4 probabilistic modelling are not feasible, as information required to perform such analyses is not readily available. For the purpose of this research, we will apply the Level 2 probabilistic model, as it satisfies relevant requirements as well as being computationally fast and efficient. The Level 2 structural reliability analysis will be carried out using the First Order Reliability Method (FORM), as the physical embankment model can be easily integrated within the applied methodology (Halder & Mahadevan, 2000).

3.4 Level 2 Reliability Analysis

Here we assume that each random variable is represented by its two moments, mean and standard deviation. The fundamental principles for the theory of probability and the commonly used probability distributions are summarised in *Appendix III*. The first step in the reliability analysis is to identify the relevant failure modes, which provide a base for $g(x_i)$. The safety margin (M) can be determined from the limit state function, Eqn.

(3.2). It is the safety margin (M) that is of interest in the reliability analysis and is either an implicit, or an explicit, function of the basic random variables (x_i).

$$M = g(x_i) = g(x_1, x_2, \dots\dots, x_n) = 0 \tag{3.2}$$

Figure 3.1 shows the safety margin in the design parameter space of two arbitrary variables (x_1 and x_2) (Haldar & Mahadevan, 2000). For clarity we refer to $g(x_i)$ as the limit state function and consider the safety margin as $M = g(x_i) = 0$.

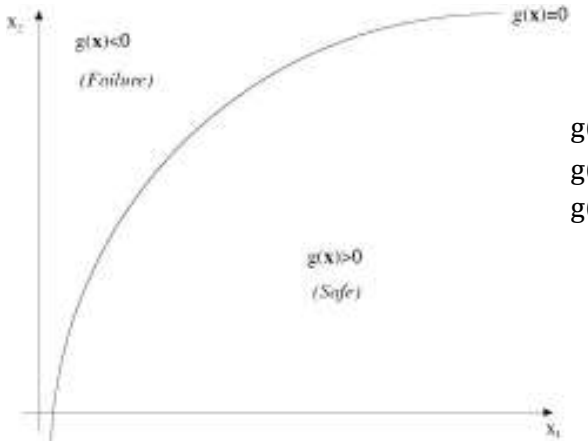

KEY

$g(x_i) > 0$	$x_i \in$ Safe domain
$g(x_i) < 0$	$x_i \in$ Failure domain
$g(x_i) = 0$	Safety margin (Boundary between the domains of the design parameter space)

Figure 3.1 Safety margin (M) in the design parameter space of two arbitrary variables[5]

For the limit state function, $g(x_i)$, the probability of failure (P_f) of the structure is evaluated over its failure domain, as defined in Figure 3.1, Eqn. (3.3).

$$P_f = P\left[g(x_i) \le 0\right] = \int_{g(X_i)\le 0} f_g(x_i)\,dx_i \tag{3.3}$$

where: $f_g(x_i)$ is the cumulative distribution function.

However, Eqn. (3.3) is deceptively simple as the integral includes uncertainties associated with the joint density function and the failure domain (when $g(x_i) \le 0$) (Vrijling, van Gelder & Voortman, 2004). In reality, it is virtually impossible to obtain the joint probability density function, $f_{g(x_i)}$, so an analytical approximation has to be applied to Eqn. (3.3). Frequently in engineering, we use the reliability index (β) for the limit state function that is directly related to P_f, Eqn. (3.4).

[5] Extracted from Vrijling, van Gelder and Voortman (2004)

$$P_f = \Phi(-\beta) = 1 - \Phi(\beta) \tag{3.4}$$

where: Φ = Standard normal distribution function.

Also as a complement to P_f, the structure's reliability (P_s) can be obtained, Eqn. (3.5).

$$P_s = 1 - P_f \tag{3.5}$$

Hence, β can be found by applying Eqn. (3.6) where a higher reliability index will reflect a lower probability of failure, as shown in Table 3.1.

$$\beta = -\Phi^{-1}(P_f) \tag{3.6}$$

Table 3.1 Relationship between the reliability index (β) and probability of failure (P_f)

β	1.3	2.3	3.1	3.7	4.2	4.7	5.2
P_f	10^{-1}	10^{-2}	10^{-3}	10^{-4}	10^{-5}	10^{-6}	10^{-7}

3.4.1 Linear limit state function

The simplest case in a reliability analysis is to consider a linear limit state function $g(x_i)$ where resistance (x_R) and load effect (x_S) are defined in terms of their mean values and standard deviation. Here, both random variables (x_R and x_S) are normally distributed and uncorrelated, $N(\mu_R, \sigma_R)$ and $N(\mu_S, \sigma_S)$ respectively.

$$g(x) = M = x_R - x_S = 0 \tag{3.7}$$

The linear limit state, Eqn. (3.7), can also be shown conceptually by plotting the graphs of the probability density functions for the load effect $f_S(s)$ and resistance $f_R(r)$ of the random variables, Figure 3.2. The area where the graphs overlap indicates the quantitative measure of the probability of failure and is a measure of the bar's likelihood of failure (Haldar & Mahadevan, 2000). The area of overlap has its own distribution calculated by applying the integral expressed in Eqn. (3.8). In most cases, this equation is difficult to evaluate, especially when nonlinear limit sate functions are considered.

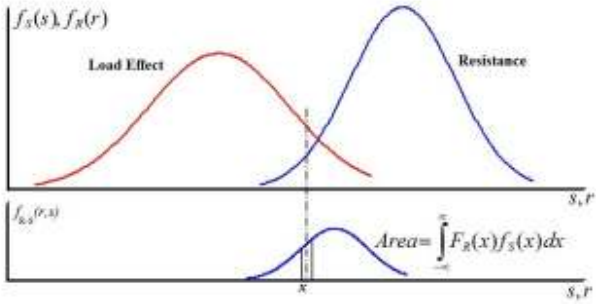

Figure 3.2. Probability densities for resistance and load effect demonstrating measure of failure

$$P_f = P\left(g(x) \le 0\right) = \int_{-\infty}^{\infty} F_R(x) f_S(x)\, dx \tag{3.8}$$

By taking the ratios of the mean (μ_M) and standard deviation (σ_M), the reliability index (β) can be obtained using Eqn. (3.9) as defined by Cornell (1969). β is therefore expressed as '*the mean margin of safety from its critical value (M=0) in units of standard deviation*' (Baecher & Christian, 2003: p.304), when x_R and x_S are uncorrelated normally distributed variables.

$$\beta = \frac{\mu_M}{\sigma_M} = \frac{\mu_R - \mu_S}{\sqrt{\sigma_R{}^2 + \sigma_S{}^2}} \tag{3.9}$$

where: μ_M is the mean and σ_M is the standard deviation of the safety margin.

The reliability index (β) is related to the probability of failure, as defined in Eqn. (3.6). Hence, the probability of failure (P_f) can be easily obtained.

3.4.2 Nonlinear limit state function

Several strategies for evaluation of reliability index for nonlinear limit state functions are now presented.

3.4.2.1 Taylor series approximation for nonlinear function

When the limit state function is nonlinear, the nonlinear function can be linearized using a Taylor series expansion about the mean values of the random variables, Eqn. (3.11), to obtain approximate values for the mean (μ_M) and standard deviation (σ_M) (Thoft-Christensen & Baker, 1982). Eqn. (3.10) shows the linearized safety margin (M) where only the linear terms are retained from the expanded Taylor series.

$$M \cong g\left(\mu_X\right)+\sum_{i=1}^{n}\frac{\partial g}{\partial X_i}\left(X_i-\mu_{X_i}\right)+\frac{1}{2}\sum_{i=1}^{n}\sum_{j=1}^{n}\frac{\partial^2 g}{\partial X_i \partial X_j}\left(X_i-\mu_{X_i}\right)\left(X_j-\mu_{X_j}\right)+\ldots=0 \qquad (3.10)$$

By linearizing the safety margin (M), the joint density function, $f_{g(x_i)}(x_i)$, could be characterized. Thus, applying First Order Second Moment Method (FOSM), irrespective of whether the random variables are correlated or uncorrelated, the mean and variance of the safety margin (M) as defined by Eqn. (3.10), can be found (Hartford & Baecher, 2004). If the variables are uncorrelated, then the variance of the random variables, $\mathrm{Var}(x_i)$, is determined using Eqn. (3.12), whereas Eqn. (3.13) is applied when the variables are correlated (Haldar & Mahadevan, 2000).

$$\mu_{g(x_i)} \cong g\left(\mu_{x_1}, \mu_{x_2}, \ldots\ldots, \mu_{x_n}\right) \qquad (3.11)$$

$$\sigma_M{}^2 \approx \sum_{i=1}^{n}\left(\frac{\partial g}{\partial x_i}\right)^2 \mathrm{Var}\left(x_i\right) \qquad (3.12)$$

$$\sigma_M{}^2 \approx \sum_{i=1}^{n}\sum_{j=1}^{n}\frac{\partial g}{\partial x_i}\frac{\partial g}{\partial x_j}\mathrm{COV}\left(x_i, x_j\right) \qquad (3.13)$$

where: $\mathrm{Var}(x_i)$ is the variance of the random variables x_i and $\mathrm{COV}(x_i, x_j)$ is the covariance of the random variables x_i and x_j.

This is an effective strategy, but its main drawback is the lack of invariance (Thoft-Christensen & Baker, 1982), as for different but deterministically equivalent safety margins the reliability index, Eqn. (3.9), obtained would have been the same.

3.4.2.2 The Hasofer-Lind transformation method (FORM)

The alternative to the above strategy is FORM analysis as proposed by Hasofer and Lind. The first stage in the Hasofer-Lind transformation is to map all the random variables (x_i) into their standardized form N(0,1) using Eqn. (3.14) (Hasofer & Lind, 1974), where x_i' is defines the normal random variable with zero mean ($\mu_{x_i} = 0$) and unit standard deviation ($\sigma_{x_i} = 1$) (Baecher & Christian, 2003). The original safety margin, $g(x) = 0$, is then also mapped to produce the reduced safety margin, $g(x') = 0$ (Haldar & Mahadevan, 2000).

$$X_i' = \frac{x_i - \mu_{x_i}}{\sigma_{x_i}} \qquad g(x') = 0 \qquad (3.14)$$

By applying Eqn. (3.14), it enables the transformation to occur without any complications, if all the random variables are uncorrelated. The reliability index (β_{HL}) for both the linear and nonlinear limit state functions, over any n^{th} dimensional space with a hyperplane limit state, can therefore be found by applying Eqn. (3.15), as shown in Figure 3.3. Thus, the reliability index, as defined by Hasofer and Lind (1974), is the shortest distance from the origin of the axes in the reduced coordinate system to the limit state surface, defined as the failure surface ($g(x) = 0$).

$$\beta_{HL} = \min\left(\sum_{i=1}^{n} x_i^{\,2}\right)^{\frac{1}{2}} = \min\sqrt{\left(x'^*\right)^T\left(x'^*\right)} \tag{3.15}$$

where: x'^* is the vector in the reduced coordinate system at the design point in standard normal space.

As shown in Figure 3.3 as the vector in the reduced coordinate system gets closer to the origin, the probability of failure (P_f) increases. This is dependent on the shape of the graph produced when $g(x') = 0$, where the random variables (x') are in the reduced coordinate system. The most probable failure point (x'^*) is effectively at the minimum distance from the origin to the design point on the limit state surface, Figure 3.3, where X'^* represents the coordinates of the design point (Thoft-Christensen & Baker, 1982). There are many strategies available to find this critical point, but here the standard Rackwitz-Fiessler iterative approach (Haldar & Mahadevan, 2000) is applied. This methodology is therefore the foundation for finding the first order second moment reliability index for any given structure with linear and nonlinear failure functions.

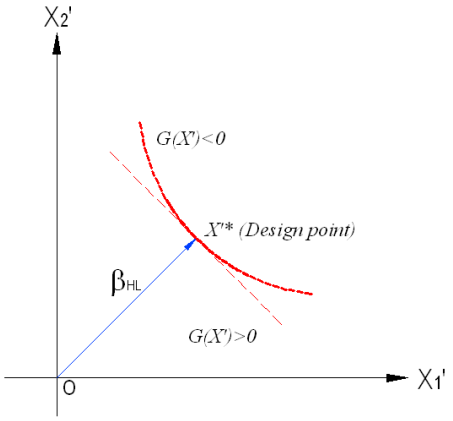

Figure 3.3. Hasofer-Lind relaiblity index for nonlinear limit state function in standard normal space

For the linear state function with normally distributed variables, $g(x_i) = x_R - x_S$, defined by Eqn. (3.7), its reliability index can be determined by applying Eqn. (3.15). However, it will reduce to the formulation defined in Eqn. (3.9).

The Hasofer-Lind reliability index (β_{HL}) defined as the first-order second-moment mean value reliability index, as derived in Eqn. (3.18), can be obtained in several ways, but the classical calculus of variations method or Lagrangian multiplier approach is used here (Haldar & Mahadevan, 2000). The first step is to minimise the problem and apply a Lagrangian multiplier (λ) to the problem (Baecher & Christian, 2003). By minimising the distance from the origin to a point on the failure surface, minΔ in Eqn. (3.16) becomes and optimum problem, assuming all finite points are stationary and equal to zero, Eqn. (3.17).

$$Min\ \Delta = \sqrt{(x'^{*})^{T}(x'^{*})} + \lambda g(x') \tag{3.16}$$

$$\frac{\partial \Delta}{\partial x_i'} = 0 \qquad \text{and} \qquad \frac{\partial \Delta}{\partial \lambda} = g(x') = 0 \tag{3.17}$$

where: $(x'^{*})^{T}$ indicates the transpose of a matrix.

$$\beta_{HL} = -\frac{\sum_{i=1}^{n} x_i'^{*}\left(\frac{\partial g}{\partial x_i'}\right)^{*}}{\sqrt{\sum_{i=1}^{n}\left(\frac{\partial g}{\partial x_i'}\right)^{2*}}} \tag{3.18}$$

By applying Eqn. (3.19), the design point $x_i'^{*}$ in the reduced coordinates is identified, where α_i, Eqn. (3.20), are the direction cosines along the coordinate axes x_i'.

$$x_i'^{*} = -\alpha_i \beta_{HL} \qquad (i = 1, 2, \ldots\ldots, n) \tag{3.19}$$

$$\alpha_i = \frac{\left(\frac{\partial g}{\partial x_i'}\right)^{*}}{\sqrt{\sum_{i=1}^{n}\left(\frac{\partial g}{\partial x_i'}\right)^{2*}}} \tag{3.20}$$

Finally, by applying Eqn. (3.21), the design point (x_i^{*}) in the original space can be established.

$$x_i^{*} = \mu_{x_i} - \alpha_i \sigma_{x_i} \beta_{HL} \tag{3.21}$$

By implementing Eqn. (3.20), the sensitivity indices (α_i) of the individual variables are identified.

3.4.2.3 Random variable modelling

The main advantage of applying FOSM is that it *'reveals the relative contribution of each variable to the overall uncertainty in a clear and easily tabulated manner'* (Baecher & Christian, 2003: p.342). The disadvantage of using FOSM is that it does not consider the form of the probability density function, which describes the individual random variables and their subsequent mean and standard deviation (Griffiths, Fenton & Tveten, 2005). Hasofer and Lind (1974) solved this problem by developing the Hasofer-Lind transformation method, which is applied within the advanced first order second moment method (AFOSM) for normal random variables, to find the minimum distance between the mean points from the origin and the failure surface (Hartford & Baecher, 2004; Pereira & Caldeira, 2011).

3.4.3 Sensitivity Index

In addition to the notional reliability index (β) that is a direct function of the probability of failure (P_f), the sensitivity factor, Eqn. (3.20), or sensitivity index, for each random variable is obtained. This factor represents a rational measure of importance of specific variables. By implementing Eqn. (3.20), α_i defines the unit vector in the direction of the gradient vector. The calculated sensitivity indices (α_i) therefore reflect the contribution of the inherent variability of the random variable on the reliability in respect to each limit state. For instance, if α_i has a low value it indicates that the variable does not greatly affect the model and could be defined as deterministic. However, if the sensitivity index is high, then the variable has a greater influence on the model's reliability.

3.4.4 Reliability Analysis with Correlated Variables

As sometimes random variables can be dependent on the other, their correlation has to be considered. This is important as correlated variables can affect the reliability index for both linear and nonlinear limit state functions. To quantify the relationship between the correlated random variables, the correlation coefficient is established.

Assuming that the random variables x_R and x_S, as defined in Eqn. (3.7), are correlated it is possible to determine their correlation coefficient, $\rho(x_R, x_S)$. The first step is to calculate the covariance of the two variables $COV(x_R, x_S)$, which defines the second moment about their respective means μ_R and μ_S (Thoft-Christensen & Baker, 1982), indicating the linear relationship between the two variables (Haldar & Mahadevan, 2000). Once the variables covariance is established then their correlation coefficient, $\rho(x_R, x_S)$, can be defined using the following equation:

$$\rho\left(x_R, x_S\right) = \rho_{x_R x_S} = \frac{COV\left(x_R, x_S\right)}{\sigma_R, \sigma_S} \qquad -1 \le \rho_{X_R X_S} \le 1 \tag{3.22}$$

Haldar and Mahadevan (2000: p.52) state that *'two random variables can be considered to be statistically independent if the correlation coefficient is less than ± 0.3; they can be considered to be perfectly correlated if the correlation coefficient is greater than ± 0.9.'* The correlation coefficient is non-dimensional, as the deviations for the two random variables have the same units as their respective means (Hartford & Baecher, 2004). To take into account the correlated variables, the covariance matrix, [C], for the random variables (x_i) has to be established.

$$\left[C\right] = \begin{bmatrix} \sigma_{x_1}{}^2 & COV\left(x_1, x_2\right) & & COV\left(x_1, x_n\right) \\ COV\left(x_2, x_1\right) & \sigma_{x_2}{}^2 & \cdots & COV\left(x_2, x_n\right) \\ \vdots & \vdots & \ddots & \vdots \\ COV\left(x_n, x_1\right) & COV\left(x_n, x_1\right) & \cdots & \sigma_{x_n}{}^2 \end{bmatrix} \tag{3.23}$$

where: $\sigma_{X_n}{}^2 = Var(x_i)$

As most 'real' cases consider the Hasofer-Lind transformation method (FORM), the covariance matrix can be expressed in terms of the correlation coefficients for the reduced random variables (x_i'), Eqn. (3.24).

$$\left[C'\right] = \begin{bmatrix} 1 & \rho_{x_1, x_2} & & \rho_{x_1, x_n} \\ \rho_{x_2, x_1} & 1 & \cdots & \rho_{x_2, x_n} \\ \vdots & \vdots & \ddots & \vdots \\ \rho_{x_n, x_1} & \rho_{x_n, x_2} & \cdots & 1 \end{bmatrix} \tag{3.24}$$

3.5 Alternative Reliability Index Evaluations

An alternative analytical methodology is the Second Order Reliability Method (SORM). SORM applies second order representation to approximate the nonlinear state function, with correlated non-normal variables to determine the probability of failure (Haldar & Mahadevan, 2000; Baecher & Christian, 2003). A further alternative approach is the Monte Carlo (MC) simulation that involves solving a deterministic problem numerous times, usually ranging from 100 to 1000 simulations, to develop the statistical distribution of the limit state function (Mostyn & Li, 1993; Chowdhury, Flentje & Bhattacharya, 2010).

Applying Monte Carlo simulations is simple, and can easily deal with an extensive range of functions, including those that cannot be defined in explicit form (Hartford & Baecher, 2004), providing the components of the random variables are uncorrelated (Mellah, Auvinet & Masrouri, 2000). However, there are disadvantages to using MC simulations when evaluating slope failure. For instance, if the slope has a very small probability of failure, it will take a very larger number of simulations to establish the slope's probability of failure to an acceptable level of confidence. The other disadvantage relates to the soil properties of the embankment fill, which are modelled as spatially perfectly correlated random variables (Mostyn & Li, 1993). For further literature regarding the theory and implementation of SORM and Monte Carlo simulations in reliability analysis, refer to Haldar and Mahadevan, (2000) and Baecher and Christian (2003).

3.6 Reliability Analysis for Small Embankment Dams

The first step in the reliability analysis is to identify the relevant failure modes (FM) that govern the dam's long-term performance. Here, the relevant failure modes refer to upstream (FM1) and downstream (FM2) slope failure (slope instability). Thus, their linear limit state functions, defined using sliding block assumptions, are given by Eqns. (3.25 and 3.26), with reference to Figure 2.9 in *Chapter 2: Subsection 2.9*.

$$g(upstream) = \tau_U' - \left(P_{x_C} + P_{x_D}\right) - \left(P_w + P_{p_U}\right) \quad (3.25)$$

$$g(downstream) = \tau_D' - \left(P_{x_C} + P_{x_U}\right) - P_{p_D} \quad (3.26)$$

where: $\tau_{U/D}$ = Vertical effective shear stress for the upstream and downstream slopes respectively; P_w = Pore water pressure; P_{x_C} = Total active earth pressure force exerted by the core; $P_{x_{U/D}}$ = Total active earth pressure force exerted by the upstream and downstream slopes respectively; $P_{p_{U/D}}$ = Total passive earth pressure force acting on the upstream and downstream slopes respectively.

While Eqns. (3.25 and 3.26) appear linear, in reality, they are non-linear and include a number of variables that depend on the position of the phreatic line and the soil properties of the embankment fill. Subsequently, the input variables are identified. Those assumed as deterministic are defined in terms of their characteristic value (e.g. the moisture content of the soil), whereas the variables taken as probabilistic are defined in terms of their mean (μ) and standard deviation (σ) or they have been derived as a function of the random variables, such as the position of the idealised phreatic line. Here, the selected probabilistic variables represent the aleatory uncertainties concerned with the embankment's geometry, embankment fill's soil properties and the reservoir's headwater height.

For the limit state functions defined in Eqns. (3.25 and 3.26), a generic notation x_i was introduced and the reliability index (β), Eqn. (3.15), and probability of failure (P_f) for FM1 and FM2 evaluated by implementing Eqn. (3.4). The probability distribution functions reflect the nature of uncertainty and in this case there is a significant diversity between geometric and soil properties. For the variables that define the geometry of the embankment, the equipment tolerances used to measure the embankment would be a significant factor, and the lack of sufficient samples from soil testing would have a major influence on the slope's probability of failure. As a complement to P_f, the structure's reliability (P_s) can be obtained by applying Eqn. (3.6).

The First Order Second Moment method (FOSM) is integrated with the modified deterministic slope stability model to create the probabilistic slope stability model

(PSSM). This methodology can be applied when the limit state functions, Eqns. (3.25 and 3.26), have correlated or non-correlated random variables.

3.6.1 Example for application of the probabilistic slope stability model (PSSM)

A simple slope stability problem is considered here, to demonstrate how the First Order Second Moment method (FOSM) is integrated into the deterministic upstream and downstream slope stability models defined in *Chapter 2*. For this example, the physical embankment model (Upstream 1: 3.0 and Downstream 1: 4.0) constructed of London Clay (LC), illustrated in Figure 2.13, *Chapter 2: Subsection 2.10*, is considered for the probabilistic slope stability model (PSSM).

To demonstrate the application of PSSM, the limit state functions, defined by Eqns. (3.25 and 3.26), have been used as the relevant failure modes (FM1 and FM2) governing the dam's long-term performance. The soil properties and derived unit weights of soil for LC summarised in Table 2.4, *Chapter 2: Subsection 2.10*, are implemented into the probabilistic model.

Here the mean values and standard deviation of the variables relating to the embankment's geometry and soil properties of the embankment fill are assumed uncertain and modelled as probabilistic with normal distribution, Table 3.2.

Table 3.2 Probabilistic modelling of the input parameters: Variables are normally distributed

Variable	Unit	Mean (μ)	Standard deviation (σ)
Height of Embankment (H)	m	3.0	$0.01 \cdot \mu$
Crest Width (CW)	m	2.8	$0.01 \cdot \mu$
Height of Foundation (H_f)	cm	50.0	$0.02 \cdot \mu$
Headwater height (H_w)	m	2.0	$0.05 \cdot \mu$
Unit weight of soil factor (γ_{fct})	kN/m^3	1.0	$0.10 \cdot \mu$
Internal friction of soil* (φ')	^{o}	20	$0.15 \cdot \mu_\varphi$
Cohesion of soil* (c')	kN/m^2	5.0	$0.30 \cdot \mu_c$

*Negatively correlated (-0.5)

As an extension, by probabilistically modelling the embankment's geometry, the trajectory of the idealised phreatic line will be able to reflect variations in the upstream

and downstream slope gradients caused by localised changes. For instance, dipping or crest reduction due to soil degradation at the embankment's surface, external erosion of the slopes, bulging at the downstream toe and improvements to the slopes during maintenance or repair. For that reason, the headwater height is treated as uncertain and its mean value and standard deviation are presented in Table 3.2.

The advantage of the probabilistic approach is that the variables are defined in terms of their mean (μ) and standard deviation (σ), or have been derived as a function of the random variables such as the position of the phreatic line, whereas the variables are defined taken as deterministic are defined in terms of their characteristic value. Therefore, the variable's standard deviation is able to capture the inherent randomness or natural variations associated with the parameter, such as limited data, variations between samples, accuracy of measurements, etc. Thus, the reliability index obtained for both failure modes will be able to take into account the effect these variables have on the performance of the embankment's individual slopes.

The results presented below compare the reliability index (β_U and β_D) obtained for failure modes FM1 (upstream) and FM2 (downstream) with the slope's deterministic factor of safety (FoS_U and FoS_D), for the London Clay embankment defined in *Chapter 2: Subsection 2.10*. Furthermore, the percentage difference between the reliability indices is approximately 10 %, whereas the factors of safety have a percentage difference of 23 %. It would be wrong to compare these percentages directly. However, reliability is a more comprehensive measure as has taken into account uncertainties associated with the embankment and its site-specific conditions.

Upstream (FM1) ⇒ Reliability index: $\beta_U = 3.28$; Factor of safety: $FoS_U = 3.05$

Downstream (FM2) ⇒ Reliability index: $\beta_D = 2.94$; Factor of safety: $FoS_D = 2.42$

In summary, as the reliability index is associated with the slope's critical slip surface, the likelihood of slope failure occurring has been quantified while taking into account:

- Site-specific and slope specific information.
- Outcomes of tests carried out at the dam site.
- Variability of the embankment's geometry and soil properties of the embankment fill.

Thus, the proposed probabilistic slope stability model (PSSM) will offer a rational way of approaching slope stability analysis, in which probabilities of failure can be assessed.

For those earthfill embankment dams, which until now were not covered by the Reservoirs Act 1975, it is unlikely that detailed, consistent, data is available. This could be due to inconsistent monitoring of the dam and/or only a small number of data samples taken over the course of its lifecycle. Consequently, certain properties will either be largely unknown or noticeably differ between the data samples. By implementing PSSM, it will therefore be possible to determine how such dams could be classified according to the risk classification stated within the Flood and Water Management Act 2010.

It should be noted that for both failure modes their reliability index is a relative measure and not an absolute measure of the slope's overall reliability. This is due to simplification of the limit state functions (FM1 and FM2), defined using sliding block assumptions, as well as site-specific data relating to the earthfill embankment dam. In order to improve the accuracy of the slope's calculated reliability, alternative limit states such as those associated with overtopping or internal erosion would need to be considered in addition to the availability of more detailed and consistent data.

3.7 Flowchart for the Applied Probabilistic Slope Stability Analysis (PSSM)

The flowchart in Figure 3.4 presents the key stages in the proposed probabilistic slope stability analysis (PSSM) and interpolation of the results obtained. Uncertainties associated with the embankment's geometry, the soil properties of the homogeneous embankment fill and the reservoir's headwater height, as indicated by step 1 in Figure 3.4 represent the input parameters. Traditional steady seepage model is implemented to

establish the saturation levels of the partially saturated fill, above the phreatic line, step 2 in Figure 3.4. For the probabilistic analysis of the embankment's slopes, step 3 in Figure 3.4, the slope stability model is defined using the sliding block equilibrium equations derived in *Chapter 2: Subsections 2.9*.

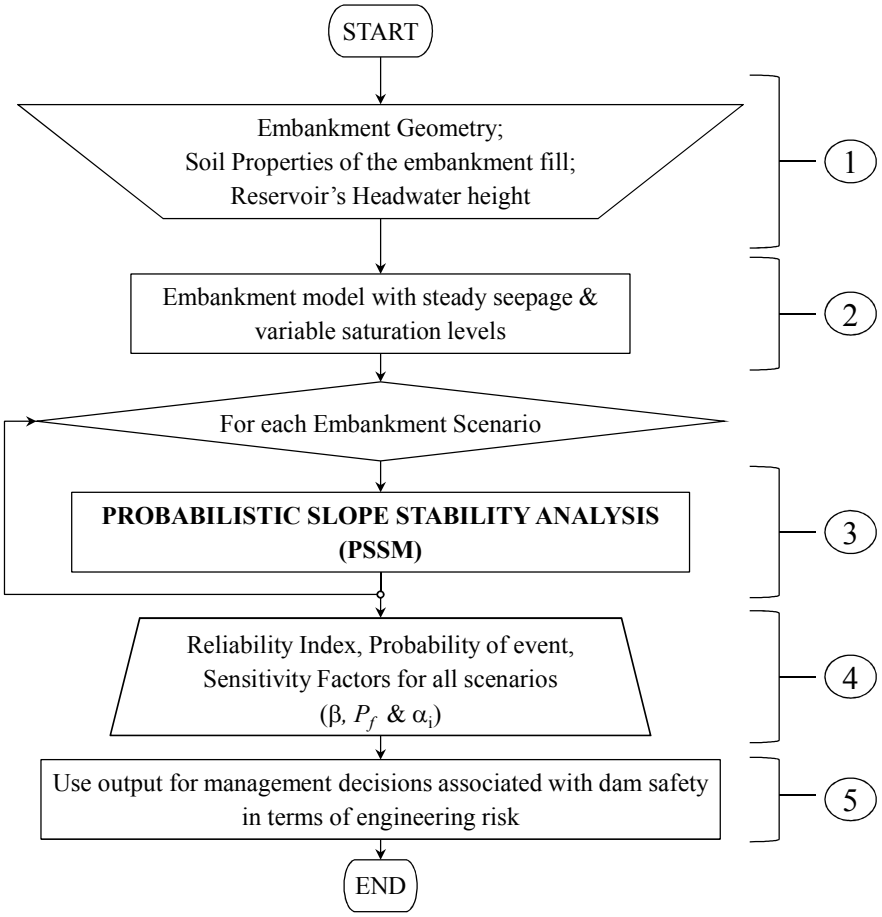

Figure 3.4 Flowchart of the applied probabilistic slope stability analysis

The results obtained for each failure mode (FM1 and FM2) using PSSM, step 4 in Figure 3.4, include the reliability index (β), probability of failure (P_f) and sensitivity indices (α_i) that reflect the importance of the uncertain variables. The output of the probabilistic slope stability analysis will represent a tool for decision-makers (Undertakers, Panel Engineers, Environment Agency, etc.) regarding future inspections, monitoring, discontinuing, etc. of such dams, step 5 in Figure 3.4. The aim is not to replace existing risk assessments, but to improve the quality of data used by the decision-makers.

The probabilistic model (PSSM) contains a set of routines that integrate FOSM with the sliding block formulation for upstream and downstream slope stability models, derived in *Chapter 2: Subsections 2.9*. To determine the structural reliability of the embankment's individual slopes the optimization as described in Eqn. (3.15) is carried out using the Rackwitz-Fiessler iterative approach. This iterative approach is incorporated within the PSSM using the Rely routine developed by the Department of Civil Engineering at Imperial College. An outline of the Rely routine is summarised in *Appendix V*.

3.8 Engineering Risk Analysis

Now that we have a means of calculating the probability of failure for the embankment's slopes, we can consider engineering risk. Engineering risk is the product of the probability of the event (P_f) and the consequence of the event (such as the cost of dam failure, fatalities, loss of services, etc.), Eqn. (3.27), (Hartford & Baecher, 2004).

$$\text{Risk} \equiv P_f \times \text{Consequence} \tag{3.27}$$

Consequently, the dam's risk classification, subject to its current conditions, could be ascertained. Currently the Flood and Water Management Act 2010 reflects the view that dam failure is a low probability, high-consequence event.

By analysing the notional reliability and probability of failure, established using PSSM, for the upstream and downstream slopes it will be possible to ascertain the site-specific engineering risk, Eqn. (3.27), associated with specific slopes, individual limit states, etc. With respect to dam failure of small homogeneous earthfill embankment dams, it is unlikely to be a low probability, high-consequence event. Such structures could have a high probability of failure due to accumulated uncertainties due to poor and/or inconsistent monitoring and maintenance.

Furthermore, as stated by Faber and Stewart (2003: p.174) '*Risk analyses may be represented in a generic format, which is largely independent from the application or whether the risk analysis is performed in order to document that the risks associated with a given activity are acceptable or is performed to serve as a basis for a*

management decision.' Figure 3.5 presents a well-established approach to classification of the engineering risk, where the consequence of the event and the notional probability of the event are considered. As indicated in Figure 3.5, if the event probability remains constant and the consequence of the event increases, or the event probability increases and the consequence of the event remains constant, then the level of risk, in terms of its risk classification, will also change.

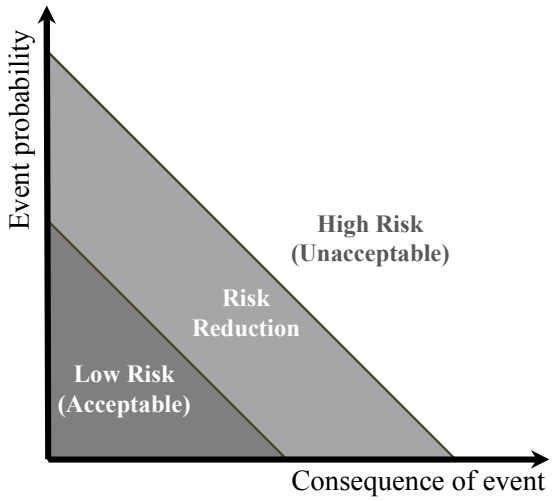

Figure 3.5 Classification of the risk targets associated with engineering risk

In the current study, the critical event is associated with structural failure of the slope. Therefore, using the outcomes of the probabilistic analysis it is possible to relate the risk classifications defined in Figure 3.5 with the engineering risk associated with upstream and downstream slope failure.

3.9 Concluding Remarks

This chapter has summarised the different forms of uncertainty that can be identified for homogeneous earthfill embankments. Different forms of probabilistic modelling have been discussed, focusing on Level 2 structural reliability analysis. The approximate analytical methods, such as First Order Reliability Method (FORM) and Second Order Reliability Method (SORM), including Monte Carlo simulations, have been identified. For the reliability analysis, the Level 2 probabilistic model has been implemented, as it satisfies the relevant requirements as well as being computationally fast and efficient.

Finally, the newly developed hybrid probabilistic slope stability model (PSSM) has been presented, which integrates the First Order Second Moment method (FOSM) into the deterministic slope stability model, for upstream and downstream slopes, outlined in the previous chapter. The failure modes associated with the structure and their limit state functions, defined by sliding block equilibrium equations, were established. The variables modelled as deterministic and probabilistic have been identified. To demonstrate the application of PSSM, a simple slope stability problem was presented and the notional reliability indices (β_D and β_U), for each failure mode, were compared with the slope's deterministic factors of safety (FoS_U and FoS_D). Furthermore, the methodology used to establish site-specific engineering risk associated with the applied limit states was also presented.

In the following chapter, the application of the newly developed methodology for a generic small homogeneous earthfill embankment dam will be demonstrated, which will encompass the aleatory uncertainties associated with the embankment's geometry, the embankment fill's soil properties and the reservoir's headwater height. This will also enable a better understanding of the notional reliability of the upstream and downstream slopes under specific conditions.

CHAPTER 4 : PROBABILISTIC SLOPE STABILITY MODEL FOR SMALL EMBANKMENT DAMS

4.1 Introduction

This chapter focuses on the implementation of the new probabilistic slope stability model (PSSM) for assessment of small homogeneous earthfill embankment dams, as described in *Chapter 3*. Here, the probabilistic model encompasses the uncertainties associated with the soil's mechanical soil properties and the embankment's geometry. Failure of the upstream and downstream slopes is defined by their failure modes (FM1 and FM2) and associated limit state functions as defined in *Chapter 3: Subsection 3.6*. From the parametric, probabilistic slope stability analysis, the reliability index (β) and probability of failure (P_f) for each failure mode, including the sensitivity factors that reflect the importance of all random variables for each limit state, will be established. This will provide a quantitative measure of the notional reliability against upstream and downstream slope failure for different embankment configurations when subjected to specific conditions.

To demonstrate the usability of PSSM, the performance level of the embankment's upstream and downstream slopes, as a function of their notional reliability, will be assessed by taking into account different slope configurations, headwater height scenarios and saturation levels of the partially saturated fill above the phreatic line. Selected soil types, with respect to their mechanical properties, will also be considered using various sources and exposed to the same dam site conditions.

The results will therefore provide a benchmark with which to compare the effect of precipitation on the reliability of the individual slopes. Thus, indicating the change, if any, in the classification of the slope's behaviour and performance level.

4.2 Slope Gradient Configurations (SG)

When carrying out the probabilistic slope stability analysis for a given soil model, soil type effectively, different embankment geometries are considered. To establish a range of embankment profiles, different slope configurations will be considered although for small earth embankments their upstream and downstream slopes must not exceed 1: 2.0 and 1: 1.75 respectively (Stephens, 2010). To establish the range of embankment profiles used in the analysis, the upstream and downstream slope gradients will vary from 1: 2.5 to 1: 4.0. Table 4.1 outlines the different configurations for the set of slope gradients applied to different embankment geometries. Figure 4.1 illustrates how these configurations influence the total base width of the embankment when its height and crest width are constant.

Table 4.1. Slope configurations for different embankment geometries (SG1 – SG13)

SLOPE GRADIENT CONFIGURATIONS (SG)				
Upstream → / Downstream ↓	1 : 2.5	1 : 3.0	1 : 3.5	1 : 4.0
1 : 2.5	SG1	SG2	SG3	SG4
1 : 3.0		SG5	SG6	SG7
1 : 3.5		SG8	SG9	SG10
1 : 4.0		SG11	SG12	SG13

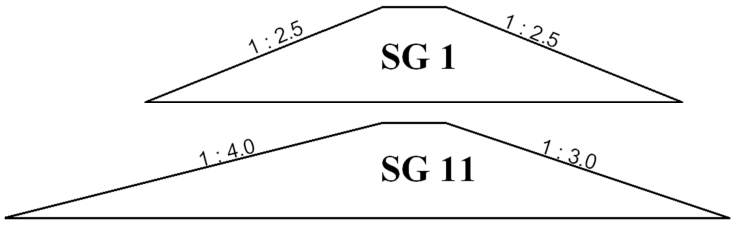

Figure 4.1 Sketch of embankment's physical model with two slope configurations: SG and SG7

4.3 Probabilistic Modelling

Unlike newer dams, where the soil materials used could be identified with respect to their hydraulic and mechanical properties, in older dams these are largely unknown. In an ideal situation, detailed data of the embankment and reservoir, including geological and geotechnical reports, review reports as well as monitoring and surveillance data could be available (Fell et al, 2000). However, when analysing older, small dams, for the majority, their data has been found to be incomplete, outdated or lost over the years since their construction. Due to the lack of available information, a degree of uncertainty arises when carrying out a slope stability analysis (Abramson et al., 2002). Therefore, in order to apply the probabilistic method, based on the slope stability model, it is required to take into account the uncertainties in the input parameters, which describe the possible failure modes (Kortenhaus et al, 2002).

4.3.1 Geometry modelling

The embankment's physical model, Figure 2.2 in *Chapter 2: Subsection 2.5*, is dependent on its height, crest width, along with the upstream and downstream slope. These variables determine the total base width of the embankment, as shown in *Chapter 2: Subsection 2.5*. However, accurately measuring the embankment's geometry is difficult to achieve, especially if the dam is still operational so, indirectly, the embankment's geometry is treated as uncertain. Thus, the embankment's height (H) and crest width (CW) are modelled as random variables using normal distribution. Furthermore, as it is difficult to accurately measure the height of the embankment's foundation (H_f), its true physical magnitude may never be known. Therefore, it will also be modelled as variable with normal distribution within the probabilistic analysis. Here the embankment's mean height and crest width are equal to 3m and 2.8m respectively (Stone, 2003), and its foundation has a mean depth of 0.5m (Creager et al., 1945a), as shown *Chapter 2*. The mean values and standard deviations of the geometry's variables are defined in Table 4.2.

Table 4.2 Probabilistic modeling of geometry parameters: Variables are normally distributed

Variable	Unit	Mean (μ)	Standard deviation (σ)
Height (H)	m	3.0	0.03
Foundation Height (H_f)	cm	50.0	1.00
Crest Width (CW)	m	2.8	0.028

By probabilistically modelling the embankment's key geometry parameters (H, CW and H_f), it will be possible to take into account any variations in the upstream and downstream slope gradients caused by:

- Localised dipping or reduction of the embankment's crest due to soil degradation.
- External erosion of the upstream slope due to rainfall washing away the surface layers of its fill into the reservoir.
- Bulging at the downstream toe and external erosion of its embankment fill.
- Improvements to the embankment's individual slopes during maintenance, repair, etc.

4.3.2 Modelling of the reservoir's headwater height

As the trajectory of the phreatic line is largely dependent on the reservoir's headwater height, when carrying out the probabilistic analysis, it is assumed the reservoir has remained at a constant level over a significant period of time (Preziosi & Micic, 2009; 2011a). However, during the dam's lifetime, the reservoir level is never truly constant due to changes to its headwater height. Small changes in its headwater height could result from:

- Sedimentation of silt in the reservoir's basin.
- Environmental effects (such as rainfall, evaporation, etc.), resulting in fluctuations in the volume of water stored by the reservoir.
- Inconsistent, and/or inaccurate measurements taken of the reservoir level by the inspecting engineer.

Larger, more visible, changes in its headwater height are more commonly associated with rapid drawdown, overtopping or flooding of the reservoir, as stated by Hughes and Hoskins (1994) and ter Horst, Jonkman and Vrijling (2006). These would initiate a

separate failure mode and are not taken into account here, as they would not sufficiently affect the position of the idealised phreatic line.

When modelling the reservoir's headwater height, van Noortwijk et al. (1999) assumed that the inner water level between two embankments had a normal distribution when determining the probability of dikes failing due to uplifting and piping. Buijs et al. (2005) also assumed that the horizontal seepage length, calculated using the water level within the reservoir, through the embankment was normally distributed. For that reason, the reservoir's headwater height will be modelled as an uncertain random variable with normal distribution. Table 4.3 shows the mean and standard deviation of three headwater height scenarios (R1, R2 and R3) considered for the, parametric, probabilistic slope stability analysis.

Table 4.3 Probabilistic modelling of three headwater heights: Variables are normally distributed

Variable	Unit	Mean (μ)	Standard deviation (σ)
Headwater height (R1)	m	1.0	0.05
Headwater height (R2)	m	1.5	0.075
Headwater height (R3)	m	2.0	0.1

These scenarios represent different operations and conditions of the dam's reservoir, and are defined as:

R1 (H_w = 1.0m) Could represent a reservoir where sedimentation has reduced its storage capacity or simply a disused reservoir.

R2 (H_w = 1.5m) Corresponds to a reservoir normally kept at half capacity.

R3 (H_w = 2.0m) Refers to the critical scenario, as it represents a reservoir at its maximum allowable capacity.

4.3.3 Modelling of the embankment fill's soil properties

It is difficult to obtain reliable, and consistent, experimental data samples for the soil properties of the embankment fill without disturbing the embankment. Therefore, probabilistic modelling of the soil parameters was developed from reported sample soils, assuming a homogeneous earthfill embankment, to account for the limitations of the statistical sample and variations at different locations across the embankment.

As outlined by Liang, Nusier and Malkawi (1999); Pumjan and Young (1999); Bhattacharya et al. (2003); Baker and Calle (2006) and Bay, J. (2008) when modelling the embankment fill's geotechnical parameters, the following soil properties are frequently treated as uncertain random variables:

- Unit weight of soil (γ)
- Cohesion (c)
- Angle of internal friction (φ)

Derived unit weights of soil (dry, moist, saturated and partially saturated), above and below the phreatic line, are directly affected by the soil's moisture content or degree of saturation, which are themselves variable between soil samples. Therefore, for modelling the unit weight of the soil within the upstream, core and downstream sections of the embankment, a factor representing the unit weight of soil (γ_{fct}) is introduced to account for variations between soil samples. It is assumed that the unit weight of soil is normally distributed, and its mean value and standard deviation are presented in Table 4.4.

As defined in the JCSS Probabilistic Model Code (Baker, Calle & Rackwitz, 2006) and by Liang, Nusier and Malkawi (1999), for any geotechnical reliability analysis, the uncertainties resulting from the unit weight, internal friction and cohesion of the soil are assumed to have normal (Gaussian) probability distribution. Pumjan and Young (1999) observed that when modelling the geotechnical strength parameters (cohesion, internal friction and density variables), cohesion and internal friction were found to be interdependent and negatively correlated. Cherubini (2000) also noted that when performing a probabilistic analysis on shallow foundations, when cohesion and internal friction were negatively correlated ($\rho_{\varphi',c'}$ = 0 to -0.75), the evaluated reliability index was higher than that obtained when the variables were uncorrelated. Therefore, the soil's internal friction (φ') and cohesion (c') are said to be normally distributed and assumed to be negatively correlated (-0.5) to reflect the linear relationship between the two variables. Their mean and standard deviations are shown in Table 4.4.

Table 4.4 Probabilistic modelling of soil properties: Variables are normally distributed

Variable	Unit	Mean (μ)	Standard deviation (σ)
Unit weight of soil factor (γ_{fct})	kN/m^2	1.0	0.1
Internal friction (φ')*	°	μ_φ	$\mu_\varphi \cdot 0.15$
Cohesion (c')*	kN/m^2	μ_c	$\mu_c \cdot 0.3$

* Negatively correlated (-0.5)

The evaluated reliability index and probability of failure of both failure modes (FM1 and FM2) will therefore assess the effect these specific uncertain soil variables have on the embankment dam's performance.

4.3.3.1 Soil types modelling the soil properties of the homogeneous embankment fill

To demonstrate how the type of soil used for the embankment fill can directly affect the notional reliability of the embankment's slopes, different soil types were selected. Here, soil models (M1 to M7), as listed in Table 4.5, were considered for the homogeneous embankment fill and exposed to the same dam site conditions. Two London Clay soil samples (M3A and M3B) are considered, in order to determine whether the applied soil model is able to capture the effect of different soil properties. As shown in Preziosi and Micic (2011a).

As the soil properties applied for London Clay were obtained from actual site investigations (Kovacevic, Potts & Vaughan, 2001; Davis et al., 2008; & Rouainia et al., 2009), it is a well-characterised soil model that could establish a benchmark for future research when effects of the embankment age, fill composition due to any deterioration or strengthening are taken into account.

Table 4.5 Soil type and applied soil properties for soil models (M1-M7)

Soil Type	Soil Model	Void ratio	Specific gravity	Cohesion	Internal friction	Saturated hydraulic conductivity
		e	Gs	c'	φ'	K_s
				(kN/m^2)	°	(cm/hr)
Alluvial Soil	M1[6]	0.600	2.67	1.0	35.0	0.02
Gault Clay	M5[7]	0.831	2.71	12.0	23.0	0.26
London Clay	M3A[8]	0.794	2.73	7.0	20.0	0.10
London Clay	M3B[9]	0.690	2.77	5.0	20.0	0.10
Lower Oxford Clay	M4[10]	0.295	2.63	10.0	24.75	0.26
Medium Silt	M7[11]	0.430	2.65	n/a	26.0	0.25
Moist Clay	M2[12]	0.487	2.72	10.0	20.0	0.02
Silty Gravely Clay	M6[13]	0.542	2.72	14.4	20.0	0.07

In general, in almost all site investigations the soil profile examined and modelled usually represents only a small fraction of the total volume of soil (White, 1993). Due to limited access to dam site data, the soil properties for the different soil models are either, derived, collated or extracted from various sources, as referenced in Table 4.5. Hence, for this analysis, the depth and distance the soil sample/samples taken at various locations across the embankment have been ignored. Thus, the probabilistic modelling of the soil properties, as listed in Table 4.5, is simplified but relevant to soils that can be found in United Kingdom. In practice, inspecting engineers would have access to real dam site, which could enable a more comprehensive characterisation of the embankment fill.

It is well known that soil type M7 (Medium Silt) is not an ideal soil for construction of homogeneous earthfill embankments. However, it has been considered for this analysis,

[6] Extracted (Gens & Alonso, 2006)
[7] Extracted (Carder & Barker, 2005)
[8] Extracted (Davis et al., 2008)
[9] Extracted (Kovacevic et al., 2001)
[10] Extracted (Reeves, Sims & Cripps, 2006)
[11] Extracted (Bell, 1992)
[12] Extracted (Smith, 1982)
[13] Extracted (Cherubini, 2000)

to demonstrate that the probabilistic slope stability model produces a viable set of reliability indices for upstream and downstream slope failure.

4.4 Parametric Studies for Generic Earthfill Embankment Dams

For the parametric, probabilistic slope stability analysis, the embankment's reliability was evaluated as a function of:

Variable slope gradients: The embankment's geometry is modified by applying the upstream and downstream slope gradient configurations (SG1 to SG13), defined in Table 4.1.

Headwater height effects: Here, the headwater height scenarios R1 to R3, defined in Table 4.3, are applied to the physical model of the embankment.

Degree of saturation: For each soil model (M1 to M7), the degree of saturation (S_r) of the partially saturated embankment fill, above the phreatic line, is varied between 56 - 59.4 %, 72.0 - 76.5 % and 86.5 - 89.8 %.

In total, 117 dam scenarios were considered for each soil model and the reliability index for the upstream and downstream slopes obtained using the PSSM. From these parametric studies, the behaviour of the embankment's slopes can be determined for varying degrees of saturation for each soil model (M1 to M7), Table 4.5, embankment geometry (SG1 to SG13), Table 4.1, and headwater height (R1, R2 and R3), Table 4.3.

To provide a point of reference with which to compare the reliability indices obtained, the following parameter codes R1SG1 - R1SG13, R2SG1 - R2SG13 and R3SG1 - R3SG13 were developed. These parameter codes provide a simple way of evaluating and comparing the reliability indices, for FM1 and FM2, obtained for each soil model. For example, soil model M1 is labelled as M1R1SG1 to M1AR1SG13 if considering only headwater height R1. The complete index of the applied parameter codes for soil models M1 to M7 are clearly tabulated in *Appendix VI*. Thus, a quantitative measure of the reliability index against upstream and downstream slope failure can be established.

4.5 Benchmarking of Probabilistic Analysis

With the recent introduction of the Flood and Water Management Act 2010, reservoir safety in England and Wales should now be carried out using a risk-based approach in order to identify whether those classified as large raised reservoirs should be categorised as high-risk (UK Statute Law Database, 2010). The implementation of the risk-based approach is a relatively new development and it is inevitable that further clarifications and amendments to the legislation could follow as it is put in practice. Most of all quantifying acceptable risk target levels can present a challenge.

To qualify the embankment's expected performance level as a relative measure of its current conditions and physical performance, one can consider different criteria. The U.S. Army Corps of Engineers (USACE) (1997) developed a set of target reliably indices (β) and associated probabilities of failure using specific data, obtained from case histories and engineering judgement for existing USA levees and by implementing basic reliability analysis (see Table I.8, *Appendix I*). However, embankments are complex structures and have many modes of failure, as summarised in Chapter 2: Subsection 2.4. Therefore, the generalization implemented by the USACE described above, while well thought-out, could be difficult to implement in practice.

For slope instability that is considered in the current research, the approach identified by USACE could be used as guidance in order to assess the effect of slope failure. Thus, a distinct classification is developed that reflects site-specific conditions and, as a result, the target reliability indices and performance levels associated with structural failure of the upstream and downstream slopes have been identified in Table 4.6. Here, the slope's performance level is a quantitative measure (reliability index), whereas its behaviour is a classification for slope management. Furthermore, different levels of engineering risk, as illustrated in Figure 3.5, corresponding probabilities of failure, and associated performance levels are included in Table 4.6.

Table 4.6 Target reliability indices (β), probabilities of failure (P_f), and associated performance levels and risk targets for structural form of failure

Target reliability index (β)	Probability of failure (P_f)	Performance level	Slope behaviour	Risk targets
$\beta > 2.5$	$P_f < 0.006$	Satisfactory	Safe (stable)	Low Risk (Acceptable)
$1.5 < \beta \leq 2.5$	$0.07 > P_f \geq 0.006$		Slope is 'vulnerable'	Risk Reduction Required
$1.0 < \beta \leq 1.5$	$0.16 > P_f \geq 0.07$	Unsatisfactory		
$\beta \leq 1.0$	$P_f \geq 0.16$	Hazardous	Failed	High Risk (Unacceptable)

As defined in Table 4.6, a reliability index greater than 2.5 indicates the slope is safe (stable) and is likely to be associated with an acceptable risk level, whereas a reliability index between 1.5 and 1.0 reflects unsatisfactory performance and a reliability index less than 1.0 signifies high risk due to complete slope failure, most likely irrespective to consequences. Here, when the slope's behaviour is classified as 'vulnerable', it indicates that risk reduction measures might be required. As Faber and Stewart (2003) pointed out engineering risk represents a measure that could be taken into account within the decision making process.

By comparing the slope's reliability index obtained using PSSM with the target reliabilities defined in Table 4.6, a point of reference is provided that can be used to compare the results for the same dam conditions when subjected to certain alternative environmental effects, such as precipitation. However, it is prudent to say that the applied target reliability indices and associated performance levels defined in Table 4.6 are notional and can only be used as a benchmark. These classifications are dependent on the complexity of the applied methodology used to model the selected failure mode and random variables, but they do represent a sample demonstration for practical implementations.

In the following subsections, 4.5.1 to 4.5.3, the reliability indices, β_{up} and β_{dwn}, for FM1 and FM2 have been extracted for selected soil models and parameter codes. Here, only soil models M3A (London Clay), M3B (London Clay), M4 (Lower Oxford Clay), M5

(Gault Clay) and M7 (Medium Silt), with comparable degrees of saturation, will be examined. To compare β_{up} and β_{dwn} between the selected soil models, the same slope configurations and headwater heights are considered. In order to monitor changes in the notional reliabilities of the different soil models, soil model M3A (London Clay) was selected as a benchmark, as its soil properties were obtained from actual dam site investigations. By analysing these results, it will be possible to quantify how different soil types, used to construct the homogeneous earthfill embankment behave under similar conditions. The complete set of reliability indices (β_{up} and β_{dwn}) for upstream (FM1) and downstream (FM2) slope failure, for all soil models (M1 to M7) are tabulated in Appendix VII.

In the following sections, extracts from the complete set of results are presented to demonstrate the procedure and the target reliabilities presented in Table 4.6 can be used as a benchmark for classifying the embankment's upstream and downstream slopes under different conditions. In addition, to the reliability indices the sensitivity factors were also collated to identify the random variables that have the significant impact on the reliability of each limit state, in this case upstream (FM1) and downstream (FM2) slope failure.

4.5.1 Performance of the embankment's slopes as a function of their slope gradient

For this parametric analysis, the reservoir's headwater height and the embankment fill's degree of saturation were kept constant and different slope configurations implemented. Slope configurations SG1 (USlope 1: 2.5, DSlope 1: 2.5), SG5 (USlope 1: 3.0, DSlope 1: 3.0) and SG13 (USlope 1: 4.0, DSlope 1: 4.0) are considered. The reliability indices (β_{up} and β_{dwn}) for both failure modes, FM1 and FM2, are shown in Figure 4.2 for M3A (London Clay), M3B (London Clay), M4 (Lower Oxford Clay), M5 (Gault Clay) and M7 (Medium Silt).

Figure 4.2 only charts the reliability indices when the critical headwater height scenario R3 (H_w = 2m) and the high degree of saturation (S_r = 86.5 - 89.8 %) of the partially saturated fill, above the phreatic line, are applied.

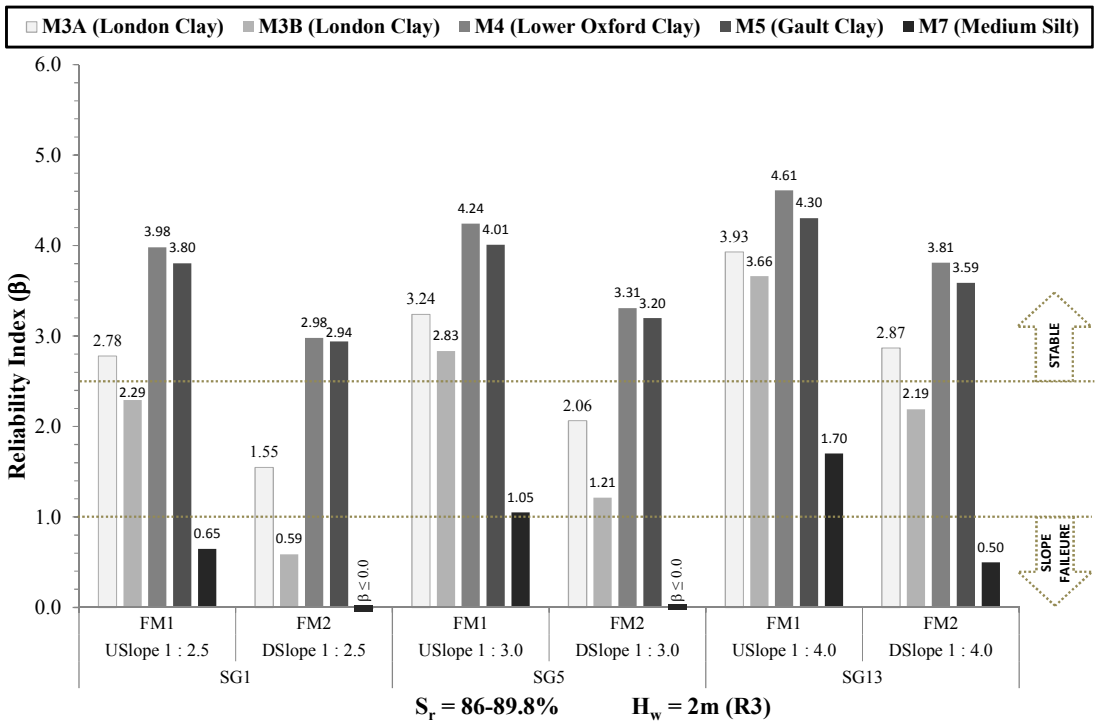

Figure 4.2 Demonstration of reliability indices for upstream (FM1) and downstream (FM2) slope failure for selected soil models with slope configurations SG1, SG5 and SG13

From the bar chart in Figure 4.2, as the upstream and downstream slope gradients become shallower for the selected soil models, there is a noticeable improvement in reliability. However, when comparing the reliability index between the individual slopes within a single slope configuration (e.g. SG5) there is a clear difference between their reliability, with the upstream slope consistently the more reliable slope. The applied probabilistic slope stability analysis therefore backs up the deterministic approach to requirements for dam design, such as those stated by Stephens (2010), and improves on this by also making it easier to take into account any variation in the slope's gradient due to external erosion, bulging at the downstream toe and other deformations.

Considering the reliability indices in Figure 4.2, for the selected soil models and slope configurations, and using the target reliability indices developed in Table 4.6 the slopes expectant behaviour and performance level can be ascertained. For this parametric analysis, $\beta = 1.0$ is selected as complete failure of the embankment's slopes, as indicated in Figure 4.2. Therefore, if the embankment were constructed of Medium Silt (M7) with slope configurations SG1 and SG5, the upstream slope is deemed hazardous ($\beta \leq 1.0 : P_f \geq 16.0$ %) and slope failure is likely to occur, whereas failure of the

downstream slope would have already occurred ($\beta \leq 0.0$), given the dam's current conditions (S_r = 86.5 - 89.8 % and H_w = 2m). If classification from Table 4.6 is applied for slope configuration SG13, the upstream slope would be classified as 'vulnerable', whereas the downstream slope has failed as its performance is deemed hazardous ($\beta \leq 1.0 : P_f \geq 16.0$ %). For soil models M3A, M4B, M4 and M5, the performance level of their embankment's upstream and downstream slopes, in terms of notional reliability, as a function of their slope gradients is quantitatively captured in Figure 4.2.

The following bar chart, Figure 4.3, shows the reliability indices obtained for slope configurations SG1 and SG4 for the same soil models selected in Figure 4.2, assuming the same critical headwater height scenario and degree of saturation. Here, the downstream slope (FM2) remains constant and only the slope gradient of the upstream slope (FM1) is changed. As the upstream slope becomes shallower, the slope's expectant behaviour and performance level clearly improve, as indicated by the increase in its notional reliability index, irrespective of the soil type. There is also a slight improvement in the downstream slope's structural reliability, even though its slope gradient is constant. However, this change does not affect its behaviour and performance if classification defined by Table 4.6 is used.

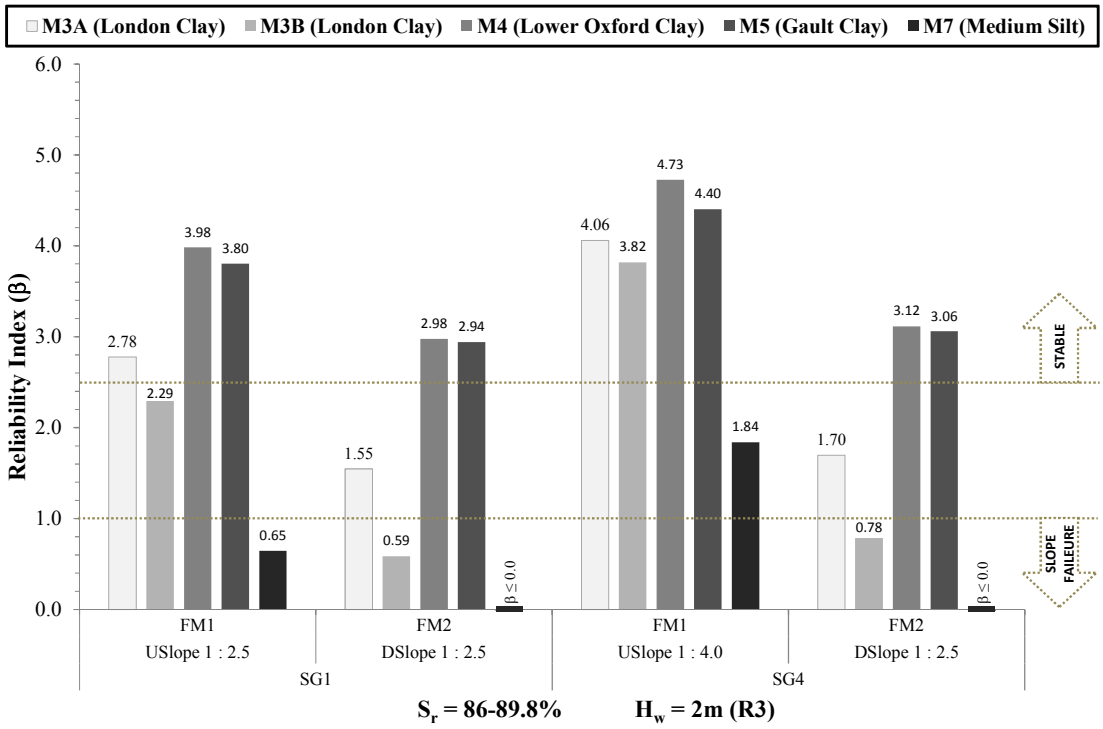

Figure 4.3 The effect of irregular slope configurations (SG1 and SG4) on the reliability indices for upstream (FM1) and downstream (FM2) slope failure, for selected soil models

To demonstrate the effect of embankment configuration, the reliability indices for slope configurations SG5 and SG11 for the same soil models as shown in Figures 4.2 and 4.3, assuming the same conditions, are considered and results presented in Figure 4.4. Here the downstream slope (FM2) is varied from 1: 3.0 to 1: 4.0 and the upstream slope (FM1) remains unchanged. The results presented indicate that there is an improvement in the behaviour and performance of the downstream slope, i.e. increase in its recorded reliability, when it has a shallower slope gradient (DSlope 1: 4.0). However, the upstream slope's performance, and slope behaviour, is unaffected. As the performance classification remains unchanged for SG5, comparison between slope configurations, such as SG5 and SG11, is feasible.

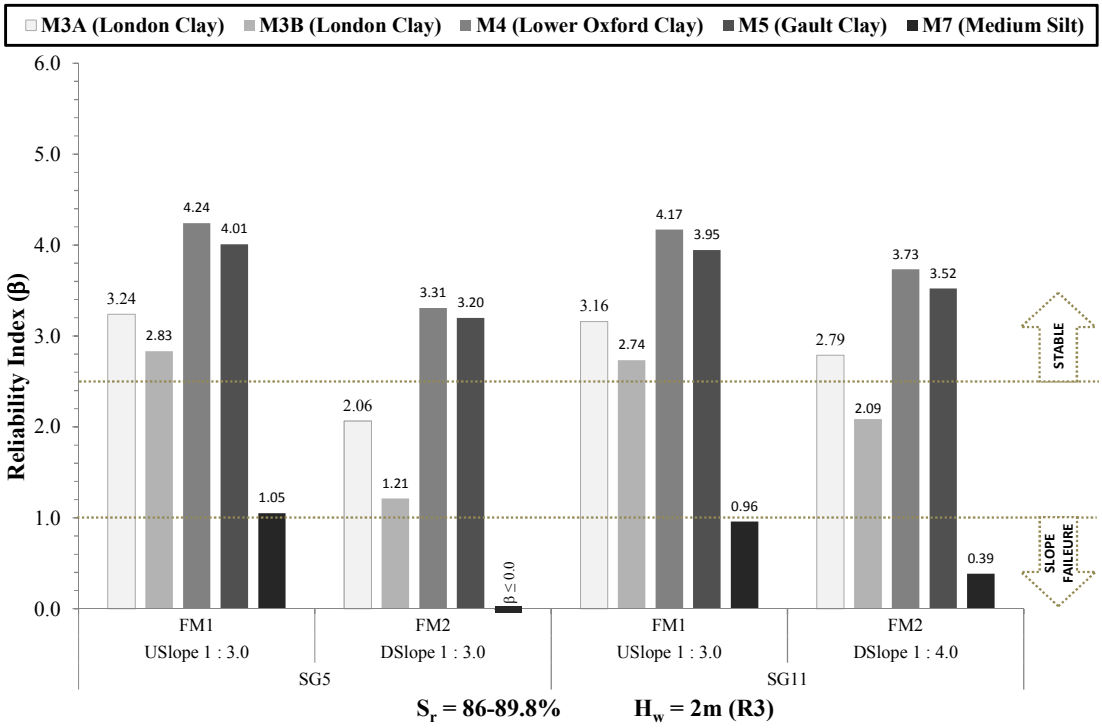

Figure 4.4 The effect on the reliability index for upstream (FM1) and downstream (FM2) slope failure when the downstream slope becomes shallower (SG5 and SG11), for selected soil models

From the complete data set showing the reliability indices (β_{up} and β_{dwn}) for failure modes FM1 and FM2 tabulated in *Appendix VII*, and for all other soil models (M1, M2 and M6), a variety of comparative analyses, as shown above, can be carried out. Thus, the embankment's geometry, specifically the total base width of the embankment that is directly dependent on its slope configuration, will affect the curvature of the phreatic line through the cross section of the embankment and associated notional reliability

index. As a result of the parametric study, the classification of the slope's behaviour and associated performance level can be established.

4.5.2 Performance of the embankment's slopes as a function of H_w effects

To understand how the reservoir's water level can influence the overall reliability of the embankment's slopes, if maintained for a significant period of time, headwater height scenarios R1 (H_w = 1.0m) and R3 (H_w = 2.0m) will be considered here. The bar charts presented in Figures 4.5 to 4.8, correspond to a specific slope configuration, in this case SG2, SG4, SG8 and SG10 respectively, and shows the reliability indices (β_{up} and β_{dwn}) for FM1 and FM2, assuming the fill's degree of saturation, above the phreatic line, is between 56 - 59.4 % for soil models M3A, M3B, M4, M5 and M7.

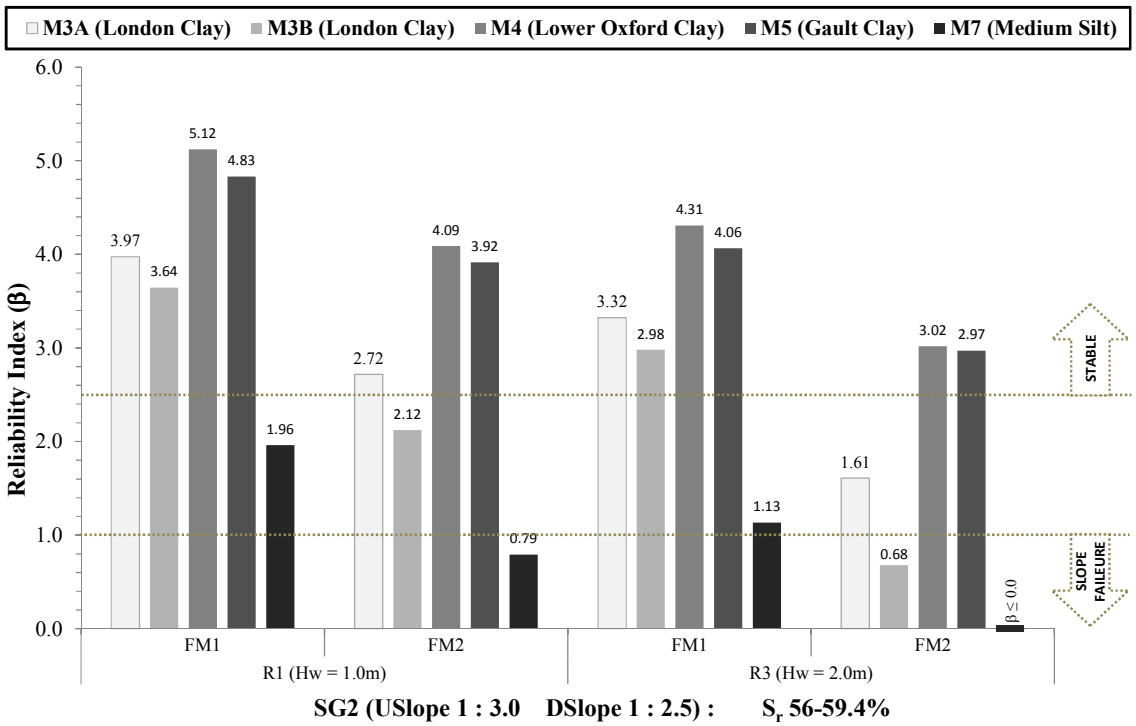

Figure 4.5 The effect of different headwater height scenarios on the reliability indices for upstream (FM1) and downstream (FM2) slope failure for slope configuration SG2

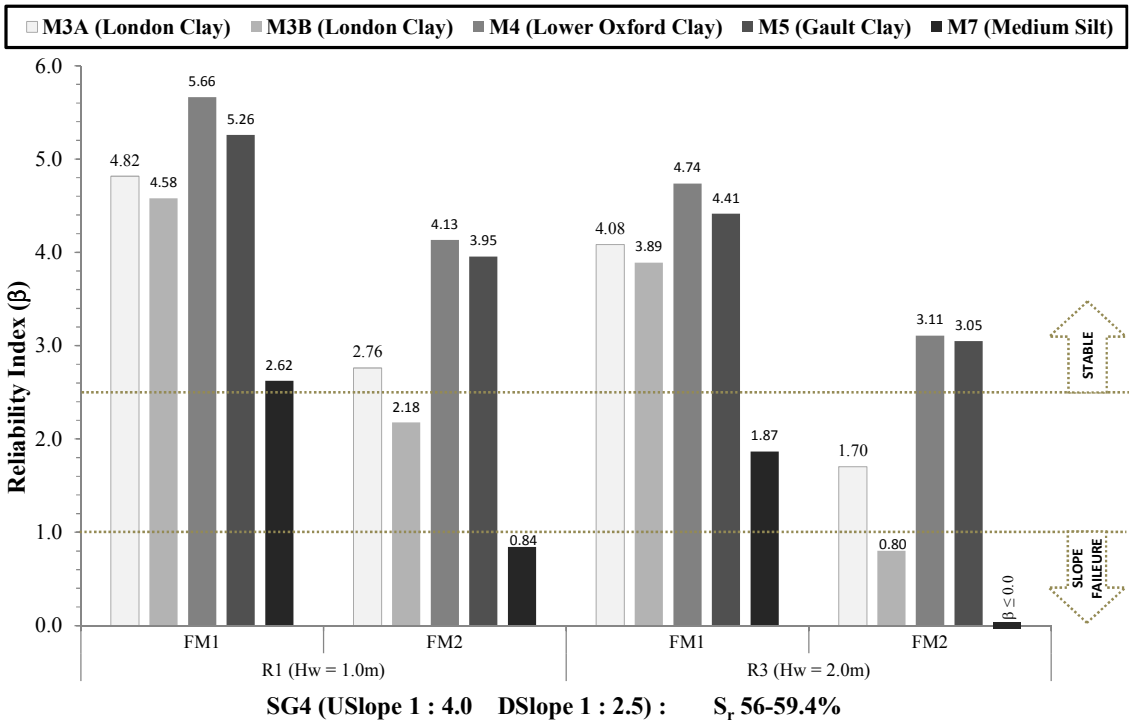

Figure 4.6 The effect of extreme headwater height scenarios on the reliability indices for upstream (FM1) and downstream (FM2) slope failure for slope configuration SG4

The results presented in Figures 4.5 and 4.6, show that when the embankment's reservoir is maintained at its maximum allowable capacity (H_w = 2.0m), scenario R3, the reliability index of the upstream and downstream slopes is noticeably lower compared to those recorded for scenario R1 (H_w = 1.0m), irrespective of the embankment's slope configuration. The bar charts also show that the reservoir's headwater height has a greater impact on the overall stability and performance of the downstream slope (FM2) compared to the embankment's upstream slope. This is primarily due to the increased trajectory of the phreatic line, defined by the steady seepage flow model, as it influences the distribution of the unit weights of the embankment fill, above and below the phreatic line, and the pore water pressures below the phreatic line.

Comparing the bar charts for slope configurations SG2 and SG4, Figures 4.5 and 4.6, when the embankment has a shallower upstream slope (USlope 1: 4.0), there is a slight improvement in the stability of both embankment slopes, as reflected by the increase in their reliability index. However, the change in the individual slope's reliability is also

dependent on the embankment fill's soil type, as demonstrated when comparing the slope's notional reliability between the selected soil models.

The following bar charts, Figures 4.7 and 4.8, compare the reliability indices for FM1 and FM2 obtained for slope configurations SG8 and SG10 for soil models M3A, M3B, M5 and M7. As demonstrated in Figures 4.5 and 4.6, the critical headwater height scenario R3 visibly reduces the reliability of both the upstream and downstream slopes. However, there is larger change in the downstream slope's structural reliability compared to only a slight decrease in the reliability of the upstream slope. Comparing the bar charts in Figures 4.5 to 4.8, the shallower the downstream slope gradient, the better it performs reducing the likelihood of slope failure occurring when the reservoir is maintained at its critical headwater height (R3).

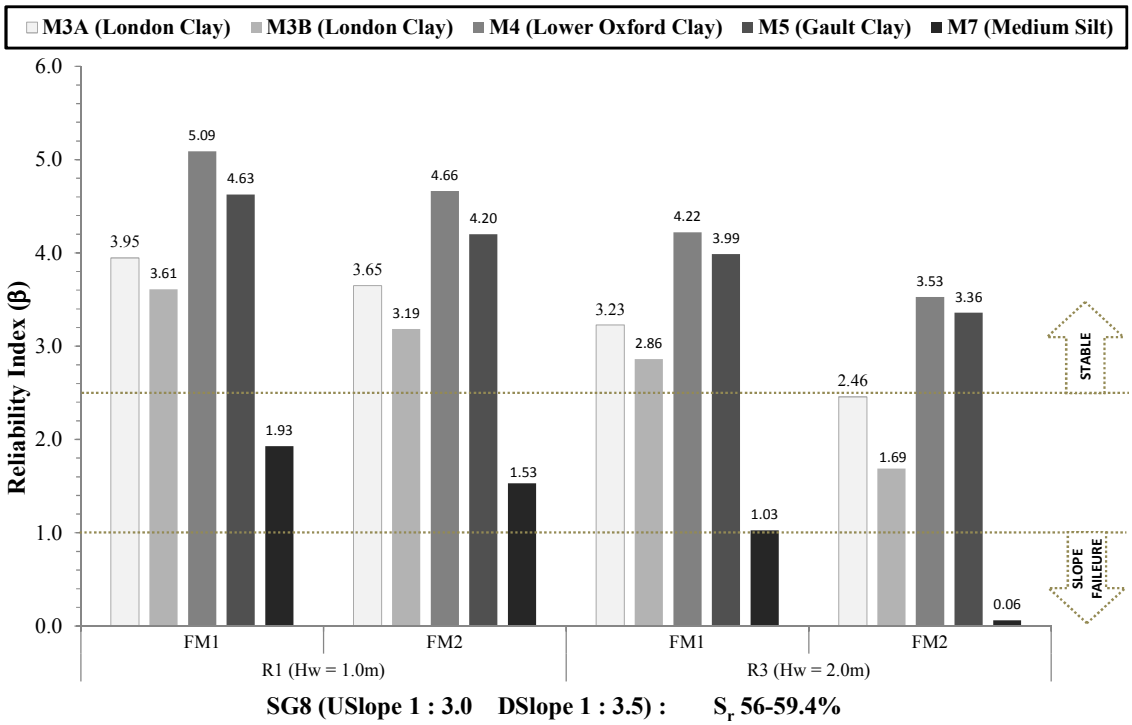

Figure 4.7 The effect of extreme headwater height scenarios on the reliability indices for upstream (FM1) and downstream (FM2) slope failure for slope configuration SG8

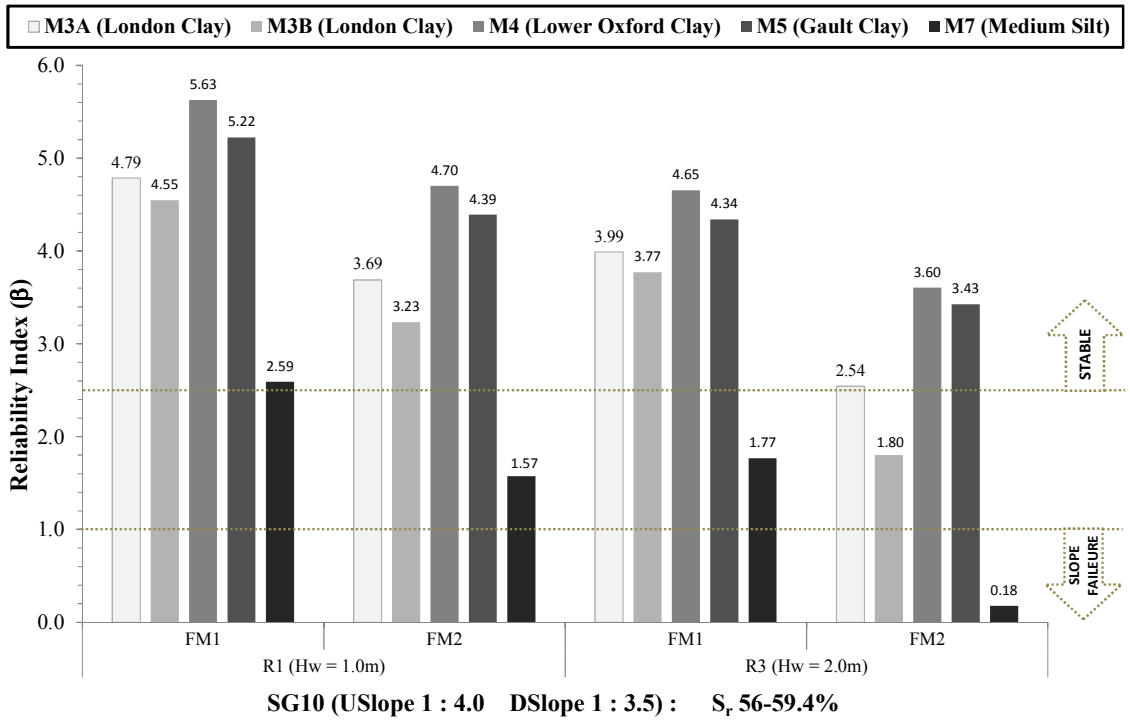

Figure 4.8 The effect of extreme headwater height scenarios on the reliability indices for upstream (FM1) and downstream (FM2) slope failure for slope configuration SG10

In conclusion, this parametric study demonstrates how the water level in the dam's reservoir, if maintained, directly affects the stability of the embankment's upstream and downstream slopes. Here, the two extreme headwater height scenarios R1 and R3 (H_w = 1m and H_w = 2m) were presented. From the reliability indices obtained for both failure modes, there will be a gradual, but small, decrease in the upstream slope's reliability, irrespective of its slope gradient. In contrast, the reservoir's headwater height and the embankment's slope configuration have a greater effect on the reliability of the downstream slope.

Similar outcomes were also observed for the other soil models (M1, M2 and M6), see results tabulated in *Appendix VII*, when comparing the same slope configurations and headwater height scenarios, assuming the same degree of saturation for the partially saturated embankment fill above the phreatic line. Thus, the performance level, in terms of the notional reliability index, indicates that the dam will have to be reassessed to ensure stability of the slopes.

4.5.3 Performance of the embankment's slopes as a function of the fills degree of saturation (S_r)

During the dam's lifetime its embankment, and reservoir, are continually exposed to changes in its surrounding environment that result in fluctuations in the degree of saturation, and the unit weight of soil, of the embankment fill's surface layers above the phreatic line. This will impact on the slope's reliability to noticeably change as the forces acting on the slopes are primarily affected by the soil's mechanical and hydraulic properties. For instance, during the winter months, the partially saturated embankment fill will have a higher degree of saturation, and unit weight of soil, compared to that recorded over the summer months.

For this parametric, probabilistic slope stability analysis, the degree of saturation (S_r) of the partially saturated embankment fill, for each soil model and slope configuration was increased from 56 - 59.4 % to 86.5 - 89.8 %. To understand how the soil's degree of saturation influences the reliability of both FM1 and FM2, headwater height scenario R3 (H_w = 2.0m) has been considered, as its represents the reservoirs maximum allowable capacity.

The following bar charts, Figures 4.9 and 4.10, refer to relatively shallow slope configurations SG5 and SG11 respectively and compare the reliability indices (β_{up} and β_{dwn}) for FM1 and FM2, for soil models M3A, M3B, M4, M5 and M7. Each bar chart shows how the soil's degree of saturation influences both upstream and downstream failure. To determine the slopes predicted performance, its reliability index was compared to the target reliability indices and associated performance levels classified in Table 4.6.

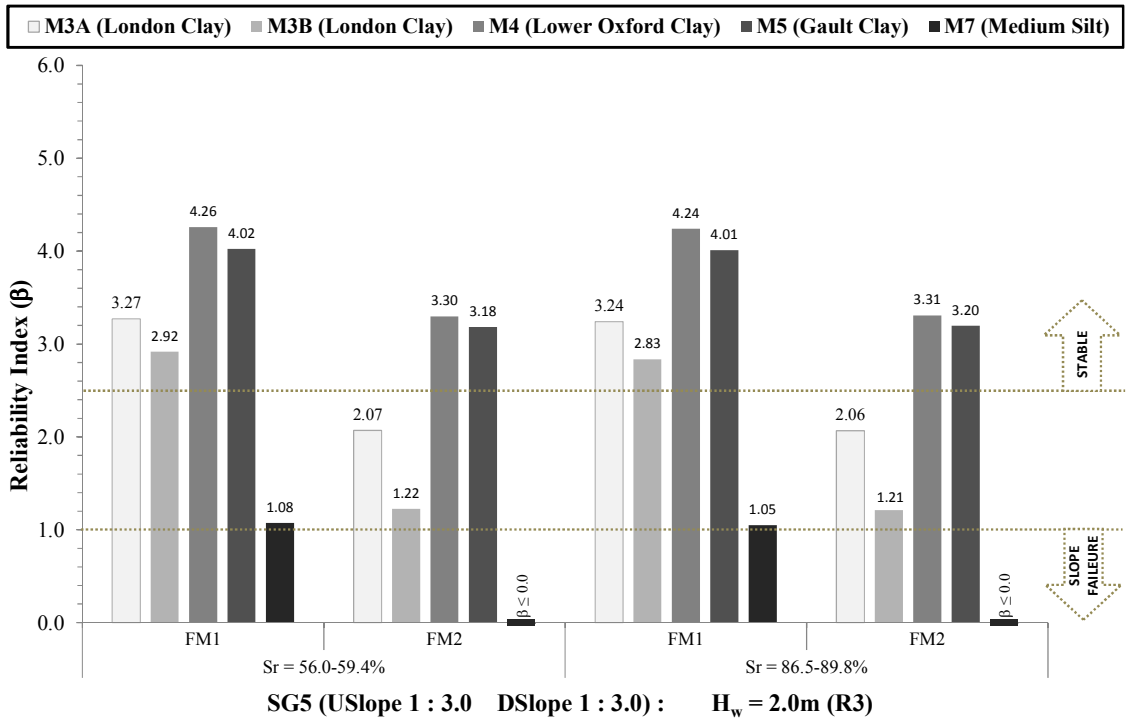

Figure 4.9 The effect of variable saturation level on the reliability for upstream (FM1) and downstream (FM2) slope failure for slope configuration SG5

Figure 4.9 shows that for the selected soil models, irrespective of their soil type and the embankment's slope configuration, there is a small change in the overall reliability of the embankment's slopes when the embankment fill above the phreatic line is deemed saturated (S_r > 80 %). Thus, using the target reliabilities presented in Table 4.6 as a benchmark, the overall classification of the individual slope's performance, and predicted slope behaviour, will remain unchanged.

Comparing the notional reliability indices recorded for FM1 and FM2, for slope configuration SG11, see Figure 4.10 below, with those presented in Figure 4.9, the same outcomes can be noticed. However, downstream failure (FM2) is less likely to occur, as it has a shallower slope gradient (DSlope 1: 4.0).

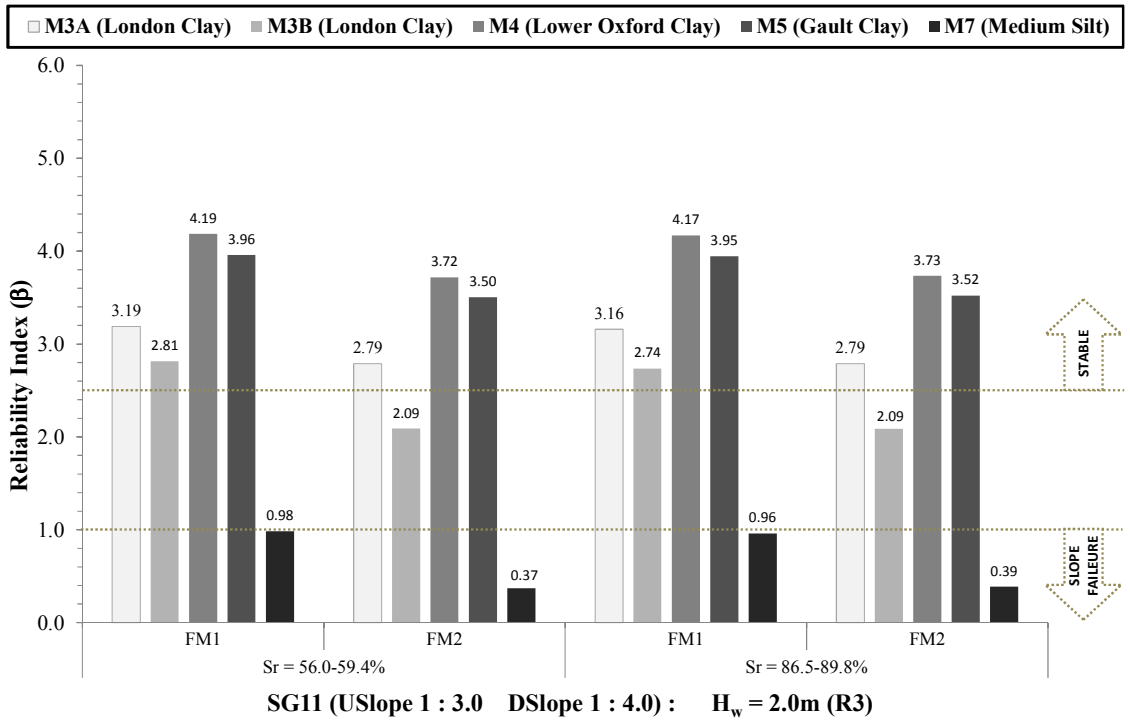

Figure 4.10 The effect of variable saturation level on the reliability for upstream (FM1) and downstream (FM2) slope failure for slope configuration SG11

Comparing the results tabulated in *Appendix VII* for the other soil models (M1, M2 and M6), for slope configurations SG5 and SG11, taking into account headwater height scenario (R3) and the same degrees of saturation (S_r = 56 - 59.4 % to 86.5 - 89.8 %) similar outcomes were observed. Therefore, comparative analyses can be carried out for all soil models (M1 to M7) to take into account alternative headwater height scenarios and slope configurations when implementing PSSM.

Thus, the slope's notional reliability and associated performance level will remain unchanged, even when the embankment fill's saturation level above the phreatic line varies. Hence, the slope's overall performance level in terms of its notional reliability can be quantitatively captured as a function of the fill's degree of saturation, as illustrated in Figures 4.9 and 4.10.

4.5.4 Summary of observations from the applied parametric studies

The parametric studies demonstrated how the probabilistic slope stability model (PSSM) is able to comprehensively capture the effect different parameters have on the notional reliability, probability of failure and associated performance level, of the embankment's upstream and downstream slopes. By applying the target reliably indices (β) and probabilities of failure (P_f), developed in Table 4.6, it was possible to classify the expectant behaviour and associated performance level of the individual slopes. For consistency within the modelling, complete failure of the embankment's slopes was said to have occurred when $\beta = 1.0$.

Comparing the soil properties for the different soil models, see Table 4.5, when the soil has a higher cohesion and/or internal friction, the overall reliability, level of performance, of the embankment's upstream and downstream slopes is noticeably improved. Furthermore, the probabilistic analyses presented for upstream and downstream slope stability provide useful information about the behaviour of slopes in the presence of site-specific uncertain factors. The notional reliability indices for the selected soil models, taking into account variable upstream and downstream slope configurations, headwater height scenarios, and the fill's degree of saturation above the phreatic line were shown to provide a quantitative measure of the likelihood of slope failure and can provide improved risk estimates for the dam.

Failure of the embankment's slopes also appear to occur independently from one another when comparing the complete set of results tabulated in *Appendix VII* for all soil models, when considering different headwater height scenarios, while varying the embankment's geometry, slope configuration effectively, and the fill's degree of saturation. As demonstrated in the parametric studies, irrespective of the fill's degree of saturation, failure of the upstream slope is less likely to occur compared to the downstream slope when comparing the results for the different soil models, which reflect different homogeneous earthfill embankments.

In the case of the embankment constructed of medium silt (M7),as expected its slopes are classified as unsatisfactory to hazardous due to their low reliability indices, especially when considering the reservoir's critical headwater height scenario (R3, H_w = 2.0m). In comparison, embankments constructed of soils such as London Clay (M3A and M3B) and Gault Clay (M5) indicate, notionally, better performance as demonstrated in the bar charts presented in Figures 4.2 to 4.10. Therefore, if the probabilistic slope stability model (PSSM) were applied to a real dam, the results obtained would enable a better evaluation of the engineering risk, subject to the dam's current status.

For this analysis, the same probabilistic model is applied throughout, however, in reality, uncertainty in the parameters will be site-specific and therefore the quantitative measures obtained would reflect genuine conditions. As the reliability indices of each failure mode are dependent on the uncertain random variables, it is important to quantify the effect each random variable has on the individual failure modes (FM1 and FM2). Therefore, by analysing both the reliability index and the sensitivity factor (α_i), Eqn. (3.19): *Chapter 3: Subsection 3.4.2.2*, of the individual variables tabulated in Tables 4.2 to 4.4, for each failure mode, it will be possible to establish a more site specific probabilistic slope stability model.

4.6 Sensitivity Factors for Three Soil Models with Identical Slope Configuration, Degree of Saturation and Headwater Height

From the probabilistic slope stability analysis, the sensitivity factors (α_i) for upstream (FM1) and downstream (FM2) failure, when slope configuration SG11 (USlope 1: 3.0, DSlope 1: 4.0) and the critical headwater height scenario (R3) are considered, were collated for soil models M3A (London Clay), M5 (Gault Clay) and M5 (Medium Silt) when their degree of saturation is varied (S_r = 56.0 - 59.4 % and 86.5 - 89.8 %). The following table, Table 4.7, shows the uncertain random variables for both limit state under the said conditions.

Table 4.7 Sensitivity factors (α_i) for all uncertain variable (defined in Tables 4.2 to 4.4) for FM1 and FM2: Comparing M3A, M5 and M7 when H_w = 2.0m and S_r = 56.0-59.4 % and 86.5-89.8%

Random Variables	SENSITIVITY FACTORS (α_i)					
	S_r = 56.0 - 59.4 %			S_r = 86.5 - 89.8 %		
	M3AR3SG11	M5R3SG11	M7R3SG11	M3AR3SG11	M5R3SG11	M7R3SG11
	FM1 (Upstream failure)					
Cohesion	0.7019	0.8028		0.5349	0.7985	
Crest Width	1.98E-07	9.07E-08	2.59E-07	1.97E-07	9.22E-08	2.15E-07
Foundation Height	1.73E-04	1.67E-04	3.47E-04	1.44E-04	1.66E-04	3.48E-04
Headwater Height	1.09E-02	8.43E-03	1.64E-02	9.71E-03	8.65E-03	1.67E-02
Height of Embankment	5.35E-05	2.09E-04	2.57E-04	4.58E-06	2.15E-04	2.68E-04
Internal Friction	6.89E-04	1.62E-02	0.9228	4.63E-02	1.42E-02	0.9224
Unit weight of Soil Factor	2.26E-02	5.12E-02	6.03E-02	5.13E-03	4.93E-02	6.03E-02
	FM2 (Downstream failure)					
Cohesion	0.7799	0.8593		0.6254	0.8534	
Crest Width	1.36E-07	1.21E-07	4.26E-07	1.72E-07	1.33E-07	4.51E-07
Foundation Height	2.16E-05	3.47E-07	2.61E-06	6.07E-06	1.26E-07	3.53E-06
Headwater Height	9.82E-03	5.29E-03	1.70E-02	9.19E-03	5.47E-03	1.70E-02
Height of Embankment	3.49E-04	4.25E-04	1.29E-03	2.50E-04	4.26E-04	1.26E-03
Internal Friction	2.40E-03	2.88E-02	0.9231	1.60E-02	2.59E-02	0.9247
Unit weight of Soil Factor	4.37E-03	1.99E-02	5.85E-02	2.13E-03	2.00E-02	5.71E-02

Least impact, Greatest impact on the reliability of the each limit state (FM1 and FM2)

By comparing the sensitivity factors, it will be possible to determine which variables have the greatest and least impact on the overall reliability and associated performance level of the upstream and downstream slopes. Including, how their level of importance is related:

- The embankment fill's degrees of saturation above the phreatic line.
- The soil models, effectively different soil types used to construct the embankment.
- Upstream (FM1) and downstream (FM2) failure for the embankment's slope configuration. In this case, slope configuration SG11.

Comparing the sensitivity factors of the variables between FM1 and FM2 for parameter codes M3AR3SG11 and M5R3SG11, there are notable changes in the order of

importance between the uncertain variables. In addition, the soil's degree of saturation also appears to have some effect on the variables order of importance, see Table 4.7. As highlighted in Table 4.7, the cohesion (c') for soil models M3A (London Clay) and M5 (Gault Clay) has the greatest impact, whereas the embankment's crest width (CW) has the lowest sensitivity factor overall. This indicates that the embankment's crest width has little or no effect on the overall stability of the individual slopes. Furthermore, for both soil models (M3A and M5) their internal friction (φ) has a higher impact on the downstream slope's reliability compared to the embankment's upstream slope.

As indicated in Table 4.7, the unit weight of soil also has a degree of importance as the distribution of the different unit weights of soil within the upstream, core and downstream sections of the embankment are modelled using the steady seepage model. This is indicated by the unit weight of soil factor (γ_{fct}) in Table 4.7. The reservoir's headwater height (H_w) also has an effect on the reliability of both failure modes as the trajectory and position of the phreatic line is dependent on the reservoir's headwater height. The remaining variables, the embankment's height (H) and foundation height (H_f), each have some degree of influence on the individual slope's reliability and there is merit in treating them as probabilistic.

The sensitivity factors also show that the height of the embankment's foundation has a slightly higher impact on upstream failure (FM1) compared to the height of the embankment. In comparison, the embankment's height is slightly more important compared to the height of the embankment's foundation when analysing the sensitivity factors for FM2. However, when the embankment fill is constructed of Gault Clay (M5), defined by M5R3SG11 in Table 4.7, and is deemed saturated (S_r = 86.5 - 89.8 %), the level of importance between the embankment's crest width and foundation height differ between the two failure modes. In this case, for FM1, the crest width has the lowest sensitivity factor whereas for FM2, it is the height of the foundation with the lower sensitivity factor.

Table 4.7 also includes the sensitivity factors for all uncertain variables obtained for FM1 and FM2 when the embankment was constructed of Medium silt (M7), indicated

by parameter code M7R3SG11. As M7 is defined as a cohesionless soil, it is the soil's internal friction (φ) that has the greatest influence on the reliability of the embankment's slopes. The variable unit weights of soil, indicated by the unit weight of soil factor (γ_{fct}), also has a much higher level of importance when comparing it to the reservoir's headwater height. Furthermore, as observed for the other soil models (M3A and M5) the impact of the embankment's crest width remains insignificant. From this probabilistic analysis, it is clear that site investigations would inevitably focus on soil properties first as the variables, which have the greatest impact on the limit state's reliability, are associated with:

- The fill's soil properties, namely, cohesion, internal friction.
- The unit weights of the soil.

However, if results such as those for Medium Silt were obtained in practice, further investigations that are more comprehensive would have to be performed, to ensure the dam was safe. Such investigations would include:

- Carrying out detailed lab and dam site tests in addition to regular site inspections to ensure the dam's long-term reliability would not be an immediate cause for concern.
- Determining whether the dam should be discontinued if no improvements to the dam site are feasible.

4.7 Concluding Remarks

The parametric studies using PSSM, for soil models M1 to M7, confirmed that it is possible to identify the performance level of the embankment's slopes, as a function of its reliability index, given the dam's current conditions. This makes it possible to prioritise monitoring or modifications so as to reduce the likelihood of upstream and/or downstream failure. Furthermore, by comparing the reliability indices (β_{up} and β_{dwn}) with the target reliability indices presented in Table 4.6, the performance level for the upstream and downstream slopes can be estimated for the different soil models prior to precipitation occurring.

By examining the sensitivity factors for each random variable, in addition to the notional reliability index, the 'leading' uncertain variables that influence the stability of the embankment's upstream and downstream slopes can be ascertained – thus providing a quantitative measure of how the notional reliability of such structures is directly affected by the embankment's design, composition and surrounding environment. As demonstrated, the soil properties of the embankment fill are the leading variables. In general, this quantitative information about sensitivity factors can be used to identify variables, which should be investigated further to update the probabilistic model reducing the uncertainty and, consequently increasing the reliability as also shown by Preziosi and Micic (2011a). It is evident that targeted site investigations would enable valuable cost control.

While the results collated from the applied probabilistic slope stability analysis are only valid within the limits set for the embankment's geometry and the soil properties assumed for the embankment fill. The results therefore provide a benchmark which will be used to analyse the effect of precipitation on the reliability of the individual slopes, and so also indicate the change, if any, in the classification of the slope's behaviour and performance level.

CHAPTER 5 : CLIMATE EFFECTS FOR ASSESSMENT OF SMALL EMBANKMENT DAMS

5.1 Introduction

Having developed the probabilistic slope stability model (PSSM) to determine the performance level of the embankment's upstream and downstream slopes, as a function of their notional reliability index, the effect of precipitation, in the form of rainfall will be investigated here. To achieve this, a new and more sophisticated deterministic slope stability model needs to be established, which incorporates explicit formulation for rainfall infiltration within the sliding block method (SBM).

Before modifying the deterministic slope stability models, derived in *Chapter 2: Subsection 2.9*, this chapter will first present a summary of the terminology used to distinguish between climate change, the Earth's global climate and their associated common climate variables. Common climate variables and climate change scenarios associated with UK climate change are identified and their current and future trends discussed. The impact that external and internal threats have on the long-term performance of small UK earthfill embankment dams is categorized and their influence on the failure modes, relating to upstream and downstream slope stability, examined. This will be accomplished by carrying out a parametric analysis and deterministically modelling precipitation associated with climate change, in the form of rainfall, as it directly affects the embankment's slope stability.

Thus, the deterministic slope stability model, which can take into account the pore water pressures that have developed in the embankment fill's newly saturated surface layers, due to the depth of infiltrated rainfall, within the sliding block formulation (SBM), are considered. The effect of precipitation and its infiltration rate through the embankment fill, as well as ponding, in the form of runoff or water that has remained on the embankment's surface will be quantified using the governing principles for infiltration.

As a result, the advanced deterministic slope stability model with precipitation (ASMP), for the upstream and downstream slopes, will be developed. Several worked examples will be presented, demonstrating how the modified deterministic slope stability model for the embankment's upstream and downstream slopes, using ASMP, is implemented.

5.2 Climate Change and Its Effect on the UK's Climate

Climate change refers to changes in the Earth's global climate or to regional climate changes over a period of time, such as those recorded within the United Kingdom (Hulme et al., 2002). Gething (2010: p.7) states that '*climate change must be regarded as an ongoing phenomenon, not a defined step change*.' This means that as the climate changes, the weather we experience both globally and regionally will also vary and can be defined in terms of day-to-day, year-to-year, season-to-season, etc. variations.

As a result, future climate change is largely uncertain and so, it represents a source of risk. It is therefore important to understand not only how the Earth's global climate is changing, but also how it directly affects the UK's climate. Hulme et al. (2002) define global climate change as the gradual warming of the earth caused by the greenhouse effect and can result from either natural or man-made causes, identified in Table 5.1 (Hulme, Turnpenny & Jenkins, 2002).

Table 5.1 Natural and man-made causes of global climate change[14]

Global Climate Change		
Natural Causes		**Man-made Causes**
Solar variation	Glacial variations	Greenhouse gases
Orbital variations	Ocean variability	Aerosols
Volcanism	Ocean and atmosphere interactions	Radioactive forcing
Seismic effects		Changes in land use

Natural causes are a result of either natural processes within the climate system or natural factors, whereas man-made causes are due to human activities that can alter both the atmosphere's composition and the earth's surface. Consequently, global climate change is more likely to be a combination of both natural and man-made causes (U.S. Environmental Protection Agency, 2008). Even though global climate change is important, local and regional climate change must be considered, as the impact of local and regional climate change differs between countries. We first briefly review how different aspects of global climate change can influence common climate variables associated with a particular country, in this case UK climate.

5.2.1 UK common climate variables

Common climate variables quantify the effects of climate in terms of its average/maximum/minimum temperature, precipitation, cloud cover etc. (Hulme et al., 2002) and are used to identify and carry out primary climate change risk assessments. Willows and Connell (2003) classified these climate variables in the form of primary, synoptic, compound and proxy climate variables. This framework has been adopted, and recommended, by Defra and the Environment Agency when carrying out a climate change risk assessment *'that includes consideration of the probability or uncertainty associated with the consequences of climate variability or climate change'* (Willows & Connell, 2003: p.70). As this research is only interested in how UK climate affects the reliability of small UK earthfill embankment dams, only the common climate variables associated with UK climate will be considered here. These are defined within the following table, Table 5.2.

[14] Table summarised using extracts from Hulme, Turnpenny and Jenkins (2002).

Table 5.2 Common climate variables specific to UK climate[15]

UK Common Climate Variables			
Primary	**Synoptic**	**Compound**	**Proxy**
Temperature	Weather types	Evapo-transpiration	Soil moisture
Precipitation	Storm tracks	Marine climate	Wave climate
Snowfall	Pressure	Relative humidity	Water run-off
Wind	Pressure gradient	Relative mist and fog	Seasonality variability
Cloud cover	Ocean/ Marine climatology	Growing season	Soil moisture
Carbon dioxide	Moisture content in the air/material/etc...		
Sea level	Lightning		

Primary variables are the principal common climate variables and are predicted using complex global and regional climate models. The synoptic climate variables are dependent on the spatial resolution of the climate models and are measured over a large domain. Compound variables are dependent on, or are a function of, one or more of the primary and/ or synoptic climate variables.

The relationship between the UK common climate variables defined in Table 5.2 are presented in Table VIII.1, *Appendix VIII*, indicating how:

- Primary variables directly affect the synoptic, compound and proxy variables.
- Synoptic variables affect the compound and proxy variables, including specific variables within its own category.
- Compound variables only affect those variables defined as proxy climate variables.

However, UK primary and synoptic climate variables are themselves directly affected by variables associated with the Earth's global climate. Table VIII.2 in *Appendix VIII* shows how the UK primary and synoptic climate variables are directly affected by the natural and man-made causes presented in Table 5.2. From the set of common climate variables associated with UK climate, specific variables are considered and their effect on the safety of small earthfill embankment dams established.

[15] Summary of UK common climate variables extracted from Willows and Connell (2003: p.23)

5.3 UK Climate Change Impacts on Small Earthfill Embankment Dam Safety

Over the years, there has been an increased interest in UK climate change issues concerning the safety of dams, as the changing climate has resulted in failure of several embankment dams (Tedd, Skinner & Charles, 2000; Hamilton-King, 2010; Charles, Tedd & Warren, 2011; Hughes & Hunt, 2012). Due to the changing climate those dams that were legally outside the Reservoir Act 1975, but are now governed by the Flood and Water Management Act 2010, and are classified as old, well-established, homogeneous earthfill embankment dams are likely to be at risk to variations associated with their embankment fill, or reservoir capacity, compared to concrete or masonry dams.

As recorded by Johnston et al. (1999) and Midttømme (2004), including incident reports published by the Environment Agency (EA), slope instability (structural failure), overtopping (hydraulic failure) and seepage failure can all be attributed to the failure of earthfill embankment dams that are influenced by variations in the surrounding environment due to climate change (Preziosi & Micic, 2009; 2011a). With respect to stability of embankment slopes, Vaughan, Kovacevic and Ridley (2002) indicate that extreme changes in the dam's surrounding environment may in some cases cause slope failure. As small homogeneous earthfill embankments are already partially saturated by design, a certain number will be more vulnerable to slope instability, due to changes in their embankment fill's physical and mechanical properties (Baxter & Hope, 2009), which governs the rate at which rainfall seeps through the embankment fill (infiltration rate).

Prior to developing a more sophisticated methodology for determining upstream and downstream slope failure, the threats associated with UK climate change scenarios must also be identified. These threats are described as *'random natural events or potential internal instability that poses a threat to the integrity of the dam'* (Babtie Group the

Centre for Ecology and Hydrology, 2002: p.13). The most important threats associated with the structural reliability of an embankment dam are:

External threat (random natural event)	⇨	Associated with both the common climate variables and potential human factors
Internal threat (potential internal instability)	⇨	Relates to the embankment's slope instability during its lifecycle

To establish the relationship between the external and internal threats and the failure modes associated with earthfill embankment dams, Table 5.3 was developed. The table clearly shows the failure modes (hydraulic, structural and leakage/seepage failures) that are directly affected by particular forms of external and internal threats.

For old, well-established earthfill embankment dams, structural, hydraulic and seepage failures are relevant. By using Table 5.3, it is possible to consider either a particular threat establishing which failure modes it affects, or identify the threats (external and internal) that influence an individual failure mode. Due to the complexity of climate change models, specific common climate variables are more relevant than others when analysing the reliability of earthfill embankment dams. Babtie Group the Centre for Ecology and Hydrology (Defra) (2003) summarised that '*embankment dams might be vulnerable to the effects of increased rainfall on their surface and that the predictions of climate change might therefore cast doubt on their future integrity.*' (p.3). This is indicated in Table 5.3, which shows the relationship between the external threat 'precipitation' and all failure modes (structural, hydraulic and seepage) associated with earthfill embankment dams. Therefore, if we select 'precipitation' from the subdivision external threat and 'embankment material (geotechnical, soil mechanics etc.)' from the internal threat, as highlighted in Table 5.3, we can see that they both directly influence slope stability of the embankment.

Table 5.3 Relationship between external and internal threats and failure modes of an earthfill embankment dam[16]

				Failure Modes														
				Hydraulic			Leakage/ Seepage	Structural										
					External Erosion								Instability					
				Overtopping	Top erosion	Gullying	Seepage through embankment fill	Embankment and/or reservoir foundation	Sliding	Reduced freeboard	Settlement	Internal erosion	Micro-instability	Slope instability	Cracking/Slough s/ Bulges/ Other irregularities	Piping	Outlet works
External Threats	Climate variables	Primary	Temperature		*	*		*			*	*	*	*	*	*	
			Precipitation	*	*	*	*	*	*	*	*	*	*	*	*	*	*
			Snowfall	*	*	*	*	*	*	*	*	*	*	*	*	*	*
			Wind	*	*	*							*	*	*		
			Cloud cover														
			Carbon dioxide		*		*					*	*		*	*	
		Synoptic	Weather types	*	*	*	*	*	*	*	*	*	*	*	*		*
			Storm tracks	*	*	*	*		*	*			*	*			*
			Pressure		*	*	*						*	*		*	
			Pressure gradient		*	*	*									*	
			Moisture content in the air /material/etc.		*	*	*	*	*		*	*	*	*	*	*	
			Lightning		*	*								*	*		
		Compound	Evapo-transpiration		*	*	*	*	*	*	*	*	*	*	*	*	*
			Relative humidity		*	*	*	*	*		*	*	*	*	*		
			Relative mist and fog														
			Growing season		*		*	*	*		*	*	*	*	*	*	*
		Proxy	Water run-off	*	*				*	*			*	*	*		*
			Season specific variables	*	*	*	*	*	*		*	*	*	*	*	*	*
	Potential Human Factors		Poor surveillance of dam		*		*	*	*						*		*
			Inadequate design of embankment and/or its reservoir				*	*	*		*	*	*	*	*	*	*
			Lack of maintenance and/or upgrading of embankment due to budget limitations		*		*	*	*	*	*	*	*	*	*	*	*
			Accidental damage to the embankment's surface		*			*	*	*	*	*	*	*	*		*
			Damage to crest due to human and/or vehicle traffic		*			*	*	*	*	*	*	*	*	*	*
			Damage to embankment due to vandalism/terrorism/etc.		*		*	*	*	*	*	*	*	*	*	*	*
Internal Threats	Internal stability		Embankment material (geotechnical, soil mechanics, etc.)	*	*	*	*	*	*		*	*	*	*	*		
			Appurtant works	*		*		*	*	*	*						

* Relationship between failure modes, external and internal threats; ■ Threats and failure mode considered.

[16] Data collated from Johnston et al. (1999); Babtie Group the Centre for Ecology and Hydrology (2002); and Willows and Connell (2003: p.23).

Considering that most external threats in Table 5.3 are uncertain, it is evident how complex the full assessment of the embankment for climate change effects would be. Therefore, we start with precipitation as the representative primary variable.

5.3.1 Common climate variable: precipitation

For clarity, only the environmental factor precipitation, in the form of rainfall, is considered as it directly influences the embankment's slope stability. A simple representation of the hydrologic cycle concerning a generic earthfill embankment, when precipitation (rainfall) occurs is shown in Figure 5.1. This cycle has no real beginning or end, as it is a continuous sequence of events.

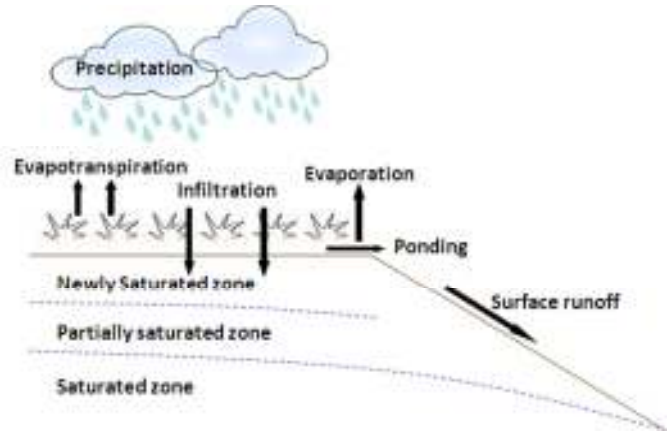

Figure 5.1 Simplistic diagram showing the hydrologic cycle relating to a generic embankment

The effect rainfall can have on an earthfill embankment can be defined as a decrease in shear strength due to an increase in pore pressure on the potential failure surface, which finally results in slope failure (Terlien, 1998). This implies that variations in the rainfall intensity and infiltration rates can change the unit weight of the embankment fill and its water content. Therefore, rainfall-induced slope failure has to be considered.

The method with which rainfall is measured is relatively straight forward, but the data collated is notoriously inaccurate and can vary in any given catchment area. The rainfall rate is also highly variable in time and space. Over the years, the effect of precipitation on earthfill embankments has been studied in detail and more sophisticated models that can be used to determine the effect of rainfall infiltration and its infiltration rate through such structures have emerged. The following subsections will present the methodologies

that will be incorporated within the deterministic slope stability models in order to determine the effect of precipitation on the stability of the embankment's slopes.

5.4 Modelling of Precipitation through the Embankment

Detailed modelling for slope instability due to variable precipitation is now presented, as the fundamental mechanisms of rainfall infiltration through unsaturated soils are still not easily understood (Ng et al., 2003). Variable precipitation is expected to have a noticeable impact on the embankment's reliability. Here, modelling of precipitation effects through the embankment fill will be characterised and the following parameters are evaluated.

- The soil's relative hydraulic conductivity (K_r) at a given depth in the embankment fill.
- The rainfall's infiltration rate (i) through the embankment fill.
- Depth of infiltrated water through the crest and slopes of the embankment.

5.4.1 Infiltration and infiltration rate

Infiltration of the water through the embankment fill is considered first. The rate at which water infiltrates through the soil is dependent on the condition of the embankment's surface and vegetation cover, and on the fill's soil properties such as its porosity, moisture content and hydraulic conductivity (Chow, Maidment & Mays, 1988; Leong, Low & Rahardjo, 1999; and McCarthy, 2006). Figure 5.2 highlights the four moisture zones and the soil moisture path within a soil profile when infiltration occurs, as illustrated by Chow, Maidment and Mays (1988).

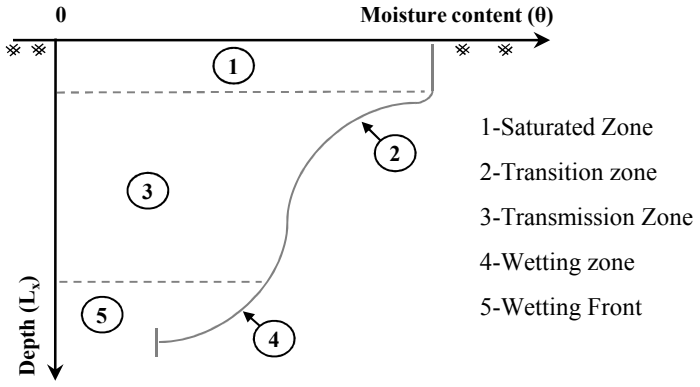

Figure 5.2 Diagram of moisture zones during infiltration

As stated by Linsley, Kohler and Paulhus (1988) and Preziosi and Micic (2011a), during rainfall the surface layers of the embankment fill become saturated causing the soil's unit weight within these layers to change. Once the water has infiltrated the soil, it advances through the fill saturating further soil layers until the phreatic line is reached, as illustrated in Figure 5.3. The amount of rainfall absorbed by the soil is dependent on the soil's hydraulic conductivity and corresponding infiltration rate, and the time until ponding occurs on the soil's surface. Furthermore, as the rainfall infiltrates the fill above the phreatic line, pore water pressures develop within the embankment fill's newly saturated surface layers, as indicated by y_1, y_2 and y_3 in Figure 5.3. Therefore, their effect will have to be included in the sliding block formulation.

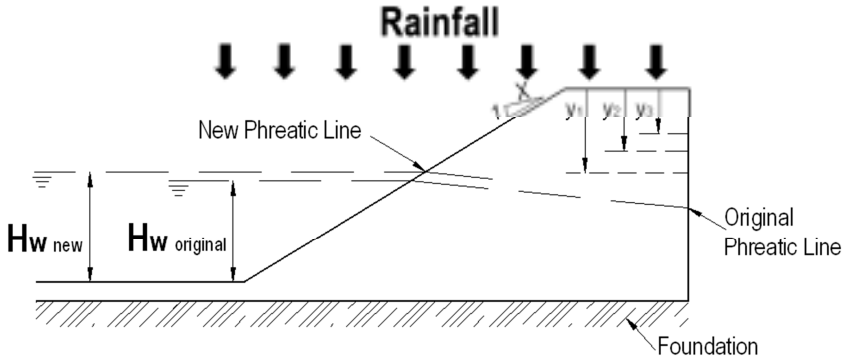

Figure 5.3 Sketch showing infiltration of water through the embankment's upstream section (y_1, y_2 and y_3 = depth of infiltrated water)

During rainfall, the soil and vegetation cover become wet as they completely absorb the initial drops of water. Once they are completely saturated, either the remaining rainfall permeates through the surface layers of the soil or runoff occurs (McCarthy, 2006). For instance, when there is a low intensity rainfall event, the soil's infiltration rate could allow all the rainfall to be absorbed by the soil in a continuous stream. In contrast, when there is a high intensity rainfall event, the impact of the raindrops tends to reorder the grains in the soil's surface, resulting in small grains being pushed into air voids between the larger grains (Potts & Zdravkovic, 2001). This in turn reduces the soil's surface permeability, causing water to collect on the soil's surface as the amount of water exceeds the rate at which the soil can absorb the water (Manning, 1987).

In the case of the dam's embankment, the rainwater will continue to percolate through the embankment fill until it reaches the phreatic line. Different types of soils allow the

water to infiltrate at different rates (Wilson, 1990). Any changes in the measure of rainfall and its infiltration rate result in variations in the depth of the wetted soil rather than a continued increase in the moisture content of the surface layers of the embankment, as illustrated in Figure 5.3. The percentage of rainfall that is absorbed by the embankment fill is dependent on the infiltration rate, measured in mm/hr, and the amount of time the water remains on the surface of the soil. Initially, the infiltration rate is highest through the partially saturated fill, but as the fill becomes saturated, the infiltration rate gradually decreases. This is a direct consequence of changes in the soil's hydraulic conductivity. In addition, as the top layers of the embankment fill become saturated, the unit weight of soil within these layers also changes. Figure 5.4 shows a simple representation of how the embankment fill is affected during rainfall.

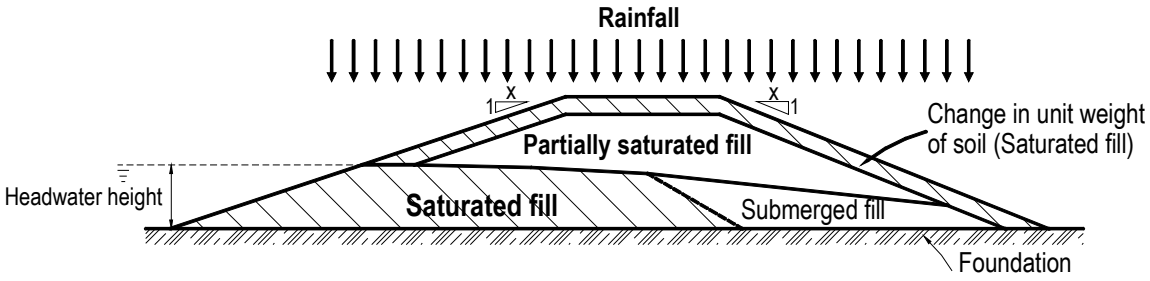

Figure 5.4 Modelling of rainfall infiltration through the surface layers of the embankment fill

Thus the soil properties of the embankment fill, hydraulic conductivity, wetting front suction head and rainfall rate that are variable and never constant (Sako, Kitamura & Fukagawa, 2006) are considered in the following text.

5.4.2 Soil-water characteristic function (SWCC)

The depth water will permeate through the soil depends to a large extent on the soil's hydraulic properties (Wang, Shao & Horton, 2003) and is represented as the wetting front. It is these hydraulic properties, which control the infiltration characteristics of the core and slopes of the embankment. Gasmo, Rahardjo and Leong (2000) state that as the soil's volumetric moisture content decreases, its wetting front suction head (ψ) increases as illustrated in Figure 5.5 for three different soil types.

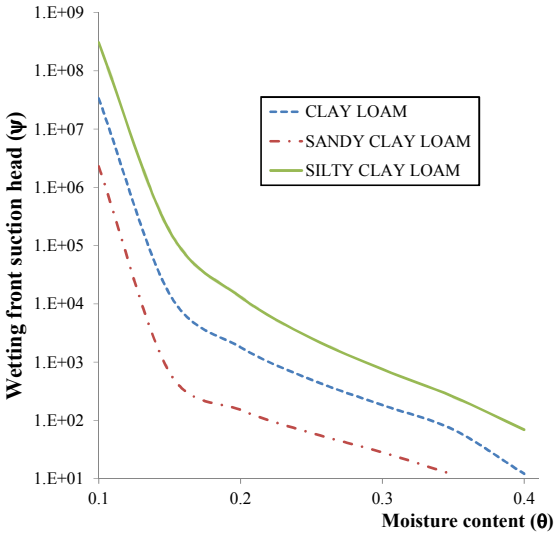

Figure 5.5 A simple representation of the SWCC graph for 3 soil types using the widely used van Genuchten method

Due to the high variability of the soil's hydraulic conductivity through the depth of the embankment, representing it as a random variable would be too significant a simplification. Thus, the soil-water characteristic curve is applied to characterise the relative hydraulic conductivity at a specific depth (function of the moisture content effectively).

The soil water characteristic curve (SWCC) can be obtained either by direct experiment or by using well-established empirical formulation. Many tests have been carried out to obtain the SWCC for different soils, under various conditions. However, even this available data must be treated carefully when applying it to the soil mode. This is largely due to the number of variables that have to be considered according to Zhou and Yu (2005):

- The type of soil, including its hydraulic and mechanical soil properties.
- The soil's initial moisture content and void ratio.
- The mineralogy and compaction of the soil.

However, when taking soil samples from the site, the data obtained may be incomplete due to the great diversity of experimental methods and the quantity of data that can be collected.

Thus, empirical models are applied to predict the unsaturated hydraulic conductivity from more easily available soil properties, e.g. saturated hydraulic conductivity and empirical fitting parameters (Zhang & van Genuchten, 1994), such as those proposed by Brooks and Corey (1964), Mualem (1976) and van Genuchten (1980) as they produce suitable analytical expressions. As a result, the wetting front suction head (ψ) and the unsaturated hydraulic conductivity (K) of the soil at varying moisture contents (θ) are established using the soil-water characteristic curve (SWCC). The ability to model this process is imperative to perform an accurate assessment of slope stability (Gavin & Xue, 2008), as direct hydraulic conductivity measurements of the soil, obtained from either laboratory or on site tests, are *'time consuming, expensive and require extensive preparation'* as indicated by Sidiropoulos and Yannopoulos (1984: p 295).

To capture the variability in the soil's hydraulic properties for the embankment model in relation to the specific moisture content, the van Genuchten method (van Genuchten, 1980) has been selected, as it is widely used due to its flexibility and simplicity (Zhou & Yu, 2005). Thus, the expressions for the unsaturated hydraulic conductivity as a function of the moisture content, also known as soil-water characteristic curve (SWCC), can be established.

5.4.3 van Genuchten method (VG)

To obtain the relative unsaturated hydraulic conductivity at a given depth, as a function of the saturated hydraulic conductivity (K_s), the effective saturation of the soil (Θ) is obtained using either of the expressions in Eqn. (5.1).

$$\Theta = \left[\frac{1}{1+(\alpha\psi)^n} \right]^m \quad \text{or} \quad \Theta = \frac{\theta - \theta_r}{\theta_s - \theta_r} \tag{5.1}$$

where: θ_s = Saturated moisture content; θ_r = Residual moisture content; θ = Measured moisture content; Θ = Effective saturation of the soil; n and α are the empirical non-dimensional fitting parameters of the soil; m is related to n as m=(1-1/n).

Subsequently the unsaturated hydraulic conductivity $K(\Theta)$, can be expressed as a function of the effective saturation of the soil, Eqn. (5.2) or, we can apply $K(\psi)$ as a

function of the soil water potential as given in Eqn. (5.3) (Philip, 1956; Jaynes & Taylor, 1984).

$$K(\Theta) = \Theta^{\frac{1}{2}}\left[1-\left(1-\Theta^{\frac{1}{m}}\right)^{m}\right]^{2} \tag{5.2}$$

$$K(\psi) = \frac{\left\{1-(\alpha\psi)^{n-1}\left[1+(\alpha\psi)^{n}\right]^{-m}\right\}^{2}}{\left[1+(\alpha\psi)^{n}\right]^{\frac{n}{2}}} \tag{5.3}$$

Hence, the soil's relative hydraulic conductivity (K_r) can be obtained, as a function of either $K(\Theta)$ or $K(\psi)$ divided by the saturated hydraulic conductivity (K_s), Eqn. (5.4).

$$K_r(\psi) = \frac{K(\psi)}{K_s} \qquad \text{or} \qquad K_r(\Theta) = \frac{K(\Theta)}{K_s} \tag{5.4}$$

To determine $K(\Theta)$ and $K(\psi)$ for soil models (M1 to M6) the fitting parameters have to be ascertained. Rawls, Brakensiek and Saxton (1982) and Carsel and Parrish (1988) both provide comprehensive information relating to specific soil types and their corresponding fitting parameters, as shown in Tables VI.1 and VI.2 in *Appendix VI*. It is these fitting parameters, which determine the shape of the SWCC (Sidiropoulos & Yannopoulos, 1984). Thus using soil specific fitting parameters the value for relative hydraulic conductivity (K_r) at specific depths is determined for partially and/or completely saturated conditions.

For this analysis, the fitting parameters provided by Carsel and Parrish (1988) were implemented, Table 5.4, as they directly relate to the van Genuchten model. Even though the derived soil properties of soil models M3A and M3B (London Clay) are variable, other authors such as Davis et al. (2008) and Rouainia et al. (2009) followed the same approach and applied the same fitting parameters so the same parameters have been adopted in this analysis.

Table 5.4 Soil water retention and hydraulic conductivity parameters for soils models M1 to M6

Soil Type	Soil Model	Saturated Hydraulic Conductivity (K_s)	Fitting parameters (van Genuchten method)		
		(cm/hr)	n	m	α
Alluvial Soil	M1[17]	0.02	1.090	0.083	0.005
Gault Clay	M5[17]	0.20	1.090	0.083	0.008
London Clay	M3A[18]	0.10	1.443	0.307	0.458
London Clay	M3B[18]	0.10	1.443	0.307	0.458
Lower Oxford Clay	M4[17]	0.20	1.090	0.083	0.008
Moist Clay	M2[17]	0.02	1.090	0.083	0.005
Silty Gravely Clay	M6[17]	0.07	1.230	0.187	0.010

While the uncertainty associated with measured saturated hydraulic conductivity is high, it will remain constant for the selected site and all corresponding applied precipitation scenarios. In this analysis, as in Chen and Young (2006) saturated hydraulic conductivity is assumed to be a, site specific, deterministic variable without undermining consistency.

As demonstrated by Cai and Ugai (2002), it is possible to connect landslides and slope failures with rainfall intensities, duration and antecedent rainfall by carrying out both deterministic and probabilistic analyses. Lee, Gofar and Raharjo (2009) also identified that carrying out a reliability analysis that can consider soil uncertainties, gives quantitative evidence to assess the stability of rainfall-induced slope failure. Once the relative hydraulic conductivity (K_r)and the wetting front suction head (ψ) are obtained for the soil's saturation level, the specific depth of rainfall infiltration through the embankment needs to be established and, therefore, the slope failure investigated as a function of realistic physical properties (Nishigaki, Tohari & Komatsu, 1999).

[17] Fitting parameters according to Carsel & Parrish (1988)
[18] Fitting parameters extracted from Davis et al. (2008) and Rouainia et al. (2009)

5.4.4 Governing principles for modelling infiltration

There are many well-established empirical methodologies, such as Horton's equation (Chow, Maidment & Mays, 1988); Philip's equation, Philip (1957); and the Green-Ampt method (Green & Ampt, 1911) that can be applied in order to quantify the infiltrated depth of water through the soil. These methods produce an analytical solution for Richard's equation developed by Richards (1931), which is the partial differential equation for infiltration in unsaturated soils for one-dimensional vertical flow (Chow, Maidment & Mays, 1988). The theory relating to Horton's and Philip's equations is summarised in *Appendix I: Subsection I.6*, as these empirical methodologies are well documented and have been widely used.

The method developed by Green and Ampt (1911) is based on actual soil types and requires estimates of the soil's hydraulic conductivity, porosity and wetting front suction head (Bedient, Huber & Vieux, 2008). The Green-Ampt method also provides a conceptual representation of the infiltration process and produces accurate analytical solutions (McCuen, 1989). Thus, it is possible to plot the cumulative infiltration of the water through the soil as a function of time. Furthermore, as stated by Cho (2009: p.33-34), '*the Green–Ampt model has received considerable attention in recent years and, although it is an approximate equation, it has been shown to have a theoretical basis, as well as measurable parameters*'.

Thus, for depth dependent relative hydraulic conductivity associated with partially saturated soil, the depth that the water has permeated for specific rainfall durations and intensities, using actual infiltration rate (i) through the soil will be quantified using the Green-Ampt method.

5.4.5 Applied Green-Ampt method (G-A)

Here, the Green-Ampt (G-A) method has been applied for the homogeneous earthfill embankment with a uniform moisture content, subject to rainfall. Figure 5.6 shows the variables required to carry out the Green-Ampt (G-A) method.

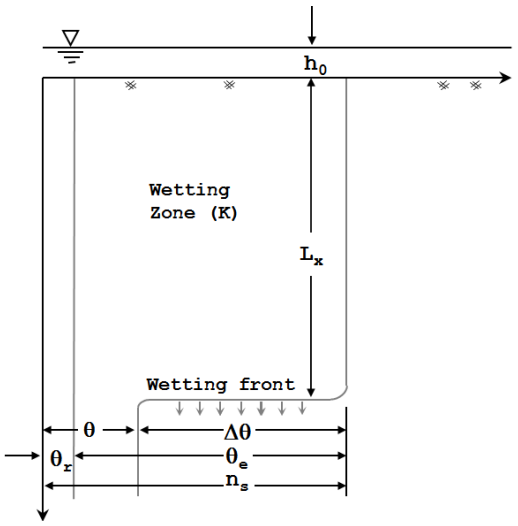

VARIABLES

n_s	Porosity
θ_e	Effective moisture content
Θ_r	Residual moisture content
θ	Measured moisture content
h_o	Depth of ponded water on the soil's surface
L_x	Depth of infiltrated water through the soil over time

Figure 5.6 Diagram identifying the variables required to carry out the G-A method

The G-A method provides an appropriate formulation for determining the depth rainfall has traversed through the embankment fill over the rainfall's duration while still taking into account the hydraulic properties of the soil and the time till ponding (t_p) occurs on the soil's surface. Ponding only occurs once the infiltration rate is greater than the infiltration capacity of the soil (Chow, Maidment & Mays, 1988). Thus, during and after ponding the surface layers of the soil become saturated causing either overtopping or surface runoff to develop. However, prior to ponding, the soil's surface layers remain unsaturated.

As the standard G-A model can only be applied to a horizontal soil surface, it cannot be used to determine the depth of water infiltrated through the embankment's slopes. To solve this problem, a modified G-A method was developed by Chen and Young (2006) who extended the standard G-A method to include sloping surfaces subjected to steady rainfall. By applying this modified G-A method, the impact the embankment's upstream and downstream slopes on the depth of water infiltrated during, and just after, a rainfall event can be modelled and accurately quantified. As with most infiltration models, the

modified G-A method also assumes the soil properties are both homogeneous and isotropic (Chen & Young, 2006).

As the embankment's crest and slopes are incorporated into the modified slope stability model, for this analysis, the standard G-A method will be applied to the crest while the modified G-A method developed by Chen and Young (2006) will be applied to both slopes to take into account the slope angle, see Table 5.5. Hence, when the modified formulation is used the depth of water infiltrated can be expressed in the direction normal to embankment's surface. As illustrated in Figure 5.4 the embankment fill, above the phreatic line, will be divided into a saturated zone, depth rainfall has traversed through the embankment fill, and an unsaturated zone which retains the initial soil profile prior to rainfall occurring.

The G-A methods must be applied in a consistent manner as illustrated in Table 5.5. Here, Case 1 refers to circumstances when all rainfall is infiltrated and ponding does not occur; Case 2 refers to situations when ponding can and will occur, where Case 2a defines conditions when all rainfall has infiltrated prior to ponding ($t < t_p$) and Case 2b denotes when ponding occurs and runoff develops ($t \geq t_p$). Table 5.5 lists the detailed expressions required to calculate the depth of infiltrated water through the crest and sloped surfaces of the earthfill embankment, bearing in mind that the results obtained using the G-A method rely on values for K_r, ψ and θ obtained above.

Table 5.5 Green-Ampt formulation implemented to determine the depth of water infiltrated through the embankment's crest and slopes, following Maidment (1993) and Chen and Young (2006) respectively

<table>
<tr><th rowspan="2">EMBANKMENT SURFACE</th><th rowspan="2">CASE 1</th><th colspan="2">CASE 2</th></tr>
<tr><th>CASE 2A
$(t < t_p)$</th><th>CASE 2B
$(t \geq t_p)$</th></tr>
<tr><td rowspan="3">CREST
(Standard G-A method applied)
 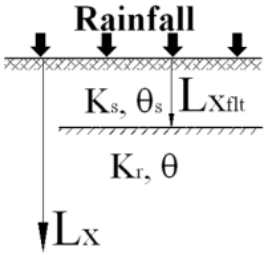
</td><td>$i_{flt} = i \leq K_r$</td><td colspan="2">$i_{flt} = i > K_r$
$F_{P_{flt}} = \frac{\psi(n_s-\theta)}{\left(i_{flt}/K_r\right)-1}$; $t_{P_{flt}} = \frac{F_{P_{flt}}}{i_{flt}}$
$t_{e_{flt}} = \frac{F_{P_{flt}}}{K_r} - \frac{\psi(n_s-\theta)}{K_s} ln\left(1+\frac{F_{P_{flt}}}{\psi(n_s-\theta)}\right)$</td></tr>
<tr><td rowspan="2">$L_{x_{flt}} = \frac{i_{flt}}{n_s-\theta}$</td><td rowspan="2">$L_{x_{flt}} = \frac{i_{flt}}{n_s-\theta}$</td><td>$t = t_{P_{flt}} - t_{e_{flt}} + \frac{F_{x_{flt}}}{K_s} - \frac{\psi(n_s-\theta)}{K_s} \ln\left(1+\frac{F_{x_{flt}}}{\psi(n_s-\theta)}\right)$</td></tr>
<tr><td>$L_{x_{flt}} = \frac{F_{x_{flt}}}{n_s-\theta}$</td></tr>
<tr><td rowspan="4">SLOPE
(Modified G-A method applied)
 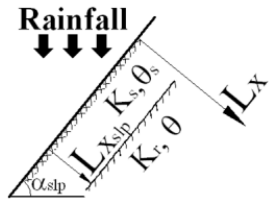
</td><td>$i_{slp} = i \cos \alpha_{slp}$
$i_{slp} \leq K_r$</td><td colspan="2">$i_{slp} = i \cos \alpha_{slp}$
$i_{slp} > K_r$
$F_{P_{slp}} = \frac{\psi(n_s-\theta)}{\left(\frac{i_{slp}}{K_r}\right)-\cos \alpha_{slp}}$; $t_{P_{slp}} = \frac{F_{P_{slp}}}{i_{slp}}$
$t_{e_{slp}} = \frac{F_{P_{slp}}}{K_r \cos \alpha_{slp}} - \frac{\psi(n_s-\theta)}{K_s \cos \alpha_{slp}} ln\left(1+\frac{F_{P_{slp}} \cos \alpha_{slp}}{\psi(n_s-\theta)}\right)$</td></tr>
<tr><td rowspan="3">$L_{x_{slp}} = \frac{i_{slp}}{n_s-\theta}$</td><td rowspan="3">$L_{x_{slp}} = \frac{i_{slp}}{n_s-\theta}$</td><td>$\left[t - \left(t_{p_{slp}} - t_{e_{slp}}\right)\right] K_s \cos \alpha_{slp} = F_{x_{slp}} - \frac{\psi(n_s-\theta)}{\cos \alpha_{slp}} ln\left(1+\frac{F_{x_{slp}} \cos \alpha_{slp}}{\psi(n_s-\theta)}\right)$</td></tr>
<tr><td>$L_{x_{slp}} = \frac{F_{x_{slp}}}{n_s-\theta}$</td></tr>
</table>

where: i_{flt}, i_{slp} = Infiltration rate for flat and sloped surfaces respectively; t = Rainfall duration; t_{pflt}, t_{pslp} = Time to surface ponding for flat and sloped surfaces respectively; t_{eflt}, t_{eslp} = Equivalent time to infiltrate a given volume of infiltration for flat and sloped surfaces respectively; F_{xflt}, F_{xslp} = Cumulative infiltration for flat and sloped surfaces respectively; F_{pflt}, F_{pslp} = Cumulative infiltration at time of ponding for flat and sloped surfaces respectively; L_{xflt}, L_{xslp} = Wetting front depth in the direction normal to the surface; α_{slp} = Slope angle

The flowchart presented in Figure 5.7 illustrates how the applied Green-Ampt methodologies, shown in Table 5.5, will be used to determine the depth rainfall has penetrated through the embankment's crest and slopes, including the time it would take for ponding to develop on the embankment's surface in the form of surface runoff or overtopping, during a specific rainfall event.

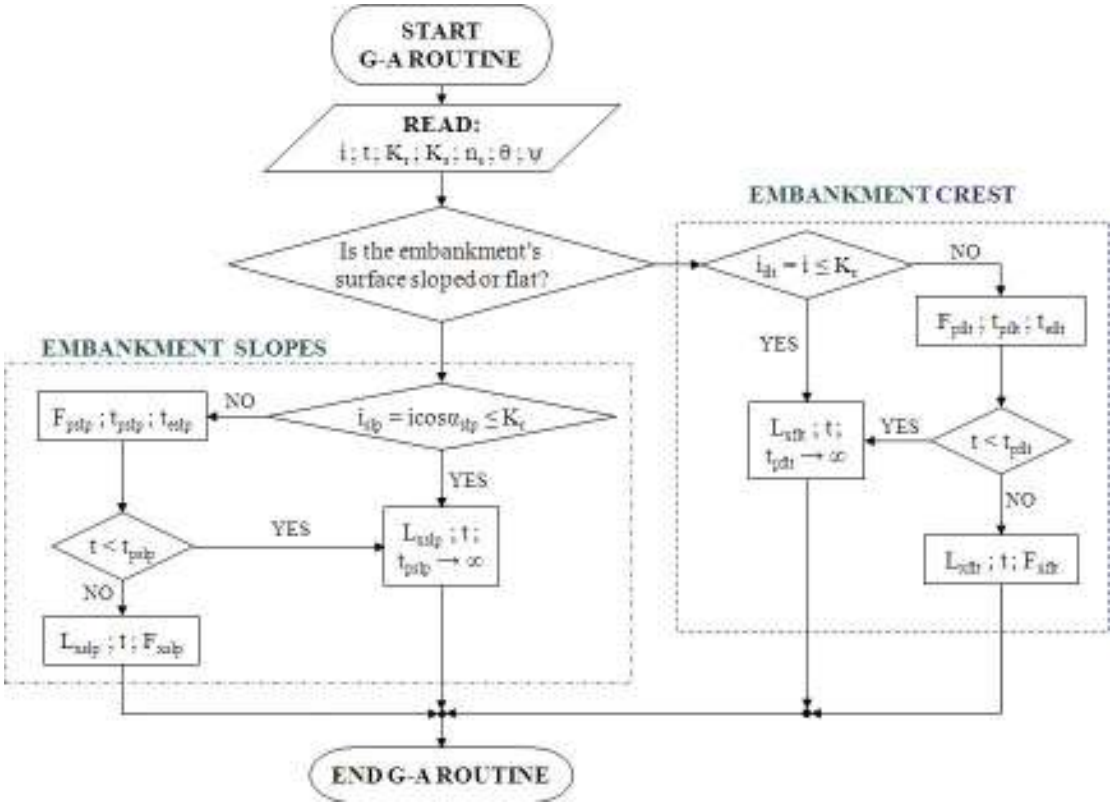

where: i_{flt}, i_{slp} = Infiltration rate for flat and sloped surfaces respectively; t = Rainfall duration; t_{pflt}, t_{pslp} = Time to surface ponding for flat and sloped surfaces respectively; t_{eflt}, t_{eslp} = Equivalent time to infiltrate a given volume of infiltration for flat and sloped surfaces respectively; F_{xflt}, F_{xslp} = Cumulative infiltration for flat and sloped surfaces respectively; F_{pflt}, F_{pslp} = Cumulative infiltration at time of ponding for flat and sloped surfaces respectively; L_{xflt}, L_{xslp} = Wetting front depth in the direction normal to the surface; α_{slp} = Slope angle.

Figure 5.7 Flowchart demonstrating the application of the applied G-A methods through the embankment's crest, upstream and downstream slopes

From the results obtained using the G-A methodologies, the infiltration rate (i) as a function of time (t) can be plotted. As sketched in Figure 5.8, Line A is produced when $i \leq K_s$, whereas when $i > K_s$ then Curves B to D are produced and over a given length of time the infiltration rate will gradually approach K_s, as indicated on the graph.

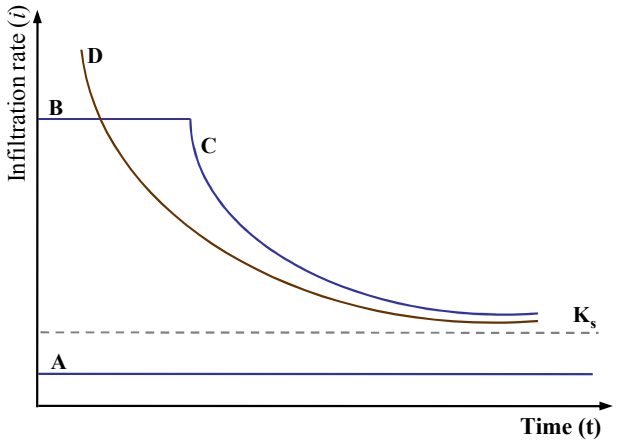

Figure 5.8 Sketch of infiltration rate as a function of time under different rainfall conditions

For the standard and modified Green-Ampt methodologies, five key assumptions have been made. These are (Bedient, Huber & Vieux, 2008):

- The soil is homogeneous and as such, the macropores and preferential migration pathways should be ignored.
- The amount of ponded water at the soil's surface is unlimited.
- A distinct and defined wetting front exists and as water infiltrates through the soil, the wetting front advances at the same rate as the depth.
- During the infiltration event, the capillary suction is uniform throughout the profile just under the wetting front and remains constant in time.
- The soil is uniformly saturated above the wetting front and the volumetric water content remains constant above and below the advancing wetting front.

The presence of ponding on the surface of the embankment's crest and slopes must also be considered, as old, well-established, small earthfill embankment dams have been subject to rainfall erosion or changes to its protective vegetation cover (Hughes & Hunt, 2012) caused by either runoff or water remaining on the embankment's surface even after the rainfall event.

However, as the embankment's physical model has a crest width of only 2.8m, the depth of ponded water on the embankment's crest and slopes will be small. Thus, we can qualify the outcomes of the standard and modified Green-Ampt methodologies as mathematical time to surface ponding (t_p) and cumulative infiltration at time of ponding (F_{pflt}, F_{pslp}).

5.5 Advanced Slope Stability Model with Precipitation Effects for Small Homogeneous Earthfill Embankment Dams

In order to assess the impact rainfall has on the stability of the embankment's upstream and downstream slopes, the standard and modified Green-Ampt methodologies, defined in Table 5.5 and summarised in Figure 5.7, coupled with the van Genuchten method were incorporated into the deterministic upstream and downstream slope stability models outlined in *Chapter 2: Subsection 2.9*. Thus, the advanced slope stability model with precipitation effects (ASMP), using sliding block formulation, was established. To take into account the increase in the fill's saturation level and the presence of pore water pressures within the newly saturated fill layers, due to the infiltrated rainfall, the embankment fill above the phreatic line is divided into two distinct zones, Figure 5.4.

Saturated zone	⇨	Embankment fill is completely saturated as rainfall infiltrates the fill's surface layers.
Partially saturated zone	⇨	Retains the original soil properties and derived unit weight of soil prior to rainfall occurring.

Once these properties are identified, the sliding block formulation (SBM) is used. For consistency within the ASMP modelling, the following assumptions have been made:

- When the depth of water infiltrated through the embankment's crest and slopes is equivalent to the average height between the embankment's surface and the calculated position of the phreatic line, the partially saturated zone is deemed completely saturated.
- The idealised phreatic line, through the foundation and cross section of the embankment, calculated using the steady seepage flow model is unaffected by the rainfall event. Hence, the soil properties and unit weights of soil in the embankment fill, below the phreatic line and in the embankment's foundation, remain unchanged.
- There is well-defined wetting front between the saturated and partially saturated zones above the phreatic line, which advances at the same rate as the depth of infiltrated water through the embankment fill's surface layers.

Consequently, if failure of the embankment's slopes occurs, it can be assumed that it is a direct result of either seepage or structural failure.

5.5.1 Slope stability model with precipitation effects (ASMP) for the upstream slope using the modified sliding block formulation

By applying the ASMP formulation, a more sophisticated upstream slope stability model has been developed, which is able to take into account the pore water pressures present within the newly saturated zone as a function of the depth of rainfall infiltration. Thus, the modified upstream slope stability model is able to capture changes in the resultant resisting and driving forces acting on the embankment's slope during a specific idealised rainfall event.

5.5.1.1 Zoning of embankment fill in the upstream slope

Firstly, the depth of infiltrated water normal to the surface of the slope during the rainfall event is established using the modified Green-Ampt method. As indicated by points *b* and *e* in Figure 5.9, there is a well-defined wetting front between the newly saturated and original partially saturated zone.

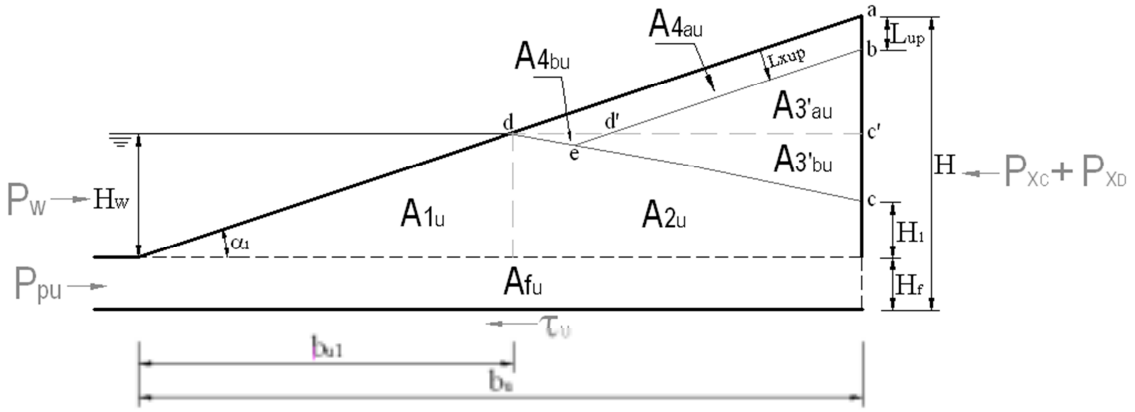

Figure 5.9 Position of the idealised phreatic line and depth of infiltrated water in the upstream slope

Once the depth of infiltrated water (L_{xup}) normal to the slope is obtained, using Eqn. (5.5) the vertical depth of infiltrated water (L_{up}), distance between points *a* and *b* in Figure 5.9, can be found. Subsequently, by amending Eqn. (2.33) to include the depth of infiltrated water (L_{up}), the average height of the partially saturated fill (H_{xU}) above the idealised phreatic line can be determined, Eqn. (5.6).

$$L_{up} = \frac{L_{x_{up}}}{\cos\alpha_1} \tag{5.5}$$

$$H_{x_U} = H - H_{av_U} - L_{up} \tag{5.6}$$

where: α_1 = Upstream slope angle; H = Embankment height; $H_{av_U} = \frac{H_w + H_1}{2}$ which is the average height of the idealised phreatic line through the upstream slope.

In order to determine the total area of the newly saturated zone (A_{4u}) and partially saturated fill (A_{3u}), indicated in Figure 5.9, a more detailed model of the area close to the phreatic line is established. By applying Eqns. (5.7 to 5.10), an approximation of the area close to the phreatic line (A_{4bu}) within the newly saturated zone can be obtained. For simplification, it has been assumed that the trajectory of the phreatic line between points *d* and *e* in Figure 5.9 becomes a straight line as the water seeps through the slope's surface.

$$bc' = (H - H_w) - L_{up} \tag{5.7}$$

$$d'c' = b_u - b_{u_1} - \left(\frac{L_{x_{up}}}{\sin\alpha_1}\right) \tag{5.8}$$

$$bd' = \sqrt{(bc')^2 + (d'c')^2} \tag{5.9}$$

$$ed' = \sqrt{\left(\frac{L_{x_{up}}}{\sin\alpha_1}\right)^2 + \left(L_{x_{up}}\right)^2} \tag{5.10}$$

where: H_w = The reservoir's headwater height.

The next step is to calculate the total area of the newly saturated embankment fill (A_{4u}), Eqn. (5.13). This is found by dividing A_{4u} into areas A_{4a_u}, Eqn. (5.11), and A_{4b_u}, Eqn. (5.12), which are bounded by points *abdd'* and points *dd'e* in Figure 5.9 respectively. Hence, A_{4u} is the sum of the two areas.

$$A_{4a_u} = L_{up} \cdot \left(\frac{L_{up} + bd'}{2}\right) \tag{5.11}$$

$$A_{4b_u} = \frac{1}{2} L_{up} \left(ed' \cdot \sin\alpha_1\right) \tag{5.12}$$

$$A_{4u} = A_{4a_u} + A_{4b_u} \tag{5.13}$$

As the area of the partially saturated fill decreases with the depth of infiltrated water, an alternate set of equations are required. Hence, by dividing the partially saturated fill into areas $A_{3'a_u}$, Eqn. (5.14), and $A_{3'b_u}$, Eqn. (5.15), bounded by points *bc'd'* and points *cc'd'* in Figure 5.9 respectively, the revised total area of the partially saturated zone ($A_{3'u}$) can be found by applying Eqn. (5.16). As the distribution of the partially saturated zone, above the phreatic line, is in reality unlikely to be so clearly differentiated as in Figure 5.9, the methodology used to determine the different zones within the embankment is the best approximation available to us. Therefore, there will be a degree of error within the ASMP formulation. However, the proposed methodology is detailed enough to determine the area close to the phreatic line and the scale of the error will be consistent for all analyses carried out using the ASMP model.

$$A_{3'a_u} = \frac{1}{2} \cdot bc' \cdot d'c' \tag{5.14}$$

$$A_{3'b_u} = A_{3u} - A_{3'a_u} - A_{4u} \tag{5.15}$$

$$A_{3'_u} = A_{3'a_u} + A_{3'b_u} \tag{5.16}$$

where: A_{3u} is the total area of the partially saturated embankment fill above the phreatic line prior to rainfall occurring, Eqn. (2.39).

5.5.1.2 Pore pressures present in the upstream slope

As the rainfall infiltrates through the surface layers of the embankment fill, the pore pressures u_{1u} (above the phreatic line), u_{2u} (below the phreatic line) and u_{3u} (within the upstream slope and its foundation) will vary. Therefore, the effect of pore pressure within the newly saturated zone has to be taken into account. This is established by dividing the pore pressure zones u_{1u} into u_{1a_u} (pore pressure present within the newly saturated zone) and u_{1b_u} (pore pressure acting through the newly saturated and partially saturated zones). By applying Eqns. (5.17 to 5.20), the change in the pore pressures u_{1a_u}, u_{1b_u}, u_{2_u} and u_{3_u} can be established. However, there will still be no hydrostatic pressure present within the partially saturated fill above the phreatic line.

$$u_{1a_u} = \gamma_w \cdot L_{up} \tag{5.17}$$

$$u_{1b_u} = \gamma_w \cdot L_{up} \tag{5.18}$$

$$u_{2u} = \gamma_w \cdot \left(H_{av_U} + L_{up}\right) \tag{5.19}$$

$$u_{3u} = \gamma_w \cdot \left(L_{up} + H_{av_U} + H_f\right) \tag{5.20}$$

where: H_{av_U} = Average height of the idealised phreatic line; H_f = Foundation height; γ_w = Unit weight of water.

5.5.1.3 Vertical effective stresses present in the upstream slope

To determine the vertical effective stresses acting on the upstream slope, the first step is to establish the vertical stresses (σ_{v1a_u} and σ_{v1b_u}) in the newly saturated and partially saturated zones, above the phreatic line, using Eqns. (5.21 and 5.22). Once σ_{v1a_u} and σ_{v1b_u} are obtained, the revised vertical stress (σ_{v2_u}), just below the phreatic line, and the vertical stress (σ_{v3_u}), acting on the entire upstream slope and its foundation, can be found by applying Eqns. (5.23 and 5.24).

$$\sigma_{v1a_u} = \gamma_{sat}(L_{up}) \tag{5.21}$$

$$\sigma_{v1b_u} = \sigma_{v1a_u} + \gamma_m(H_{x_U}) \tag{5.22}$$

$$\sigma_{v2_u} = \sigma_{v1_u} + \gamma_{sat}(H_{av_U}) \tag{5.23}$$

$$\sigma_{v3_u} = \sigma_{v2_u} + \gamma_{f_{up}}(H_f) \tag{5.24}$$

where: γ_{sat} = Saturated unit weight of soil; γ_m = Partially saturated unit weight of soil; γ_{fup} = Average unit weight of foundation (upstream).

Subsequently, by applying Eqn. (2.43), *Chapter 2: Subsection 2.9.1.2*, the vertical effective stresses (σ_{v1a_u}', σ_{v1b_u}', σ_{v2_u}' and σ_{v3_u}') are obtained, Eqns. (5.25 to 5.28).

$$\sigma_{v1a_u}' = \sigma_{v1a_u} - u_{1a_u} \tag{5.25}$$

$$\sigma_{v1b_u}' = \sigma_{v1b_u} - u_{1b_u} \tag{5.26}$$

$$\sigma_{v2_u}' = \sigma_{v2_u} - u_{2u} \tag{5.27}$$

$$\sigma_{v3_u}' = \sigma_{v3_u} - u_{3u} \tag{5.28}$$

5.5.1.4 Total passive earth pressure force (P_{pU})

In order to obtain the total passive earth pressure force (P_{pU}), acting in the same direction as the water pushing against the upstream slope, the first step is to calculate the horizontal passive earth pressure (σ_{pU}) and passive effective earth pressure (σ_{pU}'). These are found by applying the same equations defined in *Chapter 2: Subsection 2.9.1.4*, Eqns. (2.51 to 2.52). Once σ_{pU} and σ_{pU}' are established, the total passive earth pressure force (P_{pU}) can be ascertained using Eqn. (2.53), *Chapter 2: Subsection 2.9.1.4*.

5.5.1.5 Pore water pressure force (P_w)

By applying Eqn. (2.54), stated in *Chapter 2: Subsection 2.9.1.5*, the pore water pressure force (P_w), can be calculated. Thus, the force of the water acting on the slope's surface from the reservoir is ascertained.

5.5.1.6 Total active earth pressure force (P_{aU}) acting on the upstream slope

As the rainfall infiltrates through the surface layers of the embankment fill, it causes the forces acting on the upstream slope from the embankment's core (P_{XC}) and downstream slope (P_{XD}), indicated in Figure 2.9, to change. Therefore, the equations used to evaluate P_{XC} and P_{XD} prior to rainfall occurring, see *Chapter 2: Subsection 2.9.1.6*, have to be revised in order to take into account the effect of rainfall. Hence, the revised total horizontal driving force (H_U) of the upstream slope can be found.

5.5.1.6.1 Active earth pressure force (P_{XC}) from the embankment's core

For the total active earth pressure force of the core (P_{XC}), the equations used to determine the pore pressures, stresses and effective stresses in the vertical and horizontal direction are amended to include the depth water has infiltrated through the core during the rainfall event.

The vertical stresses (σ_{v1a_c}, σ_{v1b_c}, σ_{v2_c} and σ_{v3_c})

The pore pressures (u_{1a_c}, u_{1b_c}, u_{2_c} and u_{3_c})

The vertical effective stress (σ_{v1a_c}', σ_{v1b_c}', σ_{v2_c}' and σ_{v3_c}')

The horizontal effective stresses (σ_{h1a_c}', σ_{h1b_c}', σ_{h2_c}' and σ_{h3_c}')

The horizontal stresses (σ_{h1a_c}, σ_{h1b_c}, σ_{h2_c} and σ_{h3_c})

To ensure that the core's unit weights of soil, see Figure 5.10, and the pore pressures in the newly saturated and partially saturated zones, above the phreatic line, are included, the first step is to identify the depth of infiltrated water through the core's surface (L_c), Figure 5.10, using the standard Green-Ampt method.

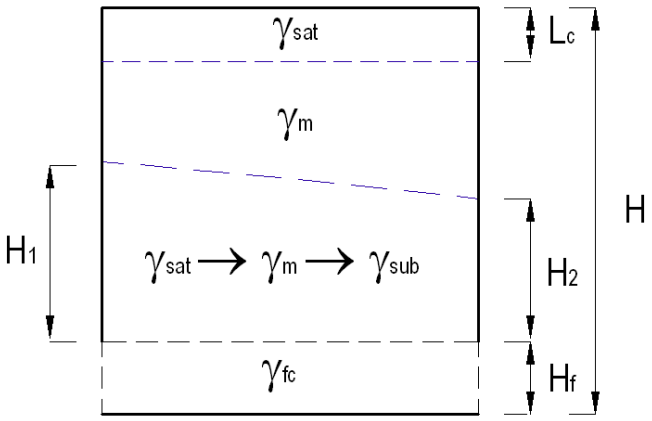

Figure 5.10 Idealised allocation of the different unit weights of soil defined in the core

Hence, the core's vertical stresses and pore pressures can be found by applying the following set of equations.

Above the phreatic line:

$$\sigma_{v1a_c} = \gamma_{sat} \cdot L_c \qquad (5.29)$$
$$u_{1a_c} = \gamma_w \cdot L_c$$

$$\sigma_{v1b_c} = \gamma_m(H - H_{av_c} - L_c) \qquad (5.30)$$
$$u_{1b_c} = \gamma_w \cdot L_c$$

Below the phreatic line:

$$\sigma_{v2_c} = \sigma_{v1_c} + \left(\frac{\gamma_{sat} + \gamma_m + \gamma_{sub}}{3}\right) H_{av_c} \qquad (5.31)$$
$$u_{2c} = \gamma_w(H_{av_c})$$

Core and foundation:

$$\sigma_{v3_c} = \sigma_{v2_c} + \gamma_{fc}(H_f) \qquad (5.32)$$
$$u_{3c} = \gamma_w(H_{av_c} + H_f + L_c)$$

where: L_c = Depth of infiltrated water through the core; $H_{av_c} = \frac{H_1+H_2}{2}$ = Average height of the idealised phreatic line through the core; H_f = Foundation height; γ_w= Unit weight of water; γ_{sat} = Saturated unit weight of soil; γ_m = Partially saturated unit weight of soil; γ_{sub} = Effective (submerged) unit weight of soil; γ_{fc} = Unit weight of foundation (core).

Thus, the core's vertical effective stresses (σ_{v1a_c}', σ_{v1a_c}', σ_{v2_c}' and σ_{v3_c}') can be found using the following set of equations.

$$\sigma_{v1a_c}' = \sigma_{v1a_c} - u_{1a_c} \qquad (5.33)$$

$$\sigma_{v1b_c}' = \sigma_{v1b_c} - u_{1b_c} \qquad (5.34)$$

$$\sigma_{v2_c}' = \sigma_{v2_c} - u_{2c} \qquad (5.35)$$

$$\sigma_{v3_c}{}' = \sigma_{v3_c} - u_{3c} \tag{5.36}$$

By applying Eqn. (2.23) defined in *Chapter 2: Subsection 2.8.2.1*, Eqns. (5.37 to 5.40) can be established and the core's horizontal effective stresses ($\sigma_{h1a_c}{}'$,$\sigma_{h1b_c}{}'$, $\sigma_{h2_c}{}'$ and $\sigma_{h3_c}{}'$) calculated.

$$\sigma_{h1a_c}{}' = \sigma_{v1a_c}{}'(K_a) - 2c'\sqrt{K_a} \tag{5.37}$$

$$\sigma_{h1b_c}{}' = \sigma_{v1b_c}{}'(K_a) - 2c'\sqrt{K_a} \tag{5.38}$$

$$\sigma_{h2_c}{}' = \sigma_{v2_c}{}'(K_a) - 2c'\sqrt{K_a} \tag{5.39}$$

$$\sigma_{h3_c}{}' = \sigma_{v3_c}{}'(K_a) - 2c'\sqrt{K_a} \tag{5.40}$$

where: K_a = Active earth pressure coefficient; c' = Cohesion of the soil.

Thus, the horizontal stresses (σ_{h1a_c}, σ_{h1b_c}, σ_{h2_c} and σ_{h3_c}) can be evaluated using Eqns. (5.41 to 5.44), derived using Eqn. (2.64) stated in *Chapter 2: Subsection 2.9.1.6.1*.

$$\sigma_{h1a_c} = \sigma_{h1a_c}{}' + u_{1a_c} \tag{5.41}$$

$$\sigma_{h1b_c} = \sigma_{h1b_c}{}' + u_{1b_c} \tag{5.42}$$

$$\sigma_{h2_c} = \sigma_{h2_c}{}' + u_{2c} \tag{5.43}$$

$$\sigma_{h3_c} = \sigma_{h3_c}{}' + u_{3c} \tag{5.44}$$

Therefore, by applying Eqns. (5.45 to 5.48), the core's individual active earth pressure forces (P_{XC1a}, P_{XC1b}, P_{XC2} and P_{XC3}) can be determined and the total active pressure force (P_{XC}) obtained, Eqn. (5.49).

$$P_{XC1a} = \frac{1}{2} \cdot \sigma_{h1a_c} \cdot L_c \tag{5.45}$$

$$P_{XC1b} = \left(\frac{\sigma_{h1a_c} + \sigma_{h1b_c}}{2} \right) \cdot \left(H - H_{av_c} - L_c \right) \tag{5.46}$$

$$P_{XC2} = \left(\frac{\sigma_{h1b_c} + \sigma_{h2_c}}{2} \right) H_{av_c} \tag{5.47}$$

$$P_{XC3} = \left(\frac{\sigma_{h2_c} + \sigma_{h3_c}}{2} \right) H_f \tag{5.48}$$

$$P_{XC} = P_{XC1a} + P_{XC1b} + P_{XC2} + P_{XC3} \tag{5.49}$$

5.5.1.6.2 Active earth pressure force (P_{XD}) from the downstream slope

Applying the same approach used to calculate P_{XC} above, the total active earth pressure force (P_{XD}) acting on the upstream slope from the downstream slope can be determined, see Figure 5.11. Therefore, the following pore pressures, stresses and effective stresses in the vertical and horizontal direction are established:

The vertical stresses (σ_{v1a_d} , σ_{v1b_d} , σ_{v2_d} and σ_{v3_d})

The pore pressures (u_{1a_d} , u_{1b_d} , u_{2_d} and u_{3_d})

The vertical effective stress (σ_{v1a_d}' , σ_{v1b_d}' , σ_{v2_d}' and σ_{v3_d}')

The horizontal effective stresses (σ_{h1a_d}' , σ_{h1b_d}' , σ_{h2_d}' and σ_{h3_d}')

The horizontal stresses (σ_{h1a_d} , σ_{h1b_d} , σ_{h2_d} and σ_{h3_d})

Before the vertical stresses and pore pressures can be found, the depth of infiltrated water normal to the slope's surface (L_{xdwn}), Figure 5.11, has to be evaluated using the modified Green-Ampt method. Once L_{xdwn} is obtained, the vertical depth of infiltrated water (L_{dwn}) can be calculated by applying Eqn. (5.50). Here, the embankment fill's unit weight of soil is classified as saturated in the newly saturated zone, partially saturated above the phreatic line and effective below the phreatic line.

$$L_{dwn} = \frac{L_{x_{dwn}}}{\cos\alpha_2} \tag{5.50}$$

where: α_2= Downstream slope angle.

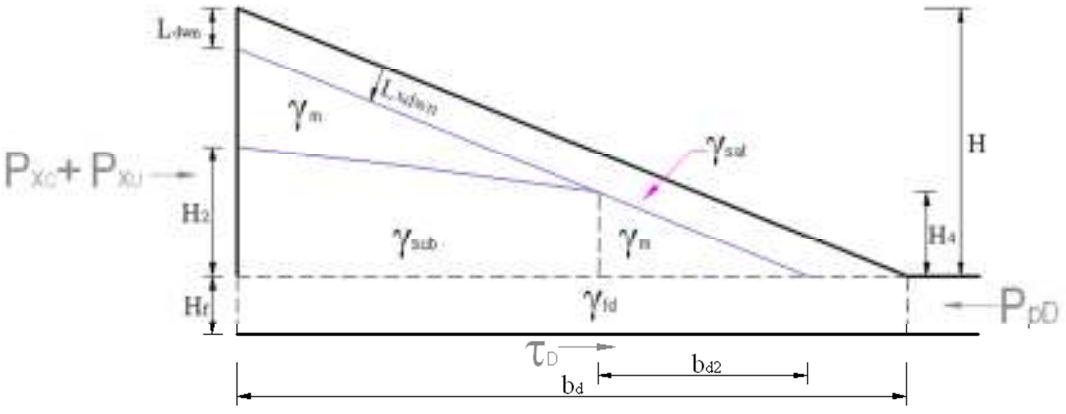

Figure 5.11 Idealised position of the phreatic line and depth of infiltrated water in the downstream slope

The next step is to determine the vertical stresses (σ_{v1a_d}, σ_{v1b_d} σ_{v2_d} and σ_{v3_d}) and pore pressures (u_{1a_d}, u_{1b_d}, u_{2_d} and u_{3_d}), by applying the following set of equations.

Above the phreatic line:

$$\sigma_{v1a_d} = \gamma_{sat} \cdot L_{dwn}$$
$$u_{1a_d} = \gamma_w \cdot L_{dwn} \quad (5.51)$$

$$\sigma_{v1b_d} = \sigma_{v1a_d} + \gamma_m \left(H - H_{av_d} - L_{dwn}\right)$$
$$u_{1b_d} = \gamma_w \cdot L_{dwn} \quad (5.52)$$

Below the phreatic line:

$$\sigma_{v2_d} = \sigma_{v1b_d} + \left(\gamma_{sub} \cdot H_{av_d}\right) + \left(\gamma_m \cdot \frac{H_4}{2}\right)$$
$$u_{2d} = \gamma_w \cdot \left(H_{av_d} + \frac{H_4}{2}\right) \quad (5.53)$$

Downstream slope and foundation:

$$\sigma_{v3_d} = \sigma_{v2_d} + \gamma_{fd}(H_f)$$
$$u_{3d} = \gamma_w \cdot \left(H_{av_d} + \frac{H_4}{2} + H_f\right) \quad (5.54)$$

where: H_4 = Height of the phreatic line between points *F* and *D′* in Figure 5.12; $H_{av_d} = \frac{H_2+H_4}{2}$ = Average height of the idealised phreatic line through the downstream slope (mean point between points *B′* and *F* in Figure 5.12); H = Height of embankment; H_f = Foundation height; γ_{fd} = Unit weight of foundation (Downstream); γ_w = Unit weight of water; γ_m = Partially saturated unit weight of soil; γ_{sub} = Effective (submerged) unit weight of soil.

Subsequently, the vertical effective stresses (σ_{v1a_d}', σ_{v1b_d}', σ_{v2_d}' and σ_{v3_d}') can be established using the following equations.

$$\sigma_{v1a_d}' = \sigma_{v1a_d} - u_{1a_d} \quad (5.55)$$

$$\sigma_{v1b_d}' = \sigma_{v1b_d} - u_{1b_d} \quad (5.56)$$

$$\sigma_{v2_d}' = \sigma_{v2_d} - u_{2d} \quad (5.57)$$

$$\sigma_{v3_d}' = \sigma_{v3_d} - u_{3d} \quad (5.58)$$

Once the vertical effective stresses have been equated, the horizontal effective stresses can be found by applying the following equations.

$$\sigma_{h1a_d}{}' = \sigma_{v1a_d}{}'(K_a) - 2c'\sqrt{K_a} \quad (5.59)$$

$$\sigma_{h1b_d}{}' = \sigma_{v1b_d}{}'(K_a) - 2c'\sqrt{K_a} \quad (5.60)$$

$$\sigma_{h2_d}{}' = \sigma_{v2_d}{}'(K_a) - 2c'\sqrt{K_a} \quad (5.61)$$

$$\sigma_{h3_d}{}' = \sigma_{v3_d}{}'(K_a) - 2c'\sqrt{K_a} \quad (5.62)$$

where K_a = Active earth pressure coefficient; c' = Cohesion of the soil.

Thus, adding the horizontal effective stresses and pore pressures together, the horizontal stresses (σ_{h1a_d}, σ_{h1b_d}, σ_{h2_d} and σ_{h3_d}) are obtained, Eqns. (5.63 to 5.66).

$$\sigma_{h1a_d} = \sigma_{h1a_d}{}' + u_{1a_d} \quad (5.63)$$

$$\sigma_{h1b_d} = \sigma_{h1b_d}{}' + u_{1b_d} \quad (5.64)$$

$$\sigma_{h2_d} = \sigma_{h2_d}{}' + u_{2d} \quad (5.65)$$

$$\sigma_{h3_d} = \sigma_{h3_d}{}' + u_{3d} \quad (5.66)$$

Finally, by applying Eqns. (5.67 to 5.70) the downstream slope's individual active earth pressure forces (P_{XD1a}, P_{XD1b}, P_{XD2} and P_{XD3}) can be determined and the total active pressure force (P_{XD}) obtained, Eqn. (5.71).

$$P_{XD1a} = \frac{1}{2} \cdot \sigma_{h1a_d} \cdot L_{dwn} \quad (5.67)$$

$$P_{XD1b} = \left(\frac{\sigma_{h1a_d} + \sigma_{h1b_d}}{2} \right) \cdot \left(H - H_{av_d} - L_{dwn} \right) \quad (5.68)$$

$$P_{XD2} = \left(\frac{\sigma_{h1b_d} + \sigma_{h2_d}}{2} \right) H_{av_d} \quad (5.69)$$

$$P_{XD3} = \left(\frac{\sigma_{h2_d} + \sigma_{h3_d}}{2} \right) H_f \quad (5.70)$$

$$P_{XD} = P_{XD1a} + P_{XD1b} + P_{XD2} + P_{XD3} \quad (5.71)$$

5.5.1.7 Total horizontal driving force (H_U) acting on the upstream slope

As defined in *Chapter 2: Subsection 2.9.1.7*, by applying Eqn. (2.88), the total horizontal driving force (H_U) can be calculated by subtracting the total active earth pressure forces from the core and downstream slope (P_{XC} and P_{XD}) with the total passive earth pressure force (P_{pU}) and the pore water pressure force (P_w).

5.5.1.8 Total vertical effective stress (σ_{vu}') acting on the upstream slope

In order to calculate the total vertical effective stress (σ_{vu}'), acting through the upstream slope, the total effective weight of the slope (ω_{eu}), which is dependent on the total area of the slope's embankment fill and corresponding unit weights of the soil is established. This is equal to the vertical stress (σ_{Fu}), including the pore pressure acting in the vertical direction (u_{vu}). As the upstream slope's surface layers are affected by the depth water will have infiltrated through its embankment fill, the first step is to establish the slope's individual effective weights (ω_{eu1a}, ω_{eu1b}, ω_{eu2} and ω_{eu3}) by applying Eqns. (5.72 to 5.75). Thus, the slope's total effective weight (ω_{eu}) can be found, Eqn. (5.76).

Above the phreatic line:

$$\omega_{eu1a} = \gamma_{sat}(A_{4u}) \tag{5.72}$$

$$\omega_{eu1b} = \gamma_{m}(A_{3'u}) \tag{5.73}$$

Below the phreatic line:

$$\omega_{eu2} = \gamma_{sat}(A_{1u} + A_{2u}) \tag{5.74}$$

In the foundation:

$$\omega_{eu3} = \gamma_{fd}(A_{fd}) \tag{5.75}$$

$$\omega_{eu} = \omega_{eu1a} + \omega_{eu1b} + \omega_{eu2} + \omega_{eu3} \tag{5.76}$$

The next step is to calculate the total vertical effective stress (σ_{vu}'), Eqn. (2.94) in *Chapter 2: Subsection 2.9.1.8*. This is found by subtracting the total vertical stress (σ_{Fu}) with the pore pressure (u_{vu}) acting in the vertical direction of the upstream slope, Eqn. (2.93) in *Chapter 2: Subsection 2.9.1.8*, and then dividing by the width of the base of the upstream slope (b_u). Thus, the total vertical effective shear stress (τ_U') and resultant shearing force (R_U) for the upstream slope can be evaluated.

5.5.1.9 Resultant shearing force (R_U)

The resultant shearing force (R_U) is simply calculated in terms of the total effective shear stress (τ_U') and the total width of the base of the upstream slope (b_u).

$$R_U = \tau_U' \cdot b_u \tag{5.77}$$

where: $\tau_U' = \sigma_{vu}' \tan\varphi' + c'$

5.5.1.10 Factor of safety (FoS_U) of the upstream slope

From Eqn. (2.30), *Chapter 2: Subsection 2.9*, the upstream slope's factor of safety can therefore be established by dividing the total resultant shearing force (R_U) by the slope's horizontal driving force (H_U).

5.5.2 Slope stability model with precipitation effects (ASMP) for the downstream slope using the modified sliding block formulation

In order to capture the effect a specific rainfall event has on the downstream slope's factor of safety (FoS_D), a more sophisticated downstream slope stability model has been developed by applying the ASMP formulation. Here, the modified slope stability model, Figures 5.11 and 5.12, is noticeably different to the downstream slope stability model illustrated in Figure 2.12, *Chapter 2: Subsection 2.9.2*. This is due to the toe and surface layers of the downstream slope becoming saturated and pore water pressure developing within the newly saturated zone, as a function of the depth of infiltrated water normal to the slope's surface. Thus, the modified slope stability model is able to capture changes in the resultant resisting and driving forces acting on the embankment's slope during a specific rainfall event and the likelihood of downstream slope failure occurring can be evaluated.

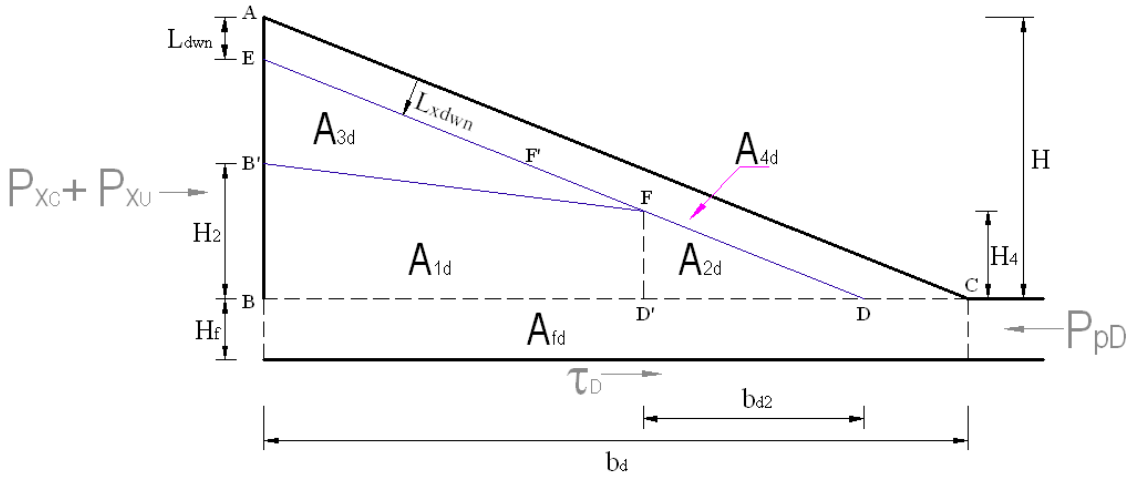

Figure 5.12 Modified downstream slope stability model

5.5.2.1 Zoning of embankment fill in the downstream slope

Figure 5.12 shows the depth of infiltrated water normal to the slope's surface (L_{dwn}), evaluated using the modified Green-Ampt method, and the idealised position of the phreatic line through the downstream slope. As the water infiltrates through the surface layers of the downstream slope, the total horizontal projection (d) of the phreatic line and the height of the phreatic line (H_4) will change as the depth of infiltrated water increases. Therefore, the distance 'a' on the surface of the downstream slope is now measured between points *F* and *D* in Figure 5.12, as the wetting front advances at the same rate as the depth of infiltrated water. Hence, distance 'a' is found by first calculating the distance d_F, Eqn. (5.78), which is the revised horizontal projection of the phreatic line, taking into account the depth of infiltrated water (L_{dwn}) through the downstream slope, and then applying Eqn. (5.79).

$$d_F = \left[b_u + CW + \left(b - L_{dwn} \right) \right] - \left(S - S' \right) \tag{5.78}$$

$$a = \frac{d_F}{\cos \alpha_2} - \sqrt{\frac{d_F^{\,2}}{\cos^2 \alpha_2} - \frac{H_w^{\,2}}{\sin^2 \alpha_2}} \tag{5.79}$$

where: S = The horizontal projection of the wetted upstream slope, Eqn. (2.7) in *Chapter 2: Subsection 2.6.1*; S' = The horizontal distance, Eqn. (2.8) in *Chapter 2: Subsection 2.6.1*; α_2 = Downstream slope angle.

The height of the phreatic line (H_4) is measured at the point where the phreatic line intersects the newly saturated fill, point *F* in Figure 5.12, and is calculated using Eqn. (2.97) defined in *Chapter 2: Subsection 2.6.1*. Thus, the average height (H_{avd}) of the phreatic line, Eqn. (2.99) in *Chapter 2: Subsection 2.6.1*, will also change in the downstream slope.

Here, the downstream slope and its foundation have been divided into areas A_{1d} to A_{4d} and A_{fd}, see Figure 5.12. However, further dimensions are required to calculate areas A_{1d} to A_{4d}. These are found using the coordinates defined in Figure 5.12 and by applying Eqns. (5.80 to 5.82).

$$BD = b_d - \frac{L_{x_{dwn}}}{\cos \alpha_2} \tag{5.80}$$

$$ED = \sqrt{\left(BD\right)^2 + \left(H - L_{dwn}\right)^2} \tag{5.81}$$

$$B'F' = \left(\frac{H_2}{H - L_{dwn}}\right) \cdot BD \tag{5.82}$$

The area of the newly saturated fill (A_{4d}), the areas above (A_{3d}) and below (A_{1d} and A_{2d}) the phreatic line, and the area of the slope's foundation (A_{fd}) are determined using Eqns. (II.26 to II.29) in *Appendix II: Subsection II.2.1*.

5.5.2.2 Pore pressures, vertical stresses and vertical effective stresses present in the downstream slope

Using the same set of equations defined in *Subsection 5.5.1.6.*2, the vertical stresses ($\sigma_{v1a_d}, \sigma_{v1b_d}$ σ_{v2_d} and σ_{v3_d}), pore pressures ($u_{1a_d}, u_{1b_d}, u_{2_d}$ and u_{3_d}), and vertical effective stresses ($\sigma_{v1a_d}', \sigma_{v1b_d}'$, σ_{v2_d}' and σ_{v3_d}') present in the downstream slope are obtained. The vertical stresses (σ_{v1a_u} and σ_{v1b_u}) and pore pressures (u_{1a_d} and u_{1b_d}) present above the phreatic line are calculated by applying Eqns. (5.51 and 5.52), whereas the vertical stress (σ_{v2_u}) and pore pressure (u_{2_d}) present below the phreatic line are found using Eqn. (5.53). Lastly, the vertical stress (σ_{v3_u}) and pore pressure (u_{3_d}) acting on the entire downstream slope and its foundation are calculated by implementing Eqn. (5.54). Thus, the vertical effective stresses ($\sigma_{v1a_d}', \sigma_{v1b_d}'$, σ_{v2_d}' and σ_{v3_d}') present in the downstream slope, are simply found by applying Eqns. (5.55 to 5.58).

5.5.2.3 Total passive (P_{pD}) and active (P_{aD}) earth pressure forces acting on the downstream slope

In order to determine the total passive earth pressure force (P_{pD}), acting on the downstream slope from its foundation, Eqns. (II.6 to II.8) in *Appendix II: Subsection II.1.*2 are applied, where σ_{v3_d}' is obtained using Eqn. (5.58) in *Subsection 5.5.1.6.2*. As outlined in *Chapter 2: Subsection 2.9.2.3*, the total active earth pressure force (P_{aD}), acting on the downstream slope, is the sum of the forces acting on the slope from the embankment's core (P_{XC}) and upstream slope (P_{XU}).

Applying the methodology defined in *Subsection 5.5.1.6.1*, the active earth pressure force (P_{XC}), Eqn. (5.49), acting on the downstream slope from the core is established.

To determine the total active earth pressure force (P_{XU}) acting on the downstream slope from the upstream slope, the first step is to establish the vertical effective stresses (σ_{v1a_u}', σ_{v1b_u}', σ_{v2_u}' and σ_{v3_u}'), Eqns. (5.25 to 5.28), by subtracting the pore pressures (u_{1a_u}, u_{1b_u}, u_{2_u} and u_{3_u}), Eqns. (5.21 to 5.24), from the vertical stresses (σ_{v1a_u}, σ_{v1b_u}, σ_{v2_u} and σ_{v3_u}), Eqns. (5.17 to 5.20).

The next step is to apply Eqns. (II.30 to II.37), derived in *Appendix II: Subsection II.2.2*, to establish the horizontal effective stresses (σ_{h1a_u}', σ_{h1b_u}', σ_{h2_u}' and σ_{h3_u}') and horizontal stresses (σ_{h1a_u}, σ_{h1b_u} σ_{h2_u} and σ_{h3_u}). Thus, the individual active earth pressure forces (P_{XU1}, P_{XU2} and P_{XU3}), and the total active earth pressure force (P_{XU}), acting on the downstream slope from the upstream slope can be found by applying Eqns. (II.38 to II.42) in *Appendix II: Subsection II.2.2*.

5.5.2.4 Total horizontal driving force (H_D) acting on the downstream slope

Applying Eqn. (2.100), *Chapter 2: Subsection 2.9.2.4*, the total horizontal driving force (H_D) acting on the downstream slope can be determined. However, here, the passive earth pressure force (P_{pD}) and total active earth pressure forces (P_{XC} and P_{XU}) calculated using the ASMP formulation, as defined in *Appendix II: Subsection II.2*, are inserted into Eqn. (2.100).

5.5.2.5 Total vertical effective stress (σ_{vd}') acting on the downstream slope

In order to determine the vertical effective stress (σ_{vd}') acting through the downstream slope, when rainfall has occurred, the first step is to calculate the change in the slope's total effective weight (ω_{ed}) and pore pressure (u_{vd}) acting vertically through the downstream slope. Here, Eqns. (II.43 to II.46), derived in *Appendix II: Subsection II.2.3*, are applied and the effective weights within the 'newly' saturated fill (ω_{ed1a}), above (ω_{ed1b}) and below (ω_{ed2}) the phreatic line, and within the slope's foundation (ω_{ed3}) obtained. Thus, the total effective weight (ω_{ed}) can be found using Eqn. (II.47), *Appendix II: Subsection II.2.3*, which is equivalent to the total vertical stress (σ_{Fd}).

The next step is to calculate change in the pore pressure (u_{vd}) using Eqn. (5.83). Once u_{vd} and σ_{Fd} are calculated, Eqn. (5.84) can then be applied and the total vertical effective stress (σ_{vd}') obtained.

$$u_{vd} = \frac{\left(\gamma_w H_f b_d\right) + \left[\gamma_w H_{av_d}\left(\frac{b_d - \left(b_{d2}\right)}{2}\right)\right] + \left[\gamma_w L_{dwn}\left(\frac{b_d}{2}\right)\right]}{b_d} \tag{5.83}$$

$$\sigma_{vd}' = \sigma_{Fd} - u_{vd} \tag{5.84}$$

where: H_{av_d} = Average height of the idealised phreatic line (downstream); H_f = Foundation height; L_{dwn} = Depth of infiltrated water vertically through the slope (downstream); γ_w = Unit weight of water; $b_{d2} = a \cdot \cos\alpha_2$, where 'a' is the distance on the downstream slope's surface, see Figure 2.3 in *Chapter 2: Subsection 2.6*, and α_2 is angle of the downstream slope.

5.5.2.6 Resultant shearing force (R_D)

Applying Eqn. (2.103), defined in *Chapter 2: Subsection 2.9.2.6*, the resultant shearing force (R_D), acting on the downstream slope, can be calculated.

5.5.2.7 Factor of safety (FoS_D) of the downstream slope

As presented in *Chapter 2: Subsection 2.9*, the calculated total resultant shearing force (R_D) and horizontal driving force (H_U) are inserted into Eqn. (2.31) in order to determine the downstream slope's factor of safety (FoS_D). Hence, FoS_D is able to capture the effect the depth of infiltrated water through the surface layers of the embankment's individual slopes and core has on the slope's overall stability, during a specific rainfall event.

5.6 Deterministic Example of the Upstream and Downstream Slope Stability Model

To demonstrate how the modified ASMP model is able to capture the effect rainfall has on the upstream and downstream slope's factor of safety, several worked examples will be presented. For consistency, the physical embankment model defined in *Chapter 2: Subsection 2.10.1* has been applied here, in order to compare the slope's factor of safety prior to, and after, selected rainfall events. Therefore, it was assumed that:

- The embankment's upstream and downstream slopes have a gradient of 1: 3.0 and 1: 4.0 respectively (SG11).
- The reservoir has been maintained at half capacity R2 (H_w = 1.5m).
- The embankment fill was constructed of London Clay (LC).

When carrying out the deterministic analysis, two soil saturation levels were considered for the partially saturated fill above the phreatic line, S_r = 56 % and 75 %, as the soil's degree of saturation (S_r) varies between seasons. The soil properties, derived unit weights of soil (partially saturated, saturated and effective) and fitting parameters for LC (London Clay) are summarised in Table 5.6.

Table 5.6 London Clay (LC): Soil properties, unit weights of soil and fitting parameters

Soil properties		**Units**	**M3B**
Moisture content (θ)		%	56 and 75
Cohesion (c)		kN/m^2	5
Internal friction (φ)		°	20
Saturated hydraulic conductivity (K_s)		cm/hr	0.1
Unit weight of embankment fill	γ_d	kN/m^3	16.1
	γ_m		17.0
	γ_{sat}		20.1
	γ_{sub}		10.3
Unit weight of foundation	γ_{fup}		20.1
	γ_{fc}		23.7
	γ_{fd}		13.6
Fitting parameters (van Genuchten method)	n		1.443
	m		0.307
	α		0.458

To understand how the intensity and duration of the rainfall event can directly affect the stability of the individual slopes, indicated by the change in the slope's factor of safety, two rainfall scenarios have been considered:

- High rainfall intensity over a short duration (1hr).
- Prolonged rainfall (24hrs) with low rainfall intensity.

The first rainfall scenario assumes that 70mm of rain fell in one hour at the dam site, whereas the second scenario assumes it rained continuously for 24hrs at a rainfall rate of 10mm/hr. Thus, for each rainfall scenario and saturation level, the factor of safety and associated depth of infiltrated water, were obtained for the embankment's upstream and downstream slopes.

5.6.1 Deterministic results: Depth of infiltrated water through the embankment's slopes (L_{up} and L_{dwn}) and core (L_c)

For each analysis, the depth of infiltrated water through the upstream (L_{up}) and downstream (L_{dwn}) slopes, including the core (L_c) of the embankment were recorded for the selected rainfall scenarios and saturation levels. These results are presented in Table 5.7.

Table 5.7 Depth of infiltrated water through the embankment's slopes and core

Soil Model	Rainfall duration	Average rainfall rate	Cumulative rainfall	Depth of water infiltration through the embankment's slopes and core (cm)					
				S_r = 56 %			S_r = 75 %		
	(hr)	(mm/hr)	mm	L_{up}	L_c	L_{dwn}	L_{up}	L_c	L_{dwn}
LC	1	70	70	0.62	0.63	0.62	3.12	3.15	3.14
	24	10	240	3.07	3.10	3.08	9.65	10.18	9.87

When S_r = 56 % the amount of rainfall infiltrated through the embankment is relatively small. This means that the residual rainfall retained on the embankment's surface could instigate slope failure in the form of runoff or overtopping. In the case of the first rainfall scenario (high intensity over a short duration), only the surface layers of the embankment are completely saturated as the depth of water infiltrated is small. However, the rainfall duration clearly influences the depth of water infiltrated through the embankment's surface layers, as indicated by the results in Table 5.7. This demonstrates the effect of prolonged rainfall on the depth of water infiltrated as a function of the embankment fill's saturation level, rainfall intensity and duration.

However, when the fill has a high saturation level, S_r = 75 %, there is a noticeable increase in the recorded depth of infiltrated water through the embankment, irrespective of the rainfall's intensity and duration. This occurs as the amount of rainfall absorbed by the embankment fill is dependent on the soil's relative hydraulic conductivity (K_r) and wetting front suction head (ψ), which will have changed due to the fill's increased saturation level. In addition, the time until ponding occurs on the surface of the embankment's crest and slopes is also dependent the soil's hydraulic conductivity and corresponding infiltration rate, as shown in Table 5.8.

Table 5.8 Time to ponding (t_p) on the surface of the embankment's crest and slopes

Soil Model	Rainfall duration	Average rainfall rate	Time to ponding (t_p) (hr)					
			S_r = 56 %			S_r = 75 %		
	(hr)	(mm/hr)	L_{up}	L_c	L_{dwn}	L_{up}	L_c	L_{dwn}
LC	1	70	1.37E-04	1.31E-04	1.23E-04	7.40E-04	7.08E-04	6.66E-04
	24	10	1.70E-01	1.63E-01	1.53E-01	0.0	0.0	0.0

5.6.2 Comparison between the slope's factor of safety (FoS) prior to and just after rainfall

From the deterministic analyses, the factors of safety for the upstream and downstream slopes, FoS_U and FoS_D, were also obtained and presented in Table 5.9. The results clearly show that the rainfall's intensity and duration influence the slope's factor of safety.

Table 5.9 Factor of safety of the upstream and downstream slopes (USlope 1: 3.0, DSlope 1:4.0)

Soil Model	Rainfall duration	Average rainfall rate	Cumulative rainfall	Factor of safety			
				S_r = 56 %		S_r = 75 %	
	(hr)	(mm/hr)	mm	FoS_U	FoS_D	FoS_U	FoS_D
LC	No rainfall			3.09	2.41	3.00	2.39
	1	70	70	2.25	2.09	2.10	2.04
	24	10	240	2.14	2.04	1.87	1.91

By comparing FoS_U and FoS_D with the depth of infiltrated water through the embankment's slopes, there is a clear correlation between their factor of safety, the fill's saturation level and the rainfall scenario. This is evident when the partially saturated fill above the phreatic line, prior to rainfall occurring, has a high saturation level, S_r = 75 %.

As indicated in Tables 5.7 and 5.8, a short-high intensity rainfall event does not appear to affect the stability of the individual slopes, irrespective of the fill's saturation level. Failure of such dams is therefore more likely to occur in the form of hydraulic failure (overtopping, runoff, external erosion, etc.). However, when there is prolonged rainfall with low rainfall intensity, there is a noticeable drop in the upstream and downstream slopes factor of safety (FoS_U and FoS_D). This occurs as the rainfall's duration, and the saturation level of the partially saturated fill prior to rainfall occurring, influence the depth of infiltrated water through the embankment. Therefore, structural failure in the form of slope instability is more likely to develop.

By carrying out the advanced slope stability model with precipitation effects (ASMP), using the modified sliding block formulation, for the upstream and downstream slopes it will be possible to obtain quantitative information about the performance of the embankment's slopes, as well as providing an indication of the time when slope failure could occur. This level of information is useful when assessing the future precipitation scenarios and their possible effect on a specific small homogeneous earthfill embankment.

5.7 Concluding Remarks

This chapter summarised the terminology used to differentiate between climate change, global climate change and their associated common climate variables, focusing on common climate variables specific to UK climate. The climate change scenarios associated with UK climate change were identified and the current and future trends discussed. The relationship between the external and internal threats and the failure modes (hydraulic, structural and leakage/seepage failures), relating to upstream and downstream slope stability, were categorized and the impact such threats have on the structural reliability of a small UK earthfill embankment dam addressed. Different common climate variables were identified and the environmental factor precipitation, in the form of rainfall, was selected.

The new advanced slope stability model with precipitation effects (ASMP) was established by modifying the applied sliding block formulation. This involved incorporating the standard and modified Green-Ampt methodologies, coupled with the van Genuchten method, into the deterministic upstream and downstream slope stability models, defined in *Chapter 2: Subsection 2.9*. The equations used to develop the modified deterministic slope stability models for the embankment's upstream and downstream slopes using ASMP formulation are outlined in detail in this chapter. Therefore, by implementing the ASMP formulation, quantitative information about the behaviour of the embankment's upstream and downstream slopes in the presence of site-specific information and variable rainfall scenarios can be obtained for variable target time frames.

A deterministic example has been presented, demonstrating the application of the ASMP formulation, for a generic embankment taking into account the embankment fill's seasonal saturation level and two different rainfall scenarios (rainfall duration and intensity effectively). The depth of infiltrated water through the embankment's core, upstream and downstream slopes was recorded for each rainfall scenario, including the time until ponding occurs on the embankment's surface. From the deterministic analysis, the results obtained demonstrate that there is a clear correlation between the slope's factor of safety, the saturation level of the partially saturated fill above the phreatic line, and the rainfall scenario.

In the next chapter the probabilistic slope stability model (PSSM) for assessment of small homogeneous earthfill embankment dams, outlined in *Chapter 3* and implemented in *Chapter 4*, will be amended to incorporate formulation for precipitation effects (ASMP). Thus, the modified probabilistic analysis will also encompass the uncertainty associated with rainfall intensity.

CHAPTER 6 : PROBABILISTIC ASSESSMENT OF SMALL EMBANKMENT DAMS FOR CLIMATE EFFECTS

6.1 Introduction

This chapter presents the development and application of the complete advanced probabilistic slope stability model with precipitation effects (APSMP). It provides a facility to quantitatively measure the notional reliability for small, well-established, homogeneous earthfill embankment dams against upstream and downstream slope failure when exposed to variable precipitation scenarios. As before, we consider that failure of the upstream and downstream slopes are representative limit state functions. Furthermore, the probabilistic modelling is now encompassing the aleatory uncertainties associated with precipitation, specifically the rainfall's intensity, the embankment's geometry, the fill's mechanical soil properties and the reservoir's headwater height.

Selected precipitation scenarios will be obtained from historic rainfall records, using the Met Office records, and by applying the latest probabilistic model for predicting future climate change projections for the UK (UKCP09). In addition to the selected precipitation scenarios future extreme rainfall scenarios will be developed using the UKCP09 User Interface.

The performance of the embankment's upstream and downstream slopes is a function of their notional reliability (probability of failure), which is evaluated for:

- Selected soil models that reflect site-specific conditions.
- Different slope configurations.
- Variable precipitation scenarios to represent climate effects.
- To represent seasonal variations, two extreme saturation levels of the partially saturated fill above the phreatic line, prior to rainfall occurring.
- The critical headwater height scenario (R3).

In addition, assuming the same dam site conditions and precipitation scenario, the sensitivity factors, which reflect the importance of uncertain variables, for each limit state will be assessed.

By applying the APSMP model, it will be possible to establish the engineering risk associated with such earthfill embankment dams and relate it to the risk classification, as categorized by the Flood and Water Management Act 2010, in respect to the effect of precipitation.

6.2 Precipitation Modelling

It is well understood that the soil's average saturation level will vary noticeably both between the seasons and the regions. Using UKCP09 climate projections and specific past extreme events such as those reported by the Met Office, including short and prolonged rainfalls, different rainfall scenarios will be established to analyse their impact on the overall stability of the embankment's slopes.

6.2.1 UK Met Office data

The UK has a relatively humid climate, thus, precipitation occurs primarily as rain and is recorded by the Meteorological Office (Met Office). The Met Office keeps detailed records dating from 1854 to the present day of the annual, monthly and daily rainfall intensities (mm), in a given catchment area (Met Office, 2011). However, only data obtained from weather stations that use the standard instruments and exposure practices is documented. From these records the Met Office Hadley Centre, for Climate Change Research, developed the climate model HadCM3 simulating future climate change projections (Murphy et al., 2009).

The Met Office also keeps records of extreme past and historic weather events. For instance, in England the highest recorded rainfall over 24 hours was 279mm in Martinstown on 18th July 1955, whereas the highest recorded rainfall over an hour was 92mm in Maidenhead on 12th July 1901 (Met Office, 2010). Table 6.1 shows the data that has been extracted from the Met Office for selected daily and monthly rainfall records, as well as extreme rainfall events. Within this thesis, these specific rainfall conditions are used within the APSMP model in order to analyse how different rainfall patterns influence the overall stability of the embankment's slopes.

Table 6.1 Selected historic daily, monthly and extreme UK rainfall

Rainfall Scenario	Location and Date	Cumulative Rainfall Intensity (mm)	Rainfall Duration	Average Rainfall Rate
A[#]	Martinstown 18th July 1955	279.00	24 hr	11.63 mm/hr
B[##]	England 22nd August 2010	29.25	24 hrs	1.22 mm/hr
C[#]	Maidenhead on 12th July 1901	92.00	60 min	92.00 mm/hr
D[#]	Hampstead 14th August 1975	169.00	2.5 hr	67.60 mm/hr
E[##]	S England November 1940	185.60	30 days	6.19 mm/day
F[##]	SE England January 1988	158.20	31 days	5.10 mm/day

[#]Extreme rainfall events not used for precipitation statistics (Met Office, 2010); [##]Extracted from UK Climate Summaries (Met Office, 2011)

6.2.2 UKCP09 - future climate projections

Future UK climate change scenarios have been continually developed since 1991 and are a prediction of how the climate may change over the next 100 years. The Climate Change Impacts Review Group (CCIRG) developed the first generation of climate scenarios from data obtained using the Met Office Hadley Centre coupled ocean-atmosphere model (HadCM1), (Hulme & Jenkins, 1998; Hulme & Dessai, 2008). These climate predictions were published as CCIRG91 scenarios and later as CCIRG96 scenarios (Hulme & Jenkins, 1998; Hulme et al., 2002).

A new set of UK climate scenarios, UKCIP98, were later published by the UK Climate Impacts Programme (UKCIP), who took into account the '*natural climate variations including a range of future greenhouse gas emissions scenarios and different assumed sensitivities of the climate system to these emissions*' (Hulme & Jenkins, 1998: p.2).

These scenarios were based on the results obtained from two sets of climate change experiments completed in 1996, by the Hadley Centre, using the Met Office Hadley Centre global climate model (HadCM2) (Hulme & Dessai, 2008).

Prior to UKCP09 climate projections the last set of climate scenarios, published by the Intergovernmental Panel on Climate Change (IPCC), were the UKCIP02 scenarios in 2000 (Hulme et al., 2002). UKCIP02 presents four climate change scenarios based on Low, Medium-Low, Medium-High and High Emissions scenarios (Hulme, Turnpenny & Jenkins, 2002). These are considered the fourth generation of UK climate scenarios.

Using the latest regional climate model HadRM3, the UKCP09 climate projections were developed, which present the climate scenarios as probabilistic ranges over seven overlapping 30-year time periods (2010 - 2039, 2020 - 2049,…, 2070 - 2099) (Gething, 2010). These are the fifth generation climate scenarios superseding those detailed in UKCIP02 (Hulme et al., 2002). These climate projections can be found in UKCP09 Scientific Reports published by UKCIP. The fundamental difference between UKCIP02 and UKCP09 is that the Probabilistic Climate Projections (PCP), defined in UKCP09, are based on various probabilistic climate models and not just on the Hadley Centre Regional Climate Model.

The UKCP09 climate projections reflect the uncertainties caused by the climate's natural variability and the limitations of the climate model (HadCM3), by taking into account the main uncertainties associated with future climate predictions (Jenkins et al., 2009). These projections provide a standard reference with which to evaluate the UK's future climate changes, including climate variability in the 21st century, and are defined by three future emissions scenarios, Murphy et al. (2009), High, Medium and Low. These scenarios are commonly derived using observed data, obtained from 20th and 21st Century historical information regarding trends in UK Climate, and the results obtained experimentally from the climate change projections (Hulme et al., 2002).

Based on these projections, a detailed assessment of the uncertainties associated with future Climate Projections (UKCP09), for specific variables, were further developed by

the UK Climate Impacts Programme (UKCIP). UKCP09 presents these projections as probabilistic ranges (Gething, 2010), which reflect the uncertainties associated with the limitations of the climate model as well as the climate's natural variability (Jenkins et al., 2009). Jenkins et al. (2009) observed that these uncertainties arise from:

- Natural climate variability.
- Uncertainties in future man-made emissions.
- Uncertainties in the different global, local or regional scale climate models (modelling uncertainty).

From UKCP09, future trends for UK seasonal, annual and monthly temperature, precipitation, etc. can be obtained in probabilistic form (Jenkins, Perry & Prior, 2008). However, UKCP09 cannot be used to estimate probabilistic projections of future changes relating to snowfall rate, latent heat flux, wind speed or soil moisture (Hulme et al., 2002). Variations in the soil's moisture content are dependent on changes in temperature, precipitation, wind speed and solar radiation (Hulme et al., 2002) and will be simulated in simple terms in the following analysis.

As reported in UKCP09, since 1766 the recorded annual mean precipitation over England and Wales has remained relatively consistent. However, Jenkins et al. (2009) observed that '*seasonal-mean precipitation is highly variable, but appears to have decreased in summer and increased in winter, although with little change in the latter over the last 50 yr*' (p.12). This has resulted in a clear shift in seasonal rainfall patterns, including an increase in average rainfall intensity over winter and a change in average seasonal rainfall durations (Jenkins et al., 2009; Gething, 2010). From the data presented in the UKCIP02 briefing report, the biggest contrast in precipitation patterns are predicted to occur in Eastern and Southern England (Hulme, Turnpenny & Jenkins, 2002).

It is well understood that the soil's average moisture content will vary noticeably both between the seasons and the regions. Here, the UKCP09 User Interface will be applied to develop future precipitation projections for a given region and 30-year time period. By applying the predicted UKCP09 climate projections and specific past extreme events

such as those reported by the Met Office, including short and prolonged rainfalls, different rainfall scenarios will be developed. It will therefore be possible to quantify how different rainfall patterns could affect the notional level of engineering risk associated with the embankment dam (slope instability).

6.2.2.1 Application of the UKCP09 User Interface

To determine the future precipitation projections, UKCP09 combines the probabilistic climate change projections with the precipitation recorded during the baseline period (1961 - 1990). Using the UKCP09 User Interface, these projections are obtained as a Cumulative Distribution Function (CDF) providing the projected distributions for specific climate variables relative to the baseline climate. The CDFs are available for the projected annual/monthly/seasonal change in precipitation for a given emission scenario (low, medium and high), probability level, 30-year time period and location (Jenkins et al., 2009).

Using the UKCP09 User Interface sample CDF were produced for the London region, Figures 6.1 and 6.2. These graphs show the seasonal (winter and summer) changes in precipitation for high (A1FI) and low emission (B1) scenarios for three 30-year time periods (2010 - 2039, 2020 - 2049 and 2070 - 2099).

To demonstrate how the change in precipitation also varies regionally, the following CDF graphs, Figures 6.3 and 6.4, are presented for the Martinstown/ Dorset region, for the same future climate projections, as the highest 24hr rainfall was recorded in Martinstown, see Table 6.1.

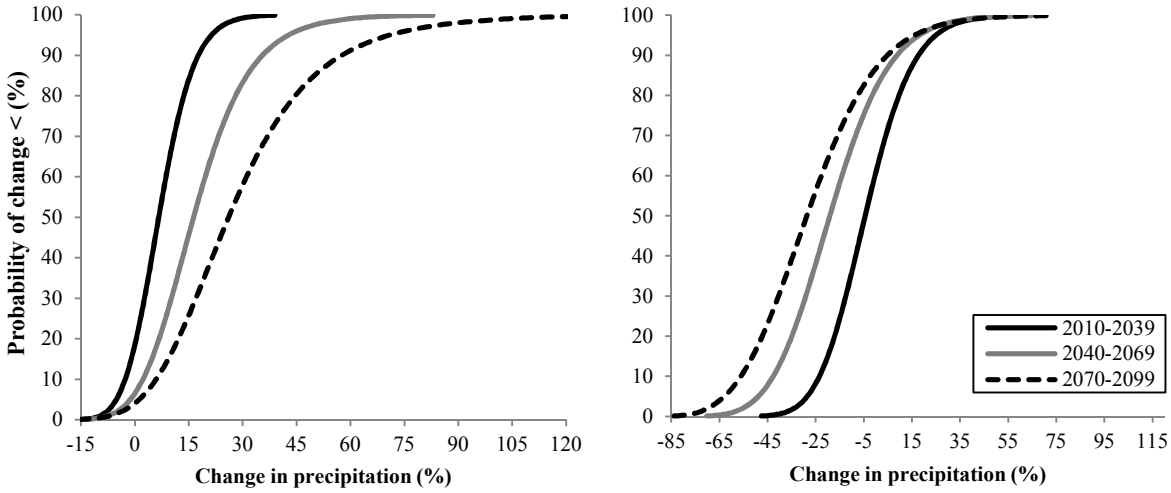

(Winter) (Summer)

Figure 6.1 CDF of change in precipitation for high emission (A1FI) scenario in the London region: data source UKCP09

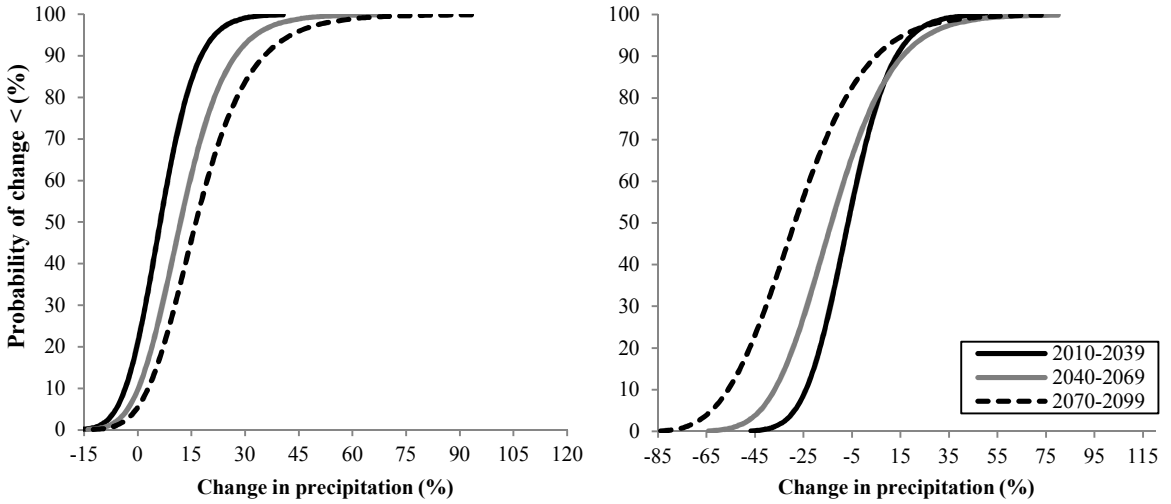

(Winter) (Summer)

Figure 6.2 CDF of change in precipitation for low emission (B1) scenario in the London region: data source UKCP09

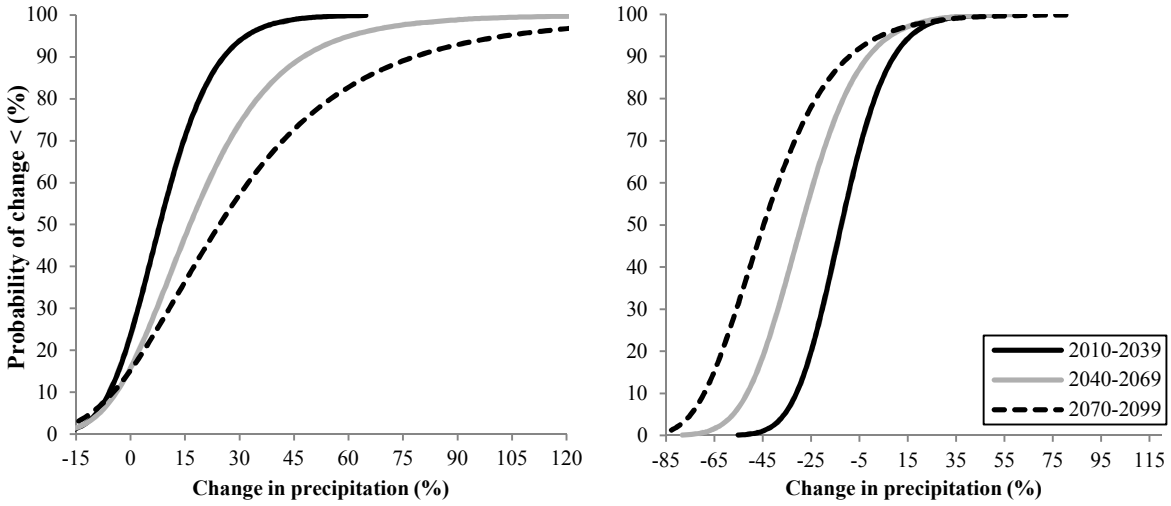

(Winter) (Summer)

Figure 6.3 CDF of change in precipitation for high emission (A1FI) scenario in the Martinstown/Dorset region: data source UKCP09

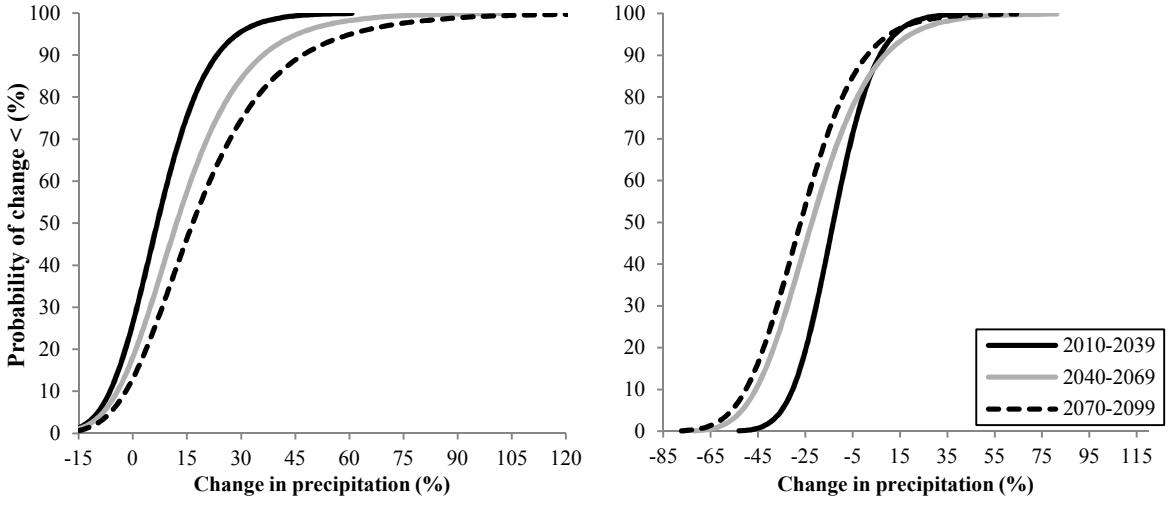

(Winter) (Summer)

Figure 6.4 CDF of change in precipitation for low emission (B1) scenario in the Martinstown/Dorset region: data source UKCP09

Comparing the CDF graphs in Figures 6.1 to 6.4, the change in precipitation during winter and summer follow diverging trends for both high and low emission scenarios. For the winter season, there is a projected increase in future winter precipitation over the 30-year time periods, irrespective of the emission scenarios. However, this trend is

clearly reversed for summer, as the CDF graphs indicate drier summers due to decreasing precipitation in the future. Similar results were also documented in the UKCIP02 scientific and briefing reports (Hulme et al., 2002; Hulme, Turnpenny & Jenkins, 2002).

From the data generated in UKCP09, Table 6.2 presents the characteristic values for the 90 % probability level, or extreme possible case, for the UKCP09 change in precipitation recorded during the baseline period (1961 - 1990) for the selected regions, London and Martinstown/Dorset, for the future time periods 2010 - 2038 and 2079 - 2099 under high and low emission scenarios. Comparing the changes in precipitation for the selected regions, the differences between the values in either season and with the same emission scenario, have a similar order of magnitude. The table also shows that the change in precipitation in the Martinstown/Dorset Region follows a similar pattern to that observed over London. However, the Martinstown/Dorset Region will experience much drier summers, with very low rainfall expectancy.

Table 6.2 UKCP09 change in seasonal precipitation at 90 % probability level for the London and Martinstown/ Dorset regions

Region	Emission Scenario	UKCP09 change in precipitation (%): 90 % probability level			
		Winter		Summer	
		2010-2039	2079-2099	2010-2039	2079-2099
London	High (A1FI)	17.7	57.5	17.7	4.8
	Low (B1)	17.7	35.3	13.3	12.9
Martinstown/ Dorset	High (A1FI)	25.6	67.1	9.3	-9.2
	Low (B1)	23.3	47.1	6.5	3.2

Using UKCP09 climate projections for high (A1FI) emission scenarios, such as those presented in Figures 6.1 to 6.4, future precipitation patterns were identified. High emission scenarios were selected, or extreme possible case, by encompassing a higher estimate of future global emissions, or greenhouse gases. These results were then used to extrapolate extreme future rainfall events for January and July between 2010 - 2039 and 2070 - 2099.

To obtain the quantitative measure of change in precipitation, the 95th fractile of the percentage increase in average rainfall for UKCP09 climate projections for high

emission scenarios was selected. The application of the UKCP09 User Interface used to obtain the 95th fractile is demonstrated in *Appendix IX*. Table 6.3 shows the probable future rainfall intensities for January and July between 2010 - 2039 and 2070 - 2099, assuming prolonged and short rainfall events. Here, the future UKCP09 precipitation scenarios FP1 and FP2 define prolonged (monthly) rainfall events, whereas FP3 and FP4 correspond to short (1 hour) rainfall patterns. The average rainfall rates for the different UKCP09 precipitation scenarios were then incorporated into the probabilistic model.

Table 6.3 Probable future rainfall intensities incorporating UKCP09 climate projections

UKCP09 precipitation scenario*	Month and 30-year period	UKCP09 change in precipitation for high emission (%)†	Predicted future rainfall intensity (mm)	Rainfall duration	Average rainfall rate
FP1	January 2010-2039	16.98 %	174.13	31days	5.62/ mm/day
FP2	January 2070-2099	53.46 %	238.47	31days	7.69 mm/day
FP3	July 2010-2039	44.23 %	133.61	1hr	133.61 mm/hr
FP4	July 2070-2099	26.81 %	113.33	1hr	113.33 mm/hr

†95th fractile of the percentage increase in average rainfall for UKCP09 climate projections for High Emission Scenarios.

6.2.3 Selected precipitation scenarios incorporated within APSMP using Met Office and UKCP09 data

To quantify the effect different precipitation scenarios can have on the notional reliability of the upstream and downstream slopes, selected historic and future UKCP09 precipitation scenarios from Tables 6.1 and 6.3 will be considered. The rainfall patterns and rainfall intensities, including their average rainfall rates, for the selected historic and UKCP09 precipitation scenarios are presented in Table 6.4.

Table 6.4 Selected historic and UKCP09 scenarios used within APSMP

Precipitation Scenario		Location and Date	Rainfall Intensity (mm)	Rainfall Duration	Average Rainfall Rate
Historic Scenarios	A	Martinstown 18th July 1955	279.00	24 hr	11.63 mm/hr
	D	Hampstead 14th August 1975	169.00	2.5 hr	67.60 mm/hr
	F	SE England January 1988	158.20	31 days	5.10 mm/day
UKCP09 Scenarios	FP1	January 2010 - 2039	174.13	31days	5.62/ mm/day
	FP2	January 2070 - 2099	238.47	31days	7.69 mm/day
	FP3	July 2010 - 2039	133.61	1hr	133.61 mm/hr

By incorporating the rainfall patterns and rainfall intensities defined in Table 6.4 within APSMP, variations in the depth of water infiltrated through the dam's embankment fill can be established and the slope's notional reliability ascertained. Thus, it will be possible to detect if the embankment's upstream and downstream slopes are at risk when subject to specific conditions. Here, variable soil saturation levels will be considered for the partially saturated fill, above the calculated idealised position of the phreatic line, as the embankment's slopes are more vulnerable during the wetter months, primarily in winter and at the beginning of spring.

6.3 Probabilistic Modelling

The advanced probabilistic slope stability model with precipitation effects (APSMP) is a probabilistic model that encompasses the uncertainties associated with the embankment fill's mechanical and hydraulic properties, the geometry of the embankment, the reservoir's headwater height and the rainfall parameters. For this applied probabilistic analysis the linear limit state functions during the rainfall event, $g_{RI}(.)$, for FM1 and FM2, defined using the modified sliding block formulation, are given by Eqns. (6.1 and 6.2) with reference to Table 6.1 and Figure 2.9 in *Chapter 2: Subsection 2.9*.

$$g_{RI}(upstream) = \tau_{U_{RIup}}{}' - \left(P_{x_{C_{RIup}}} + P_{x_{D_{RIup}}}\right) - \left(P_w + P_{p_{U_{RIup}}}\right) \quad (6.1)$$

$$g_{RI}(downstream) = \tau_{D_{RIdwn}}{}' - \left(P_{x_{C_{RIdwn}}} + P_{x_{U_{RIdwn}}}\right) - P_{p_{D_{RIdwn}}} \quad (6.2)$$

where: P_w = Pore water pressure from the reservoir acting on the upstream section; $P_{aRIup/RIdwn}$ = Total active pressure acting on the upstream/downstream sections during the rainfall event; $P_{pRIup/RIdwn}$ = Total passive earth pressure on the upstream/downstream sections; $\tau'_{RIup/RIdwn}$ = Coulomb's shear strength during rainfall event.

6.3.1 Probabilistic modelling of uncertain variables

As outlined in *Chapter 4: Subsection 4.3*, the following variables have been selected to represent the uncertainties associated with the dam's embankment and reservoir itself:

Embankment's geometry ⇒
- Embankment's height (H)
- Crest width (CW)
- Foundation height (H_f)

Embankment fill's soil properties ⇒
- Unit weight of soil factor (γ_{fct})
- Internal friction (φ')
- Cohesion (c')

Their mean values and standard deviation are summarised in Table 6.1 and are modelled using normal distribution. When modelling the idealised trajectory of the phreatic line, only the critical headwater height scenario (R3), as defined in *Chapter 4: Subsection 4.3.2*, has been applied to the embankment's physical model. R3 has been considered for illustrative purposes, as during specific rainfall events, such as prolonged rainfall, it will take less time for the infiltrated water to reach the calculated position of the idealised phreatic line (Preziosi & Micic, 2011a; Preziosi & Micic, 2011b).

Table 6.5 Probabilistic modelling of soil properties: Variables are normally distributed

Variable	Unit	Mean (μ)	Standard deviation (σ)
Rainfall intensity factor (RI_{fct})	mm	1.0	0.1
Height (H)	m	3.0	0.03
Foundation Height (H_f)	cm	50.0	1.0
Crest Width (CW)	m	2.8	0.028
Headwater height (H_w)	m	2.0	0.1
Unit weight of soil factor (γ_{fct})	kN/m^2	1.0	0.1
Internal friction (φ')*	°	μ_φ	$\mu_\varphi \cdot 0.15$
Cohesion (c')*	kN/m^2	μ_c	$\mu_c \cdot 0.3$

* Negatively correlated (-0.5)

The rainfall's intensity and duration are highly variable within a given catchment area. Thus, to account for the variability between the rainfall intensity measurements over the rainfall duration a rainfall intensity factor (RI_{fct}) has been introduced, whose mean value and standard deviation are shown in Table 6.1.

From the results obtained, the change in the embankment's upstream and downstream slope's evaluated reliability index (β) and probability of failure (P_f) will be extracted. This will enable the evaluation of the notional level of engineering risk associated with small homogeneous earthfill embankment dams associated with slope instability, including any decisions relating to future conditions at the dam site. Effectively, APSMP models the change in the embankment's strength due to rainfall infiltration.

6.3.2 Selected clay like soil models

To demonstrate the applied probabilistic methodology (APSMP) for failure modes FM1 (upstream slope failure) and FM2 (downstream slope failure), the clay like soil models M3A (London Clay), M3B (London Clay), M5 (Gault Clay) and M6 (Silty Gravely Clay) have been selected for the homogeneous embankment fill. The applied standard, deterministic, embankment fill properties, effective internal friction and cohesion for the selected soil models are summarised in Table 4.4 in *Chapter 4: Subsection 4.3.3*. Thus, it will be possible to understand how variable precipitation, in the form of rainfall, directly affects the reliability of the embankment's slopes. For simplification of the embankment's physical model, it has been assumed that the soil properties, hydraulic parameters and derived unit weights of soil are homogeneous throughout the embankment fill and exposed to the same dam site conditions.

6.4 Flowchart for the Applied Probabilistic Slope Stability Model with Precipitation Effects (APSMP)

The following flowchart, Figure 6.5, presents the key stages required to carry out the applied probabilistic slope stability model with precipitation effects (APSMP). Here, the input parameters incorporated into the probabilistic model correspond to the uncertainties associated with the rainfall intensity, the embankment's geometry, the embankment fill's mechanical soil properties and the reservoir's headwater height, indicated by step 1 in Figure 6.5. Prior to the rainfall event, the different saturation levels within the embankment fill (above and below the position of the idealised phreatic line) are established, step 2 in Figure 6.5, by applying the traditional steady seepage model.

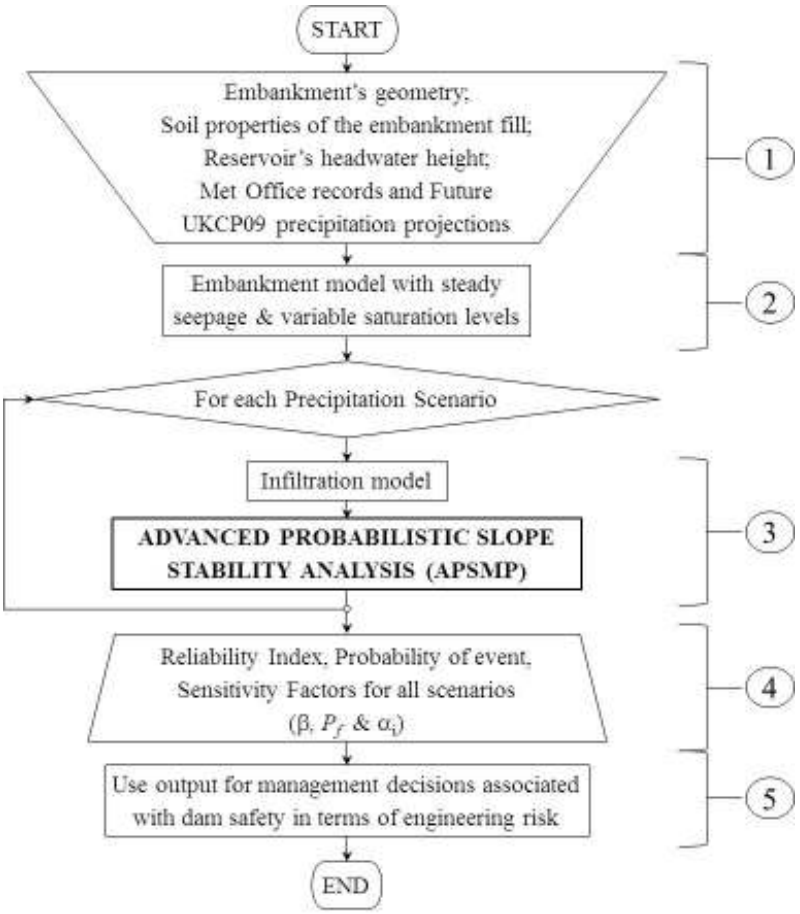

Figure 6.5 Flowchart of the applied probabilistic slope stability model with precipitation effects (APSMP)

For the advanced probabilistic analysis of the embankment's slopes, step 3 in Figure 6.5, the infiltration model is defined using the standard and modified Green-Ampt methodologies, coupled with the van Genuchten method. Thus, the new and sophisticated upstream and downstream slope stability models are defined using the modified sliding block equilibrium equations derived in *Chapter 5*. Here, APSMP integrates FOSM with the modified sliding block formulation for upstream and downstream slope stability models, derived in *Chapter 5*.

For the selected dam site, specific soil type and climate scenario, the output data relating to the reliability index (β), probability of failure (P_f) and the sensitivity factors (α_i) are obtained for the individual failure modes, FM1 and FM2, Step 4 in Figure 6.5. Using data collated from APSMP, the impact variable future climate change scenarios could have on the engineering risk associated with upstream and downstream slope failure, of well-established dams, will be established and how it relate to the risk classification

categorized by the Flood and Water Management Act 2010, step 5 in Figure 6.5. Furthermore, it will be possible to reflect on the implication of the inclusion of probabilistic climate models on associated risks.

6.5 Parametric Studies for Clay Like Soil Models Subject To Selected Precipitation Scenarios

To account for the high variability in relative hydraulic conductivity, the coupled van Genuchten-Green Ampt approach described in *Chapter 5* has been implemented. For instance, during the winter months the partially saturated fill will have a high saturation level resulting in a higher unit weight of soil, compared to those recorded over the summer months. Therefore, the shear stress of the slopes will increase while simultaneously decreasing their shear strength. This will be reflected in the reliability indices, β_{up} and β_{dwn}, for upstream (FM1) and downstream (FM2) slope failure.

In the following subsections, 6.5.1 to 6.5.4, the effect that the precipitation scenarios, defined in Table 6.4, effectively rainfall intensity and its duration, have on β_{up} and β_{dwn} for FM1 and FM2 have been extracted for the clay like soil models M3A (London Clay), M3B (London Clay), M5 (Gault Clay) and M6 (Silty Gravely Clay) with comparable degrees of saturation. For the current parametric study, only slope configurations SG5 (USlope 1: 3.0, DSlope 1: 3.0) and SG11 (USlope 1: 3.0, DSlope 1: 4.0), as defined in Table 4.1 in *Chapter 4: Subsection 4.2*, and the critical headwater height scenario R3 (H_w = 2m) will be considered. As the soil's degree of saturation (S_r) will vary between seasons, two extreme soil saturation levels were considered, S_r = 57 % and 75 %, to represent the average soil conditions during summer and winter respectively. Thus, for the selected precipitation scenarios and applied degrees of saturation, the reliability index and associated depth of infiltrated water for each failure mode, as defined in Eqns. (6.1 and 6.2), were obtained.

To demonstrate how the target reliabilities presented in Table 4.6, *Chapter 4: Subsection 4.5*, can be used as a benchmark for classifying the change in the upstream and downstream slopes expectant behaviour and performance level under different

precipitation scenarios, extracts from the complete set of results for the selected soil models, using APSMP, are presented in the following subsections. In addition to the reliability indices, the change in the probability of failure (P_f) for downstream slope failure, under variable precipitation scenarios for two comparable soil models, is also presented. The sensitivity factors are also presented to identify the variables that have the greatest impact on the limit state's reliability, in this case upstream (FM1) and downstream (FM2) slope failure, for slope configuration SG5 and SG11. The complete set of reliability indices (β_{up} and β_{dwn}) for upstream (FM1) and downstream (FM2) slope failure, for the clay like soil models (M3A, M3B, M4, M5 and M7) subjected to the precipitation scenarios defined in Table 6.4 can be found in the CD labelled *Appendix X*.

For the following parametric analyses, complete failure of the embankment's slope is identified when:

1. The infiltrated water has reached the idealised position of the phreatic line during the rainfall event.
2. The reliability index against slope failure has reached hazardous level (according to Table 4.6 in *Chapter 4: Subsection 4.5*) i.e. $\beta \leq 1.0$, $P_f \geq 16.0$ %.

It is fair to emphasise that such criteria is selected as illustrative, somewhat non-conservative, and in practice it will be the statutory bodies, such as the Environment Agency and Panel Engineers, who would make the required recommendations as already explained in *Chapter 4*.

6.5.1 Analysis of the embankment's slopes for soil model M3A (London Clay)

i) Infiltration

For both limit states and saturation cases, the depth to which the water has infiltrated through the slopes, L_{up} and L_{dwn}, was obtained for the different precipitation scenarios and are shown in Table 6.6 for M3A (London Clay). When S_r = 57 % the amount of rainfall infiltrated through the surface layers of the partially saturated embankment fill is relatively small. Therefore, any residual rainfall retained on the embankment's surface could result in runoff or overtopping developing.

Table 6.6 Depth of infiltrated water through the slopes, including time taken to reach the phreatic line for M3A (London Clay) with varying S_r for the selected precipitation scenarios

Precipitation Scenario†		Rainfall Duration	Depth of infiltrated water through the embankment's slopes (cm) or time for complete failure (days) for M3A (London Clay)							
			SG5 (1: 3.0, 1: 3.0)				SG11 (1: 3.0, 1: 4.0)			
			S_r = 57 %		S_r = 75 %		S_r = 57 %		S_r = 75 %	
			L_{up}	L_{dwn}	L_{up}	L_{dwn}	L_{up}	L_{dwn}	L_{up}	L_{dwn}
No Rainfall			-	-	-	-	-	-	-	-
Historic Scenarios	A	24 hrs	3.42	3.42	16.90	16.90	3.42	3.42	16.91	17.08
	D	2.5 hrs	1.05	1.05	3.87	3.87	1.05	1.05	3.87	3.89
	F	31 days	25.45	25.45	26 days♦	26 days♦	25.45	25.65	26 days♦	25 days♦
UKCP09 Scenarios	FP1	31 days	25.50	25.50	24 days♦	24 days♦	25.50	25.70	23 days♦	23 days♦
	FP2	31 days	25.59	25.59	17 days♦	17 days♦	25.59	25.79	17 days♦	17 days♦
	FP3	1 hr	0.66	0.66	2.28	2.28	0.66	0.66	2.28	2.29

†*See Table 6.5 for definitions of the abbreviations used for precipitation scenarios;* ♦*Approximate time taken for the infiltrated water to reach the calculated idealised position of the phreatic line during the rainfall event.*

In the case of precipitation scenarios A, D and FP3, high rainfall intensity over a short duration, only the surface layers of the embankment are completely saturated as the depth of water infiltrated is small. However, the rainfall duration clearly influences the depth of infiltrated water, as shown by the results for precipitation scenarios F, FP1 and FP2 in Table 6.6. Comparing the prolonged rainfall scenarios (F, FP1 and FP2) the infiltrated water has reached the idealised position of the phreatic line in the embankment's slopes between 24 and 26 days, precipitation scenario F and FP1 respectively, and in 17 days for precipitation scenario FP2, resulting in the partially saturated fill above the phreatic line becoming completely saturated (S_r > 80 %).

When the partially saturated embankment fill has a high saturation level, S_r = 75 %, there is a significant increase in the recorded depths of infiltrated water through the slopes, regardless of the rainfall's intensity and duration, as indicated in Table 6.6. This occurs as the soil's hydraulic conductivity (K_r) and wetting front suction head (ψ) change with increased S_r, enabling a greater amount of rainfall to percolate through the embankment fill. For example, when the moisture content (θ_r) of the fill's surface layers, for M3A, increases from 56 % to 76 % its relative hydraulic conductivity (K_r) will vary from 4.9×10^{-8} to 5.7×10^{-7} m/s, while the wetting front suction head (ψ) decreases from approximately 7.3 to 2.8 cm (Preziosi & Micic, 2011b).

As this parametric study demonstrates, the depths of infiltrated water through slope configurations SG5 and SG11 for the UKCP09 precipitation scenarios FP1, FP2 and FP3, see Table 6.6, follow a very similar pattern to those recorded for the selected past precipitation scenarios A, D and F. The results presented in Table 6.6 also show the effect of prolonged rainfall on the depth of infiltrated water as a function of the saturation level of the partially saturated embankment fill, rainfall intensity and duration. By recording the depth that the water has infiltrated through the embankment fill for each precipitation scenario, it will be possible to obtain qualitative information about the slopes notional reliability index and associated performance level. While only extreme saturation scenarios have been considered here, in practice it is possible to consider genuine, site-specific conditions.

ii) Reliability

Table 6.7 shows the reliability indices (β_{up} and β_{dwn}) for FM1 and FM2, obtained for slope configurations SG5 and SG11 for the soil model M3A (London Clay), assuming the same degrees of saturation. The results presented show that variable rainfall intensity and duration greatly affect the slope's overall reliability.

Table 6.7 Reliability indices for upstream (FM1) and downstream (FM2) slope failure, for soil model M3A (London Clay), with varying S_r for the selected precipitation scenarios

Precipitation Scenario†		**Rainfall Duration**	**Reliability Index (β) for M3A (London Clay)**							
			SG5 (1: 3.0, 1: 3.0)				SG11 (1: 3.0, 1: 4.0)			
			S_r = 57 %		S_r = 75 %		S_r = 57 %		S_r = 75 %	
			β_{up}	β_{dwn}	β_{up}	β_{dwn}	β_{up}	β_{dwn}	β_{up}	β_{dwn}
No Rainfall			3.31	1.96	3.28	1.96	3.22	2.55	3.19	2.55
Historic Scenarios	A	24 hrs	3.03	1.81	2.27	1.39	2.93	2.47	2.13	2.04
	D	2.5 hrs	3.15	1.89	2.97	1.82	3.06	2.56	2.87	2.49
	F	31 days	1.83	1.09	F^* (11 days)	F^* (8 days)	1.68	1.71	F^* (10 days)	F^* (13 days)
UKCP09 Scenarios	FP1	31 days	1.83	1.08	F^* (10 days)	F^* (7 days)	1.68	1.71	F^* (9 days)	F^* (12 days)
	FP2	31 days	1.82	1.08	F^* (7 days)	F^* (5 days)	1.67	1.71	F^* (7 days)	F^* (9 days)
	FP3	1 hr	3.17	1.90	3.05	1.87	3.08	2.57	2.96	2.55

†See Table 6.5 for definitions of the abbreviations used for precipitation scenarios; F^* Indicates slope failure has occurred as $\beta \leq 1.0$ (F = Slope Failure).

Comparing β_{up} and β_{dwn} with the depth rainfall has infiltrated through the upstream and downstream slopes (L_{up} and L_{dwn}), there is a clear correlation between outcomes. This is evident when the embankment fill has a high saturation level, S_r = 76 %. As indicated in

Table 6.7, if there is prolonged rainfall over a month (precipitation scenario F, FP1 and FP2) the reliability indices clearly show that complete slope failure will occur ($\beta \leq 1.0$) between 7 and 11 days for FM1 and 5 and 13 days for FM2, depending on the rainfall intensity. Taking into account the outcomes in Table 6.6, slope failure will be deemed to occur prior to the infiltrated water reaching the phreatic line and the partially saturated fill, above the phreatic line, becoming completely saturated. Therefore, the indication is that time to perceived failure is shorter then that obtained from deterministic analysis.

Referring to the target reliabilities presented in Table 4.6, *Chapter 4: Subsection 4.5*, when $S_r = 57$ % upstream and downstream slopes are deemed stable ($\beta > 2.5$) prior to rainfall occurring, however, when there is prolonged rainfall at the dam site, they become 'vulnerable' in terms of classification even though their performance level remains within the satisfactory bounds.

From Table 6.7, short rainfall scenarios A, D and FP3 will not significantly affect the reliability index and the overall classification of the slope's performance level, irrespective of the fill's degree of saturation. However, as the behaviour of the individual slopes is still dependent on site-specific conditions, such as the fill's soil properties and saturation level, including the rate of precipitation, alternative failure modes (such as overtopping, runoff and surface erosion) could become more critical.

6.5.2 Analysis of the embankment's slopes for soil model M3B (London Clay)

For this parametric analysis, the impact the selected precipitation scenarios have on the reliability indices (β_{up} and β_{dwn}) for failure modes FM1 and FM2, for slope configurations SG5 and SG11 and saturation levels $S_r = 57$ % and 75 %, were evaluated for M3B (London Clay). As soil model M3B and M3A are both London Clay soil samples, there are noticeable similarities between their recorded depths of infiltrated water through the embankment's slopes and the reliability indices for FM1 and FM2 when exposed to the same dam site conditions.

i) Infiltration

The recorded deterministic depths of infiltrated water through the upstream (L_{up}) and downstream (L_{dwn}) slopes for soil model M3B are presented in the following table. As indicated by the results in Table 6.8, when the fill is highly saturated (S_r = 75 %) and there is prolonged rainfall (precipitation scenario F, FP1 and FP2) the infiltrated water will reach the idealised position of the phreatic line, in the upstream and downstream slopes, between 14 and 21 days.

Table 6.8 Depth of infiltrated water through the slopes, including time taken to reach the phreatic line for M3B (London Clay) with varying S_r for the selected precipitation scenarios

Precipitation Scenario†		**Rainfall Duration**	**Depth of infiltrated water through the embankment's slopes (cm) or time for complete failure (days) for M3B (London Clay)**							
			SG5 (1: 3.0, 1: 3.0)				SG11 (1: 3.0, 1: 4.0)			
			S_r = 57 %		S_r = 75 %		S_r = 57 %		S_r = 75 %	
			L_{up}	L_{dwn}	L_{up}	L_{dwn}	L_{up}	L_{dwn}	L_{up}	L_{dwn}
No Rainfall			-	-	-	-	-	-	-	-
Historic Scenarios	A	24 hrs	4.07	4.07	27.08	27.08	4.07	4.07	27.08	27.44
	D	2.5 hrs	1.23	1.23	5.46	5.46	1.23	1.23	5.46	5.50
	F	31 days	23.19	23.19	21 days♦	21 days♦	23.19	23.36	21 days♦	21 days♦
UKCP09 Scenarios	FP1	31 days	23.22	23.22	19 days♦	19 days♦	23.22	23.39	19 days♦	19 days♦
	FP2	31 days	23.29	23.29	14 days♦	14 days♦	23.29	23.45	14 days♦	14 days♦
	FP3	1 hr	0.62	0.62	3.12	3.12	0.62	0.62	3.12	3.14

†*See Table 6.5 for definitions of the abbreviations used for precipitation scenarios;* ♦*Approximate time taken for the infiltrated water to reach the calculated idealised position of the phreatic line during the rainfall event.*

Comparing precipitation scenarios A, D and FP3 (high rainfall intensity over a short duration) when S_r = 56 %, rainfall only infiltrates a short distance through the surface layers of the embankment fill. However, when S_r = 75 %, and subjected to the same precipitation scenarios, the depth of infiltrated water through the slopes is increased, most significantly for historic precipitation scenario A.

ii) Reliability

Table 6.9 shows the change in the reliability index for upstream (FM1) and downstream (FM1) slope failure, for M3B (London Clay), for the selected slope configurations and saturation levels, prior to and just after the rainfall event.

Table 6.9 Reliability indices for upstream (FM1) and downstream (FM2) slope failure, for soil model M3B (London Clay), with varying S_r for the selected precipitation scenarios

Precipitation Scenario†		Rainfall Duration	Reliability Index (β) for M3B (London Clay)							
			SG5 (1: 3.0, 1: 3.0)				SG11 (1: 3.0, 1: 4.0)			
			S_r = 57 %		S_r = 75 %		S_r = 57 %		S_r = 75 %	
			β_{up}	β_{dwn}	β_{up}	β_{dwn}	β_{up}	β_{dwn}	β_{up}	β_{dwn}
No Rainfall			2.91	1.22	2.88	1.22	2.81	2.09	2.77	2.09
Historic Scenarios	A	24 hrs	2.43	$F^*_{(23\ hrs)}$	$F^*_{(23\ hrs)}$	$F^*_{(2\ hrs)}$	2.32	1.96	$F^*_{(21\ hrs)}$	1.03
	D	2.5 hrs	2.58	1.11	2.31	$F^*_{(2\ hrs)}$	2.49	2.08	2.19	1.93
	F	31 days	1.26	$F^*_{(2\ days)}$	$F^*_{(6\ days)}$	$F^*_{(1\ day)}$	1.08	1.15	$F^*_{(5\ days)}$	$F^*_{(6\ days)}$
UKCP09 Scenarios	FP1	31 days	1.26	$F^*_{(2\ days)}$	$F^*_{(5\ days)}$	$F^*_{(1\ day)}$	1.08	1.15	$F^*_{(5\ days)}$	$F^*_{(6\ days)}$
	FP2	31 days	1.25	$F^*_{(2\ days)}$	$F^*_{(4\ days)}$	$F^*_{(1\ day)}$	1.07	1.14	$F^*_{(4\ days)}$	$F^*_{(4\ days)}$
	FP3	1 hr	2.62	1.14	2.43	1.06	2.53	2.10	2.33	2.03

†*See Table 6.5 for definitions of the abbreviations used for precipitation scenarios;* F^* *Indicates slope failure has occurred as* $\beta \leq 1.0$ *(F = Slope Failure).*

Comparing the change in the upstream slope's reliability index with the target reliabilities presented in Table 4.6, *Chapter 4: Subsection 4.5*, for both slope configurations, the upstream slope's behaviour and performance level is not significantly affected by precipitation scenarios A, D and FP3 when S_r = 56 %. However, for precipitation scenario A (24 hrs) when the fill is highly saturated the downstream slope has failed as its performance is deemed hazardous.

From Table 6.9, precipitation scenario FP3 will not affect the classification of the downstream slope's behaviour and performance level irrespective of the fill's degree of saturation for slope configurations SG5 and SG11, as there is only a small decrease in its notional reliability. The same outcome is observed for precipitation scenario D when S_r = 56 %. Yet when S_r = 75 %, precipitation scenarios A and D cause failure of the downstream slope for SG5 to occur within 2 hours, as its performance is deemed hazardous ($\beta \leq 1.0$), whereas for slope configuration SG11 its performance level remains satisfactory ($1.5 < \beta \leq 2.5$). Therefore, if there is a short-high intensity rainfall event (such as precipitation scenarios A and FP3), overtopping or runoff could develop leading to flooding downstream of the reservoir, as the embankment fill cannot absorb the excess rainfall.

Comparing slope configurations SG5 and SG11, when the fill has a high degree of saturation (S_r = 75 %), slope failure will occur during prolonged rainfall (precipitation scenarios F, FP1 and FP2). For SG5 downstream slope failure (FM2) will occur in 1 day, as its performance level even before rainfall occurs, can be classified as unsatisfactory ($\beta < 1.5$: $P_f > 7.0$ %). When its downstream slope gradient is 1 : 4.0 (SG11) slope failure will occur within 4 or 6 days. As shown in Table 6.9, depending on the rainfall intensity, failure of the upstream slope (FM1) will eventually occur between 4 and 6 days.

As expected, when comparing the results in Tables 6.7 and 6.9, change in β_{up} and β_{dwn} for FM1 and FM2, and Tables 6.6 and 6.8, depth of infiltrated water through the embankment's slopes, for M3A and M3B, the slopes behave in a similar manner. This is because the same hydraulic conductivity parameters, defined in Table 5.4 in *Chapter 5: Subsection 5.4.3*, have been applied for M3A and M3B, which have the same effective internal friction, but different void ratios, specific gravity and cohesion, as shown in Table 4.5, *Chapter 4: Subsection 4.3.3.1*. This implies that the soil properties of the embankment fill and precipitation scenario control the notional reliability of the upstream and downstream slopes.

As the results for soil types M3A and M3B demonstrate, the APSMP model can quantify the effect of uncertainties associated with the specific soil properties, as well as different dam geometries and rainfall parameters.

6.5.3 Analysis of the embankment's slopes for soil model M5 (Gault Clay)

i) Infiltration

Table 6.10 shows the evaluated depth of infiltrated water through the upstream and downstream slopes (L_{up} and L_{dwn}) for soil model M5 (Gault Clay), the slope configurations SG5 and SG11 when S_r = 57 % and 75 %.

Table 6.10 Depth of infiltrated water through the slopes, including time taken to reach the phreatic line for M5 (Gault Clay) with varying S_r for the selected precipitation scenarios

Precipitation Scenario†		**Rainfall Duration**	**Depth of infiltrated water through the embankment's slopes (cm) or time for complete failure (days) for M5 (Gault Clay)**							
			SG5 (1: 3.0, 1: 3.0)				SG11 (1: 3.0, 1: 4.0)			
			S_r = 57 %		S_r = 75 %		S_r = 57 %		S_r = 75 %	
			L_{up}	L_{dwn}	L_{up}	L_{dwn}	L_{up}	L_{dwn}	L_{up}	L_{dwn}
No Rainfall			-	-	-	-	-	-	-	-
Historic Scenarios	A	24 hrs	11.67	11.67	35.61	35.61	11.67	11.68	35.61	35.69
	D	2.5 hrs	3.74	3.74	10.74	10.74	3.74	3.74	10.74	10.75
	F	31 days	62.43	63.43	22 days♦	22 days♦	62.45	62.84	22 days♦	22 days♦
UKCP09 Scenarios	FP1	31 days	63.64	63.64	21 days♦	21 days♦	63.65	63.99	21 days♦	20 days♦
	FP2	31 days	66.24	66.24	15 days♦	15 days♦	66.24	66.47	15 days♦	15 days♦
	FP3	1 hr	2.36	2.36	6.71	6.71	2.36	2.36	6.71	6.71

†*See Table 6.5 for definitions of the abbreviations used for precipitation scenarios;* ♦*Approximate time taken for the infiltrated water to reach the calculated idealised position of the phreatic line during the rainfall event.*

Unlike previous soil models, M3A and M3B, when S_r = 57 % the depth of infiltrated water through the slopes is significantly higher even when there is a high intensity, short rainfall event (such as precipitation Scenario D). Looking at the prolonged precipitation scenarios F, FP1 and FP2, continuous rainfall for a month, the infiltrated water has almost reached the idealised position of the phreatic line when S_r = 57 %. Therefore, any excess water contained within the saturated layers of the embankment fill will continue to seep through the partially saturated fill until it reaches the phreatic line where it will either follow the trajectory of the phreatic line, towards the downstream toe, or continue to seep through the embankment towards its foundation. When S_r = 75 %, during short rainfall events with high intensity (precipitation scenarios A, D and FP3) the depth of infiltrated water through the individual slopes is more than three times that recorded when the partially saturated fill has a lower degree of saturation.

ii) Reliability

As shown in Table 6.11, for each slope configuration there is only a small decrease in the failure mode's notional reliability, upstream and downstream slope failure effectively, when subjected to short-high intensity rainfall (precipitation scenarios A, D and FP3), irrespective of the fill's saturation level. However, during prolonged rainfall (precipitation scenarios F, FP1 and FP2) the behaviour and performance classification for both slopes is significantly reduced, from above average and safe ($\beta > 2.5$:

P_f < 0.6 %) to the possibility of slope failure occurring (β < 1.5 : P_f > 7.0 %). similar outcomes are observed for both SG5 and SG11, indicated in Table 6.11.

Table 6.11 Reliability indices for upstream (FM1) and downstream (FM2) slope failure, for soil model M5 (Gault Clay), with varying S_r for the selected precipitation scenarios

Precipitation Scenario†		Rainfall Duration	Reliability Index (β) for M5 (Gault Clay)							
			SG5 (1: 3.0, 1: 3.0)				SG11 (1: 3.0, 1: 4.0)			
			S_r = 57 %		S_r = 75 %		S_r = 57 %		S_r = 75 %	
			β_{up}	β_{dwn}	β_{up}	β_{dwn}	β_{up}	β_{dwn}	β_{up}	β_{dwn}
No Rainfall			3.85	2.99	3.83	3.00	3.78	3.29	3.77	3.30
Historic Scenarios	A	24 hrs	3.41	2.78	2.44	2.30	3.32	3.09	2.34	2.56
	D	2.5 hrs	3.73	2.96	3.44	2.83	3.65	3.29	2.35	3.15
	F	31 days	1.44	1.76	F* (17 days)	1.24	1.38	1.96	F* (17 days)	1.33
UKCP09 Scenarios	FP1	31 days	1.40	1.74	F* (16 days)	1.24	1.34	1.93	F* (15 days)	1.33
	FP2	31 days	1.31	1.70	F* (11 days)	1.24	1.26	188	F* (11 days)	1.32
	FP3	1 hr	3.79	2.99	3.60	2.92	3.71	3.32	3.52	3.25

†See Table 6.5 for definitions of the abbreviations used for precipitation scenarios; F Indicates slope failure has occurred as β ≤ 1.0 (F = Slope Failure).*

Comparing the prolonged rainfall events in Tables 6.10 and 6.11, when the fill has a high degree of saturation (S_r = 75 %) upstream failure will occur between 11 and 17 days, depending on the average rainfall rate, even before the infiltrated rainfall has reached the phreatic line completely saturating the partially saturated fill. However, failure of the downstream slope is now likely, as its performance level is downgraded to unsatisfactory (β < 1.5 : P_f ≥ 7.0 %). As indicated by the results presented in Tables 6.10 and 6.11, further monitoring will be required, specifically at the downstream slope, to establish the level of emergency at the dam site if there is continuous rainfall for a significant length of time, even with low intensity rainfall.

6.5.4 Analysis of the embankment's slopes for soil model M6 (Silty Gravely Clay)

For this parametric analysis, the embankment has been constructed of a Silty Gravely Clay (M6). This soil type contains a greater percentage of gravel particles and has a higher cohesion, but lower void ratio and saturated hydraulic conductivity compared to the other clay like soil models (M3A, M3B and M5), as defined in Table 4.5 in *Chapter 4: Subsection 4.3.3.1*. However, M6 has the same effective internal friction as the London clay soil models M3A and M3B.

i) Infiltration

The following table, Table 6.12, shows that the recorded depth of infiltrated water L_{up} and L_{dwn}, for both SG5 and SG11, for soil model M6 are similar to those recorded for M3A and M3B. The deterministic results clearly show that during winter, when the fill above the phreatic line has a high saturation level, and there is continuous rainfall for a month (precipitation scenarios F, FP1 and FP2), the rainfall will completely saturate the embankment fill within 12 and 18 days, depending on the rainfall intensity. Yet when there is prolonged rainfall during summer, and the partially saturated fill has a lower degree of saturation (S_r = 57 %), approximately 30cm of fill's surface layers are completely saturated.

Table 6.12 Depth of infiltrated water through the slopes, including time taken to reach the phreatic line for M6 (Silty Gravely Clay) with varying S_r for the selected precipitation scenarios

Precipitation Scenario†		**Rainfall Duration**	**Depth of infiltrated water through the embankment's slopes (cm) or time for complete failure (days) for M6 (Silty Gravely Clay)**							
			SG5 (1: 3.0, 1: 3.0)				SG11 (1: 3.0, 1: 4.0)			
			S_r = 57 %		S_r = 75 %		S_r = 57 %		S_r = 75 %	
			L_{up}	L_{dwn}	L_{up}	L_{dwn}	L_{up}	L_{dwn}	L_{up}	L_{dwn}
No Rainfall			-	-	-	-	-	-	-	-
Historic Scenarios	A	24 hrs	5.26	5.26	43.34	43.34	5.23	5.25	43.34	43.37
	D	2.5 hrs	0.27	0.27	13.77	13.77	0.16	0.41	13.77	13.77
	F	31 days	30.54	30.54	18 days♦	18 days♦	30.52	30.53	18 days♦	17 days♦
UKCP09 Scenarios	FP1	31 days	30.62	30.62	17 days♦	17 days♦	30.55	30.64	17 days♦	16 days♦
	FP2	31 days	30.75	30.75	12 days♦	12 days♦	30.77	30.74	12 days♦	12 days♦
	FP3	1 hr	0.01	0.01	8.68	8.68	0.02	0.15	8.68	8.69

†*See Table 6.5 for definitions of the abbreviations used for precipitation scenarios;* ♦*Approximate time taken for the infiltrated water to reach the calculated idealised position of the phreatic line during the rainfall event.*

Comparing the results for short-high intensity rainfall events (precipitation scenarios A, D and FP3), when S_r = 57 % virtually no rainfall is absorbed by the embankment fill during 1 hour and 2.5 hours of rainfall, whereas only 5cm of the fill's surface layers are completely saturated when it rains for 24 hrs (precipitation scenario A). Therefore, other forms of failure, such as runoff or surface erosion due to the water remaining on the embankment's surface even after the rainfall event, would have to be considered when monitoring the embankment's expectant performance level, as a relative measure of the structure's current conditions. When it rains continuously for 24 hrs (precipitation

scenario A) there is a significant increase in L_{up} and L_{dwn} for both slopes and configurations during the winter months.

ii) Reliability

The following table, Table 6.13, shows the change in the reliability index for upstream (FM1) and downstream (FM2) obtained for each slope configuration for M6.

Table 6.13 Reliability indices for upstream (FM1) and downstream (FM2) slope failure, for soil model M6 (Silty Gravely Clay), with varying S_r for the selected precipitation scenarios

Precipitation Scenario†		**Rainfall Duration**	**Reliability Index (β) for M6 (Silty Gravely Clay)**							
			SG5 (1: 3.0, 1: 3.0)				SG11 (1: 3.0, 1: 4.0)			
			S_r = 57 %		S_r = 75 %		S_r = 57 %		S_r = 75 %	
			β_{up}	β_{dwn}	β_{up}	β_{dwn}	β_{up}	β_{dwn}	β_{up}	β_{dwn}
No Rainfall			3.53	2.89	3.53	2.89	3.49	3.19	3.48	3.20
Historic Scenarios	A	24 hrs	3.40	2.84	2.35	2.29	3.34	3.18	2.29	2.59
	D	2.5 hrs	3.54	2.88	3.15	2.71	3.49	3.23	3.08	3.05
	F	31 days	2.69	2.45	$F^*_{(18\ days)}$	1.68	2.63	2.76	1.10	1.85
UKCP09 Scenarios	FP1	31 days	2.70	2.45	$F^*_{(16\ days)}$	1.68	2.62	2.76	1.09	1.85
	FP2	31 days	2.69	2.45	$F^*_{(12\ days)}$	1.68	2.62	2.76	1.09	1.85
	FP3	1 hr	3.55	2.91	3.29	2.80	3.49	3.27	3.23	3.14

†See Table 6.5 for definitions of the abbreviations used for precipitation scenarios; F^* Indicates slope failure has occurred as $\beta \leq 1.0$ (F = Slope Failure).

It is evident in Table 6.13, for both configurations that when exposed to short-high intensity rainfall there is no threat of failure as defined in Table 4.6, *Chapter 4: Subsection 4.5*. When there is prolonged-low intensity rainfall, with low saturation levels, failure of both slopes is still unlikely to occur even though there is a decrease in the slope's notional reliability. Table 6.13 also shows that for SG5 and SG11, when S_r = 75 % failure of the embankment's slopes is unlikely to occur when there is short-high intensity rainfall (precipitation scenarios A, D and FP3) at the dam site. However, for SG5, when S_r = 75 % and there is prolonged rainfall, the upstream slope is deemed hazardous on both failure criteria. The downstream slope's behaviour is now poor with slope failure likely to develop ($1.5 < \beta < 2.5$), although the partially saturated fill above the phreatic line has become completely saturated (S_r > 80 %) within 12 to 18 days, as indicated in Table 6.12. This could be due to the soil's high cohesion (c = 14.4 kN/m^2), low void ratio and saturated hydraulic conductivity, see Table 4.5 in *Chapter 4: Subsection 4.3.3.1*, resulting in the downstream slope failing due to surface runoff, as the embankment fill can no longer absorb the rainfall.

By comparing these three soil models, the analysis outcomes demonstrate that APSMP is able to provide qualitative information on:

- The slope's notional reliability index for variable precipitation scenarios.
- The effect of the embankment fill's soil properties and the degree of saturation of the partially saturated fill, prior to rainfall occurring at the dam site.
- The depth that the water has infiltrated through the embankment.

Thus it has been demonstrated how sophisticated the APSMP model has become. However, it remains important to bear in mind that, for the purpose of comparative analysis, the obtained probabilities can only be taken as notional values, rather than manipulated as fixed values. This also reveals that the model can be improved further to take more specific information about the correlation between cohesion and internal friction and include better model for downstream toe and effect of vegetation.

6.5.5 Sensitivity factors for two comparable clay like soil models with identical slope configuration, degree of saturation and headwater height

From the completed analyses the sensitivity factors (α_i), which reflect the contribution of the inherent variability of the random variables, for downstream (FM2) failure were collated for soil models M3A (London Clay) and M5 (Gault Clay) respectively. Here, only slope configuration SG11 (USlope 1: 3.0, DSlope 1: 4.0) with variable S_r (S_r = 56 % and 75 %), representing summer and winter soil conditions, and the historic precipitation scenarios A and F, defined in Table 6.4, will be considered. By comparing precipitation scenarios A and F, it will be possible to identify which variables have the greatest and least impact on the overall reliability and associated performance level of the individual slopes during short-high intensity and prolonged-low intensity rainfall events. Furthermore, it will become evident how their level of importance is linked to:

- The effect of the rainfall event, in this case rainfall intensity.
- The type of soil used in the embankment's construction.
- The partially saturated fill's degree of saturation (variable between seasons).
- Downstream (FM2) failure for the given slope.

The following table, Table 6.14, shows the sensitivity factors for the uncertain random variables with the greatest and least impact for limit state FM2 under the said conditions. As highlighted in Table 6.14, the soil's cohesion (c') has the greatest impact on the notional reliability of the embankment's upstream and downstream slopes. Now that the rainfall's intensity is also modelled probabilistically, different unit weights of soil, indicated by the unit weight of soil factor (γ_{fct}), have a much higher level of importance when comparing it to the soil's internal friction (φ). However, the rainfall intensity, defined by the rainfall intensity factor (RI_{fct}), has a very small impact, due to high uncertainties in the soil parameters.

Table 6.14 Sensitivity factors (α_i) for all uncertain variables (defined in Tables 6.5) for FM2 for M3A and M5: Comparing precipitation scenarios A and F when S_r = 56 % and 75 %

Random Variables	**SENSITIVITY FACTORS (α_i)**			
	S_r = 56 %		S_r = 75 %	
	M3A (London Clay)	M5 (Gault Clay)	M3A (London Clay)	M5 (Gault Clay)
	Precipitation scenario A (short-high intensity rainfall)			
Cohesion (c')	0.7220	0.8793	0.7467	0.8793
Headwater Height (H_w)	2.33E-02	7.98E-03	2.50E-02	1.27E-02
Internal Friction (φ)	1.63E-05	4.81E-02	2.30E-03	6.95E-02
Rainfall intensity factor (RI_{fct})	3.17E-09	4.73E-07	1.47E-08	6.90E-08
Unit weight of Soil Factor (γ_{fct})	1.82E-02	2.90E-02	3.13E-02	5.13E-02
	Precipitation scenario F (prolonged-low intensity rainfall)			
Cohesion (c')	0.7718	0.8908	0.7823	0.8904
Headwater Height (H_w)	2.51E-02	1.26E-02	2.76E-02	6.18E-04
Internal Friction (φ)	7.81E-03	1.06E-01	3.92E-02	1.49E-01
Rainfall intensity factor (RI_{fct})	2.18E-06	7.49E-04	2.95E-02	4.28E-04
Unit weight of Soil Factor (γ_{fct})	3.86E-02	6.70E-02	8.08E-02	9.83E-02

Comparing the sensitivity factors for the selected variables in Table 6.14, with those in Table 4.7 in *Chapter 4: Subsection 4.6*, when rainfall is taken into account there is a noticeable increase the importance of the reservoir's headwater height (H_w). Lastly, the least important variables are still linked to the embankment's geometry. Namely its crest width (CW), height (H) and foundation height (H_f) regardless of the fill's degree of saturation and the rainfall intensity. However, they still have some degree of influence on the slope's reliability.

Comparing soil models M3A (London Clay) and M5 (Gault Clay), when their partially saturated fill has a high degree of saturation (S_r = 75 %) and the same prolonged-low

intensity rainfall event (precipitation scenario F) is applied, the soil's cohesion (c') remains the leading variable, but its impact has been reduced, due to the increase in the sensitivity factors for the soil's internal friction (φ) and the rainfall intensity factor (RI_{fct}). However, the different unit weights of soil, denoted by γ_{fct}, for both soil models and failure modes, remains more important than RI_{fct}, but not compared to φ.

In general, this information about sensitivity factors can be used to identify variables, which should be investigated further to update the probabilistic model reducing the uncertainty and, consequently increase the reliability as shown by Preziosi and Micic (2011a). The sensitivity factor for rainfall intensity will be variable to a high level between different limit states, e.g. slope stability, overtopping or runoff. The high sensitivity for variables that represent soil properties can be reduced with targeted experimental measurements.

6.5.6 Summary of observations from the applied parametric studies

From the parametric studies carried out for soil models M3A (London Clay), M3B (London Clay), M5 (Gault Clay) and M6 (Silty Gravely Clay), the results demonstrate that the APSMP model is an effective tool that can quantify the effect of variable precipitation scenarios on the notional reliability of the embankment's slopes. It is also able to take into account the soil properties and saturation level of the embankment fill.

As identified in the parametric studies, the embankment's slopes will be more reliable in summer when the fill has a lower degree of saturation rather than during winter when the fill will have a higher saturation level. Hence, the slope's overall performance in terms of its notional reliability can be quantitatively captured as a function of the fill's degree of saturation and the precipitation scenario, rainfall intensity and duration. Regardless of the rainfall's intensity and duration, it is clear from the parametric studies that the upstream and downstream slope gradients also influence the reliability of the slopes, as they regulate the calculated position of the phreatic line through the embankment. The main benefit here comes from quantitative measures that have included uncertainties and could be used with confidence as a comparative tool.

The APSMP model can also be used to assess the impact that the reservoir's headwater height has on the upstream and downstream slopes during a period of rainfall. While this effect has not been specifically considered here, *Chapter 4* has already established that when the dam's reservoir headwater height lowers the embankment's slopes are more reliable, compared to those whose reservoir has been maintained at its maximum allowable capacity. Therefore, precipitation will have less of an impact on the slope's notional reliability and associated performance level when the dam's reservoir has remained at a low level over a significant period of time.

Furthermore, it is clear from the results presented that when considering structural failure (slope instability) both the reliability index and depth of infiltrated water should be taken into account when defining the failure criteria.

6.6 Climate Scenario Implications on Engineering Risk

The reliability index obtained for failure modes FM1 and FM2 in previous sections has an associated probability of failure (P_f). This can provide information on the engineering risk associated with each limit state. By applying Eqn. (3.27) and Figure 3.5 in *Chapter 3: Subsection 3.8*, the engineering risk, which is the product of the probability of the event (P_f) and the consequence of the event, can be determined. Current guidelines have been developed with a view that dam failure is defined as low probability, high-consequence events, where consequence of dam failure is linked to:

- The potential loss of life due to a breach downstream of the dam.
- Damage to, or loss of, critical infrastructures (i.e. properties, services, roads, rail, etc.).
- Environmental and economic loss.

However, a small embankment dam in a specific location, could have a high probability of failure (P_f = 2.3 %) and low consequence (no loss of life and limited economic loss should dam failure occur). Whereas the same type of embankment dam, but in a different location could meet the safety standards (P_f = 0.003 %) and yet have high consequence due to high economic loss, linked to damage of critical infrastructures such

as motorways, railways, etc. As a result, the latter would be considered as currently presenting a greater risk to public when climate change scenarios are included, due to high level of associated uncertainties. However, the former is also relevant.

By using data collated from APSMP, it will be possible to consider different limit states and consequences (such as loss of life, economic loss, etc.) associated with dam failure when determining the dam's risk classification. Furthermore, by applying the benchmark classifications defined in Table 4.6, *Chapter 4: Subsection 4.5*, the slopes expected performance level, as a function of its notional probability of failure, can be established and the dam's risk classification reassessed in terms of engineering risk.

To demonstrate the application of APSMP to quantify the impact future precipitation scenarios can have on the notional level of engineering risk associated with small earthfill embankment dams, the following graphs, Figures 6.6 and 6.7, are presented. Here, the graphs show the change in P_f for FM2 (downstream slope failure) for soil models M5 (Gault Clay) and M6 (Silty Gravely Clay) when exposed to different prolonged precipitation scenarios (7 days), such as those defined in Table 6.3. For this specific analysis, it was assumed that the partially saturated fill has a high saturation level (S_r = 75 %) and the considered consequences are identical for the selected precipitation scenarios.

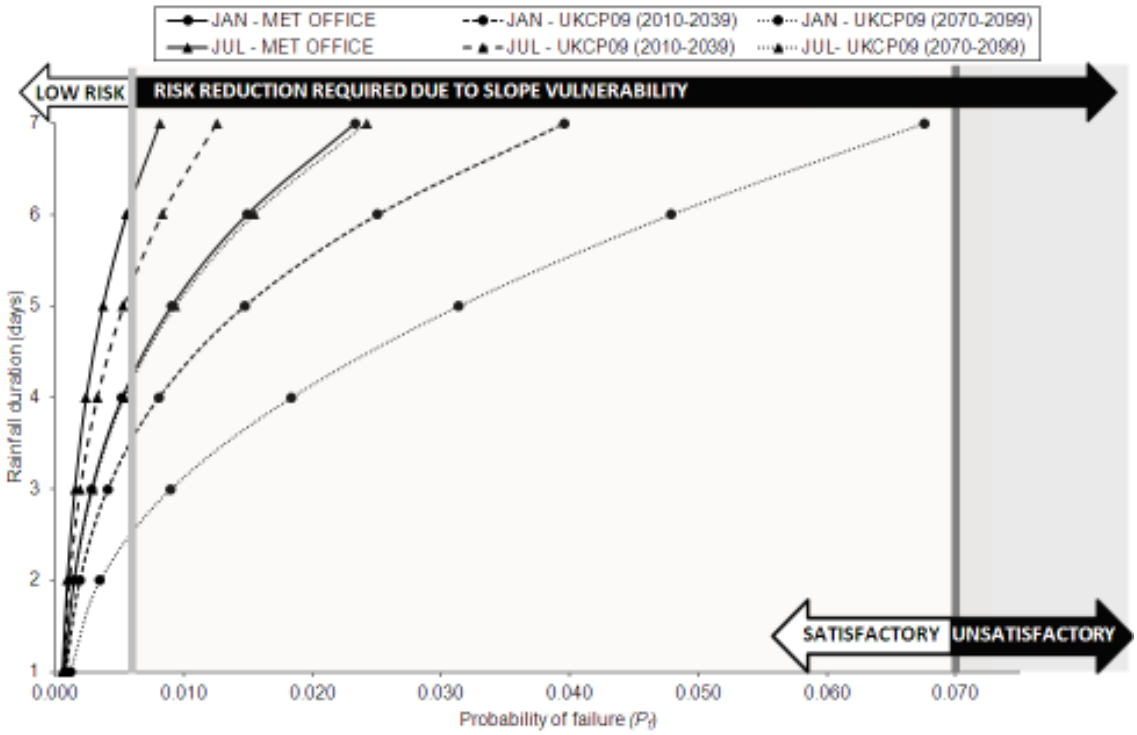

Figure 6.6 Change in P_f for downstream slope failure under variable precipitation scenarios for soil model M5 (Gault Clay)

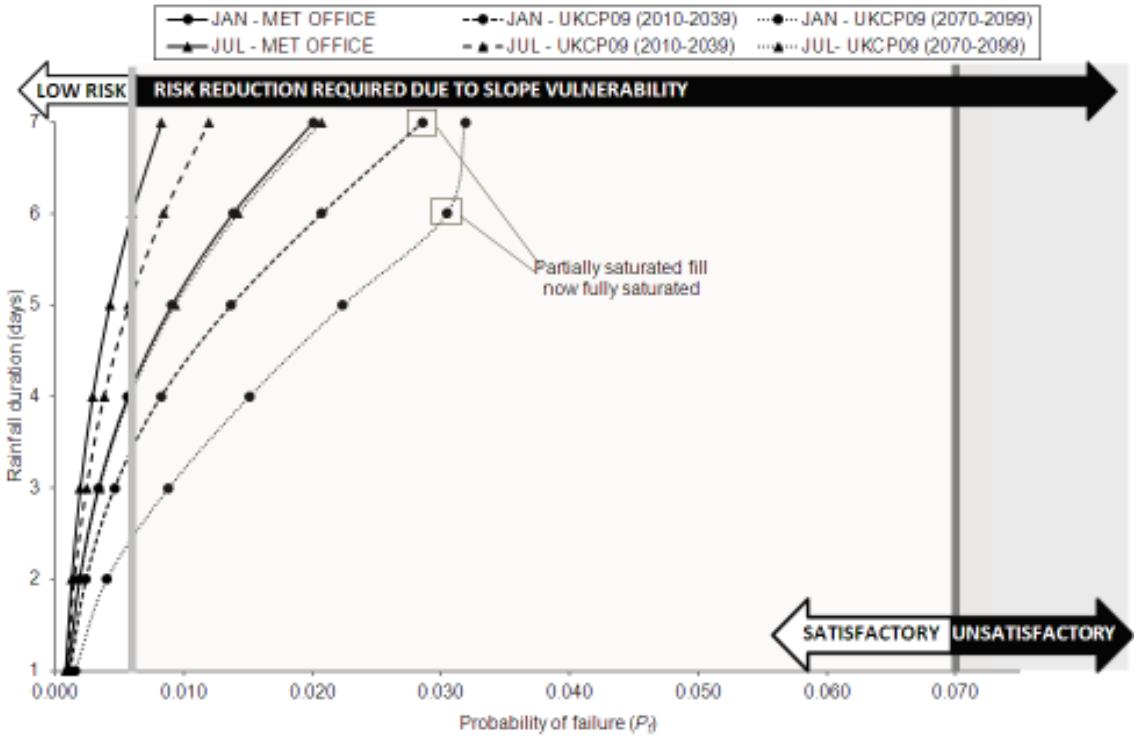

Figure 6.7 Change in P_f for downstream slope failure under variable precipitation scenarios for soil model M6 (Silty Gravely Clay)

As demonstrated in Figures 6.6 and 6.7, the performance of the downstream slope is noticeably variable over the rainfall's duration. This indicates slope vulnerability emerging and a requirement for risk reduction measures due to the changes in the dam's conditions. In addition, probabilities of failure indicate satisfactory and unsatisfactory performance levels and corresponding critical precipitation effects.

Small homogeneous earthfill embankment dams, such as those modelled here, are at present often classified as low risk. However, even if it is the case when consequences of failure are constant, it is evident that associated risk will be variable. When there is prolonged rainfall at the dam site its risk classification would need to be amended, as significant damage (not only in loss of life) could threaten the area downstream of the embankment due to complete slope failure. In contrast, when there is short-high intensity rainfall at the dam site, the embankment fill cannot absorb the excess rainfall. This could eventually lead to flooding, due to overtopping or surface runoff, downstream of the embankment. Thus, alternative limit states, such as those relating to overtopping or surface runoff would become a base for risk classification as they have their own associated probability of occurrence, defined using Eqn. (3.27) in *Chapter 3: Subsection 3.8*.

It is evident that the engineering risk is a comprehensive and useful measure for small homogeneous earthfill embankment dams that will not only differ between seasons, time horizons and the rainfall events, but is also dependent on the embankment fill's composition (mechanical and hydraulic soil properties), vegetation cover, any past strengthening, deterioration, the presence of the toe, spillway, etc.

6.7 Concluding Remarks

The parametric studies carried out using the APSMP methodology have demonstrated the effect on upstream and/or downstream slope performance of:

- Climate scenarios defined by the rainfall's duration and rainfall intensity.
- The embankment fill's mechanical and hydraulic properties.
- Embankment configuration.

By implementing APSMP, the quantitative effect of alternative future precipitation scenarios for selected time horizons and, in particular, associated risk were investigated.

Extensive application of the new advanced probabilistic slope stability model with precipitation effects (APSMP) has been presented, which quantitatively measures the notional reliability for small, well-established, homogeneous earthfill embankment dams against upstream and downstream slope failure when exposed to variable precipitation scenarios. This form of modelling can therefore be used as an additional tool to existing deterministic methods, as it includes a comprehensive precipitation model, which takes into account the soil and hydraulic properties of the embankment fill. Hence, it can provide useful information about the behaviour of the slopes in the presence of site-specific uncertain factors and different precipitation scenarios. With a view that this approach could be used for developing statutory guidelines, failure is defined in terms of reliability index and depth of infiltration.

It is demonstrated how engineering risk associated with climate scenarios can be evaluated using APSMP. The main features of the new advanced probabilistic slope stability model with precipitation effects (APSMP) can be summarised as follows:

- The uncertainties associated with the embankment fill's soil properties are taken into account and the effect of rainfall on the embankment fill's soil characteristics quantified.
- When modelling the cross-section of the homogeneous earthfill embankment, its configuration is considered probabilistically, as the dam's geometry may have changed since its construction.

- The time to slope failure can be predicted when the embankment dam is exposed to variable, seasonal, precipitation.
- The notional reliability of the individual slopes, when exposed to future climate scenarios, in this case future rainfall events, is obtained.
- The change, if any, in the classification of the upstream and downstream slopes behaviour and performance level can be estimated by comparing their reliability index, obtained using APSMP, with the target reliability indices and performance levels.

This approach can be enhanced by considering more comprehensively correlation between the soil's mechanical characteristics as well as taking into account vegetation cover, the presence of drainage at the downstream toe and the real trajectory of the phreatic line through the embankment.

In practice, APSMP can be applied for genuine site-specific conditions and rainfall scenarios identified at the dam site. Hence, the requirement for on-site testing, which is very expensive and time consuming can be reduced. Thus, decisions about future inspections, monitoring, maintenance, discontinuity, etc. of the embankment dam can be undertaken.

In order for APSMP to be applied at multiple dam sites, specific guidelines such as the Probabilistic Model Code developed by JCSS (2006) are still required in order to fully address the quality of information and appropriate modelling techniques necessary for all relevant limit states. Therefore, by using APSMP it will be possible to quantify the impact extreme future precipitation scenarios could have on the notional level of engineering risk associated with specific dam failure.

It will also be possible to consider different limit states and consequences (such as loss of life, economic loss, etc.) associated with dam failure when determining the dam's risk classification. Hence, APSMP can provide useful information about the behaviour of the embankment's individual slopes in the presence of site-specific uncertain factors and future precipitation scenarios.

CHAPTER 7 : CONCLUSIONS AND DISCUSSION

7.1 Introduction

The probabilistic methodology has been developed that can provide quantitative measures of the notional reliability and probability of upstream and downstream slope failure for small homogeneous earthfill embankment dams subject to climate scenarios. To reflect the critical conditions conducive to slope failure, a benchmark has been developed. Using outcomes from APSMP the engineering risk associated with upstream and downstream slope failure was established and related to the performance levels associated with the site conditions. In this chapter, conclusions and recommendations for future work are presented.

7.2 Conclusions and Discussions of Findings

7.2.1 Summary of findings

Initial research has indicated that there is a need for improved engineering risk assessment, in particular, for those dams whose reservoir capacities are between 10,000 m^3 and 25,000 m^3 that were previously outside the Reservoir Act 1975, but will now be subject to the guidelines set out in the new Flood and Water Management Act 2010. Many reasons being support this view.

- The requirements at the time of design and construction for many of the UK's small, earthfill, embankment dams were generally less stringent and little information was required about their condition in the meantime.

- It is unlikely that detailed, consistent, data relating to the dam's embankment and reservoir is readily available.
- It is increasingly evident that effects of climate need to be assessed.

Probabilistic approach to dam assessment was identified as necessary to account for current conditions. Compared to conventional deterministic slope stability analyses, the probabilistic approach can incorporate uncertainties associated with specific parameters such as extreme rainfall events, the current dam site conditions, etc. Assumptions have been made that the generic physical model of the embankment had no vegetation cover, there was no drainage adopted at the downstream toe and the embankment's foundation was constructed without an incline. A mathematical representation of the idealised trajectory of the phreatic line was incorporated into the physical model by applying the steady seepage flow model, as it is theoretically independent of the embankment fill's soil type.

From a selection of failure modes that can develop within a small homogeneous earthfill embankment dam it was established that structural failure in the form of slope instability combined with the effects of seepage failure and rainfall infiltration were relevant forms of failure to establish a methodology for assessment of the slope's performance for future climate scenarios. Therefore, the physical model and explicit formulation for the relevant limit states were identified. To respond to modelling requirements in the presence of uncertainties and with the view of precipitation scenarios, the sliding block method (SBM) was selected. Unlike other limit equilibrium methods, the deterministic slope stability model formulated using SBM is suitable to characterize the behaviour of the embankment's individual slopes in relation to the complete structure including the embankment's foundation.

Different forms of probabilistic modelling were considered, but for the purpose of this research, the Level 2 structural reliability analysis in the form of First Order Reliability Method (FORM) was selected. By incorporating the deterministic slope stability methodology within the First Order Second Moment method (FOSM), the advanced deterministic slope stability model with precipitation effects (APSMP) was developed.

As a result, the performance level of the individual slopes can be quantified as a function of their notional reliability.

To assess the impact future precipitation scenarios could have on the performance of the embankment's upstream and downstream slopes, as a function of their notional reliability (probability of failure), UKCP09 future climate projections and specific past rainfall events were selected and different precipitation scenarios, for selected time horizons, developed. It was then possible to quantify the impact these precipitation scenarios would have on the notional level of engineering risk associated with slope failure of small earthfill embankment dams, in this case slope instability, by incorporating these precipitation scenarios into the APSMP formulation.

From the probabilistic analyses, as expected, the reliability of the upstream and downstream slopes is noticeably higher during summer compared to winter, when the embankment has a higher saturation level. Equally when there is prolonged rainfall, the reliability of the embankment's slopes is greatly reduced over the rainfall's duration, irrespective of the rainfall's intensity. This could eventually lead to complete failure of the individual slopes. Furthermore, the rainfall's duration also influences the time to perceived failure, as slope failure can arise prior to the infiltrated water completely saturating the embankment fill above the idealised phreatic line.

During a short-high intensity rainfall event, failure due to overtopping or surface runoff is more likely to be a cause of concern. As a result, alternative limit states would become a base for risk classification as they have their own associated probability of occurrence. From APSMP and taking into consideration a specific extreme precipitation scenario, it will be possible to categorize the change, if any, in the slope's overall performance and risk classification, as a measure of its notional probability of failure, over the rainfall's duration.

From probabilistic analyses, it was possible to identify the random variables with the greatest impact. Those associated with the embankment fill soil properties (cohesion, internal friction and the unit weights of the soil) were identified in examples. This

information can be used to identify the variables that should be investigated further to update the probabilistic model, reducing the uncertainty and consequently increase the reliability of the model. Furthermore, if Undertakers (owner or user) of small earthfill dams do not have an extensive budget to perform lab and dam site tests, the probabilistic approach enables more thorough assessments to be carried out given the same budget.

The probabilistic approach is also an appropriate method when trying to assess possible change, both short and long term, in:

- Slope's performance level as a measured by the notional probability of failure.
- Dam's risk classification.

As the UK currently does not have a consistent probabilistic risk assessment that can be drawn upon, a benchmark was developed that reflects the critical conditions conducive to slope failure. This benchmark was selected as a reference with which to compare the effect of precipitation, if any, on the predicted behaviour and performance of the embankment's individual slopes.

From the results presented, the methodology within APSMP enables an informed assessment of small homogeneous earthfill embankment dams for complex climate scenarios.

7.2.2 APSMP in relation to the Flood and Water Management Act 2010

It is right that engineering risk is now being considered as a relevant measure for dam safety under the Flood and Water Management Act 2010. However, the quantification of risk as set out in the Act is based solely on the number of lives which might be lost as a consequence of dam failure, regardless of the probability of such an outcome. As a result, if a large raised reservoir were to be categorized as high-risk, the probability of a significant impact to the public due to dam failure would likely be smaller, on account of the vigorous regulations already in place to mitigate and guard against such incidents.

Small earthfill dams are currently often considered to have a relatively low impact on loss of human life should the failure occur. However, in practice the failure of these structures can still have a significant impact through damage to neighbouring buildings and infrastructure. Moreover, due to the complexity and uncertainties associated with small earthfill embankment dams, the level of risk at a site may vary over time, as may the consequences linked to dam failure. Such variations could be caused by modifications to the dam's embankment and/or its reservoir, strengthening of the embankment, poor maintenance of the dam site or changing climate conditions.

APSMP is well-placed to assist in this process. By carrying out a more detailed engineering risk analysis using the tool, a more complete picture of the dam's behaviour during extreme precipitation events can be achieved, which can then be reconciled against existing legislation or guidelines and provide information to experts.

Using APSMP it has been possible to demonstrate that the duration of a rainfall event has a significant bearing upon the probability of failure of small earthfill dams, and specifically time to failure. Moreover, by also applying UKCP09 climate precipitation projections within APSMP, longer-term safety assessments can be made at individual dam sites, without the need for further on-site testing.

The results obtained from APSMP can also be used to identify the impact dam failure of a specific small earthfill embankment dam could have on the loss of life downstream of its embankment. In addition to loss of life, it would also be beneficial to consider additional consequences of dam failure (such as economic loss, cost to infrastructure, damage to properties, insurance expenditure, etc.) when reassessing the dam's risk classification.

7.3 Recommendations for Future Work

While slope failure is one of the most commonly recorded forms of failure, various limit states affect the overall safety of small earthfill embankment dams. In drawing up future guidelines, the interaction between the respective limit states and consequences of different failure events could also be taken into account, enabling the risk classification for a specific small earthfill embankment dam, subject to its current conditions, to be more comprehensive. This level of analysis can assist Undertakers and/or the appropriate bodies overseeing small earthfill dams to make informed decisions about future inspections, monitoring or discontinuity of the dam. The benefit of this would be a reduction in the requirements for further on-site testing, which can be both expensive and time consuming.

As the work presented here is the first attempt to incorporate future climate projections into standard engineering analysis, it is recommended that future investigations are needed, in order to address the network level implementation of the procedure. If this were the case, the application of the probabilistic approach would need to be strictly defined in the relevant regulatory documentation, such as the Flood and Water Management Act 2010. The APSMP methodology can be expanded to consider alternative dam profiles, embankment fills and varying rainfall rates. This would enable a more detailed evaluation of the current status of the dam and any future conditions at the dam site to aid planning by the Owners and/or Undertakers. To achieve this:

- The probabilistic model should be validated for a real UK dam site and site-specific precipitation data using APSMP, where the calculated reliability indices for the individual slopes are compared to the benchmark target reliability indices and associated performance levels including outcomes obtained using deterministic techniques.
- The physical model could be updated to include soil layers that can reflect either different soil types within a single layer or the variability of the soil properties relative to its depth within the embankment. Alternatively, identifying whether finite element modelling in a geotechnical engineering context, for the cross section of the embankment and its foundation, could be implemented in APSMP.

While the computational time is a significant factor here, with technological advances it might become a case that convergence will be much improved. Such improvements would provide a more accurate methodology to determine the trajectory of the phreatic line, variations in the soil's mechanical and hydraulic properties including the depth of infiltrated water through the earthfill embankment during a given rainfall event.

- A more comprehensive probabilistic soil mechanics model should be developed using relevant experimental data to establish the site-specific mechanical and hydraulic soil properties, specifically the saturated hydraulic conductivity. With intense advances in sensing technology, experimental data is continuously being improved upon and as such, more sophisticated probabilistic modelling can be envisaged.
- The modelling techniques used to define the spatial variability of the soil properties should be improved, as they are a major contributor to the overall stability of the embankment's slopes. At present, the probabilistic model assumes the soil properties are uncertain, but uniform within the embankment fill and foundation of the embankment as different sources of uncertainties are encountered and estimations of the soil properties are difficult to quantify.
- The embankment's physical model could be expanded to include a protective grass layer on the embankment (crest, downstream and upstream slopes effectively), a zoned core and the angle of the foundation's incline.
- The dam's risk classification could be refined to also include additional consequences of dam failure (such as economic loss, cost to infrastructure, damage to properties within flood zone, etc.), as their probability of occurrence will vary for different failure events.
- Expert opinion would help to review the benchmarking options, as target probabilities of failure should reflect the state of the art within practice.

In addition, further development with respect to the probabilistic approach can be achieved by:

- Identifying and incorporating detailed models for alternative failure modes associated with dams, together with their related local factors in order to establish the dam's true risk classification.

- Extending the probabilistic approach to alternative limit states and identifying, if any, the correlation between limit states, in order to develop a more comprehensive probabilistic approach, as they can be affected by a combination of site-specific local factors fundamental in the embankment's long-term performance, including the extent and location of the failure in the embankment.
- Expanding the physical model to include site-specific information, such as the effects of any maintenance or strengthening carried out on the dam's embankment and reservoir during the dam's lifetime. This could include repairs to the downstream toe or resurfacing of the embankment's slopes and crest.

Thus, APSMP provides a useful tool that is not intended to replace existing risk assessments, but to improve the quality of information used by the decision-makers when considering the likelihood of dam failure occurring and its impact on infrastructure performance and public safety, in presence to climate effects.

REFERENCES

Abramson, L. W., Lee, T. S., Sharma, S., & Boyce, G. M. (2002) *Slope Stability and Stabilization Methods*. 2nd edition. New York, John Wiley & Sons.

Agate, E. (2001) Chapter 13 Dams, Weirs and Sluices. In: Brooks, A. & Agate, E. (eds.) *Waterways and Wetlands*. BTCV Publications. pp. 109-128.

Almog, E., Kelham, P., & King, R. (2011) *Modes of dam failure and monitoring and measuring techniques*. Environment Agency, Product code: SCHO0811BUAW-E-E.

Ang, A. H-S., & Tang, W. H. (1984) Probability Concepts in Engineering Planning and Design, Vol. I - Basic Principles. New York, John Wiley & Sons.

Atkinson, J. (1993) An introduction to the Mechanics of Soils and Foundations: through critical state soil mechanics. London, McGraw-Hill.

Babtie Group and the Centre for Ecology and Hydrology. (2002) *Climate Change Impacts on the Safety of British Reservoirs*. Department of the Environment, Transport and the Regions (DETR) now DEFRA. Report: WT01002.

Babtie Group the Centre for Ecology and Hydrology (DEFRA). (2003) *Climate Change Impacts on the Safety of British Dams - Advice Note on Rainfall induced instability of Dam Embankments*, Dam Safety Research, DETR, Babtie Group & the Centre for Ecology and Hydrology. [Online] Available from: http://www.britishdams.org/reservoir_safety/defra-reports/200201Climate%20change%20impacts%20on%20the%20safety%20of%20British%20reservoirs.pdf [Accessed March 2007].

Baecher, G. B., & Christian, J. T. (2003) *Reliability and Statistics in Geotechnical Engineering*. Chichester, UK, John Wiley& Sons.

Baker, J., Calle, E., & Rackwitz, R. (2006) *JCSS Probabilistic Model Code, Section 3.7: Soil Properties, Updated Version.* Technical report, Joint Committee on Structural Safety (JCSS), Lyngby, Denmark.

Baker, R. (2006) A relation between safety factors with respect to strength and height of slopes. *Computers and Geotechnics*, **33** (4-5), 275-277.

Barnes, G. E. (2000) *Soil Mechanics: Principles and Practice*. 2nd edition. Basingstoke, MacMillan Press.

Baxter, G., & Hope, I. (2009) *Reservoir Safety Research and Development Strategy Final Report*: Flood and Coastal Erosion Risk Management Research and Development Programme. Product Code: GEHO0309BPRG-E-E.

Bedient, P. B., Huber, W. C., & Vieux, B. E. (2008) *Hydrology and floodplain analysis*. 4th edition. New Jersey, Pearson Education.

Bell, F. G. (1992) *Engineering Properties of Soils and Rocks*. 3rd edition. Oxford, Butterworth Heinemann.

Bhattacharya, G., Jana, D., Ojha, S., & Chakraborty, S. (2003) Direct search for minimum reliability index of earth slopes. *Computers and Geotechnics*, **30** (6), 455-462.

Bishop, A. W. (1955) The use of the slip circle in the stability analysis of slopes. *Géotechnique*, **5** (1), 7-17.

Bowles, J. E. (1984) *Physical and Geotechnical Properties of Soils*. 2nd edition. New York, McGraw-Hill.

British Standards Institution (2009) BS 6031:2009. *Code of Practice for Earthworks.* Milton Keynes, BSI.

Bromhead, E. N. (1992) *The Stability of Slopes*. 2nd edition. London, Blackie Academic & Professional.

Bromhead, E. N., Harris, A. J., & Watson, P. D. J. (1999) Influence of pore water pressure in partly submerged slopes on the critical pool level. In: Yagi, N., Yamagami, T. and Jiang, J-C (eds.) IS-Shikoku'99: *Volume 1 of Slope Stability Engineering: Proceedings of the International Symposium on Slope Stability Engineering- IS-Shikoku'99, 8-11 November 1999, Matsuyama, Shikoku, Japan.* London, A.A. Balkema. pp. 411-416.

Brooks, R. H., & Corey, A. T. (1964) Hydraulic properties of porous media. *Hydrololgy Paper 3*. Colorado State University, Fort Collins, CO, USA.

Brown, A., & Gosden, J. (2000) Safety issues at small reservoirs. In: Tedd, P. (ed.) Dams 2000: Risk and Reservoir Safety: *Proceedings of the 11th Conference of the British Dam Society, Dams 2000, June 2000, Bath, UK*. London, Thomas Telford. pp. 159-172.

Brown, A., & Gosden, J. (2004) *Interim Guide to Quantitative Risk Assessment for UK Reservoirs*. KBR/DEFRA. London, Thomas Telford.

Buijs, F., Simm, J., Wallis, M., & Sayers, P. (2005) *Performance and Reliability of Flood and Coastal Defences*. Joint Defra/EA Flood and Coastal Erosion Risk Management R&D Programme, DEFRA/Environment Agency, R&D Technical Report: FD2318/TR2.

Building Research Establishment (BRE). (2003) *Register of British Dams May 2003*.

Cai, F., & Ugai, K. (2002) Some aspects of finite element analysis of rainfall effects on slope stability. In: Proceedings of the 3rd International Conference on Landslides, Slope Stability & the Safety of Infra-Structures, 11-12 July 2002. Singapore. pp. 149-156.

Cameron, D. (2010) *The owner's guide to reservoir safety*. Environment Agency, Product code: GEHO0210BRRU-E-E

Carder, D. R., & Barker, K. J. (2005) *The performance of a single row of spaced bored piles to stabilise a Gault Clay slope on the M25*. Wokingham, Transport Research Laboratory (TRL). TRL Report number: TRL 627.

Carsel R. F., & Parrish, R. S. (1988) Developing joint probability distributions of soil water retention characteristics. *Water Resources Research*, **24** (5), 755-769.

Casagrande, A. (1937) Seepage through dams. *New England Water Works*. **51**(2), pp. 295-336.

Cedergren, H. R. (1989) *Seepage, Drainage, and Flow Nets*. 3rd edition. New York, Wiley-Interscience.

Charles, J. A. (2002) Internal erosion in European embankment dams. In: Tedd. P, (ed.): *Reservoirs in a Changing World: Proceedings of the 12th British Dam Society Conference, Dublin, Ireland*. London, Thomas Telford. pp. 378-393.

Charles, J. A., Tedd, P., & Warren, A. (2011) *Evidence Report - Lessons from historical dam incidents*. Environment Agency, Project: SCO80046/R1. Product Code: SCHO0811BUBA-E-E.

Charles, J. A., Tedd, P., Hughes, A. K., & Lovenbury, H. T. (1996) *Investigating embankment dams: a guide to the identification and repair of defects*. Building Research Establishment (BRE). Construction Research Communications Ltd, London. Report number: BR 303.

Chen, L., & Young, M. H. (2006) Green-Ampt infiltration model for sloping surfaces, *Water Resources Research,* **42** (7): W07420, 1-9.

Cherubini, C. (2000) Reliability evaluation of shallow foundation bearing capacity on c′, φ′ soils. *Canadian Geotechnical Journal*, **37** (1), 264-269.

Cheung, R. W. M., & Tang, W. H (2005) Realistic assessment of slope reliability for effective landslide hazard management. *Géotechnique*, **55** (1), 85–94.

Ching, J., Phoon, K-K., & Hu, Y-G. (2010) Efficient Evaluation of Slope Reliability Using Importance Sampling. In: Furuta, H. (ed.) *ICOSSAR 2009: Safety, Reliability and Risk of Structures, Infrastructures and Engineering Systems: Proceedings of the 10th International Conference on Structural Safety and Reliability, ICOSSAR 2009, Osaka, Japan*. pp. 214-221.

Cho, S. E. (2009) Infiltration analysis to evaluate the surficial stability of two-layered slopes considering rainfall characteristics. *Engineering Geology*, **105**, 32-43.

Chow, V. T., Maidment, D. R., & Mays, L. W. (1988) Chapter 4 Subsurface flow. In: Clark, B. J., & Morriss, J. (eds.) *Applied Hydrology*. New York, McGraw-Hill. pp. 99-174.

Chowdhury, R., Flentje, P., & Bhattacharya, G. (2010) *Geotechnical Slope Analysis*. The Netherlands, CRC Press/Balkema.

Craig, R. F. (1992) Chapter 9 Stability of Slopes. In: *Soil Mechanics*. 5th edition. London, Chapman & Hall. pp. 366-392.

Creager, W. P., Justin, J. D., & Hinds, J. (1945a) *Engineering for Dams Volume 1: General Design*. 6th edition. New York, Wiley.

Creager, W. P., Justin, J. D., & Hinds, J. (1945b) *Engineering for Dams Volume III: Earth, Rockfill, Steel and Timber Dams*. 6th edition. New York, Wiley.

Crookes, N. (2004a*) (WP2) – Identifying Potential Breach Location*. Investigation of Extreme Flood Process and Uncertainty (IMPACT). [Online]. Available from: http://www.impact-project.net/AnnexII_DetailedTechnicalReports/AnnexII_PartA_WP2/BreachLocationReport_v3_1.pdf [Accessed 2007].

Das, B. M (2008) Seepage. In: *Advanced Soil Mechanics*. 3rd edition. UK, Taylor & Francis. p.p 262-268.

Das, S. K. (2005) Slope Stability Analysis using Genetic Algorithm. *Electronic Journal of Geotechnical Engineering (EJGE*). [Online] **10** (Bundle A). Available from: www.ejge.com/2005/Ppr0504/Ppr0504.htm [Accessed 30 July 2007].

Davis, O., Rouainia, M., Glendinning, S., & Birkenshaw, S. (2008) Assessing the Influence of Climate Change on the Progressive Failure of a Railway Embankment.

In: *Geomechanics in the Emerging Social & Technological Age: Proceedings of the 12th IACMAG Conference, Goa, India*. Toronto: X-CD Technologies Inc., Paper No. Q06.

Ditlevsen O., Madsen H.O. (2007) *Structural reliability methods*, Internet Edition. 2.3.7, John Wiley & Sons, Chichester, UK. Available from: http://www.web.mek.dtu.dk/staff/od/books/OD-HOM-StrucRelMeth-Ed2.3.7-June-September.pdf [Accessed March 2012].

Duncan, J. M. (2000) Factors of safety and reliability in geotechnical engineering. *Journal of Geotechnical and Geoenvironmental Engineering, ASCE*, **126** (4), 307-316.

Duncan, J. M., & Wright, S. G. (2005) *Soil Strength and Slope Stability*. Hoboken, New Jersey, Wiley.

Eagleson, P. S: (1970) *Dynamic hydrology*. McGraw Hill Book Co.

Eberhardt, E. (2003) Rock Slope Stability Analysis - Utilization of Advanced Numerical Technique. *Geological Engineering/Earth and Ocean Sciences*, UBC, Vancouver, Canada.

El-Ramley, H., Morgenstein, N.R., & Cruden, D.M. (2002) Probabilistic slope stability analysis for practice. *Canadian Geotechnical Journal,* **39** (3), 665-683.

Faber, M. H., & Stewart, M. G. (2003) Risk assessment for civil engineering facilities; critical overview and discussion. *Reliability Engineering and System Safety*. **80** (2), 173-184.

Faber, M. H., & Vrouwenvelder, A. C. W. M. (2008) Background Documents on Risk Assessment in Engineering, Background Document #2: Interpretation of Uncertainties and Probabilities in Civil Engineering Decision Analysis. Joint Committee on Structural Safety (JCSS).

Fell, R., Bowles, D. S., Anderson, L. R., & Bell, G. (2000) The status of methods for estimation of the probability of failure of dams for use in quantitative risk assessment. In: *Proceedings of the 20th Congress on Large Dams, Vol. 1, Question 76, Beijing, China*. International Commission on Large Dams (ICOLD). pp. 213-235.

Fell, R., MacGregor, P., & Stapledon, D. (1992) Stability Analysis. In: *Geotechnical Engineering of Embankment Dams*. Rotterdam, A. A. Balkema. pp. 342-358.

Fellenius, W. (1936) Calculation of the Stability of Earth Dams. *In: Transactions* of *2nd International Congress on Large Dams*, Washington DC, USA, Vol 4, pp. 445-459.

Gasmo, J. M., Rahardjo, H., & Leong, E. C. (2000) Infiltration effects on stability of a residual soil slopes. *Computers and Geotechnics*, **26** (2), 145-165.

Gavin, K., & Xue, J. F. (2008) A simple method to analyze infiltration into unsaturated soil slopes. *Computers and Geotechnics*, **35** (2), 223-230.

Gens, A., & Alonso, E. E. (2006) Aznalcóllar dam safety. Part 2: Stability conditions and failure mechanism. *Géotechnique*, **56** (3), 185-201.

Gething, B. (2010). Design for Future Climate: Opportunities for Adaptation in the Built Environment. Technology Strategy Board, Swindon, UK.

Glendinning, S., Rouainia, M., Hughes, P., & Davies, O. (2006) Biological and engineering impacts of climate on slopes (BIONICS): The first 18 months. In Proc.10th IAEG Congress, Nottingham, Paper 348 (on CD). [Online] Available from: http://www.iaeg.info/iaeg2006/PAPERS/IAEG_348.PDF [Accessed January 2008].

Gosden, J., & Brown, A. (2000) A guide to the Reservoir Act 1975. In: Tedd, P. (ed.) Dams 2000: *Risk and Reservoir Safety: Proceedings of the 11th Conference of the*

British Dam Society, Dams 2000, June 2000, Bath, UK. London, Thomas Telford Ltd. pp. 120-131.

Graham, A. (1997) *The Development of World Wide Web Pages for Dam Design*. MEng final year project report, School of Engineering, University of Durham. [Online] Available from: http://www.dur.ac.uk/~des0www4/cal/dams/emba/intr.htm [Accessed June 2007].

Green, W. H., & Ampt, G. A. (1911) Studies on soil physics, 1: The flow of air and water through soils. *Journal Agricultural Science*, **4** (1), 1-24.

Griffiths, D. V., & Lane, P. A. (1999) Slope Stability Analysis by Finite Elements, *Géotechnique*, **49** (3), 387-403.

Griffiths, D. V., Fenton, G. A., & Tveten, D. E. (2005) Probabilistic passive earth pressure analysis by the Random Finite Element Method. In: Barla, G. & Barla, M. (eds.) *IACMAG 05: Proceedings of the 11th International Conference on Computer Methods and Advances in Geomechanics (IACMAG 05), Turin, Italy*. Bologna, Patron Editore, Vol. **4**, pp. 235-249.

Halder, A., & Mahadevan, S. (2000) Probability, Reliability and Statistical methods in Engineering Design. John Wiley & Sons, New York.

Hamilton-King, L. (2010) *Learning from experience: Post-Incident reporting for UK dams 2009 Annual report*. Environment Agency, Product code: SEHO1010BSOO-E-P (SEHO1010BSOO-E-E).

Hammouri, N. A., Malkawi, A. I.H., & Yamin, M. M. A. (2008) Stability analysis of slopes using the finite element method and limiting equilibrium approach. *Bulletin of Engineering Geology and the Environment*, **67** (4), 471-478.

Hartford, D. N. D., & Baecher, G. B. (2004) *Risk and uncertainty in dam safety*. Thomas Telford Publishing, London.

Hasofer, A. M., & Lind, N.C. (1974) Exact and Invariant Second-Moment Code Format. *Journal of the Engineering Mechanics Division, ASCE*, **100** (1), 111-121.

Hinks, J. L., & Williams, P. J. (2004) Some problems at small dams in the United Kingdom. In: Hewlett, H. (ed.): *Long-term benefits and performance of dams: Proceedings of the 13th Conference of the British Dam Society, Canterbury, UK*. London, Thomas Telford. pp 629-638.

Hirschfeld, R. C., & Poulos, S. J. (1973) *Embankment-Dam Engineering*. John Wiley and Sons, London.

Hoek, E. (2007) Chapter 8: Factor of Safety and Probability of Failure. In: *Practical Rock Engineering*. [Online] pp. 105-114. Available from: http://www.rocscience.com/hoek/corner/8_Factor_of_safety_and_probability_of_failure.pdf [Accessed November 2008].

Hope, I. M. (2009) Learning from experience: Post-Incident reporting for UK dams 2008 Annual report. Environment Agency, Product code: GEHO0409BPCX-E-E.

Horton, R. E. (1933) The role of infiltration in the hydrological cycle. *Transactions, American Geophysical Union*, **14**, 446-460.

Horton, R. E. (1939) Analysis of runoff-plat experiments with varying infiltration capacity. *Transactions, American Geophysical Union*, **20**, 693–711.

Hough, B. K. (1969) *Basic Soils Engineering*. 2nd edition. New York, Ronald Press.

Hsu, S. M., Ni, C-F, & Hung, P-F. (2002) Assessment of three infiltration formulas based on model fitting on Richards equation. *Journal of Hydrologic Engineering, asce*, **7** (5), 373-379.

Huber, M., Vermeer, P. A., & Moormann, C. (2011) Evaluation and implications of soil variability in tunnelling. In: Nishijima, K. (ed.) *ICASP 2011*: *Applications of Statistics and Probability in Civil Engineering: Proceedings of the 11th International Conference on Applications of Statistics and Probability in Civil Engineering (ICASP 2011), Zürich, Switzerland*. London, Taylor & Francis. pp. 2785-2791.

Hudacsek, P., Bransby, M. F., Hallet, P. D., & Bengough, A. G. (2009) Centrifuge modelling of climatic effects on clay embankments. In *Proceedings of Institution of Civil Engineering on Engineering Sustainability*, **162** (2), 91-100.

Hughes, A. K., & Hoskins, C.G. (1994). A practical appraisal of the overtopping of embankment dams. In: *Reservoir Safety and the Environment: Proceedings of the 8th British Dam Society Conference, Exeter*. London, Thomas Telford. pp. 260-270.

Hughes, A. K., Bowles, D. S., & Morris, M. (2009) *Scoping study for A Guide to Risk Assessment of Reservoirs*. DEFRA/Environment Agency, Product Code: SC070087/R1.

Hughes, A.K, & Hunt, D. (2012) A Guide to the Effects of Climate Change in Dams. In: Pepper, A. (ed.) Dams: Engineering in a Social and Environmental Context: *Proceedings of the 17th Conference of the British Dam Society, September 2012, Leeds, UK*. London, ICE Publishing. pp. 231-246.

Hulme M., & Dessai, S. (2008) Negotiating future climates for public policy: a critical assessment of the development of climate scenarios for the UK. *Environmental Science and Policy*, **11** (1), 54-70.

Hulme, M., & Jenkins, G. J. (1998) *Climate change scenarios for the UK: scientific report UKCIP*. Technical Report No.1, Climatic Research Unit, Norwich, 80pp.

Hulme, M., Jenkins, G. J., Lu, X., Turnpenny, J. R., Mitchell, T. D., Jones, R. G., Lowe, J., Murphy, J. M., Hassell, D., Boorman, P., McDonald, R., & Hill, S. (2002) *Climate Change Scenarios for the United Kingdom: The UKCIP02 Scientific Report*. Tyndall Centre for Climate Change Research, School of Environmental Sciences, University of East Anglia, Norwich, UK. 120pp.

Hulme, M., Turnpenny, J., & Jenkins, G., (2002) *Climate Change Scenarios for the United Kingdom: The UKCIP02 Briefing Report*. Tyndall Centre for Climate Change Research, School of Environmental Sciences, University of East Anglia, Norwich, UK.

Hunter, G., & Fell, R. (2003) Travel distance angle for rapid landslides in constructed and natural slopes. *Canadian Geotechnical Journal*, **40** (6), 1123–1141.

Janbu, N. (1973) Slope Stability Computations. In: Hirschfeld, R. C., & Poulos, S. J. (eds.) *Embankment Dam Engineering - Casagrande Volume*. New York, John Wiley & Sons. pp. 47-86.

Jansen, R. B., Kramer, R. W., Lowe III, J., & Poulos, S. J. (1988) Earthfill dam design and analysis. In: Jansen, R. B. (ed.) *Advanced Dam Engineering for Design, Construction, and Rehabilitation*. New York, Springer-Verlag. pp. 256-321.

Jaynes, D. B., & Taylor, E. J. (1984) Using soil physical properties to estimate hydraulic conductivity. *Soil Science*, **138** (4), 298–305.

Jenkins, G. J., Murphy, J. M., Sexton, D. M. H., Lowe, J. A., Jones, P., & Kilsby, C. G. (2009) *UK Climate Projections: Briefing report*. Meteorological Office Hadley Centre, Exeter, UK.

Jenkins, G. J., Perry, M. C., & Prior, M. J. (2008) *The Climate of the United Kingdom and Recent Trends*. Meteorological Office Hadley Centre, Exeter, UK.

Johnston, T. A., Millmore, J. P., Charles, J. A., & Tedd, P. (1999) *An Engineering Guide to the Safety of Embankment Dams In The United Kingdom*. 2nd edition. Building Research Establishment, Watford, UK, BRE Report: BR 363.

Joint Committee on Structural Safety (JCSS) (2006) *Probabilistic Model Code, Section 3.7: Soil Properties, Updated Version*. Technical report [Online] Available from: http://www.jcss.eth.ch [Accessed 1 June 2008]

KBR. (2002) *Reservoir Safety-Floods and Reservoir Safety Integration: In three Volumes*. DEFRA Research contract. Report number: XU0168 Rev A05. Available from: http://www.britishdams.org/reservoir_safety/default.htm.

Kennard, M. F., Hopkins, C. G., & Fletcher, M. (1996) Small embankment reservoirs: A comprehensive guide to the planning, design, construction and maintenance of small embankment reservoirs for water supply and amenity use. Construction Industry Research & Information Association (CIRIA), Classic House. Report number: R161.

Kilsby, C., Glendinning, S., Hughes, P. N., Parkin, G., & Bransby, M .F (2009) Climate-change impacts on long-term performance of slopes. In *Proceedings of the Institution of Civil Engineering on Engineering Sustainability*, **162** (2), pp. 59-66.

Kim, J., Jeong, S., Park, S., & Sharma, J. (2004) Influence of rainfall-induced wetting on the stability of slopes in weathered soils. *Engineering Geology*, **75** (3-4), 251-262.

Kortenhaus, A., Oumeraci, H., Weissmann, R., & Richwien, W. (2002) Failure mode and fault tree analysis for sea and estuary dikes. In: *Proceedings of the International Conference on Coastal Engineering (ICCE), ASCE, Vol. 2 Cardiff, Wales*. pp. 2386-2398.

Kovacevic, K., Potts, D. M., & Vaughan, P. R. (2001) Progressive failure in clay embankments due to seasonal climate changes. In: *Proceedings of the 15th International Conference on Soil Mechanics and Geotechnical Engineering, Istanbul, Turkey*. Rotterdam, A A Balkema Publishers. pp. 2127-2130.

Krahn, J. (2004) *Stability Modelling with SLOPE/W: An Engineering Methodology*. 1st edition. Calgary, Alberta, Canada, Geo-SLOPE/W International Ltd.

Lee, M. L., Gofar, N., & Raharjo. H. (2009) A simple model for preliminary evaluation of rainfall-induced slope instability. *Engineering Geology*, **108** (3-4), 272-285.

Lee, S. R., Choi, J. C., Song, J. C., Myoung, H., & Kim, Y. K. (2010) Wireless sensor network based slope monitoring system considering variability of matric suction. In: Furuta, H. (ed.) *ICOSSAR 2009: Safety, Reliability and Risk of Structures, Infrastructures and Engineering Systems: Proceedings of the 10th International Conference on Structural Safety and Reliability, ICOSSAR 2009, Osaka, Japan.* pp. 2588-2592.

Leong, E. C., Low, B. K., & Rahardjo, H. (1999) Suction profiles and stability of residual soil slopes. In: Yagi, N., Yamagami, T. and Jiang, J-C (eds.) IS-Shikoku'99: *Volume 1 of Slope Stability Engineering: Proceedings of the International Symposium on Slope Stability Engineering- IS-Shikoku'99, 8-11 November 1999, Matsuyama, Shikoku, Japan.* London, A.A. Balkema. pp. 387-390.

Liang, R. Y., Nusier, O. K., & Malkawi, A. H. (1999) A reliability based approach for evaluating the slope stability of embankment dams. *Engineering Geology*, **54** (3-4), 271-285.

Linsley, R. K., Kohler, M. A., & Paulhus, J. L. H. (1988) *Hydrology for engineers*, 3rd edition, McGraw-Hill, London.

Liu, C., & Evett, J. B. (2006). Chapter 2 Engineering Properties of Soils. In: *Soils and Foundations*. 7th edition. New Jersey, Pearson Education. pp. 30-45.

Madsen, H. O., Krenk, S., & Lind, N. C. (1986) *Methods of Structural Safety*. Prentice-Hall.

Mahmood, K., & Kim, J. M. (2011) Reliability Study of Unsaturated Embankment Exposed to Short Duration Rainfall Pattern. *Electronic Journal of Geotechnical Engineering (EJGE)*. [Online] **16** (Bundle F). Available from: http://www.ejge.com/2011/Ppr11.047/Ppr11.047br.pdfn [Accessed June 2011].

Maidment, D. R. (1993) *Handbook of hydrology*. McGraw Hill, New York.

Manning, J. C. (1987) *Applied Principles of Hydrology*. Ohio, Merrill.

McCarthy, D.F. (2006) *Essentials of Soil Mechanics and Foundations: Basic Geotechnics*. 7th edition. New Jersey, Prentice Hall.

McCuen, R. H. (1989) *Hydrologic Analysis and Design*. New Jersey, Prentice Hall.

Melchers, R. E. (1999) *Structural reliability analysis and prediction*. 2nd edition. New York, John Wiley & Sons.

Mellah, R., Auvinet, G., & Masrouri, F. (2000) Stochastic finite element method applied to non-linear analysis of embankments. *Probabilistic Engineering Mechanics*, **15** (3), 251-259.

Meteorological Office. (2010) [Online] Available from: http:// www.metoffice.gov.uk/climate/uk/extremes/ [Accessed 2010].

Meteorological Office. (2011) [Online] Available from: http://www.metoffice.gov.uk/climate/uk/ [Accessed 2011].

Mettananda, D. C. A., & Kulathilaka, S. A. S. (2002) Dependence of the probabilistic evaluation of slope stability on the deterministic model. In: *Proceedings of the 3rd International Conference on Landslides, Slope Stability & the Safety of Infra-Structures, 11-12 July 2002. Singapore*. pp. 333-340.

Michalowski, R. L. (1995) Slope Stability analysis: a kinematical approach. *Géotechnique*, **45** (2), 283-293.

Midttømme, G. H. T. N. (2004) Challenges on dam safety in a changed climate in Norway. In: Hewlett, H. (ed.): *Long-term benefits and performance of dams: Proceedings of the 13th Conference of the British Dam Society, Canterbury, UK*. London, Thomas Telford. pp. 339-347.

Möllmann, A. F. D., & Vermeer, P. A. (2007) Reliability analysis of a dike failure. In: *Proceedings of the 18th European Young Geotechnical Engineers' Conference (EYGEC 2007)*. June 2007, Ancona, Italy. pp. 1-10.

Mostyn, G. R., & Li, K. S. (1993) Probabilistic slope analysis – State of play. In: Li, K. S., & Lo, S-C. R. (eds.) *Proceedings of the Conference on Probabilistic Methods in Geotechnical Engineering, Canberra, Australia, 10-12 February 1993*. Rotterdam, Balkema. pp. 89-105.

Mualen, Y. (1976) A new model of predicting the hydraulic conductivity of unsaturated porous media, *Water Resources Research*, **12** (3), 513–522.

Murphy, C., Charles, E., Harris, Jr., & Gardoni, P. (2011) Classification and moral evaluation of uncertainties in engineering modelling. *Proceedings of the 11th International Conference on Applications of Statistics and Probability in Civil Engineering (ICASP 2011)*, Zürich, Switzerland. pp. 384-192.

Murphy, J. M., Sexton, D. M. H., Jenkins, G. J., Boorman, P.M., Booth, B. B. B., Brown, C.C., Clark, R. T., Collins, M., Harris, G. R., Kendon, E. J., Betts, R.A.,

Brown, S. J., Howard, T. P., Humphrey, K. A., McCarthy, M. P., McDonald, R. E., Stephens, A., Wallace, C., Warren, R., Wilby, R., & Wood, R. A. (2009) *UK Climate Projections Science Report: Climate change projections*. Meteorological Office Hadley Centre, Exeter, UK.

Ng, C.W.W., Zhan, L. T., Bao, C. G., Fredlund, D. G., & Gong, B.W. (2003) Performance of an Unsaturated Expansive Soil Slope Subjected to Artificial Rainfall Infiltration. *Géotechnique*, **53** (2), 143-157.

Nishigaki, M., Tohari, A., & Komatsu, M. (1999) Predicting rainfall-induced slope failures from moisture content measurement. In: Yagi, N., Yamagami, T. and Jiang, J-C (eds.) *IS-Shikoku'99: Volume 1 of Slope Stability Engineering: Proceedings of the International Symposium on Slope Stability Engineering- IS-Shikoku'99, 8-11 November 1999, Matsuyama, Shikoku, Japan*. Rotterdam, Balkema. pp. 465-469.

Parlange, J-Y. (1971) Theory of water movement in soils: 2. One- dimensional infiltration. *Soil Science*, **111** (3), 170-174.

Pereira, C., & Caldeira, L. (2011) Shallow Foundation Design through Probabilistic and Deterministic Methods. In: Vogt, N., Schuppener, B., Straub, D., & Bräu, G. (eds.) *ISGSR 2011: Proceedings of the 3rd International Symposium on Geotechnical Safety and Risk (ISGSR 2011), Munich, Germany*. pp. 199-207.

Philip, J. R. (1956) The theory of infiltration: 1. The infiltration equation and its solution. *Soil Science*, **83**, 345-357.

Pohl, R. (1999) Probabilistic aspects of the seepage flow in dikes. In: (eds.) *Proceedings of the XXVIII IAHR Congress,* **28** *(Theme A), 22-27 August 1999, Graz, Austria*. pp. 1-10.

Potts, D. M., & Zdravkovic, L. (2001) Finite element analysis in geotechnical engineering: application. London, Thomas Telford.

Preziosi, M-C. (2008) Probabilistic assessment of small earthfill dams. *Dams and Reservoirs*, **18** (1), 27-30.

Preziosi, M-C., & Micic, T. (2009) Probabilistic assessment of small earthfill dams subject to adverse climate effects In: Furuta, H. (ed.) *ICOSSAR 2009: Safety, Reliability and Risk of Structures, Infrastructures and Engineering Systems: Proceedings of the 10th International Conference on Structural Safety and Reliability, ICOSSAR 2009*, Osaka, Japan, pp. 137-144.

Preziosi, M-C., & Micic, T. (2011a) Probabilistic assessment of clay earthfill dams subject to variable precipitation. In: Nishijima, K. (ed.) ICASP 2011: *Applications of Statistics and Probability in Civil Engineering: Proceedings of the 11th International Conference on Applications of Statistics and Probability in Civil Engineering (ICASP 2011), Zürich, Switzerland*. London, Taylor & Francis. pp. 2118-2126.

Preziosi, M-C., & Micic, T. (2011b) Methodology for the probabilistic assessment of embankment dams for predicted climate scenarios. Manuscript submitted for publication.

Pumjan, S., & Young, D. S. (1999) Geotechnical site characterisation in localized probabilistic terms. In: *Proceedings of the 37th US Symposium on Rock Mechanics, Vail Rocks (USRMS), CO, UK*. Vol. 2, pp. 801-808.

Ramachandran, K., & Baker, M. J. (1982) *Rely: Structural reliability analysis program version 1M user manual*. Imperial College Department of Civil Engineering, London.

Raudkivi, R. J. (1979) Hydrology - An advanced introduction to hydrological processing and modeling. New York, Pergamon Press.

Rawls, W. J., Brakensiek, D. L., & Saxton, K. E. (1982) Estimating soil water properties. *Transactions of the American Society of Agricultural Engineers, ASAE*, **25** (5), 1316-1320 & 1328.

Reeves, G. M., Sims, I., & Cripps, J. C. (eds.) (2006) *Properties of clay material, soils and mudrocks. In: Clay Materials Used in Construction*. London, Geological Society Publishing House.

Richards, L. A. (1931) Capillary conduction of liquids through porous mediums. *Physics*, **1**, 138-333.

Rouainia, M., Davies, O., O'Brien, T., & Glendinning, S. (2009) Numerical modelling of climate effects on slope stability. In: *Proceedings of the Institution of Civil Engineers - Engineering Sustainability*, **162** (2), 81-89.

Sako, K., Kitamura, R., & Fukagawa, R. (2006) Study of Slope Failure due to Rainfall: A Comparison between Experiment and Simulation. In: Miller, G. A., Zapata, C. E., Houston, S. L., & Fredlund, D. G. (eds.) *Unsaturated Soils 2006 : Proceedings of the 4th International Conference Unsaturated Soils, Unsaturated Soils 2006, 2–6 April 2006, Carefree, Arizona, USA, ASCE,* (GSP 147) Vol 2. pp. 2324-2335.

Santoso, A., Phoon, K. K., & Quek, S. T. (2010) Reliability analysis of unsaturated soil slopes using subset simulation. In: Furuta, H. (ed.) *ICOSSAR 2009: Safety, Reliability and Risk of Structures, Infrastructures and Engineering Systems: Proceedings of the 10th International Conference on Structural Safety and Reliability, ICOSSAR 2009, Osaka, Japan.* pp. 252-259.

Sengupta, A., & Upadhyay, A. (2005) An Evolutionary Algorithm for Locating the Critical Failure Surface in a Soil. *Electronic Journal of Geotechnical Engineering (EJGE*). [Online] **10** (Bundle F). Available from: www.ejge.com/ */2005/Ppr0592/Ppr0592.doc* [Accessed 15 March 2007].

Sidiropoulos, E., & Yannopoulos, S. (1984) Simplified determination and sensitivity analysis of soil-moisture retention curves and hydraulic conductivity. *Journal of Hydrology*, **74** (3-4), 295-309.

Smith, G. N. (1982) Elements of Soil Mechanics for Civil and Mining Engineering. 5th edition. London, Granada.

Smith, N. (1971) *A history of dams.* London, Peter Davies.

Smout, I. K., & Shaw, R. J. (eds.) (1999) Technical Brief No: 48: Small Earth Dams. In: Shaw, R. J. (ed.): *Technical Briefs on Health, Water and Sanitation*. [Online] pp. 61-64 Available from: http://www.lboro.ac.uk/well/resources/technical-briefs/48-small-earth-dams.pdf [Accessed on 15 November 2006].

Sørensen, J. D. (2004) *Notes in Structural Reliability Theory and Risk Analysis*. [Online] Available from: http://citg.tudelft.nl/fileadmin/Faculteit/CiTG/Over_de_faculteit/Afdelingen/Afdeling_Waterbouwkunde/sectie_waterbouwkunde/people/personal/gelder/publications/citations/doc/citatie215.pdf [Accessed July 2011].

Stephens, T. (2010) *Manual on small earth dams: A guide to siting, design and construction*. Food and Agriculture Organization of the United Nations (FAO), Rome. [Online]. Available from: http://www.fao.org/docrep/012/i1531e/i1531e00.htm [Accessed November 2011].

Stone, L. J. (2003) Earthen Dams for Small Catchments: A Compilation of Design, Analysis, and Construction Techniques Suitable for the Developing World: CE5993 Field Engineering in the Developing World. Master's International Program. Department of Civil Engineering and Environmental Engineering, Michigan

Technology University. [Online] Available from: http://www.cee.mtu.edu/sustainable_engineering/resources/technical/SmallEarthDams_FINAL.pdf [Accessed 22 April 2006].

Sutton, B. H. C. (1993) *Solving Problems in Soil Mechanics*. 2nd edition. Harlow, Longman Scientific & Technical.

Tancev, L. (2005) *Dams and appurtenant hydraulic structures*. Taylor & Francis, Leiden/London.

Tedd, P., Charles, J.A., & Holton, I.R. (1997) Settlement of old embankment dams: a guide to measurement and interpretation. *Dams and Reservoirs*, **7** (1), pp. 18-23.

Tedd, P., Skinner, H. D. B. U., & Charles, J. A. B. L. U. (2000) Development in the British national dams database. In: Tedd, P. (ed.) *Dams 2000: Risk and Reservoir Safety: Proceedings of the 11th Conference of the British Dam Society, Dams 2000, June 2000, Bath, UK*. London, Thomas Telford Ltd. pp 181-189.

ter Horst, W. L. A., Jonkman, S. N., & Vrijling, J. K. (2006) Probabilistic analysis of safety of dikes during flood waves. In: Soares, C. G., & Zio, E. (eds.) *Safety and Reliability for Managing Risk*. London, Taylor & Francis. pp. 2073-2080.

Terlien, M. T. J. (1998) The determination of statistical and deterministic hydrological landslide-triggering thresholds. *Environmental Geology*, **35** (2-3), 124-130.

Thoft-Christensen, P., & Baker, M. J. (1982) *Structural Reliability Theory and its Applications*. Berlin; New York, Springer-Verlag.

U.S. Army Corps of Engineers (USACE) (2003) *Engineering and Design: Slope Stability*. Department of the Army, U.S. Army Corps of Engineers, Washington, D.C. Engineering manual: EM 1110-2-1902.

U.S. Army Corps of Engineers (USACE). (1997) *Introduction to Probability and Reliability Methods for Use in Geotechnical Engineering*. Department of the Army, U.S. Army Corps of Engineers, Washington, D.C. Engineering Technical letter number: ETL 1110-2-547.

UK Statute Law Database (2008) *Reservoirs Act 1975* (c.23).

UK Statute Law Database (2010) *Flood and Water Management Act 2010* (c.29).

van Genuchten, M. T. (1980) A closed-form equation for predicting the hydraulic conductivity of unsaturated soil. *Soil Science Society of America Journal*, **44** (5), 892-898.

van Noortwijk, J. M., Vrouwenvelder, A. C. W. M., Calle, E. O. F., & Slijkhuis, K. A. H. (1999) Probability of dike failure due to uplifting and piping. In: Schueller, G. I., & Kafka, P. (eds.) *ESREL 99: Proceedings of the 10th European Conference on Safety and Reliability*. *Rotterdam (ESREL 99), 13-17September 1999, TUM Munich-Garching, Germany*. Rotterdam, Balkema. pp. 1187–1192.

Vaughan, P. R., Kovacevic, N. G., & Ridley, A. M. (2002) The Influence of climate and climate change on the stability of abutment and reservoir slopes. In: Tedd. P, (ed.): *Reservoirs in a Changing World: Proceedings of the 12th British Dam Society Conference, Dublin, Ireland*. London, Thomas Telford. pp. 337-352.

Vrijling, J. K., van Gelder, P. H. A. J. M., & Voortman, H. G. (2004) 3.1 Design applications: state of the art of probabilistic design tools In: Lannoy, A. (ed.) *Life time management of structures*. European Safety, Reliability & Data Association. pp. 148 172.

Wahlstrom, E. E. (1974) *Dams, Dam Foundations, and Reservoir Sites*. Elsevier Science Ltd, New York.

Wang, Q., Shao, M., & Horton, R. (2003) A simple method for estimating water diffusivity of unsaturated soils. *Soil Science Society of America Journal*, **68** (3), 713-718.

White, W. (1993) Soil Variability: Characterisation and modelling. In: Li, K. S., & Lo, S-C. R. (eds.) *Proceedings of the Conference on Probabilistic Methods in Geotechnical Engineering, Canberra, Australia, 10-12 February 1993*. Rotterdam, Balkema. pp. 111-120.

Whitlow, R. (1995) Chapter 9 Stability of slopes. In: Bassett, C (ed.) *Basic Soil Mechanics*. 3rd edition. Harlow, Longman Scientific & Technical. pp. 323-373.

Willows, R. I., & Connell, R. K. (eds.). (2003) *Climate adaptation: Risk, uncertainty and decision-making.* UKCIP Technical Report. UKCIP, Oxford.

Wilson, E. M. (1990) *Engineering hydrology*. 4th edition. London, Macmillan.

Zhan, T. L. T., Zhang, W. J., & Chen, Y. M. (2006) Influence of reservoir level change on slope stability of a silty soil bank. In: Miller, G. A., Zapata, C. E.,Houston, S. L., & Fredlund, D. G. (eds.) *Unsaturated Soils 2006 (GSP 147)*: *Analysis of Slope Stability in Unsaturated Soils: Proceedings of the 4th International Conference on Unsaturated Soils, Unsaturated Soils 2006 (GSP 147), Carefree, Arizona, USA*. **189**(34), pp. 463-472.

Zhang, L. L., Zhang, L. M., & Tang, W. H. (2005) Rainfall-induced slope failure considering variability of soil properties. *Géotechnique*, **55** (2), 183-188.

Zhang, R., & van Genuchten, M. T. (1994) New Models for Unsaturated Soil Hydraulic Properties. *Soil Sciences*, **158** (2), 77-85.

Zhou, J., & Yu, J-l. (2005) Influences affecting the soil-water characteristic curve. *Journal of Zhejiang University Sciences*, **6A** (8), 797-804.